THE RECOVERY OF BIOLOGICAL PARTICLES IN HIGH-SPEED CONTINUOUS CENTRIFUGES WITH SPECIAL REFERENCE TO FEED-ZONE BREAK-UP EFFECTS

by

Klaus Mannweiler

A thesis submitted to the University of London for the Degree of

Doctor of Philosophy

October, 1989

S.E.R.C. Centre for Biochemical Engineering

Department of Chemical and Biochemical Engineering

University College London

Torrington Place, London WC1E

Acknowledgements:

I wish to thank:

my supervisor Dr. Mike Hoare, for his continuous support and encouragement throughout this work,

Prof. Peter Dunnill and Dr. Nigel Titchener-Hooker of University College for providing me the benefit of their experience and knowledge,

Dipl.-Ing. W. Kohlstette of Westfalia Separator for providing me with valuable and encouraging advice on operation and maintenance of the centrifugation equipment,

Dipl.-Ing. P. Brüning, Dipl.-Ing. W. Mackel and Dipl.-Ing. U. Wrede of Westfalia Separator AG for their valuable suggestions and technical support provided during my stay at Westfalia Separator in Oelde, West Germany,

Dipl.-Ing. H. Hemfort of Westfalia Separator for providing the financial support without which this work would not have taken place,

John Betts, Don Montgomery, Clive Osborne and all the other workshop staff of University College for the construction of equipment and their precious technical assistance,

and last but by no means least, I wish to thank my girl-friend for her substained encouragement, tolerance and invaluable assistance during the many hours I spent working on this thesis at home.

Abstract

In the first part of this thesis the means are described by which an industrial disc stack centrifuge may be scaled-down to process in a meaningful fashion small volumes of particle suspensions. The centrifuge separation characteristics so measured were suitable for direct scale-up predictions of centrifuge performance. Experiments with a dye tracer and a reduced number of discs indicated that the flow through the disc centrifuge is influenced by the position of the separating discs within the disc stack.

This influence was also reflected in the separation performance of a particulate suspension. The results were shown to be in the range obtained using a full-scale industrial disc centrifuge. Experiments also showed a distinct trend that the flow rate and in particular the single passage throughput influenced the separation performance. Using a non-linear curve-fitting algorithm it was shown that the grade efficiency curve of a disc centrifuge may be approximated by a two-parameter model equation.

In the second part of this thesis the means are described by which various feed zones designs may be examined in respect to particle breakup using small volumes of a diluted protein precipitate suspension. It has been shown that in the high shear fields which are present in the feed zones to centrifuges the precipitate particles are readily disrupted into smaller fragments, the fragment size depending on the strength of the shear field. Examination of three different feed zone types revealed that particle breakup increased in the following order:

full-hermetic < hydro-hermetic < semi-hermetic

It has also been demonstrated that the bowl speed and in particular the rotational velocity of the distributor ribs has a significant influence on the level of particle breakup in the hydro-hermetic feed zone, while the effects were less pronounced in the full-hermetic feed zone.

Based on the results obtained during the above studies the major mechanism of particle breakup is thought to be due to a combination of turbulence and collision of the particle suspension with the rotating distributor ribs. It has been shown that the level of particle breakup is directly related to the circumferential velocity of the distributor ribs.

Contents

List of Tables

List of Figures

1. Introduction

1.1 Overview and aims of research

Recent advances in biological sciences have led to a rapid development of the biotechnology-based industries. This growth has led to increased demands of separation processes including high-speed centrifuges. The advantages of centrifuges include:

- continuous processing
- small space requirements
- enclosed system
- aseptic product treatment
- adaptation to different separation requirements by variation of throughput
- clean-in-place (CIP) operation possible
- relatively insensitive to variation of process feed stream composition and to presence of foulants or extreme operating conditions.

However despite these advantages there are a series of problems associated with the centrifugal recovery of biological products. Globular proteins, for instance, tend to be unstable undergoing denaturation when subjected to air/liquid interfaces, cooling of the separator is necessary to avoid thermal damage to sensitive proteins and finally, loss of solids recovery efficiency may occur due to breakup of aggregates in the centrifuge feed zone. All of these factors may contribute to make a separator inappropriate for a particular separation problem.

This thesis examines the degree of damage to precipitated protein aggregates in the feed zone of a high speed disc centrifuge. The methods of protein precipitation and the effect of shear have been studied by a number of workers but little is known about the breakage of protein aggregates in centrifuges. The aims of the research are basically threefold:

(1) development of an experimental method to determine and quantify the breakage of protein aggregates in centrifuges

(ii) examination of the relationship between aggregate breakage and various machine operating parameters such as bowl speed and throughput capacity

(iii) improvement, redesign and testing of different feed zone types.

The study will aim to increase the basic understanding of the nature of breakup in centrifuges. The results will enable the manufacturer of centrifugal separators to improve the separation performance of their centrifuge thereby making them more economical. Alternatively the results will point out the need for more research into ways of making particles more resistant to shear.

1.2 Solids recovery by centrifugal separation

Solid-liquid separation based on centrifugal sedimentation relies on the density difference between the solid and liquid phase. In a centrifuge the solids particles are subjected to centrifugal forces which make them move radially outwards provided they are more dense than the carrier liquid and that their motion overcomes the Brownian motion.

For industrial applications five main types of centrifuges may be distinguished according to the design of the bowl and the way by which the solids are removed. Figure 1.1 shows a schematic classification of the equipment including the mode of solids discharge and centrifuge operation.

One of the most common types of centrifuges found in biochemical downstream processing is of the disc stack type. Disc stack centrifuges contain a set of truncated, conical plates or discs separated by spacer ribs, rotating at a very high angular velocity. The feed is introduced to the rotating bowl by a stationary or a rotating feed pipe for non-hermetic and hermetic (sealed) machines respectively, passes through the distributor into the narrow disc spaces of the disc stack where separation and clarification of suspended particles from the liquid phase takes place.

Solids are thrown radially outward by the centrifugal forces acting upon them. After they reach the underside of one of the conical discs, the particles slide downward and finally outward on the bottom side of the discs into the sediment holding space. The clarified liquid flows to the

top of the bowl and leaves the bowl over the inner ring dam. Alternatively a build-in centripetal pump is sometimes used for an enclosed discharge of the liquid phase.

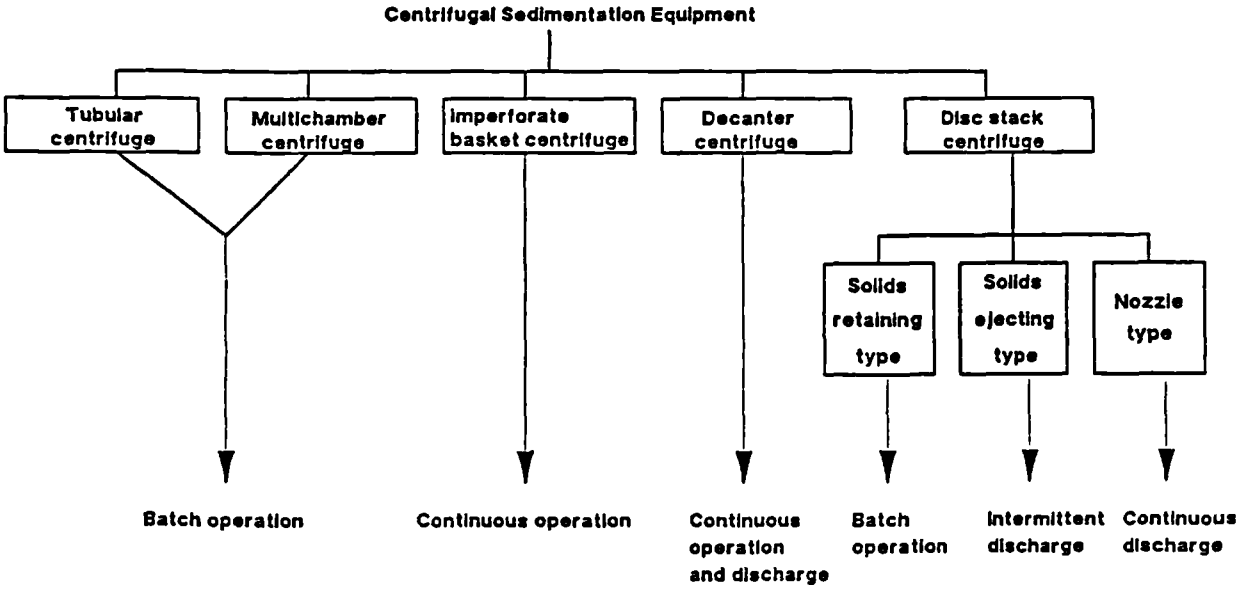

Figure 1.1: Classification of centrifugal separation equipment.

The solids that accumulate in the sediment holding space can be removed in different ways. They can be retained in the bowl and when the space is filled, the centrifuge can be stopped, the bowl dissembled and the solids can be removed by hand. However, this method is only practical when the amount of solids in the feed is very small. For feeds containing higher solids concentration the following types of machines are widely used:

1.2.1 Nozzle disc stack centrifuges

Nozzle disc stack separators, Figure 1.2 c, continuously discharge solids in form of a slurry through nozzles located at the outer diameter of the bowl. The wet solids concentration in the feed can be up to 20 % (v/v) or sometimes more depending on the flow characteristic of the ejected slurry. Nozzle centrifuges are designed to minimize plugging and nozzle erosion, and in fact they can handle solids that are too compact or sticky to discharge from other types of centrifuges. Nozzle openings range from about 0.5 to over 3 mm on the larger machines and there are up to 24 nozzles depending on the size of the machine. To avoid plugging of the nozzles, the feed is typically screened to remove solids with sizes in the order of 50 to 60% of the nozzle diameter. To protect against erosion, nozzles are hard-faced with special alloys.

In general, nozzle separators are useful where the separation is fairly easy and the quantity of solids to be handled is rather large. For separation tasks involving varying or small quantities of solids, the application of a nozzle disc stack separator would be unsuitable. A self-cleaning disc stack centrifuge should be used instead.

1.2.2 Self-cleaning disc centrifuges

In self-cleaning separators, also known as intermittent discharge disc stack centrifuges (Figure 1.2 d) the solid particles are ejected periodically from the sediment holding space while the centrifuge continues running almost at full speed and without interrupting the feed supply. The bowls of these machines have a sediment-holding space in the form of a double cone, in which the solids accumulate. When this sediment-holding space is filled, ports in the periphery of the bowl are hydraulically opened and the solids are ejected at full bowl speed.

Solids ejecting centrifuges can handle feed with a wet solids content up to 10% by volume. A higher solids content in the feed phase requires frequent solids ejection thereby exerting undue strain upon the bowl opening mechanism. The maximum volume of solids that can be handled per unit of time mainly depends on the size of the bowl.

1.2.3 Other types of centrifuges

Other types of centrifuges applied in the biotechnology-based industries are the tubular bowl centrifuge, the multichamber centrifuge and the decanter or scroll discharge centrifuge (Figure 1.2 a, b, e). Although the machines are described in detail elsewhere (Sokolow, 1971; Bell et al. 1983) a brief summary of the basic principles and field of application shall be given.

The tubular bowl centrifuge has a relatively simple design. The suspension is pumped into the rotor via a nozzle through the bottom and solids are sedimented to the rotor walls as the fluid flows upward. The supernatant is discharged via an inner ring dam or by the use of a centripetal pump. The solids that accumulate on the rotor wall need to be removed manually which requires stopping the centrifuge and interrupting the separation process. Despite its excellent clarification capabilities owing to its low solids-collecting volume the application of the tubular bowl centrifuge is limited to process fluids with low solids contents (<1% by volume).

In the downstream-processing of fermentation-based products the tubular bowl centrifuges are often used for the final polishing of preclarified solutions if a clear supernatant is required (e.g. prior to extraction or chromatography).

The multichamber centrifuge is basically a solid-wall bowl centrifuge with high solids capacity but manual discharge. The bowl is equipped with up to five concentric chamber inserts, which have the effect of extending the axial flow path and helping to improve the uniform solids distribution in the bowl, hence leading to an optimum utilisation of the sediment-holding space. The solids capacity of this bowl type varies from 1 to 65 litres of centrifuged, packed solids. The product is fed into the centre of the bowl via a closed-line system and is removed under pressure via a centripetal pump. In the inner chamber only the coarser particles are removed from the feed stream. On the way to the periphery the centrifugal force increases proportionally to the distance from the central axis, hence finer solid particles will be recovered.

The relatively low centrifugal force compared with tubular bowl or disc-type centrifuges is compensated by the high residence time of the product stream in the bowl. However long residence times require cooling of the

bowl when processing thermally sensitive products. The heat is generated during operation by air friction at the outer bowl wall, liquid friction of the centripetal pump, and mechanical friction from the clutch, gear box and bearings.

The main field of application of this type of centrifuge lies in the fractionation of human blood plasma according to the Cohn process (Foster et al. 1980) where the application of a self-cleaning separator is not suitable due to the susceptibility of the product.

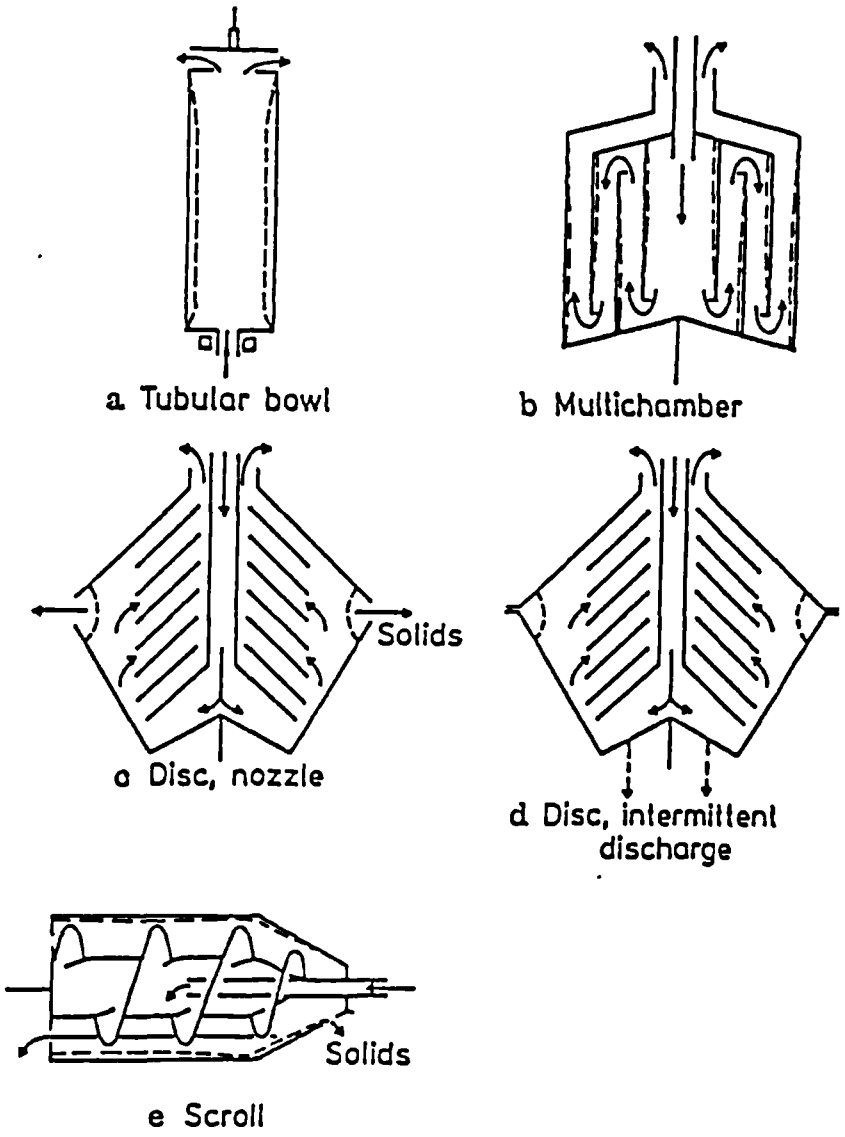

Figure 1.2: Design of five types of centrifuges commonly found in downstream processing of fermentation products.

The design of the decanter centrifuge is derived from the tubular bowl centrifuge with the modification that the solids discharge from the horizontal bowl is accomplished by means of a conveyor screw which rotates at a different speed from the bowl. The objective of this type of centrifuge is usually to concentrate the solids in process liquids with high solids content. In contrast to the disc-type centrifuges the centrifugal force is small but the ability to handle various types of solids at high concentrations and the versatility of the basic design for use in liquid-solid, liquid-liquid-solid, and for liquid-liquid separation or even extraction problems makes the decanter centrifuge very attractive for many processes. Apart from the level of the centrifugal force the performance of the decanter centrifuge is influenced by the transport of the sediment out of the bowl. Its main application is its use as a primary separation step for the clarification of fermentation broth and sludge dewatering in the waste-water industry.

1.3 Some theoretical aspects of centrifugal separation

Generally Stokes' law is used in order to describe the sedimentation process of a solid particle within a centrifugal field and is the starting point for the theoretical understanding of all sedimentation processes. Stokes' law assumes small, inert spheres, laminar flow conditions and diluted particulate dispersions and although these conditions are rarely met in practice, it is still the simplest model to describe the sedimentation of a solid particle in a centrifugal field.

The sedimentation velocity v_z of a solid particle settling in a centrifugal field is related to the gravitational sedimentation velocity, v_g, by:

$$v_z = v_g \frac{\omega^2 r}{g} \qquad 1.1$$

where ω is the angular velocity of the bowl, r is the radius of rotation and g is the gravitational constant. The gravitational sedimentation velocity v_g is calculated by:

$$v_g = \frac{\Delta\rho\ d^2}{18\ \mu} g \qquad 1.2$$

where d is the particle diameter, $\Delta\rho$ is the density difference between

solid and liquid phase and μ is the dynamic viscosity of the carrier liquid or suspension.

Equations 1.1 and 1.2 are valid in the absence of hindered settling or of turbulent settling (i.e. Re (= $v_z \cdot \rho d/\mu$) < 0.5). For higher Reynolds numbers equations have been derived by Sokolov (1971) and Hue (1981).

1.3.1 Separation in an ideal disc centrifuge

In order to describe the clarification process in a centrifuge the general "Separation Area Concept" or Sigma Theory is applied. This concept compares the settling area of a centrifuge calculated on the basis of the geometry and speed of the centrifuge with the settling area of a gravity settling tank capable of the same separation performance as the centrifuge. The derived centrifugal settling area is therefore called equivalent separation area A_{eq}. Theoretically a centrifuge with an equivalent separation area of 10,000 m^2 is capable of the same separation performance as a 100×100 m rectangular gravity settling tank while the dimension of the centrifuge are only of the order of 2×2 m.

It is important to be aware of the conditions and assumptions on which derivation of the subsequent equations are based. These assumptions, though necessary when analysing the problem, impose limitations to the sedimentation area concept which should be fully recognized. These assumptions may be divided into two groups:

a) Assumptions concerning the feed material

1. Particles are spherical in shape and and do not tend to deaggregate or flocculate during their passage through the centrifuge.

2. The particles are evenly distributed in the continuous liquid phase and their concentration is low enough to exclude inter-particle interferences, also known as hindered settling.

3. The settling velocity of the particles in the centrifugal field, v_z, does not exceed the conditions laid down by Stokes law for which the Reynolds number should be smaller than 0.5.

b) Assumptions concerning the fluid flow through the centrifuge

1. Laminar flow at all points of the disc space.

2. The continuous phase is assumed to divide evenly between all the disc spaces.

3. Particle separation is irreversible (i.e. separated particles do not reenter the liquid phase by remixing)

4. The velocity profile of the suspension normal to the disc surface is symmetrical.

5. The flow lines of the continuous liquid phase is assumed to be directed everywhere radially and that no tangential flow occurs.

In a disc stack centrifuge the separation area is enlarged by incorporating a large number of truncated, conical discs. The gaps between two adjacent discs vary according to the processed solids between 0.3 and 2.0 mm. The number of such discs in a disc stack varies from approximately 40 for small to over 250 for large centrifuges.

The general mode of separating a particle from a continuous liquid phase in an ideal disc stack centrifuge is now considered (Figure 1.3). The flow of the continuous liquid phase containing solid particles to be separated, is assumed to be evenly divided between the spaces formed by discs. The flow in each disc space is therefore Q/z where Q is the total flow through the entire disc stack and z is the number of discs. The flow of the liquid phase is also assumed to be in a radial plane and directed parallel to the surface of the rotating discs or, in other words, to have the same angular velocity as the disc stack. Under these conditions the relationship between the single passage throughput, q, and the meridian fluid velocity, v(h), is given by:

$$Q/z = q = \int_{o}^{h} 2\pi r \, v(h) \, dh \qquad 1.3$$

where z represents the number of discs, r describes a radial position in the disc space and h is the gap width.

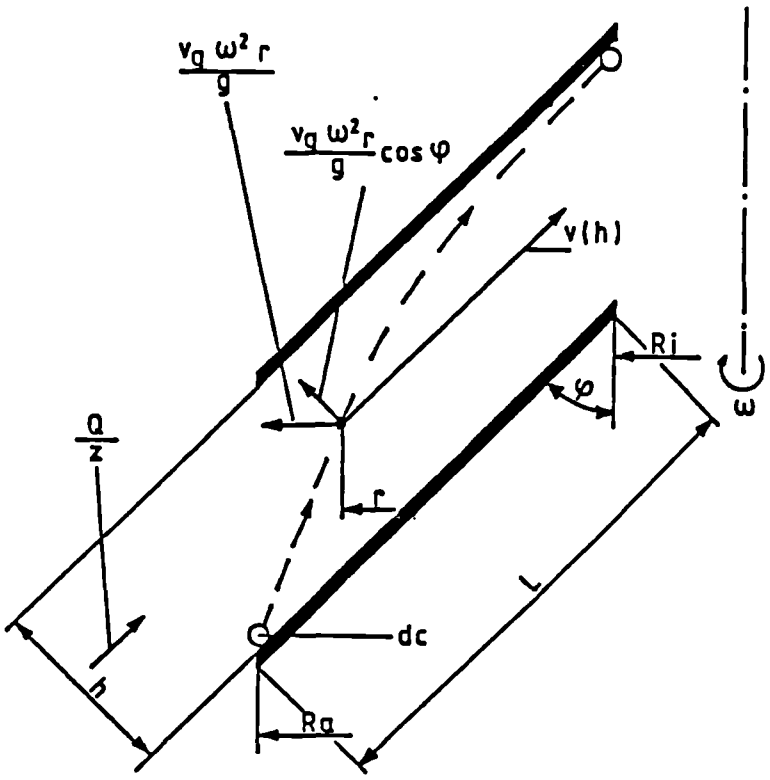

Figure 1.3: Flow through the disc space of an disc centrifuge.

In order to describe the separation capability of a disc centrifuge it is convenient to calculate the gravitational sedimentation velocity, v_g, of those particles which will just be separated from the continuous liquid phase when starting at the upper surface of the lower of the two discs defining the disc space at the outer disc radius R_a and reaching the settling wall, which is the lower surface of the upper of the two discs, before the liquid leaves the disc space at the inner disc radius R_i.

The flow velocity as a function of the radius of rotation is given by:

$$v(h) = \frac{1}{2\pi r} \frac{dq}{dh} \qquad 1.4$$

The particle trajectory in the disc spacing is composed of the radial particle settling velocity:

$$v_x = \frac{ds}{dt} = \frac{dh}{dt \cos\varphi} \qquad 1.5$$

where φ is the disc angle as defined in Figure 1.3, and the particle

velocity, v_p, parallel to the disc surface which is approximately equal to the velocity of the continuous liquid phase, v(h):

$$v_p \cong v(h) = \frac{dL}{dt} = \frac{dr}{dt \sin\varphi} \qquad 1.6$$

Writing Equations 1.5 and 1.6 for dt gives the so called "Differential Quotient" of the particle trajectory:

$$dr = \frac{v(h)}{v_z} \tan\varphi \, dh \qquad 1.7$$

Substituting the liquid phase velocity, v(h), of Equation 1.7 by the expression given in Equation 1.4 gives:

$$dr = \frac{1}{2\pi r} \tan\varphi \frac{dq}{v_z} \qquad 1.8$$

writing Equation 1.8 for dq gives:

$$dq = v_z \, 2\pi r \cot\varphi \, dr \qquad 1.9$$

The settling of a particle of size d relative to the continuous phase in the centrifugal field was defined earlier by Equation 1.2. Therefore substituting the centrifugal settling velocity of a particle, v_z, in Equation 1.9 by the expression given in Equation 1.2 gives finally:

$$dq = v_g \frac{2\pi \omega^2}{g \tan\varphi} r^2 \, dr \qquad 1.10$$

Integrating Equation 1.10 between the two boundaries R_a and R_i results in the relationship between the single passage throughput capacity, q, and the gravitational settling velocity, v_g, of those particles which are just removed from the liquid phase in the disc space.

$$q = v_g \frac{2\pi \omega^2}{3g \tan\varphi} (R_a^3 - R_i^3) \qquad 1.11$$

For a disc stack containing z discs Equation 1.11 may be modified to:

$$Q = v_g \frac{2\pi\ z\ \omega^2}{3g\ \tan\varphi} (R_a^3 - R_i^3) \qquad 1.12$$

Consideration of Equation 1.12 shows that the first factor, v_g, refers only to the settling characteristics of the particles distributed in the continuous liquid phase and the second factor refers exclusively to geometric and mechanical features of the disc stack. Separation of these two factors leads to the following relations:

$$Q = v_g\ A_\Sigma \qquad 1.13$$

where

$$A_\Sigma = \frac{2\pi\ z\ \omega^2}{3g\ \tan\varphi} (R_a^3 - R_i^3) \qquad 1.14$$

Again, A_Σ has the dimension of a length squared and corresponds to the area of a gravity settling tank capable of the same separation performance as the disc stack defined by the parameters included in Equation 1.14. Defining a specific throughput capacity:

$$q_\Sigma = \frac{Q}{A_\Sigma} \qquad 1.15$$

and comparing this expression with Equation 1.13 shows that all particles with a gravitational settling velocity of $v_g \geq q_\Sigma$ are removed from the continuous liquid phase in the disc stack.

$$q_\Sigma = v_{g,c} = \frac{Q}{A_\Sigma} = \frac{d_c^2\ \Delta\rho}{18\ \mu} g \qquad 1.16$$

Only particles which have a gravitational settling velocity greater or equal than $v_{g,c}$ will be certain to settle out in the disc stack. The separation limit, also known as the critical particle size, may be obtained after solving Equation 1.16 for the particle diameter:

$$d_c = \sqrt{\frac{18\ \mu\ Q}{\Delta\rho\ A_\Sigma\ g}} \qquad 1.17$$

According to Equation 1.17 only particles which have a diameter greater or

equal than d_c will be recovered in the disc centrifuge. However, in contrast to a filter for which the separation limit is a more or less absolute quantity, particles smaller than the critical particle diameter will, to a certain extent, also be recovered. This is due to the fact that the particles are thought to be evenly distributed across the entrance to the disc space. Hence particles starting at the outer disc radius but not necessarily at the upper surface of the lower of the two discs but somewhere in between may be of a smaller diameter than d_c and may still be separated from the continuous liquid phase. The probability of particles of gravitational settling velocity less than $v_{g,c}$ being recovered from the continuous liquid phase in a disc centrifuge is given by the grade efficiency, T (see also section 2.3.4):

$$T = \frac{v_g}{v_{g,c}} \qquad 1.18$$

The grade efficiency, T, increases linearly with the gravitational settling velocity v_g until it equals the specific throughput capacity ($v_g = v_{g,c} = q_m$). For particles for which the gravitational settling velocity, v_g, is equal or greater than $v_{g,c}$, the grade efficiency has a value of unity. Owing to the square relationship between the settling velocity and the particle size, Equation 1.18 can be formulated by:

$$\begin{aligned} T &= (d/d_c)^2 \quad \text{for } d<d_c \\ T &= 1 \quad \text{for } d\geq d_c \end{aligned} \qquad 1.19$$

In modern centrifuges, for reasons which will be explained later (see section 1.3.2), spacer ribs (usually eight ribs per disc) are used to separate the discs from each other (Figure 1.4). Therefore a correction factor, f_L, may be introduced in order to account for the small reduction of separation area due to the area occupied by the spacer ribs which are typically 6 mm wide. The equivalent separation area for a complete disc stack is then given by:

$$A_{e,L} = z \frac{2\pi\omega^2}{3g \tan\varphi} (R_a^3 - R_i^3) f_L \qquad 1.20$$

where,

$$f_L = 1 - \frac{3 z_L b_L}{4 \pi R_a} \frac{1-(R_i/R_a)^2}{1-(R_i/R_a)^3} \qquad 1.21$$

z_L is the number of spacer ribs on a single disc and b_L is their width. If point spacers rather than spacer ribs are used then $f_L = 1$. In order to calculate the corresponding throughput capacity, Q, Equation 1.12 has to be modified accordingly.

1.3.2 Separation in a real disc centrifuge

Predictions of the separation performance of a disc stack separator using the equations introduced in the previous paragraph often lack similarity to practical results (Sokolow, 1971). The main reasons for the deviation between an ideal and a real separator are essentially three:

a) Flow through the disc spacing is not necessarily laminar over the whole gap width and radius.

b) Particle sedimentation is not irreversible i.e. particles which have already settled on the underside of the disc may be remixed into the carrier liquid.

c) Unsymmetrical solids loading at the entrance to the disc and disproportionate fluid flow within the disc spacing.

Using models which apply the Navier-Stokes description of the hydrodynamics in a disc separator (Sokolow, 1971; Bohman, 1974; Brunner, 1979), it has been demonstrated that the velocity distribution across the disc spacing depends on a dimensionless number, λ

$$\lambda = h\ (\omega \sin\phi/\nu)^{1/2} \qquad 1.22$$

where h is the disc spacing, ω is the angular velocity, ϕ is the half disc opening angle and ν is the kinematic viscosity.

If λ is smaller than π, the velocity profile is parabolic. The value of λ in industrial centrifuges is usually between 5 and 28 (Sokolow, 1971). Brunner and Molerus (1979) and others have calculated profiles for a number of different λ values. The relative circumferential velocity increases from the disc surfaces to the middle of the disc spacing, and becomes - for large λ values - λ times larger than the average radial velocity. This velocity component splits at large λ values into two thin layers, one near to each disc surface. The velocity in these layers increases and their

thickness decrease with increasing λ. The Reynolds number increases and transition to turbulence can take place. The reason for this behaviour is an interplay between Coriolis, frictional and centrifugal forces.

The influence of the sediment holding space on the separation efficiency has been examined by Skortsov (1984). He showed that there is a non-uniform distribution of the solids particles entering the disc stack because coarse particles may already settle in the outer disc space. However, because of the use of feed channels (see Figure 1.6) those apparently beneficial effects of the sediment holding space are limited.

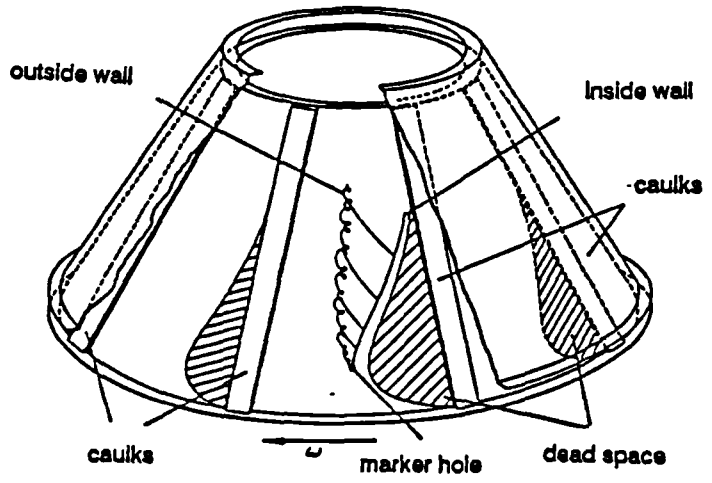

Figure 1.4: Qualitative flow profile in disc spacing (8 long caulks) observed by Brunner, 1979.

Sokolov and Dolzhanova (1972) report that the separation performance of a disc stack separator is a function of the angular velocity of the form ω^{2k}, where $k \approx 0.6-0.9$, due to an appreciable lag of the liquid behind the rotor in the peripheral direction and eddy formation in the spaces between the discs and within the rotor. On this basis, Zastrow (1976) selected

$$v_s = v_g \, (r\omega^2/g)^k \qquad 1.23$$

as an expression for the settling velocity of a particle in a centrifugal field. Under those conditions, the corresponding equivalent separation area

can be modified to:

$$A_s = (2\pi/k+2)\ \cot\varphi\ z\ (\omega^2/g)^k\ (R_s^{k+2}-R_1^{k+2}) \qquad 1.24$$

For $k = 1$ Equations 1.14 and 1.24 coincide. Good agreement between theoretical and experimental results was obtained for the separation of a polyvinylacetate/water suspension if $k = 0.71$ is used in Equation 1.24.

In advanced centrifuges, the discs have feed channels, from which the feed liquid enters the disc stack. Around each feed channel a vortex is formed due to Coriolis forces. The size of the vortex increases with bowl speed and feed flowrate (Sokolow, 1971). When leaving the flow channels, the liquid will flow in a direction counter to the bowl rotation. The existence of large vortices in the flow were photographed by Willus and Fitch (1973) who used a rotating camera to observe flow patterns in a disc centrifuge. Coarse particles are preferentially remixed by the vortex resulting in reduced separation efficiency. Similar studies on a model separator were performed by Brunner (1979). The lid of the bowl of his model separator was built of transparent perspex which made it possible to observe the streamlines of a dye tracer flowing through the disc space (Figure 1.4). Long, radial spacer ribs proved beneficial in respect to transition from laminar into turbulent flow. They suppress fluid flow in the circumferential direction and vortex formation resulting in higher critical Rossby-numbers ($= u_s/R_s\ \omega$) (Brunner and Molerus, 1979). The Rossby-number is a dimensionless flow parameter and its plot against λ is generally used to correlate the points of transition from laminar to turbulent flow for different separator specifications and operating conditions (Greenspan, 1968). The visual examination of the fluid flow through the disc gap of a centrifugal separator revealed also that the use of discs with point spacers are unsuitable for particle separation because of the premature transition from laminar to turbulent flow in the disc gap. These points of transition for discs with and without spacer ribs are plotted in Figure 1.5. For small λ-values ($\lambda < 2\pi$) only minor differences between point and rib spacers are observed. In contrast, for λ-values $> 2\pi$ the disc without caulks shows a further decrease in the critical Ro-number while the Ro remains constant at $Ro \approx 8 \cdot 10^{-3}$ for discs with caulks. Corresponding values calculated for typical operating conditions of industrial centrifuges are indicated by the hatched area of the diagram.

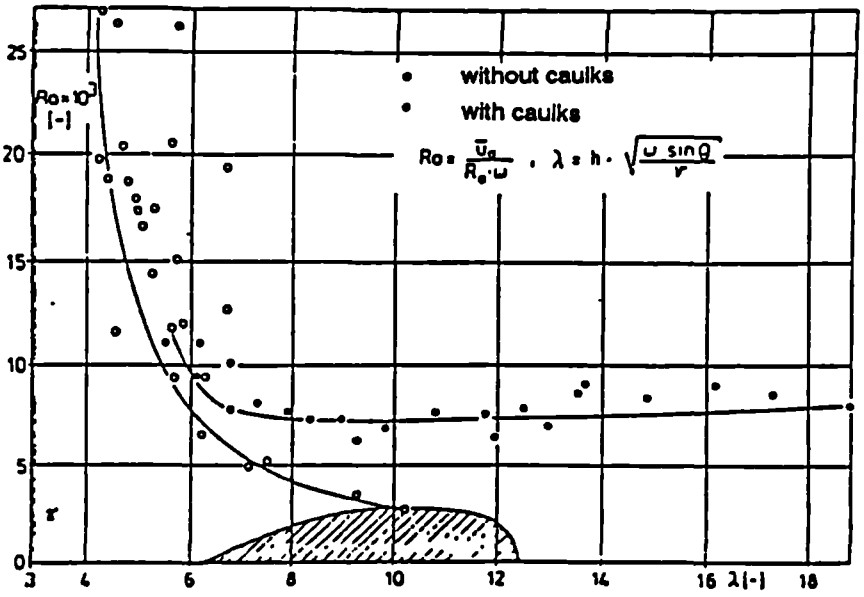

Figure 1.5: Critical Rossby-number as a function of dimensionless flow parameter λ.

The role of the distribution holes is to limit the degree of backmixing of solids sliding down the disc wall into the sediment holding space. Feeding suspension from the periphery into the disc spacing (Figure 1.6 a) gives rise to crossflow between solids on their way to the sediment holding space and freshly supplied feed suspension. By using distribution holes this cross flow situation can be avoided because the sliding solids are able to bypass the incoming suspension (Figure 1.6 b). The inevitable loss of equivalent separation area is compensated by considerably higher absolute throughput capacities if a maximum separation efficiency is the objective.

Recently, Brüning (1987) has demonstrated that owing to Coriolis forces, the use of disc stacks with feed channels cause unsymmetrical solids loading at entry to the discs and disproportionate fluid flow through the disc space, subsequently producing the deviation between the grade efficiency curve of a real and that of an ideal disc stack centrifuge. The grade efficiency, T, as a function of particle settling velocity, v_σ, and

particle diameter, d, respectively, is plotted in Figure 1.7. The graph shows that the grade efficiency approaches unity at particle velocities larger than the critical settling velocity, $v_{g,c}$, or the corresponding particle sizes greater than d_c.

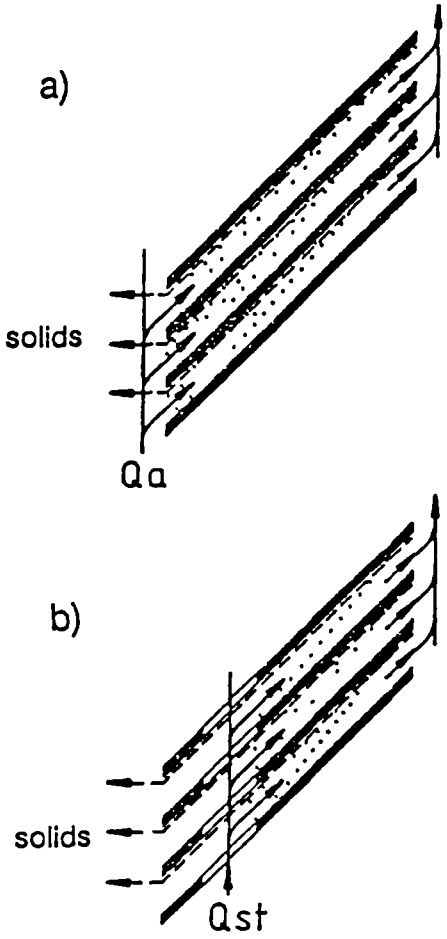

Figure 1.6: Suspension loading (a) via disc periphery and (b) via feed channels.

In a real disc centrifuge Coriolis forces and momentum conservation cause the net flow at the front side (in direction of rotation) of the caulk to be lower than the flow on the rear side of the leading caulk (Brüning, 1987). As a result a particle settling near the rear side of the leading caulk will be subjected to a higher hydraulic throughput and hence will not be recovered even if the particles are of the same size as the critical particle diameter defined by Equation 1.17. The particle size, d_{100}, defines those particles which are just completely separated in a real disc stack centrifuge i.e. no particles greater than d_{100} will be present in the clarified liquid discharge stream. For a well designed disc centrifuge, up to an equivalent separation area of up

to 300 000 m^2, the relationship between d_{100} and the separation limit d_c is generally found to be:

$$\left(\frac{d_c}{d_{100}}\right)^2 \approx 0.5 \qquad 1.25$$

Equation 1.25 is valid up to average specific throughput capacities $\bar{q}$ (= Q/A_e) of the order of 2 L/(h m^2). At higher values of $\bar{q}$ further non-ideality of flow leads to grade efficiency values lower than 1 even at high values of d/d_c.

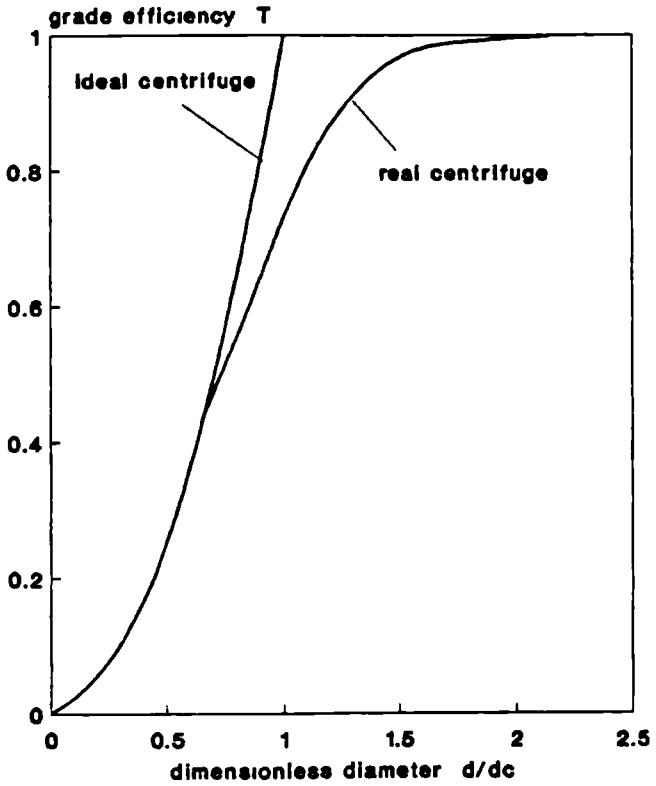

Figure 1.7: Grade efficiency T of an ideal and real disc stack separator

It is important to have clearly in mind that the above discussion only applies for dilute suspensions. Further deviations from ideality due to operation of the disc centrifuge at higher solids concentrations will be discussed later.

1.3.3 Problems associated with the centrifugal recovery of biological solids

The problems associated with the mechanical separation of solid phase bioproducts are mainly due to their small particle size, the small density difference between solid and liquid phase, high suspension viscosity, and the sensitivity of the particles to shear associated breakup effects. Also damage due to thermal effects and the existence of air/liquid interfaces must be considered. The density difference between cells and a nutrient broth is generally in the order of 10 kg/m³ with a viscosity reaching values of the order of 1 to 5 mPas. In general, bacteria exist in two different shapes which are either a spherical or a rod-like structure, with average sizes between 1 and 3 µm. Yeast cells are mainly spherical with sizes between 4 and 8 µm and therefore are fairly easy to separate. Fungi, although comparatively large in size (up to 25 µm), can be very difficult to separate because of their very shear-sensitive, mycelial structure. Major difficulties are associated with the separation of cell debris produced during homogenisation of cells in order to get access to valuable intracellular enzymes. The size of cell debris goes down to diameters of the order of 0.2 µm (Olbrich et al, 1988) and the density difference between solid and liquid phases depends on the lipid content of the debris and may be as small as 10 kg/m³. Density and sizes of protein precipitate differ considerably depending on the protein system used and on the precipitation method applied (Bell and Dunnill, 1982).

Table 1.1: Physico-chemical characteristics of some biological products (Bender and Koglin, 1986).

Product class	Example	Particle size	Density difference	Liquid viscosity	Settling speed	
					grav.	cent.
		d_p[µm]	$\Delta\rho$[kg/m³]	µ[mPas]	mm/h	mm/h
Bacteria Cells	E.coli	1.0-1.5	4-100	1-2	0.04-0.4	0.1-1
Yeast	Bakers Y.	6-8	4-100	1-2	1.5-10	4-30
Cell debris	E. coli homogenate	0.3-0.7	2-200	10	0.0004-0.02	0.001-0.05
Protein ppt.	isoelectric, ppt. Soy P.	0.1-50	5-250	1-2	0.002-200	0.007-700

ppt. = precipitate

Typical values are 5 to 15 μm for the average aggregate size and 10 to 150 kg m^{-3} for the average density difference between aggregate and mother liquor. Table 1.1 lists some typical values of particle size d_p, density difference $(\rho_p-\rho_l)$, and liquid viscosity μ for suspensions of whole cells (bacteria and yeast), cell debris and protein precipitate. In addition, the gravitational and centrifugal sedimentation rates based on the centrifuge specifications listed in Table 2.1 (section 2.1) are shown.

In practice however the actual feed rates, Q, are substantially less than the theoretically calculated feed rates shown in Table 1.2. The differences between the practical and theoretical values increases with increasing solids concentration in the feed and increasing morphological complexity of the feed solids (e.g. mycelial broth). Hence, for feed solids concentrations (0-2% v/v) the practical flowrates are of the order of two thirds of the theoretical values; at higher feed solids concentrations (ca. 5% v/v), feed rates of the order of one half of the theoretical value are recommended. Table 1.2 indicates that it becomes increasingly more difficult to remove particles in the submicron range while still providing an acceptable level of feed throughput. For instance, to remove cell debris from a homogenized cell suspension, with sizes of the order of 0.5 μm, the centrifuge has to be operated at a capacity which is far below its nominal hydraulic throughput capacity of 5 m^3 h^{-1}.

Table 1.2: Calculated hydraulic throughput capacities, Q, for complete particle removal for an intermittent disc stack centrifuge using solids of different specifications. Calculation of the Q is based on the centrifuge specifications given in Table 2.1.

Particle diameter	Solids density	Suspension density	Suspension viscosity	Throughput capacity
μm	kg m^{-3}	kg m^{-3}	mPas	L h^{-1}
1.2	1050	1020	1.02	614
1.0	1050	1020	1.02	426
0.8	1050	1020	1.02	273
0.4	1100	1020	1.02	37

The calculated settling velocities are the particle settling velocities of a single, spherical particle and are only valid for very dilute monodispersed

particle suspensions. For more concentrated suspensions, hindered settling occurs and the settling velocity of the particle is reduced. At a solids concentration of more than approximately 2% (v/v) the mean distance between two particles l_m is such that the boundary flow layers overlap (Figure 1.8) and flow of displaced liquid is created in the direction opposite to the settling particle. Hence, the particles do not sediment in a stagnant fluid but in an upward flowing liquid and as a result the settling velocity is reduced. This reduction increases with increase in solids concentration of the suspension (Muschelknautz, 1987).

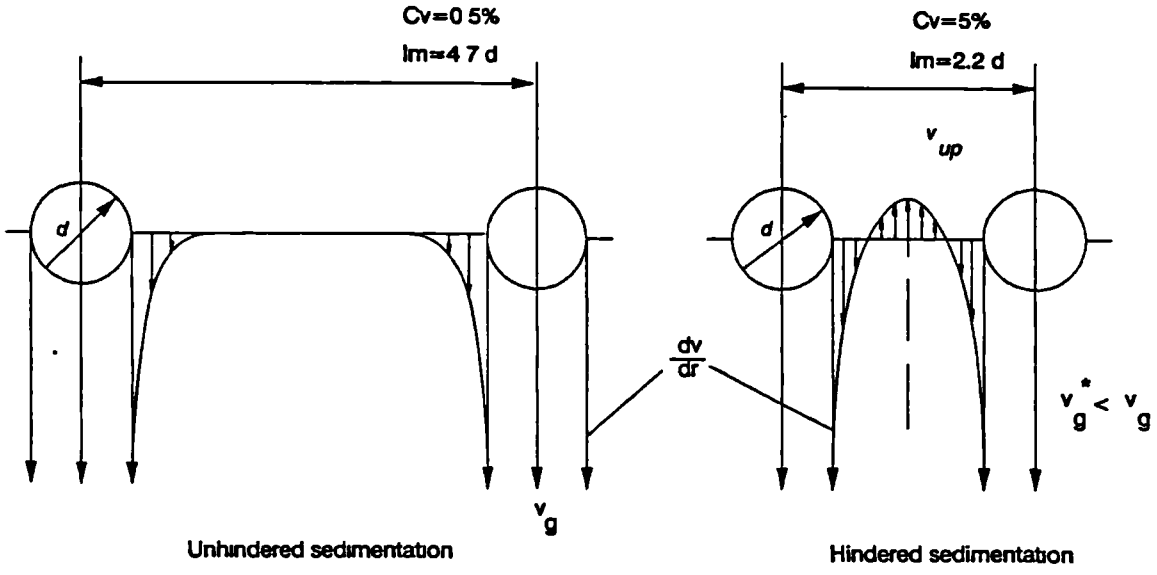

Figure 1.8: Stokes sedimentation of spherical particles.

The radial distance between two spherical particles can be calculated using the volume concentration c_v:

$$c_v = \frac{V_{sphere}}{V_{cube}} = \frac{\pi/6}{(l_m/d)^3} \qquad 1.26$$

to give:

$$l_m = \left(\frac{\pi/6}{c_v}\right)^{1/3} d \qquad 1.27$$

Experimenting with mono-sized, rigid and spherical particles Richardson and Zaki (1954) derived an empirical relationship between the terminal settling

velocity and the solids concentration:

$$v_s^* = v_s\ (1 - c_v)^{\sigma} \qquad 1.28$$

where v_s^* is the hindered settling velocity, v_s is the unhindered settling velocity given by Equation 1.2, c_v is the volume concentration of aggregate in suspension and σ is a geometrical factor. For mono-sized, rigid and spherical particles $\sigma = 4.6$, whereas for non-rigid, non-spherical particles σ can vary from values of about 10 to 100 resulting in large errors where Stokes law is assumed. For flocculated yeast suspensions measured values for σ range from about 12 to 20 (Datar, 1984).

According to Barnea (1973) correlation 1.28 does not completely reflect the reduction in settling velocity for dilute suspensions because the effects of wall hindrance are not considered. Data obtained by Ladenburg (1903) and Francis (1933) showed considerable wall effects expressed as reduction of settling velocity, when the vessel diameter was larger than particle size by one or two orders of magnitude. This is caused by the dissipation of energy as a result of friction between the the moving fluid and the walls of the settling chamber and by the restriction of the liquid flow around the particles. Incorporating effects such as the pseudo-hydrostatic effect (the relative density between particles and suspension decreases with increasing solids concentration), momentum transfer effects (the viscosity of the suspension increases with solids concentration) the gravitational settling velocity of a spherical particle is given by:

$$v_s^* = v_s \frac{1 - c_v}{(1 + K_3 c_v^{1/3})\ \exp[(K_1 c_v/(1-K_2 c_v)]} \qquad 1.29$$

From experimental data for the creeping flow range ($Re < 0.2$) using a variety of literature sources, K_2 and K_3 are found to be equal to 1.0 and K_1 has been obtained by linear regression as 5/3. Figure 1.9 compares the settling velocities calculated according to Equation 1.28 using $\sigma = 4.6$ and with the data obtained using Equation 1.29.

In contrast it is also possible that clusters of neighbouring particles sediment together resulting in higher settling velocities than v_s. In such cases it can often be observed that with increasing particle concentration the settling velocity increases accordingly and, after passing through a maximum at a solids concentration of approximately 1% (v/v), the settling velocity falls again as a result of the rising influence of the upward

flowing liquid (Koglin, 1972). These effects depend on the width and the absolute position of the particle size distribution with narrow distributions and fine particles being less affected by the velocity increasing influences.

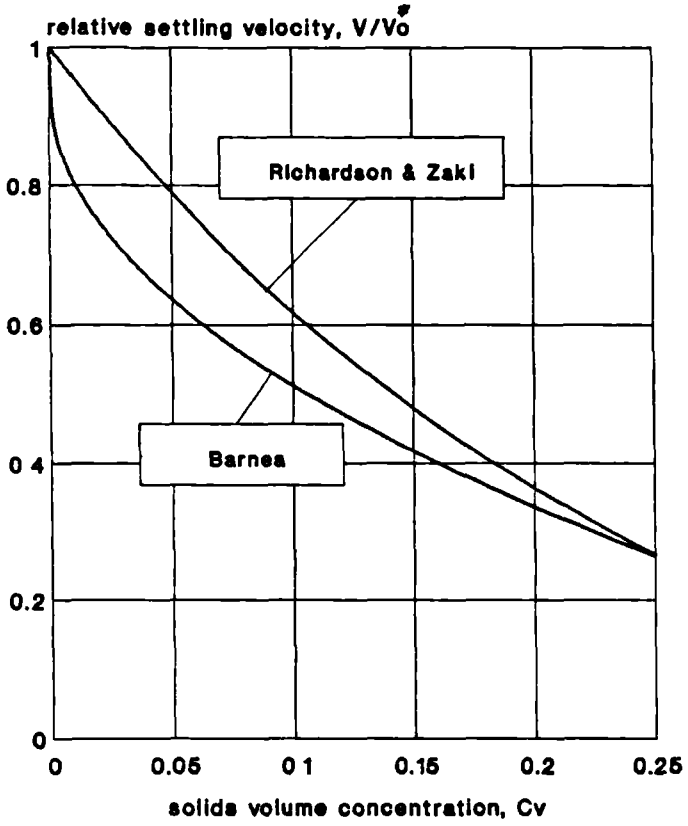

Figure 1.9: Relative settling velocities as a function of solids concentration.

Before Equation 1.12 can be applied correctly to estimate the throughput capacity of a disc stack centrifuge the physico-chemical properties of the solids and liquid phase have to be known precisely (section 1.4.3). This is the point where many problems start to emerge. For example one of the properties required is the exact density difference between aggregates (ρ_a) and liquid phase (ρ_f). Generally for aggregated particles the density decrease with increasing aggregate size; examples include precipitated protein aggregates (Bell et al, 1982), flocculated yeast cells (Brohman and McLoughlin, 1984) and other flocculated products (Tambo and Watanabe, 1979). The relationship between floc density and particle size can be expressed in the form of an empirical equation given by (see also section

1.4.3.1):

$$\rho_s - \rho_f = K_D \, d^{-n} \qquad 1.30$$

where d is the aggregate diameter. The constants K_D and n have to be found experimentally requiring several particle characterisation techniques which will be described later.

Flocs and precipitated aggregates are particularly sensitive to shear which causes the breakup into smaller fragments or primary particles, resulting in a significant loss of separation efficiency. Shear forces are particularly high in the feed zone to centrifuges (Bell and Dunnill, 1982). Research into the problem of particle breakup have led to new feed zone designs with mechanical seals between the feed pipe, the discharge line and the rotating bowl. This new design allows the bowl to be completely filled with process liquid (Hemfort et al, 1985) thus removing any present air/liquid interfaces which may cause denaturation of proteins (Virkar et al, 1982). A detailed description of three common feed zone designs of disc stack centrifuges can be found in section 4.2 of this thesis.

1.3.4 Biosafety aspects

In addition to the normal safety measures associated with recovery processes in the chemical industry, biological production plants require additional safety measures to guarantee aseptic processing of pathogenic (asepsis) microorganisms and to ensure sterile product handling to avoid infection (containment). These demands and in particular the suspicion and resentment amongst the public against new technologies involving rDNA containing organisms on the large scale (Ellmer, 1988) calls for industrial centrifuges which can be sterilised and which will permit operation as part of an entirely enclosed unit to avoid either contamination of the environment or degradation of the product. In particular the release of aerosol during the processing of both whole and disrupted cells, which has been very common in older types of intermittent discharge continuous disc centrifuges, during solids discharge (Dunnill, 1982) need to be circumvented. Further demands are due to the necessity to clean the centrifuge from time to time in order to avoid contamination of the product or to maintain a consistently good separation efficiency. Although the centrifuge may be disassembled fairly quickly and cleaned easily, clean-in-place (CIP) requirements have to be met in many cases to save

time, personnel cost and, especially in applications involving pathogenic microorganisms, where the product has to be handled in strictly enclosed systems.

These demands have led to the development of fully steam-sterilizable hermetically sealed disc centrifuges. The rotor and the housing are parts of a fully contained system that can be sterilized with steam of at least 121 °C at 1 bar excess pressure. The sterilisation procedure which includes sterilisation of the centrifuge, all pipelines, the sterile filters for air and water, and the condenser in the condensate discharge line, takes between 90 and 120 minutes and requires the flushing of the complete system with sterile water after sterilisation and cooling of the rotor (Brunner et al, 1988). Clean-in-Place operation is achieved by flushing the centrifuge with hot water for a period of 20 to 30 minutes. Cleaning of the rotor and the solids-catching chamber is enhanced by several full discharges. Additional cleaning procedures include flushing the machine with various diluted caustic solutions, solutions containing cleaning additives and hot solutions of diluted nitric acid (1-1.5 vol%). Grinding weldings and surfaces minimize solids build-up in the bowl or in the sludge-catching chamber.

During operation infection of the environment is impossible as long as no leaks occur in the system during processing. If work has to be performed on very harmful organisms, then safety is greatly enhanced by placing the equipment in separate rooms that are under a slight vacuum. A useful alternative is the use of a flexible-film isolator also known as soft film cabinet. It consist of a light framework around and under which a PVC film is welded. The operator gains access to equipment via a polyvinylchloride half-suit welded into the wall. The sealed chamber operates at a small negative pressure so that leakage, should it occur, is inward and immediately visible as a change of the chamber wall structure Dunnill, 1982).

1.4 Protein precipitation

Precipitation is a method commonly used for the isolation of proteins from solution and is one of the major steps used in protein purification. Protein precipitates are aggregates of protein molecules often large enough to be visible and to be recovered by filtration or centrifugation. Precipitation can be performed either in a continuous, semi-continuous (fed-batch) or discontinuous (batch) fashion. The primary objective is to obtain aggregates which are large in size, high in density and resistant to deagglomeration forces without denaturing the structure of the protein.

The solubility of the protein in various solvents is determined by the distribution of hydrophilic and hydrophobic residues on the surface of the protein molecule. Altering the protein environment by addition of a precipitating reagent such as salts, acids or organic solvents leads to a reduction in the barrier preventing protein association and primary protein particles emerge which grow further by diffusional transport of protein molecules to the solid protein surface and diffusion-controlled aggregation of the primary particles. Subsequently, the rate of aggregation is largely determined by orthokinetic shear-related collision; these being promoted by continued stirring or flow of the suspension and by higher concentrations. The final aggregate size is limited by the hydrodynamic forces causing disruption of the aggregates.

1.4.1 Methods of protein precipitation

1.4.1.1 Salting out

An extensive review of the subject of protein precipitation by salting out methods has been performed by Bell et al, 1983 and for this reason only a brief overview will be presented here. Salting out is largely dependent on the hydrophobic properties of the protein. High concentrations of neutral salts result in the precipitation of the protein from solution. The precipitation is caused by interactions of hydrophobic patches (side chains of Phe, Tyr, Trp, Leu, Ile, Met, Val) on the surface of the protein molecule. As the salt ions become solvated, there is a greater tendency, when freely available water molecules become depleted, to draw away water molecules ordered around the hydrophobic patches, so enabling these to interact with each other. The larger the number of hydrophobic patches on

the protein molecule the faster the aggregation process. The salting out process can generally be described in the form of an empirical formula suggested by Cohn (1947):

$$\log S = \beta - Kc \qquad 1.31$$

where S is the protein solubility, c is the salt concentration, and β and K are constants. The constant, β, varies considerably with the nature of the protein, is essentially independent of the salt used but is strongly dependent on pH and temperature of protein solution. Solubility is usually highest around pH 7, where proteins have the most charged groups. Increasing temperature generally increases the solubility of the protein. The slope, K, is found to be independent of pH and temperature but varies with the salt and protein involved.

The relative effectiveness of neutral salts in the salting out process, depends on the anions and gives rise to a series termed the lyotropic or Hofmeister series in which are, in order of effectiveness of precipitation, citrate > phosphate > sulphate > acetate ≈ chloride > nitrate > thiocyanate. The tendency for a salt to cause structural damage to the protein is found to be inversely related to its position in the Hofmeister series. Hence, sulphate ions tend to stabilise the protein structure during precipitation.

The salts most frequently used for protein precipitation are ammonium sulphate and sodium sulphate. Ammonium sulphate has the advantage of being inexpensive, of high solubility in aqueous solution even at low temperatures and of its stabilising effects on some proteins (Dixon et al, 1979). However, it does tend to become more acidic on storage and will release ammonia at higher pH. As a result of its high nitrogen content it also causes high levels of BOD (Biological Oxygen Demand - guidance for the water authorities as to what extent waste water is polluted) in the waste water. Disposal is a problem since it is highly corrosive to metals and concrete. Sodium sulphate does not have these disadvantages but must be used at 35 - 40 °C to attain adequate solubility. This may be damaging to many proteins because of their tendency to be unstable at higher temperatures. Another problem to be considered when choosing a salt for protein precipitation is its heat of solution. It is undesirable to generate excessive heating while dissolving the salt. Also the density of the final salt solution needs to be considered, since centrifugation relies on the density difference between the aggregate and the solvent.

1.4.1.2 Isoelectric precipitation

The different proportions of basic and acidic groups on the protein surface gives rise to a pH value at which the net charge of the protein becomes zero. At this point the solubility of a protein becomes a minimum (Figure 1.10) and for a pure protein this minimum will be very sharp, with greatly increased solubility at even 0.5 pH units either side of the minimum

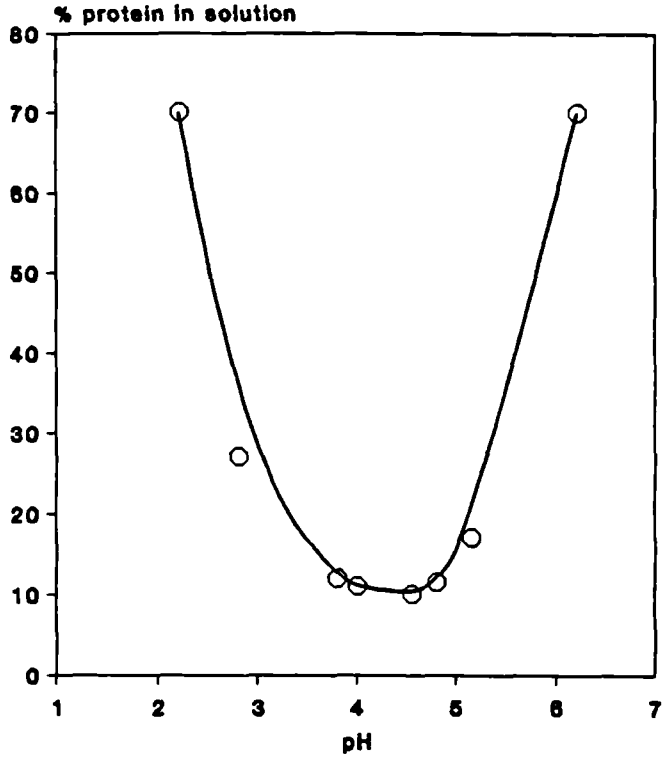

Figure 1.10: The effect of pH on the concentration of soya protein remaining in solution expressed as a fraction of initial concentration of total water extract (Virkar et al, 1982).

Precipitation of protein occurs because at the isoelectric point the electrostatic charges causing repulsion of protein molecules are removed resulting in electrostatic attraction of molecules to each other and increases the collision effectiveness of primary protein particles to form larger aggregates. Precipitation performed at acidic pH's has the advantage of the cheapness of the mineral acids, their ease of use and the fact that several are acceptable in protein food products, e.g., phosphoric, hydrochloric and sulphuric acids. Damaging effects on the protein by the used acids were found to be more severe for hydrochloric acid than for sulphuric acid or other acids with polyvalent anions (Salt, 1982).

1.4.1.3 Precipitation by organic solvents

The principal effect of precipitation is the reduction in water activity. Addition of an organic solvent to an aqueous protein solution will lower the dielectric constant and thus creates a medium less like the polar protein surface. At a low dielectric constant aggregation is promoted by increased electrostatic interactions between the dipolar protein molecules. Hydrophobic interactions are less involved because of the solubilizing influence of the organic solvent on these areas. The change of protein solubility at its isoelectric point with a change in the effective dielectric constant of the solvent can be described by:

$$\log S = K/D_m^2 + \log S_o \qquad 1.32$$

where D_m is the dielectric constant of the solvent/water mixture, K is a constant embracing the dielectric constant of the original aqueous medium and S_o is the extrapolated protein solubility.

Organic solvent precipitation has the advantage that it gives a very refined method of protein fractionation. However, its major disadvantage is the tendency of the organic solvent to cause structural damage to the protein due to the danger of protein refolding. Because refolding especially occurs at higher temperatures, low temperature processes are required for this kind of precipitation. Refolding at high temperatures is caused by small organic molecules which penetrate through 'cracks' in the surface of the protein molecule and attach themselves through hydrophobic forces to internal amino acid residues resulting in destabilisation of the protein. These 'cracks' occur due to natural flexing of the protein molecule structure. At low temperatures the lack of natural flexibility means that solvent molecules are unable to enter the internal protein structure. Although process cooling turns out to be rather expensive, the overall process of protein recovery by using an organic solvent can be economical in terms of process costs if one can easily recover the precipitating agent and re-use it. A typical example for the successful application of precipitation by organic solvents is the process of plasma protein fractionation. In this process and despite the introduction of other techniques ethanol precipitation is most widely applied and has been developed into a highly automated computer-controlled system (Foster et al, 1980).

1.4.1.4 Other methods of protein precipitation

Other precipitation methods involve non-ionic polymers, ionic polymers and metal ions. Dextrans and polyethylene glycol are among the non-ionic polymers most widely studied. The precipitation mechanism which has been described in great detail by Kula et al. (1977) and by Hao et al. (1980) assumes an exclusion effect of the polymer on access between protein molecule and water.

Ionic polyelectrolytes appear to act in a way similar to flocculating agents with some salting out and molecular exclusion action. Precipitation of the protein comes about by formation of electrostatic complexes between the polyelectrolyte and positively charged proteins at low pH values. The low pH requirement is a disadvantage because many enzymes are unstable at low pH values risking irreversible denaturation of the protein. Widely used are polyacrylic acid salts and polysaccharides such as carboxymethyl cellulose. Polyelectrolytes, even at low concentrations, tend to increase the viscosity of the solvent, therefore making downstream solid-liquid separation unit operations, such as centrifugation, more difficult.

Precipitation by metal ions is based on the formation of protein-metal salt complexes having reduced solubility. The advantage of some metal ions is their greater precipitation power with respect to proteins in dilute solutions.

1.4.2 The theory of protein precipitate formation

As discussed in the previous section, the initial stage of precipitate growth can be described as the result of collisions of protein molecules to form small 'primary' particles of protein precipitate.

The process of growth may be described using simplified models considering only aggregate growth but neglecting aggregate breakup. One of the models describing aggregate growth is the perikinetic growth theory in which aggregate growth is diffusion controlled. Von Smoluchowski (1917) first derived the basic kinetic expressions for the collision frequencies of suspended, spherical particles under Brownian motion and laminar flow regimes. He showed that for a monodispersed dispersion the initial rate of primary particle disappearance dN/dt may be described in the form of a

second order equation:

$$dN/dt = - K_A N^2 \qquad 1.33$$

where the rate constant K_A is given by:

$$K_A = \frac{4 K_B T_{abs}}{3 \mu}$$

where K_B is the Boltzman constant, T_{abs} is the absolute temperature and μ is the dynamic viscosity. The theory assumes that the interacting particles are of similar size and is therefore only applicable for systems with a narrow particle size distribution and rapid coagulation conditions. Kruyt (1952) reports that the collision rate between particles of dissimilar size is considerably faster. Colloid particles in the micron range will collect submicron particles by an order of magnitude faster than is expected from perikinetic growth theory.

To account for the long range forces of particle attraction (Van der Waals forces) and inter-particle repulsion, Smoluchowski's theory has been modified by Fuchs (1964) to give:

$$- dN/dt = \frac{4\pi D N^2}{\int_d^\infty \exp(V/K_B T_{abs})/R^2 \, dR} \qquad 1.34$$

where R is the distance between two particle centres, V is the potential energy of particle interaction, K_B is the Boltzman constant, D is the diffusivity and d is the particle diameter.

Perikinetic particle growth is only significant for particles less than approximately 1 μm in size, aggregating in the presence of a shear field of less than 10 s^{-1} and it does not contribute significantly to the collision mechanism of particles above 1 μm in size (Levich, 1962).

Camp and Stein (1943) generalised von Smoluchowski's equation to account for turbulent flow conditions. In the turbulent environment aggregate collision is not only due to random Brownian motion but to a much greater extent due to turbulent velocity fluctuations leading to turbulent shear fields, differences in the individual aggregate velocities and hence, to a greater chance of particle collision. Growth theories in which fluid motion promotes aggregation are classified as orthokinetic growth theories.

For spherical particles of similar size the rate of decrease of particle number concentration due to aggregation is given by:

$$- dN/dt = 2/3 \; K_{eff} \; d^3 \; N^2 \; G \qquad 1.35$$

which may be rewritten

$$- dN/dt = 4/\pi \; K_{eff} \; G \; c_v \; N \qquad 1.36$$

The success of flocculation is proportional to the product of collision effectiveness factor K_{eff}, the floc volume fraction c_v (= $N \pi d^3/6$) or the floc concentration present in the flocculator, the residence time of the floc in the flocculator and the specific energy input defined by Camp and Stein (1943) as the root-mean-square velocity gradient G (= $(P/\mu V)^{1/2}$) where P is the dissipated power, μ is the dynamic viscosity of the suspension and V is the volume of the precipitation vessel.

Equation 1.35 applies strictly only to laminar flow. For turbulent conditions it needs to be modified to (Levich, 1962):

$$- dN/dt = \frac{12 \; \pi}{\sqrt{15}} \; K_{eff} \; G \; d^3 \; N^2 \qquad 1.37$$

The collision effectiveness factor K_{eff} is introduced to explain such effects as interparticle repulsion and orientation requirements. It may be estimated by studying the rate of decrease of particle number during perikinetic aggregation. Based on a detailed analysis of the hydrodynamics of colliding particles, van de Ven and Mason (1977) suggest that the effectiveness of aggregate collision is a function of shear rate and particle diameter. They suggest that K_{eff} is proportional to $G^{-0.18}$ and approximately proportional to $d^{-0.73}$ for colloidal particles.

More sophisticated growth models include aggregate breakage terms to account for deagglomeration due to hydrodynamic forces acting on the aggregate surface. Aggregate breakup may be attributed to primary particle erosion, aggregate fragmentation and rupture as a result of bulgy deformation. The simplest correlation for breakup usually relates the maximum stable floc size, d_{max}, to the degree of turbulence expressed in terms of the root-mean-square (rms) velocity gradient, G:

$$d_{max} = C \; G^{-n} \qquad 1.38$$

where C is a floc strength constant and n is an exponent depending on the

hydraulic regime and type of floc involved. Experimental values for n range from 0.1 for filamentous, biological flocs (Glasgow et al, 1983) and 0.8 for Clay-Aluminium flocs (Tambo and Hozumi, 1979) to 1.1 for isoelectric soya protein precipitate (Bell et al, 1982).

Twineham et al. (1984) proposes that precipitate growth will continue until a dynamic equilibrium state between shear-controlled aggregation and shear-controlled aggregate breakup is reached.

1.4.3 Physico chemical characteristics of soya protein precipitate

1.4.3.1 Density of protein precipitates

The knowledge of the effective settling density of the solid phase is an important factor in the design of protein precipitate recovery processes. Protein recovery processes on the large scale often involve unit operations requiring settling of the solid phase in a gravitational or centrifugal field such as gravity settling tanks or disc stack centrifuges. Since protein precipitate growth involves aggregation of small protein particles, the aggregate density will be determined by its fluid voidage and the density of the protein solid phase. Koglin (1978) proposed that the mean porosity of an aggregate will increase with increasing degree of agglomeration. In the course of agglomeration the individual particles will first combine into primary agglomerates which then form larger agglomerates, the void fraction increasing during this process.

The aggregate density may be calculated using:

$$\rho_a = \rho_s - \varphi_a(\rho_s - \rho_f) \qquad 1.39$$

where ρ_a is the density of the floc, ρ_s is the density of the solids phase, ρf is the density of the liquid phase and φ_a is the porosity of the floc.

Despite its importance to centrifugal separation only little research has been performed on the subject of protein precipitate density. Generally, aggregate density decreases as aggregate size increases due to the fact that with increasing aggregate size more liquid is entrapped within the aggregate.

The aggregate density, ρ_a (kg m^{-3}) can be related to the aggregate diameter, d (μm) over a narrow size range by an empirical relationship given by:

$$\rho_a = \rho_f + K_D d^{-n} \qquad 1.40$$

where ρ_f is the liquor density, kg m^{-3}. The constant K_D depends on the nature of the solid phase and the n is a function the number of primary particles comprising the aggregate. The size at which the aggregate density is equal to the buoyant density is not defined in the equation and will depend on the molecular structure and density of the primary particles. For isoelectric soya protein precipitate the density-size relationship can be expressed in form of an empirical correlation given by:

$$\rho_a = 1004 + 246\ d^{-0.408} \qquad 1 < d < 35\ \mu m$$

Similarly for casein precipitate prepared by salting out with 1.8 M ammonium sulphate the relationship may be written as:

$$\rho_a = 1136 + 31\ d^{-0.441} \qquad 1 < d < 27\ \mu m$$

In both cases ρ_a is the aggregate density in kg m^{-3} and d is the aggregate diameter in μm. The aggregate density may be determined using a wide variety of methods but unfortunately each method gives a different aggregate density value. Some of the average results obtained by Bell (1982) for isoelectric soya protein precipitates applying various density determination methods are shown in Table 1.3.

A density-size relationship is a common characteristic of a majority of solids formed as a result of a precipitation or flocculation process. Tambo and Hozumi (1979) for instance report that the density of aluminium flocs, although much larger in size than the typical protein precipitate aggregate, is size dependent. The use of a density based on the buoyant density would overestimate the Stokes' settling velocity while assuming a constant density difference based on the density of large aggregates underestimates Stokes' law. In both cases this would result in either an over- or an underestimation of the throughput capacity of the centrifuge.

A possible solution to determine the aggregate density is to fit the volumetric median particle size (measured by the electrical sensing zone method) to the photosedimentometer volumetric median particle size and then to calculate the density difference according to Stokes' law. The

measured aggregate density may then be used to predict the required throughput capacity of a centrifuge.

Table 1.3: Density determination of isoelectric soya protein precipitate (particle size 6-8 μm mean diameter)

Method of density determination	density in kg m^{-3}
Gradient centrifugation	
a) CsCl	1292 ±5
b) sucrose/CsCl	1292 ±5
Immiscible solvent centrifugation	1080 ±15
Tracer dilution	1056 ±80
Settling velocity	1120 ±20
Coulter counter total volume	1154 ±15

Another important factor to be considered, when separating biological aggregates is the aggregate strength. Breakup of solid aggregates in hydrodynamic shear fields can adversely influence their recovery. The aggregate strength will be determined by the structure of the aggregate. Generally, aggregate strength will increase with increasing compactness of the aggregate. As for the density-size relationship a similar expression may be formulated for the relationship between aggregate size and strength. Since aggregate strength will decrease with increasing aggregate size large aggregates tend to breakup in the centrifuge thereby reducing its apparent solids recovery efficiency. The strength-size relationship is of greater importance to solids recovery processes than is apparent from examining the relevant equations. A low density difference between solid and liquid phase may be overcome by producing particles which are large in diameter. Stokes' law indicates that the sedimentation rate of a single agglomerate is proportional to the square of its diameter but only linearly dependent on the density difference between solid and liquid phase. Therefore, large particles will always be recovered even if the density difference is small. However, if the large aggregate is not strong then it will rupture when subjected to the intense hydrodynamic forces inside a centrifugal separator. As a consequence smaller agglomerates will emerge which are more difficult to recover. For this reason the objective in any agglomeration process prior to a subsequent solids recovery stage must be the production of large and dense aggregates which are resistant to shear-induced breakup.

1.4.3.2 Rheology of protein precipitate suspensions

The importance of suspension viscosity on centrifugal solid-liquid separation is clear from Stokes' equation. Treatment of a more viscous particle suspension results in an inversely proportional reduction of throughput capacity if the separation efficiency of the centrifuge is to be maintained constant. For protein concentrations up to 22 kg m^{-3} in the liquid phase (not precipitated soya protein) the dynamic viscosity may be approximated by (Deveraux, 1986):

$$\mu = 1.00 \times 10^{-3} + 10^{-5} c_s \quad \text{at } 25\ ^\circ C$$

and

$$\mu = 0.55 \times 10^{-3} + 10^{-5} c_s \quad \text{at } 50\ ^\circ C$$

where μ is the dynamic viscosity (Pa·s) and c_s is the soluble protein concentration (kg m^{-3}) in the liquid phase.

At higher protein concentrations pseudoplastic behaviour is observed. A high value of apparent viscosity of the sediment will hinder sediment flow from continuous or intermittent discharge machines. However for isoelectric precipitates, protein concentration higher than approximately 20 kg m^{-3} are very unlikely to appear in the liquid phase of a precipitate suspension since on average, approximately 80-85% (v/v) of the soluble proteins will precipitate.

An important property of a protein precipitate with respect to recovery is its resistance to movement from rest. This property effects the dewatering characteristics of the sediment. If the protein sludge inside the bowl of an intermittent discharge centrifuge is dewatered in excess, then it will be of a very plastic nature (comparable with rubber) and will tend to block the discharge nozzles. Excessive dewatering also can lead to a non-homogeneous sediment which is difficult to handle in subsequent processing. For this reason the sediment phase must always be wet enough to allow passage through the discharge nozzles. However, the water content of the protein sludge will affect the costs of unit operations downstream to the centrifuge and hence, an optimum water content of the protein sediment has to be obtained to ensure a good overall process performance.

1.4.4 Factors affecting aggregate size

For reasons described in the section on centrifugation, the aggregate size has a major influence on the solids recovery efficiency of a solid-liquid separator. Since with increasing aggregate size the ease of solids recovery increases and recovery cost decreases, the production of large, dense and strong particles must be the primary objective in any precipitation process. The size and strength of a protein precipitate will be affected by:

a) mode of precipitation, batch or continuous
b) choice of precipitating agent
c) protein concentration in mother liquor
d) degree of mixing (power input per unit volume)
e) mean residence time in reactor
f) pH and ionic strength

The effect of the mode of precipitation on the aggregate mean size has been examined by Bell and Dunnill (1982). Precipitate prepared in a continuous tubular reactor with short residence times (30-90 s) was found to be less resistant to shear associated aggregate breakup compared to precipitate prepared in a stirred tank. The difference is thought to arise from the action of a batch-turbine stirred reactor where the precipitate is exposed to high shear forces in the region near the impeller. This leads to the development of compact, regularly-shaped aggregates as compared with the loose irregularly-shaped ones obtained in a tubular one. To improve the strength of aggregates prepared in continuous precipitation processes an ageing stage is suggested where the newly formed precipitate is subjected to high shear rates for short residence times.

Chan et al. (1986) examined the effect of different precipitating agents on the kinetics of protein precipitation in a tubular flow reactor. The final mean diameter of the precipitate varied with precipitating agent used in the order: sulphuric acid (12.5 μm) > ethanol (7.5 μm) ≈ calcium ion (7.2 μm) > ammonium sulphate (3.1 μm).

The effect of the protein concentration on the final aggregate mean size has been examined by Virkar et al. (1982) and Petenate et al. (1983). Both researchers observed no effect of protein concentration on aggregate size up to a concentration of 15 kg m^{-3}.

Increasing the chance of collision may also be achieved by increasing the stirrer speed or the mean residence time of precipitate in the reactor. The maximum stable particle size is controlled by the rate of aggregate breakup. With higher stirrer speeds higher shear forces will result in the formation of smaller particles.

1.5 Breakup of aggregates under turbulent shear

The process of aggregate breakup under turbulent shear has been known for many years, but in contrast to flocculation processes, has received little attention. One reason for this may be the difficult nature of the agglomerates which may be considered as a loose, irregular, three-dimensional cluster of particles. The physico-chemical characteristics of such aggregates, for instance aggregate density and aggregate strength, are normally unclear and difficult to define.

The approaches that have been taken in the breakup studies are varied, ranging from simple deterministic models, e.g., Healy and La Mer (1964), to very complex population balances with multiple parameters, e.g., Pandya and Spielman (1982). Most of the research performed in this field is based on the breakage of polymer flocs, e.g., kaolin-polymer, kaolin-Fe^{+3} and Clay-polymer. Less is known about the breakage of precipitated protein aggregates and literature about it is scarce. The mechanisms for aggregate breakup in turbulent flow can be summarized as follows:

1) deformation and rupture due to pressure differences on opposite sides of the aggregate (bulgy rupture),
2) erosion of primary particles due to hydrodynamic shear,
3) erosion of particles larger than primary particles due to hydrodynamic shear,
4) fragmentation of aggregate by viscous drag or local shear, and
5) breakage by collisional fragmentation.

For analysis of floc breakup, the Kolmogoroff universal equilibrium range theory has proved very useful. The universal equilibrium range is defined as the range of eddies close to a characteristic microscale, where, both viscous energy dissipation and convection are the rule. The range has been further divided into a low eddy size region, the viscous dissipation subrange, and a larger size region, the inertial convective subrange. The two

subranges are divided by the Kolmogoroff microscale (Broadkey, 1966)

$$\eta = (\nu^3/\varepsilon)^{1/4} \qquad 1.41$$

In the equilibrium range theory it is assumed that the energy containing eddies and the energy dissipating eddies have widely different scales which are independent from each other (Batchelor, 1958). In addition turbulence is assumed to be homogeneous and isotropic. The energy dissipated per unit mass ε of fluid is given by:

$$\varepsilon = 2\ (\mu/\rho) \int_0^\infty k^2\ E(k,t)\ dk \qquad 1.42$$

where μ is the dynamic fluid viscosity, ρ is the fluid density, k is the wave number ($= \lambda^{-1}$) and $E(k,t)$ represents the turbulent energy spectrum or change of total kinetic energy of turbulence.

Since there are no external energy sources, this change in kinetic energy must be equal to the energy dissipated at the wavenumber k. The rate of energy removal in the high wave number range must be equal to the rate of energy insertion by inertial transfer at the lower end of the universal equilibrium range of turbulence. The relationship between ε and the more frequently used root mean square velocity gradient, G, is given by the expression:

$$G = (\varepsilon/\nu)^{1/2} \qquad 1.43$$

For the range of eddy scales in the inertial convective subrange, Batchelor (1958) has shown that when $L > \lambda > \eta$, the energy spectrum $E(k,t)$ is:

$$E(k,t) = k_1\ \varepsilon^{2/3}\ \lambda^{5/3} \qquad 1.44$$

where k_1 is a constant. For eddies in the viscous dissipation subrange, Obukhoff and Yaglom (1951) obtained for $\lambda < \eta$, the relationship:

$$E(k,t) = k_2\ (\varepsilon/\nu)\ \lambda^3 \qquad 1.45$$

where k_2 is a constant. The constants $k_1 \approx 0.73$ in accordance with Hinze and $k_2 \approx 4/15$ in accordance with Obukhoff.

The mean eddy velocity, u_λ, is a measure for the intensity of turbulence. It's relationship with the energy spectrum E(k,t) is given by:

$$u_\lambda^2 = [u(x+\lambda,t)-u(x,t)]^2 = 2/3 \int_k^\infty E(k,t)\, dk \qquad 1.46$$

By knowing the mean eddy velocity, it is possible to estimate the forces acting on a floc. A great majority of models describing floc breakup mechanisms are based on calculation of the mean eddy velocity, u_λ. Parker and Kaufman (1972) suggest that the eddies of a scale similar to the aggregate diameter have the greatest effect in terms of hydrodynamic shear. Combining Equations 1.44, 1.45 and 1.46 and replacing λ by the particle diameter d gives:

$$u_{\lambda=d} = \beta^{1/2} (\varepsilon d)^{1/3} \qquad d > \eta \quad \text{(inertial subrange)}$$

$$u_{\lambda=d} = \delta^{1/2} (\varepsilon \rho/\mu)^{1/2} d \qquad d < \eta \quad \text{(viscous subrange)}$$

where u_λ is the mean eddy velocity, ε is the energy dissipated per unit mass, v is the kinematic viscosity, η is the microscale of turbulence, β and δ are constants with values of unity and (1/15), respectively (Fuchs, 1964).

1.5.1 Mechanisms of aggregate breakage

As mentioned earlier, most of the mechanisms found in the literature about this subject are concerned with the turbulent shear disruption of flocs aggregates which are much larger (of the order of 1 mm) than the typical protein precipitate particle which is just 5 to 50 μm in size. Only little is reported on the breakup mechanisms of precipitated protein aggregates. Much of the early information appearing in the literature concerning breakage in dispersed-phase systems, dealt with the hydrodynamic splitting of liquid drops in immiscible liquids (Hinze, 1955). One of the first significant contributions to appear was the breakup analysis performed by Thomas (1964), which was based on Levich's (1962) theory of droplet splitting in two immiscible liquids. His model assumes that under turbulent flow conditions the mechanism leading to rupture is pressure difference on opposite sides of the floc. This pressure gradient is thought to cause bulgy deformation and subsequent rupture due to random velocity fluctuations of turbulent flow. Thomas suggests that the maximum stable floc size, d_{max}, i.e. the size of those flocs which are

stable and which are not further disrupted at the given shear-conditions, can be written in terms of the more convenient root-mean-square velocity gradient by:

$$d_{max} = C_1 \, G^{-5} \qquad d \gg \eta \qquad 1.47$$

$$d_{max} = C_2 \, G^{-1} \qquad d \ll \eta \qquad 1.48$$

for the inertial convective and the viscous dissipation subrange, respectively. The constants C_1 and C_2 are complex and depend on the physico-chemical state of the floc, such as floc density and floc strength and on the environment the floc is subjected to, e.g., pH-value, viscosity and temperature. It is very difficult to define or estimate these constants analytically. The severe dependence of d_{max} on G for the inertial subrange is surprising. Thomas justifies this by suggesting that at a critical value of G, a step change in aggregate size occurs. However, one would expect the function

$$d_{max} = f(G) \qquad 1.49$$

to become more continuous in the case of large aggregates for which the expression is derived. Parker et al. (1972) suggest that floc disruption is primarily due to surface erosion of primary particles from the floc surface. The study is based on Argaman and Kaufman's suggestion that the principle mode of floc breakup is surface erosion caused by turbulent drag forces acting on the floc surface. The rate at which primary particles are stripped from a floc should be proportional to the floc surface area and the shearing stress on the surface.

By assuming that the relevant eddy scales responsible for surface erosion are in the range of the floc diameter, then the maximum stable floc size for the inertial convective subrange is given by:

$$d_{max} = C \, G^{-2} \qquad 1.50$$

For the viscous dissipation subrange d_{max} is given by:

$$d_{max} = C \, G^{-1} \qquad 1.51$$

Again, as before in the Thomas model, the floc strength constant is a function of floc density, floc size and the method of flocculation. Tambo and Hozumi (1979) have proposed that a floc binding force, F_b, is proportional to the net cross sectional area A_n at the plane of rupture. The binding force can be thought of as a measure for the hydrodynamic forces acting on the floc.

By introducing a strength constant, σ, the relationship between the floc binding force, F_b, and the net sectional area, A_n, can be written as:

$$F_b = \sigma A_n \qquad 1.52$$

Presumably σ is dependent on floc size and structure. The assumption, that rupture of flocs is brought about by forces accelerating the flocs and that these forces act in opposite directions, results in another expression for the maximum stable floc size:

$$d_{max} = C G^{-n} \qquad 1.53$$

The floc strength constant and the value of the exponent are determined experimentally by plotting the floc size as a function of the root-mean-square velocity. Using Equation 1.52 the applicable microscale of turbulence can be determined and regression gives the value of the exponent and of the floc strength constant.

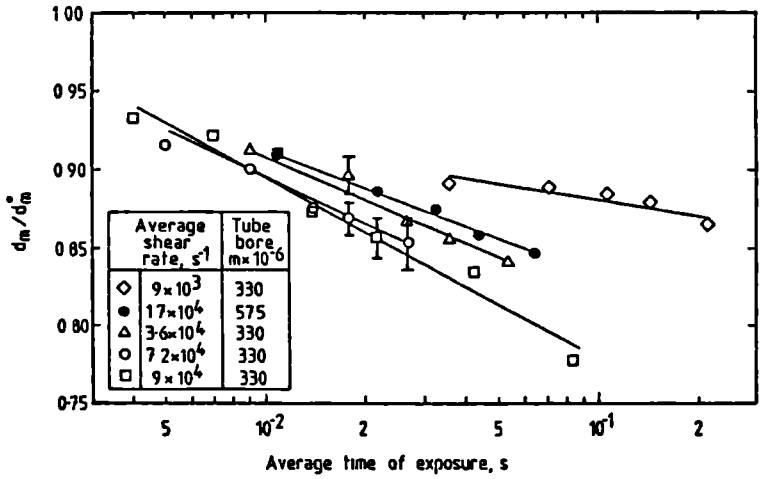

Figure 1.11: Deagglomeration of precipitated soya protein aggregates exposed to laminar shear (Bell, 1982).

The effect of shear disruption on soya protein precipitate particles was examined by Bell (1982). From experimental results using a capillary shear device it was concluded that for protein precipitate the mechanism for aggregate breakage is fragmentation with erosion occurring to a smaller extent. Aggregate disruption in a laminar flow field was observed to be dependent not only on the applied shear rate but also on the exposure time of aggregate to shear. Figure 1.11 shows the size reduction of isoelectric

precipitated soya protein aggregates subjected to different levels of shear and varying exposure times.

Petenate and Glatz (1982) proposed a breakage mechanism for soya precipitate which involves the splitting of aggregates. It was concluded that breakup of protein precipitate deagglomeration is not due to bulgy deformation as adopted from droplet breakage in emulsion formation, but due to local shear fields resulting in a breakage rate proportional to the product of parent aggregate volume and number concentration of aggregate.

Twineham et al. (1984) found evidence for collisional breakage of soya protein aggregates in Couette flow. Evidence is based on the observation that precipitate deagglomeration rate increased with precipitate concentration while extrapolated final sizes first decreased with concentration before ultimately rising again. In a paper prepared for presentation at the Annual Conference of the AIChE in Chicago, Brown and Glatz (1985) confirmed Twineham's results. In their experimental studies they found a concentration dependence of both the breakage rate constant, and the extent of breakup at various concentrations. Models of a second order rate equation were used to describe the removal of large aggregates from the initial particle size distribution.

1.5.2 Protein precipitate breakup in downstream processing equipment

Protein precipitation followed by the separation of the precipitate from the mother liquor, forms the basis of a group of unit operations commonly used for the recovery and fractionation of proteins. One unit operation involves transportation of the precipitate suspension from the precipitation vessel to a separator in order to concentrate the protein suspension. For batch precipitation reactors and ageing vessels this normally requires the use of a pump, while for continuous reactors, direct feed to a separator may be possible if the necessary pressure head required to move the fluid can be developed upstream the reactor. This has the advantage of avoiding any shear controlled damage or breakup within the pumping devices. The effect of pumps on aggregate breakage of soya protein precipitate has been examined by Hoare et al. (1982). A very rapid breakup of precipitate particles was observed in centrifugal, mono, and gear pumps over the first few passes, whereas no breakup was observed in peristaltic pumps.

Another location of concern in respect to aggregate breakage is the feed zone of centrifuges. Breakage of large aggregates into smaller fragments results in reduced solids recovery because, as shown in section 1.2, the separation efficiency of a centrifugal separator is strongly dependent on the aggregate size. The assumption that most of the breakup takes place in the feed zone and not in the bowl or between the discs is supported by the observation that the relative volume of unrecovered particles broken by shear increases as the clarification efficiency is reduced by increasing the throughput. The increased throughput corresponds with a reduced residence time in the bowl which would have resulted in fewer shear disrupted unrecovered particles if disruption was primarily due to the turbulence in the bowl (Bell and Dunnill, 1982). Although it is widely known that aggregate deagglomeration occurs in the feed zone only very little detailed research is actually done on this subject. The main reason for that may be the difficulties involved in actually measuring the degree of breakup in quantitative terms. The problem is that two separate processes happen while a solids aggregate passes through the centrifuge. These two processes are: (i) breakup of large aggregate in feed zone and (ii) particle separation.

The nature of the centrifuge gives only very limited information of the state of the particle suspension, i.e. particle concentration and size distribution, before and after the separator. It is not possible for instance, to collect a sample of feed suspension leaving the feed zone and before entering the disc stack, which would give a direct measure for the rate of breakup. Therefore, from the limited data of inlet and outlet flow one has, somehow, to derive the required information about the breakage of aggregates indirectly.

In any event, the relationship between the number and size of disrupted aggregates and the centrifuge parameters such as bowl speed and feed zone dimensions are rather complex. Gösele (1980) suggests that, based on the laws of momentum conservation, half of the power consumed by a disc separator is used to accelerate the fluid while the other half is lost as a result of power dissipation in the feed zone. The dissipated power P_f is given by:

$$P_f = 1/2\ Q\ \rho_s\ \omega^2 r_1^2 \qquad 1.54$$

where Q is the feed rate, ω is the angular velocity, r_1 is the radius of liquid discharge and ρ_s is the density of the particle suspension.

Bell et al. (1983) has shown that for protein flocs breakup is proportional to the square root of the dissipated power:

$$\ln(N/No) = k\ P^{1/2}\ t \qquad 1.55$$

For $N < N_{max}$, where N is the number of aggregates after exposure time t, No is the initial number of aggregates, and N_{max} is the maximum possible number of primary particles making up the aggregate, the following relationship between the power dissipated in the centrifugal feed zone and aggregate breakage rate using precipitated polyvinylacetate flocs in a decanter centrifuge was developed:

$$\ln(NGF/No) = 0.57\ (P_f)^{1/2} + 0.42 \qquad 1.56$$

where NGF is the number of newly generated flocs. Rearranging Equation 1.54 and substituting the total power dissipated, P_f, by the power dissipated per unit mass (Equation 1.43) results in an expression for the mean velocity gradient, G, which is frequently used to describe aggregate disintegration processes:

$$G = (\tfrac{1}{2}t\rho/\mu)^{1/2}\ \omega r_1 \qquad 1.57$$

where G is the mean velocity gradient, t is the exposure time to shear equivalent to the mean residence time of the aggregate in the feed zone, μ is the kinematic viscosity and ωr is the circumferential velocity at the point of liquid discharge.

As already mentioned in section 1.2 of this thesis, it is difficult to obtain quantitative data on the level of particle breakup in centrifuge feed zones by virtue of the fact that particle breakup and particle separation cannot be divided physically. The only variables which can be measured are the particle concentration and size distribution in the feed stream to the centrifuge and in the supernatant stream leaving the centrifuge. Figure 1.12 illustrates schematically how the particle size distribution of the feed stream may be transformed into the particle size distribution in the overflow due to aggregate breakup in the feed zone and clarification. The task is to explore a method by which the particle size distribution of the feed stream can be measured after it leaves the feed zone, before entering the disc stack. The figure expresses the particle size distribution in the feed stream in form of a frequency number distribution. Once the particle suspension enters the feed zone large particles are broken into smaller fragments By mechanismsthat are rather ill-defined in terms of the flow field in the feed zone of the centrifuge.

The resulting fragments are separated in the disc stack according to a defined separation curve leading to the size distribution in the clarified liquid discharge. More details on the mathematical evaluation of this sheared feed size distribution and the associated problems are described in section 3.5.2.2 of this thesis.

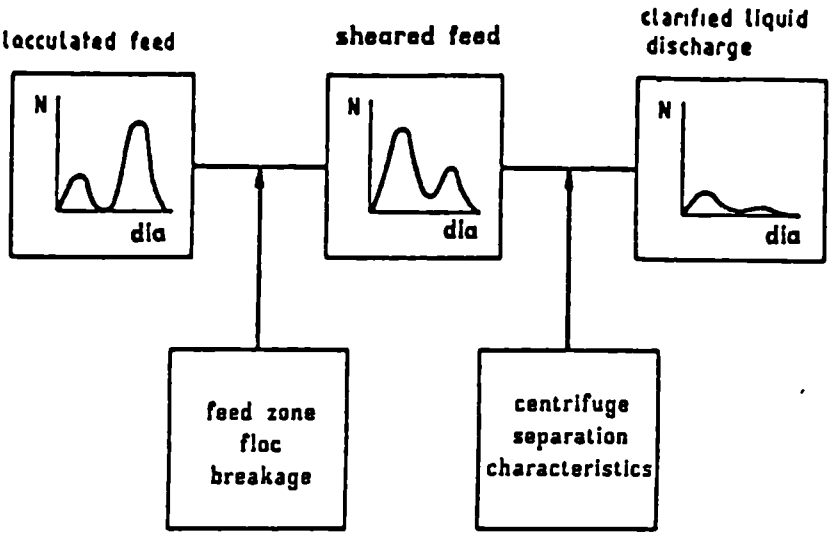

Figure 1.12: Schematic diagram of the transformation of a particle size distribution due to particle breakup in the centrifuge feed zone and particle separation in the disc stack (Bell et al, 1983).

1.6 Choice of particle systems

1.6.1 Evaluating the recovery performance of a disc centrifuge

To measure the particle recovery performance of an industrial disc stack separator it is necessary to choose a particle system which allows the grade efficiency curve of the separator to be obtained over a wide range of particle sizes. The particles should be able to withstand high tensile stresses in order to avoid breakup inside the separator. The particle must be stable in aqueous suspension and in order to obtain theoretical separation limits within measurable particle size ranges the

particle size distribution should be ideally in the order of 0.5 to 5 µm with a solids density close to the density of water.

Polyvinylacetate (PVAc) fulfils these demands. A comprehensive review on polyvinylacetate is given by W. Daniels (1983) and only some of the main characteristics will be described here. Polyvinylacetate is prepared on an industrial scale by emulsion polymerisation of vinylacetate monomers. Typical emulsions are milk-white liquids containing approximately 50 % (w/w) polyvinylacetate, the remainder being water and small quantities of wetting agents or protective colloids. Some typical physical characteristics of polyvinylacetate are listed in Table 1.4

Table 1.4: Physico-chemical constants of polyvinylacetate

Property	Value
Particle settling	
Particle size, µm	0.5 - 3
Density, kg/m³ at 20 °C	1191
25 °C	1190
Particle breakup	
Compressibility, cm³/(g kPa)	$17.8 \cdot 10^{-6}$
Elongation at break (at 20 °C and 0% rh), %	10 - 20
Surface tension (at 20 °C), N/m	0.0365
Tensile strength, MPa	29.4 - 49.0
Others	
Decomposition temperature, °C	150
Softening temperature, °C	35 - 50
Surface resistance, Ω cm^{-1}	$5 \cdot 10^{11}$

The two most important physical characteristics of polyvinylacetate as far as the separation process is concerned are the particle density and the tensile strength. The particle density of 1190 kg m^{-3} is close to the density of water which has a density of 998 kg m^{-3} at 20 °C, and the tensile strength values are high (in the range between 30 to 50 MPa) indicating high resistance against shear forces.

1.6.2 Shear-associated particle breakup

In order to study the shear-associated breakup of particles in the feed zone to disc centrifuges a suitable particle system, which is susceptible to breakup had to be obtained. Apart from the required features described earlier, some restrictions on the particle size distribution of the model system had to be made. The difficulty was finding a suitable particle size range. It was most important that the difference in particle size before and after disruption was significant and yet the particle size of the sheared product was large enough to be analysed by the electric zone sensing method and small enough not to be completely recovered in the disc stack centrifuge. It was also important that the particle size of the sheared product was related to the level of shear in the feed zone.

Isoelectric soya protein precipitate, for which an extensive review is given by Bell et al. (1983), fulfils these conditions and is a widely examined biological particle systems. The major protein fractions making-up soya protein are glycinin and β-conglycinin (Fisher and Glatz, 1986). Glycinin, represented in the 11S fraction by ultracentrifugal analysis, constitutes about 50% of the total protein, and β-conglycinin, represented in the 7S fraction, constitutes approximately 18%. Glycinin has a total molecular weight of approximately $3.2 \cdot 10^5$ D and exists in its native form as a dodecamer of associated subunits, while β-Conglycinin exists as a trimer of circa $1.5 \cdot 10^5$ D. The remaining components making up soya protein are 2S and other proteins (> 15S), fat, carbohydrates, fibre, ash, water and other tracer components.

Extreme precipitation conditions affects the 11S fraction of the protein (Nash et al, 1971) and causes irreversible denaturation of the protein. Studies by Wolf et al.(1964) demonstrated that both the 7S and 11S fractions are denatured by high concentrations of aqueous isopropanol. The 2S fraction was only denatured at higher temperatures (> 50 °C), although at a slower rate than the other fractions.

In summary soya protein is a convenient and suitable system to use due to its availability in large quantity and the ease with which a simple protein solution can be extracted from the crude soya flour. Most importantly the nature of its manufacture is such that the product is largely reproducible.

2. Scale-down of disc stack centrifuges

In the following paragraphs the experimental procedure of centrifuge scale-down will be introduced and different types of experiments are presented. The experimental results are formulated and discussed and an empirical model is set up to allow predictions of the separation performance of an industrial disc stack centrifuge.

The objective is to evaluate the feasibility of scale-down of a high speed disc stack centrifuge in order to use small quantities of test material by replacing a large portion of the active discs with solid body aluminium blocks (Figure 2.1).

2.1 Description of experimental procedure

Throughout this chapter all experimental work was performed using a Westfalia BSB 7-47-476 high speed stainless steel disc stack centrifuge (Westfalia Separator AG, 4740 Oelde, West Germany) equipped with a full-hermetic feed zone (see section 4.2.2 for further details). Some important centrifuge specifications are listed in Table 2.1. The experimental procedure is illustrated in Figure 2.2 and it can be summarised as follows:

For each trial 0.22 kg of polyvinylacetate emulsion (Hoechst AG, Frankfurt, West Germany) was diluted in 4 L of distilled water and ultrasonicated for approximately 1 hour. The conditioned particle suspension was diluted into 400 L of soft water in a 1000 Litre Chemap fermenter vessel (Chemap AG, Switzerland) to give a final particle concentration of approximately 0.05 % (w/w). The pressure inside the vessel was increased to 1.5 bar (gauge) in order to push the suspension through the disc stack centrifuge. By this means it was possible to avoid the use of valves and pumps in the feed line to the centrifuge. At least three throughput settings in the range of 300 to 700 L/h were examined. For each measurement, a total suspension mass of 15 kg were carried through the separator prior to the sampling process. In order to avoid cross contamination the separator was rinsed and totally discharged at least three times using clear water from the mains water supply. A magnetic-inductive flowmeter (Turbo AG, West Germany) was used for measuring the feed rate to the centrifuge. Such a flow meter has the advantage of being highly accurate (± 0.5% of full

scale deflection) and independent of the physico-chemical nature of the fluid provided it has a conductivity of at least 5 mS.

2.2 Measurement of solid properties

To quantify the separation performance of a disc stack separator various physico-chemical constants of the feed suspension must be evaluated. These are (i) the density and kinematic viscosity of the carrier liquid in which the particles are suspended, (ii) the density of the particles, and (iii) the size distribution and particle concentration in the feed to the separator and in the clarified liquid discharge.

2.2.1 Particle size analysis

2.2.1.1 Electric zone sensing method

The Coulter Counter is based on the electric zone sensing principle originally developed by W. H. Coulter in 1952. Although this method of particle sizing has been around for a relatively long period of time its basic principles and potential sources of error are still subject of many investigations. An extensive literature survey on the Coulter Counter principle can be obtained from Coulter Counter Ltd. Figure 2.3 illustrates the principle behind the electric zone sensing method of particle size analysis. The particle suspension is sucked from the beaker through the sizing orifice into the interior of the tube. During the passage of a particle, exhibiting a considerably different electrical conductivity from that of the suspending electrolyte, there will be a change in electrical resistance across the orifice. The constant current flowing from the current source through the platinum electrode, the orifice to the second electrode converts the resistance change into a pulse shaped electrical signal which subsequently is picked up by a signal amplifier. The number of pulses is equal to the number of particles crossing the orifice and the height of the pulse is related to the particle volume by the relationship:

$$\Delta U = \frac{E^2 f}{\rho_R I} \Delta V \qquad 2.1$$

where ΔV is the particle volume, f is a shape factor, ρ_R is the resistivity

of the suspending electrolyte, I is the electric current and E is the electric field strength.

Simultaneous measurement of particle size distribution and concentration is achieved using the electrical sensing zone method (Elzone 80XY, Particle Data Limited, England). The instrument is equipped with a statistics computing accessory (C. H. Hintze 80XY Particle Counter Support System, Version 6.4K). Size analysis was performed using a 18 μm tube, calibrated with latex standards (Particle Data Ltd.) of sizes 1.1 and 2.2 μm. Prior to size analysis the polyvinylacetate suspension was accurately diluted in 10% (w/w) sodium chloride and then analysed for 20 seconds at constant vacuum pressure (160 mbar). The counting procedure was repeated twice and the total number of particle counts was normalised to the average of three individual counts lasting 20 seconds each. In order to minimize coincidence effects (i.e. two or more particles are counted as one single particle) the counting rate did not exceed a value of more than approximately 1000 counts/second. Good dispersion was maintained during the procedure of analysis and foreign particles were excluded. Particle size data were corrected for electrolyte background count. Owing to the small density difference between the polyvinylacetate particles and the suspending electrolyte, particle sedimentation during analysis was negligible.

Special care was required for the preparation of the electrolyte since the presence of very small particles caused extensive background noise problems. In our case the application of Sartobran Filter Capsules (Sartorius AG, Göttingen, West Germany), with an average pore diameter of 0.2 μm, was sufficient in order to remove most of these small particles from the prepared electrolyte. Owing to the large filtration area (> 50 m^2) only little hydrostatic pressure was required to transport the electrolyte through the filter. The application of this technique was a major improvement compared with the earlier use of dead-end membrane filters which required considerably high pumping pressures and vacuum degassing of the filtered electrolyte. At this point it is worth mentioning that it is considered good practice not to use a freshly prepared electrolyte (unfiltered) before it had sufficient time (approximately two days) to lose most of the air introduced during the process of electrolyte preparation.

While the electric zone sensing technique is now well developed for particle size analysis there are still several potential sources of error

which should be addressed. Accuracy of size analysis may be affected by several factors namely particle material (Ullrich, 1966), particle porosity (Horak, 1982) and particle shape (Kachel, 1986).

For some classes of particles, charge transport by electrons inside the particle may occur (i.e. particle is conductive) thereby reducing the total resistance of the circuit. As a result the voltage pulse does not represent the true particle volume causing underestimation of the real particle size by the analyser. Polyvinylacetate has a very high surface resistance (5×10^{11} Ohm/cm) and therefore the chance of charge transport is remote, even when using high aperture current, small orifice diameter or low specific resistance of the electrolyte.

Particle porosity effects are negligible. Polyvinylacetate particles are virtually non-porous. Owing to their high tensile strength effects of particle shape and deformation can be excluded as a source of error during the size analysis process.

The lower and upper size limit lies roughly in the range between 2% and 40% of used aperture diameter. The lower size limit arises due to electrical background noise. The upper limit arises due to the non-linearity of response to the particle volume and the increased danger of aperture blockage. A 18 µm orifice tube was used to give a measurable particle size range between 0.6 to 6 µm.

2.2.1.2 Disc photosedimentometer

The disc centrifuge photosedimentometer has been widely applied for particle size analysis on a variety of dispersed phase systems ranging from polymer latices to herbicides and pigment. The design and operation of the sizing equipment has been described in detail elsewhere (Joyce-Loebl disc photosedimentometer manual, Vickers Co., Langer, G. (1979), Burt M. W. (1967)) and shall be recalled here only very briefly. A schematic diagram on the design and the basic operating principle of the photosedimentometer is shown in Figure 2.4. Light emitted by a mercury vapour lamp (1) is conditioned by passing it through an optical assembly consisting of a lens (2), diaphragm (3) and a 90° turnabout prism (4). At an exactly defined distance from the rotational axis of the disc the light beam crosses the disc rotor (5). The intensity of the light beam is

attenuated by particles passing through the beam while sedimenting in the centrifugal field. The change in light intensity is detected by a light sensitive photo diode (6), the resulting electrical signal amplified (7), filtered in an electronic filter circuit (8) and finaly registered on a Yt-pen recorder (9). Two modes of particle size analysis can be applied:

(i) The layer method in which all particles start from the same position.

(ii) The suspension method in which all the particles are initially uniformly distributed.

Both methods are explained in more detail in publications by Alex et al. (1974) and Brugger (1975). Owing to the mathematical difficulties associated with the suspension method the thin layer or line start method is the one mostly applied for particle size analysis using the disc photosedimentometer. A small amount of suspension (approximately 1 ml) is injected onto an exactly known volume of sedimentation fluid spinning at the same speed as the disc rotor. Near the outer edge of the rotor disc the particles cross the already described light assembly producing an electrical signal proportional to the optical density (turbidity) of the fluid in the light beam. Assuming Stokes Law, the corresponding particle diameter can be calculated from the required settling time of a particle travelling from the surface of the sedimentation fluid to the optical detector assembly. The centrifugal sedimentation rate at constant angular velocity, ω, increases proportionally to the distance from the axis of rotation, r.

$$\frac{dr}{dt} = \frac{\Delta\rho\ d^2}{18\ \mu}\ \omega^2 r \qquad 2.2$$

where $\Delta\rho$ is the density difference between the solids and liquid phase and μ is the dynamic viscosity of the sedimentation fluid. The required settling time of a spherical particle can be obtained by rearranging and integration of Equation 2.2 resulting in:

$$\ln(R_o/R_1) = \frac{\Delta\rho\ d^2}{18\ \mu}\ \omega^2 t \qquad 2.3$$

where R_o and R_1 are the start and settling radii, respectively.

In practice the settling time is recorded on a pen recorder and the particle diameter, d, is calculated after rearranging Equation 2.3 to give:

$$d = \sqrt{\frac{18\ \mu}{\Delta\rho\ \omega^2\ t}\ \ln(R_o/R_1)} \qquad 2.4$$

Determination of the particle size distribution from the pen deflection on the pen recorder trace is more complex. Because of the finite size range of the particles in the cross section of the light beam the beam attenuation is proportional to the mass of the particles and not to the particle surface (Treasure, 1981):

$$\tau(t) = f_3(d)\ \alpha\ d^3 f_o(d) \qquad 2.5$$

From Equation 2.4 we have:

$$t\ \alpha\ 1/d^2 \qquad 2.6$$

which by differentiation gives:

$$dt\ \alpha\ dd/d^3 \qquad 2.7$$

Integrating the turbidity, $\tau(t)$, over the settling time, t, gives:

$$\tau(t)\ dt\ \ \alpha\ \ f_3(d)\ dd/d^3\ \alpha\ f_o(d)\ dd \qquad 2.8$$

Hence the area under the pen recorder deflection trace represents a number distribution. Therefore integration of Equation 2.8 gives the number fraction, $F_o(d)$, of particles greater than or equal to size d, given by the expression:

$$F_o(d) = \frac{\int_0^T \tau(t)\ dt}{\int_0^\infty \tau(t)\ dt} \qquad 2.9$$

The corresponding volume- or mass (for particles where density is not a function of size) distribution can be obtained directly from the pen recorder deflection trace.

For this purpose the time axis must be transformed into a size axis via Equation 2.4.

$$F_3(d) = \frac{\int_0^d \tau(d)\, dd}{\int_0^\infty \tau(d)\, dd} \qquad 2.10$$

where $F_3(d)$ is the volume or mass fraction of particles greater than or equal to size d.

An additional level of complication is introduced if corrections for optical effects have to be included. The turbidity, τ, in Equations 2.9 and 2.10 has to be divided by a particle specific extinction coefficient, K_{ext}, which is defined as the ratio of light obscured by a particle to the light which it would have obscured if the law of geometric optics were valid for the system under consideration. If the extinction coefficient is constant, i.e. particle size independent, then its influence on the particle size distribution can be neglected. The same is valid for a narrow size distribution but a size dependent extinction coefficient (Langer, 1979). In other cases the extinction coefficient may be related to the particle size by an empirical expression developed by Kerker (1969):

$$K_{ext} = 2 - (4/\Gamma)\sin\Gamma + (4/\Gamma^2)(1-\cos\Gamma) \qquad 2.11$$

where,

$$\Gamma = \pi d/\lambda(m-1)$$

where λ is the wavelength of light in the medium (= λ_o/n, where λ_o is the wavelength of light in vacuum and n is the refractive index of the medium) and m is the relative refractive index.

In order to examine the optical effects of the particle on the light attenuation, the settling characteristics of polyvinylacetate particles in a disc photosedimentometer were examined, after its particle size distribution was analysed using the electric zone sensing method. For these experiments an ultrasonically conditioned, aqueous polyvinylacetate suspension was used. Centrifugal sedimentation was performed in a Joyce-Loebl disc photosedimentometer equipped with a turbidity meter (Vickers Instruments Co.). Instead of applying the so-called buffered line start method (recommended by the instrument manufacturer), in which a layer of

pure solvent is introduced on top of the solute containing spin fluid followed by mixing the two layers, a method proposed by Langer (1979) and by Alex and co-workers (1974) was used. In this method a preformed density gradient overcomes the difficulties associated with unstable sedimentation effects (e.g. streaming) inherent with the thin layer method.

The gradient preparation technique has been adopted from Coll (1985). Sucrose gradients were prepared in a Buchler gradient apparatus (Buchler GmbH, Switzerland) that consists of two identical wells. Well No. 1 was filled with 10 mL of distilled water and well No. 2 contained 10 mL of the higher density solution (5% (w/w) sucrose) stirred by means of a rotating spiral. The gradient solution was pumped by means of a peristaltic pump, into a holding tube made of glass (350 mm long, 10 mm inner diameter) mounted at an angle of approximately 75°. The gradient liquid (20 mL) was injected into the rotating hollow disc of the photosedimentometer by gravitational flow. After gradient injection a thin layer of dodecane (approximately 0.5 - 1 mL) was injected on top of the sucrose/water gradient using a microsyringe, with the purpose of preventing fluid from evaporation from the gradient surface. Finaly, 1 mL of suspension sample was injected on top of the dodecane layer and the sedimentation curve was recorded. To calculate the particle sizes from the sedimentation curve the arithmetic averages of spin fluid density and viscosity were used as proposed by Alex et al. (1974).

Acquisition of the optical density data and calculation of the corresponding particle size distribution was performed using a 12 bit analog-to-digital converter (Xcalibur XAD 2, 3D Digital Design & Development Ltd., England) in conjunction with an Apple IIe microcomputer. The analog signal emitted from the photoreceptor was amplified, fed to a pen recorder and from there to a 12 bit analog-to-digital converter in which the analog signal was digitized and read from a microcomputer (Apple IIe). The pen recorder served merely as a control instrument giving a visual guide as when to terminate the data acquisition process. Before injecting a sample on the gradient layer the output current of the photoreceptor was adjusted to zero on the build-in LCD display of the photosedimentometer. This corresponds to a reading below 5 mV on the computer VDU. After the sample was injected two relais associated with the analog-to-digital converter were closed by a computer controlled relays control circuit. The converted light intensity signal was fed directly into the microcomputers Random Access Memory whereby the computer was

programmed in such a way that a software-controlled timer allowed storage of signal readings every two seconds, practically copying the pen recorder deflection trace into the computer memory.

In order to maximize accuracy and signal resolution of the analog-to-digital converter and to allow measurements over a wide range the signal amplification factor was varied under software control. The data acquisition process was terminated with a punch command. If this command was given, then the software-controlled relays were opened and the stored data were recalled from the computer memory, conditioned and used for evaluation of the particle size distribution. The final particle size distribution in form of either number or volume (-mass) oversize distribution was visualized on the computer monitor or plotted as a graph or in form of a table on a DOT matrix printer (Mannesmann Tally). For documentation purposes the data were stored on a floppy disc together with all the necessary sample and operation parameters used during the process of particle size analysis.

2.2.2 Physico - chemical properties of the solids and liquid phase

The density of the carrier liquid phase was that of water which is 998.2 kg m^{-3} at 20 °C. The density of the solids phase was determined by gradient centrifugation using a sucrose-water gradient. A particle density of 1190 kg m^{-3} was determined confirming the density figure given in Table 1.4. The viscosity of the carrier fluid was assumed to be the same as water at the corresponding temperature which is 1.005 mPa·s at a temperature of 20 °C.

2.2.3 Tracer studies

A small amount of dye tracer (approximately 2 mL of methylene blue containing 10 g dye L^{-1}) was added to the in-going stream during a period of time which was very short compared with the overall residence time of the fluid in the system. The dye concentration in the exit stream was monitored on-line using a flow through colorimeter operated at a wavelength of λ = 546 nm and a cuvette pathlength of 5 mm (Isco Optical Units, Instrument Specialities Co., England). The continuous change in light absorbance was converted into an electrical current, amplified and

transferred to a microcomputer (Apple IIe, Apple Computer Inc., USA) equipped with an analog-to-digital converter (Xcalibur XAD 2, 3D Digital Design & Development Ltd., England) for data acquisition and processing. All trials were performed on pilot-plant scale on the previously described disc stack centrifuge. A gear pump, on-line controlled by an inductive flowmeter, was used to provide accurate and constant flow rates. The location of the active discs was varied by replacing part of the disc stack with the previously described blank inserts (Figure 2.5). Measurements were performed at a range of flowrates, for a rotating and non-rotating bowl and for different active disc location. Normalised exit age distribution curves and mean residence times were calculated as described by Levenspiel (1972).

Table 2.1: Disc stack centrifuge design specifications

Parameter	Value
Feed type	hermetic
Bowl speed, min^{-1}	9200
Number of discs (maximum)	72
Half disc opening angle, °	38
Outer disc radius[1], m	0.076
Inner disc radius , m	0.036
Caulk type	long
Number of caulks	8
Caulk width, m	0.006
Caulk height, mm	0.5

[1] value based on inner edge of riser channel.

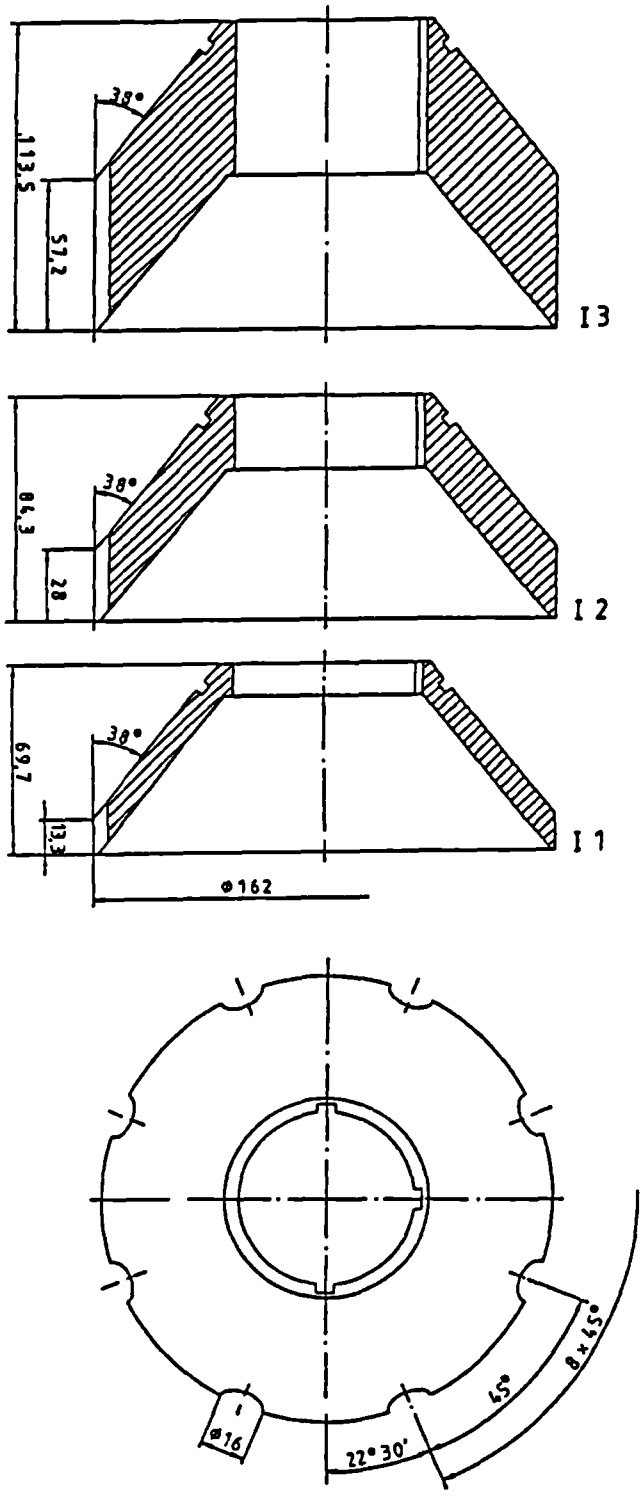

Figure 2.1: Schematic diagram of the three different sizes of blank aluminium inserts used to replace parts of the active discs inside a disc centrifuge.

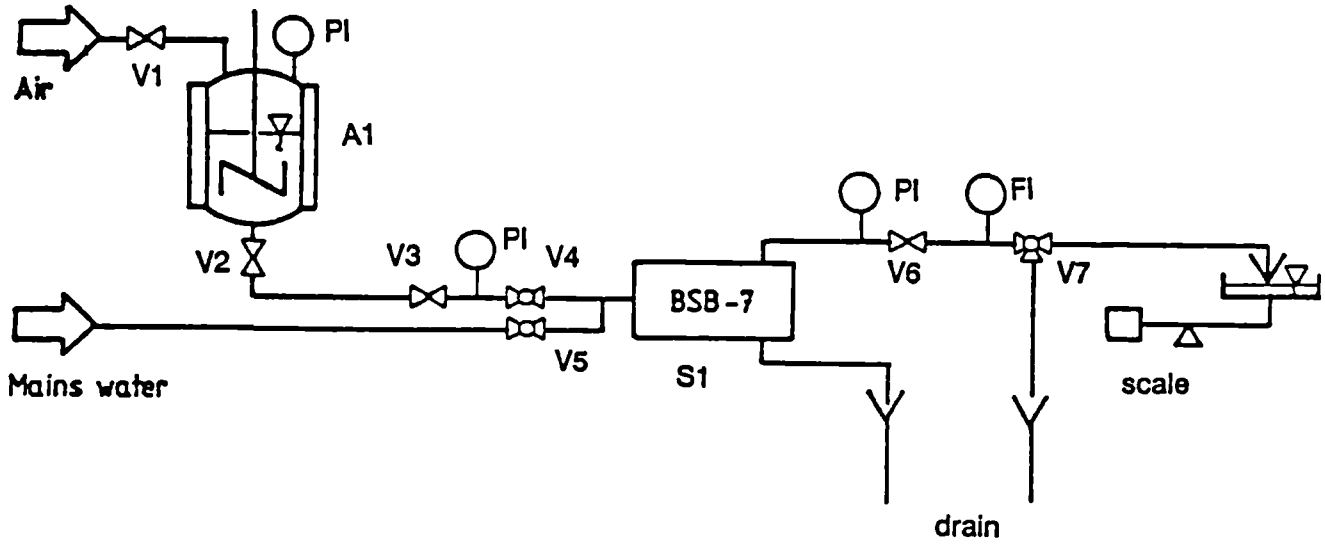

Figure 2.2: Schematic diagram of experimental setup.
A1: 1500 L feed vessel; S1: BSB 7-47-476 disc stack centrifuge (z=variable, Ri=0.036 m, Ra=0.076 m, h=0.5 mm, n=9300 min^{-1}, φ=38°); V1, V2, V3, V6: Saunders diaphragm valves; V4, V5: Ball valves; V7: 3-way ball valve; PI: pressure gauges; FI: magnetic-inductive flow meter.

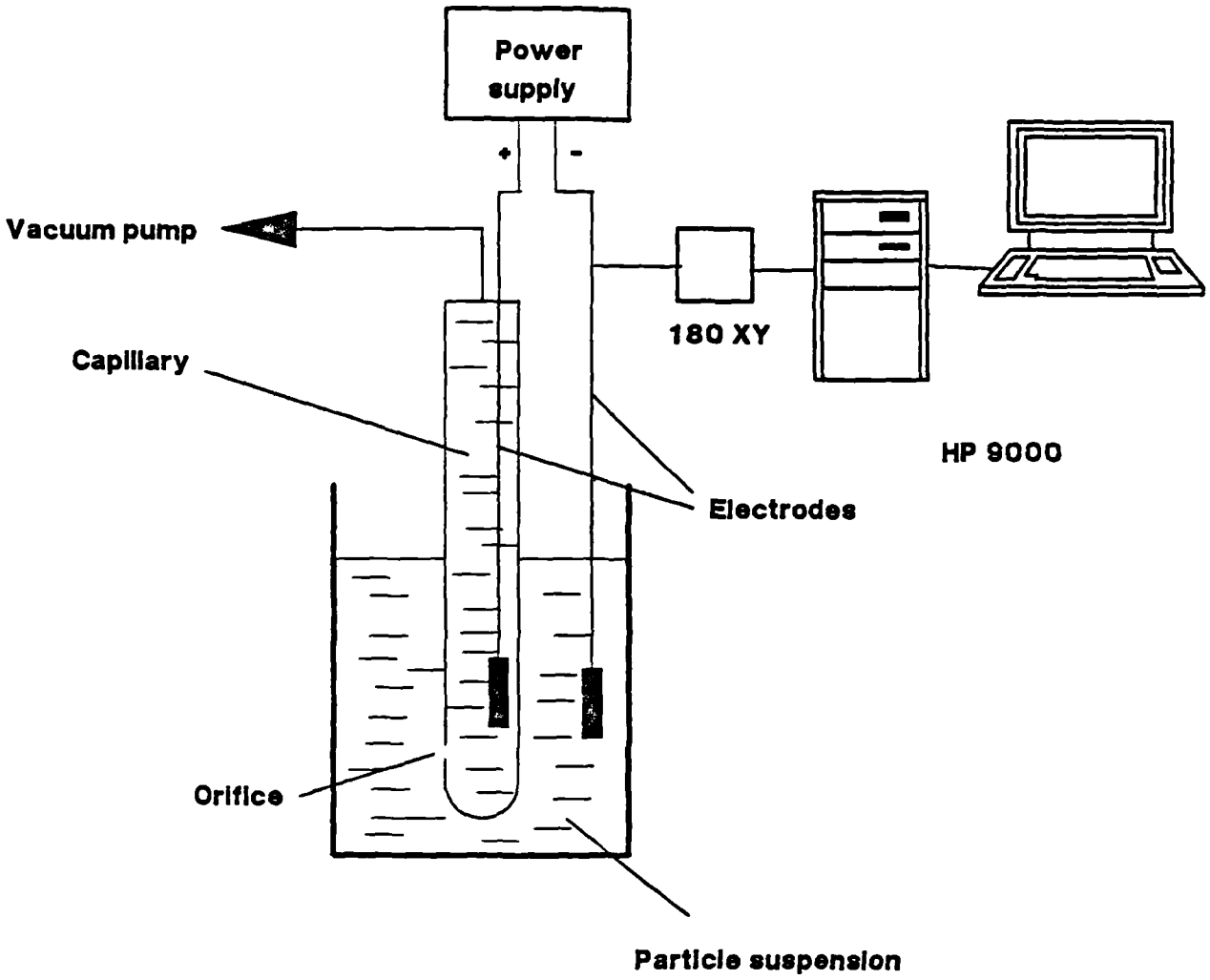

Figure 2.3: The electric zone sensing principle.

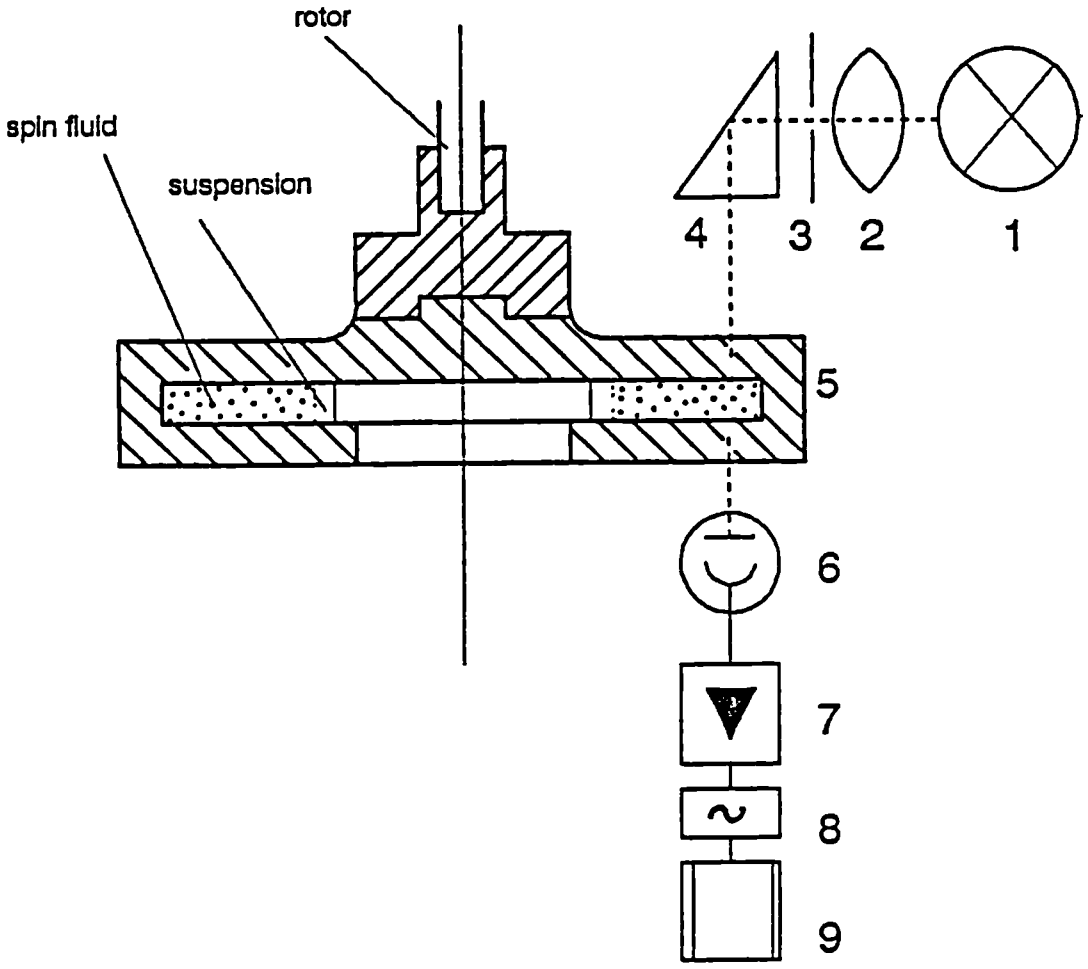

Figure 2.4 Schematic diagram of disc photosedimentometer assembly (Langer, 1979). (1) mercury vapour lamp, (2) optical lens, (3) diaphragm, (4) 90° turnabout prism, (5) disc rotor, (6) photo diode, (7) signal amplifier, (8) electronic filter circuit, (9) Yt-pen recorder.

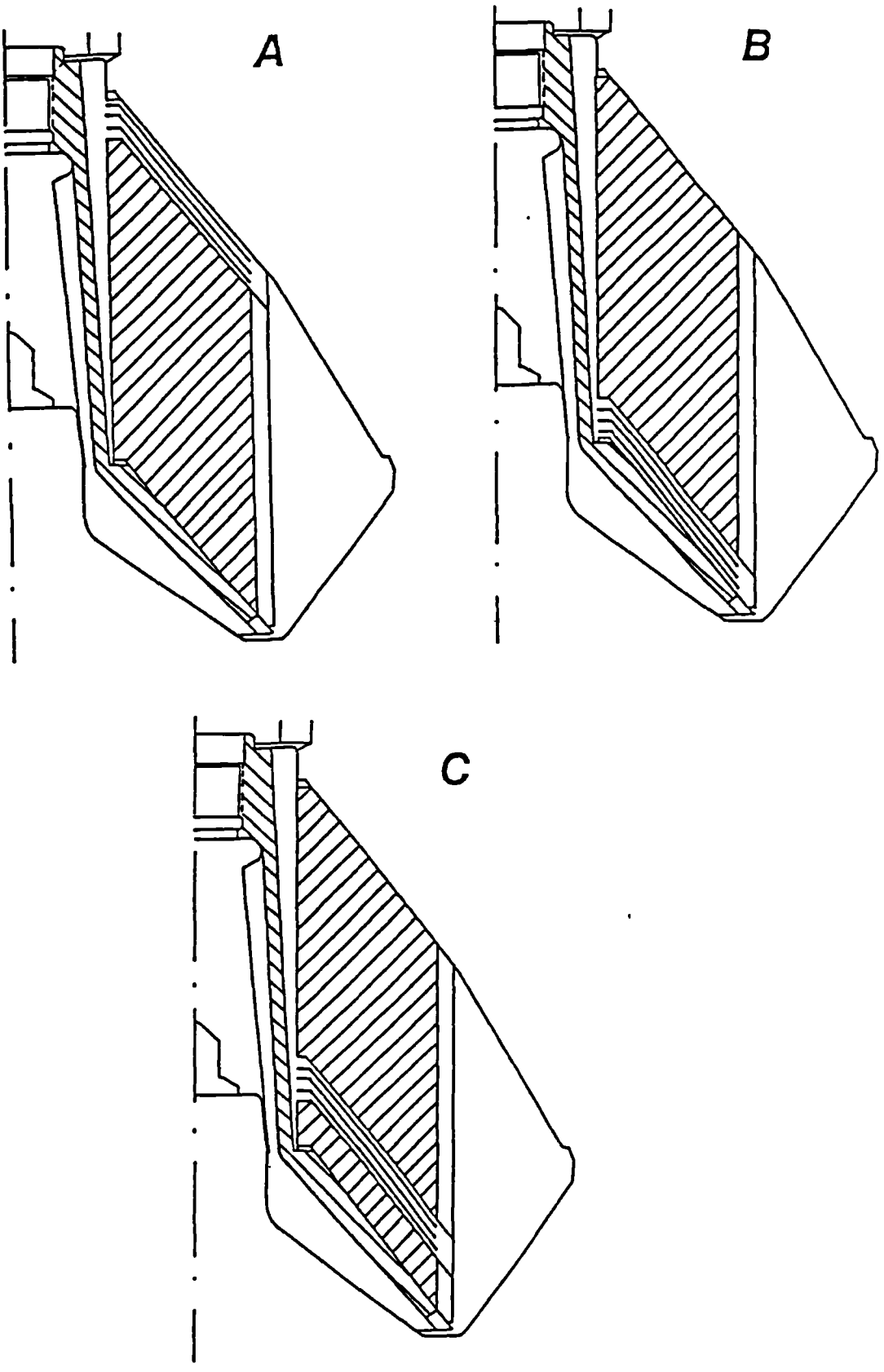

Figure 2.5: Diagram of disc stack separator showing the position of the active discs within the dummy disc stack. (A) top position; (B) bottom position; (C) top of small insert.

2.3 Results

2.3.1 Disc photosedimentometer studies

Figure 2.6 shows the extinction coefficient K_{ext} as a function of the particle diameter for polyvinylacetate particles at four wavelengths ranging from 400 to 700 nm. Calculation of the extinction coefficient is based on Equation 2.11 and a relative refractive index of m = 1.1. For small particles, the extinction coefficient rises rapidly with increasing particle diameter and then passes through a series of maxima and minima until subsequently approaching a value of K_{ext} = 2. For higher wavelength the maxima and minima are shifted to larger particle diameters.

Figure 2.7 shows the extinction coefficient as a function of the particle diameter and relative refractive index. The calculation is based on Equation 2.11 and a constant wavelength of 690 nm is assumed. The course of the extinction curve is similar to the previous plot. For small particles the extinction coefficient rises sharply with increasing particle size, then passes through a series of maxima and minima and finally converges to a value of K_{ext} = 2 for large particle sizes (> 10 µm). The effect of the relative refractive index is such that with increasing refractive index the maxima of the extinction coefficient curve are shifted to smaller particle diameters.

The specific turbidity of polyvinylacetate particles as a function of particle diameter is illustrated in Figure 2.8. Gregory (1984) has shown that the specific turbidity τ of a suspension is given by:

$$\frac{\tau}{c_v} = \frac{3}{2} \frac{K_{ext}}{d} \qquad 2.12$$

where c_v is the particle volume concentration and d is the particle diameter. Calculation of the extinction coefficient is based on Equation 2.11 and the relative refractive index for a polyvinylacetate/water suspension has a value of m = 1.1 which is obtained from dividing the refractive index of polyvinylacetate, given in Table 1.4 (= 1.4669 at 20 °C) by the refractive index of water (1.334). For small particle sizes the specific turbidity rises sharply with increasing particle size. After passing through a distinct maxima at about 2.5 µm it goes through a series of maxima and minima which are less pronounced than those in the extinction efficiency curves. For large particle diameters (> 10 µm) for

which the extinction coefficient is constant the specific turbidity falls to 1/d.

Figure 2.9 shows particle size distribution curves of polyvinylacetate particles suspended in water. The curves were obtained by using two different particle sizing methods, namely an electric sensing zone method and a centrifugal sedimentation method (Joyce-Loebl photosedimentometer). The diagram shows the cumulative volume oversize distribution curve. In contrast to a number distribution the particle volume is plotted as a function of particle diameter. All particles had a particle diameter larger than approximately 0.6 μm and no particles bigger than about 2.25 μm were detected in the examined samples. The curves obtained by using different size analysis techniques are all similar. For the electric zone sensing method a volume median diameter of 1.16 μm was measured while for the centrifugal sedimentation method a particle diameter of 1.10 μm was found.

Included in Figure 2.9 is a trace determined theoretically using the specific turbidity values shown in Figure 2.8 and the corresponding volume fractions determined by applying the electric zone sensing method. Equation 2.12 was applied to calculate the turbidity of the various size fractions and the normalised turbidity data were plotted. By using this method the calculated median particle diameter was approximately 1.21 μm. As indicated in Figure 2.6 the extinction coefficient is strongly dependent on the wavelength used for its calculation. To examine the effect of different wavelength on the turbidity distribution similar calculations as just described were performed. These calculations showed that the effect wavelength on the cumulative turbidity distribution of polyvinylacetate particles is negligible.

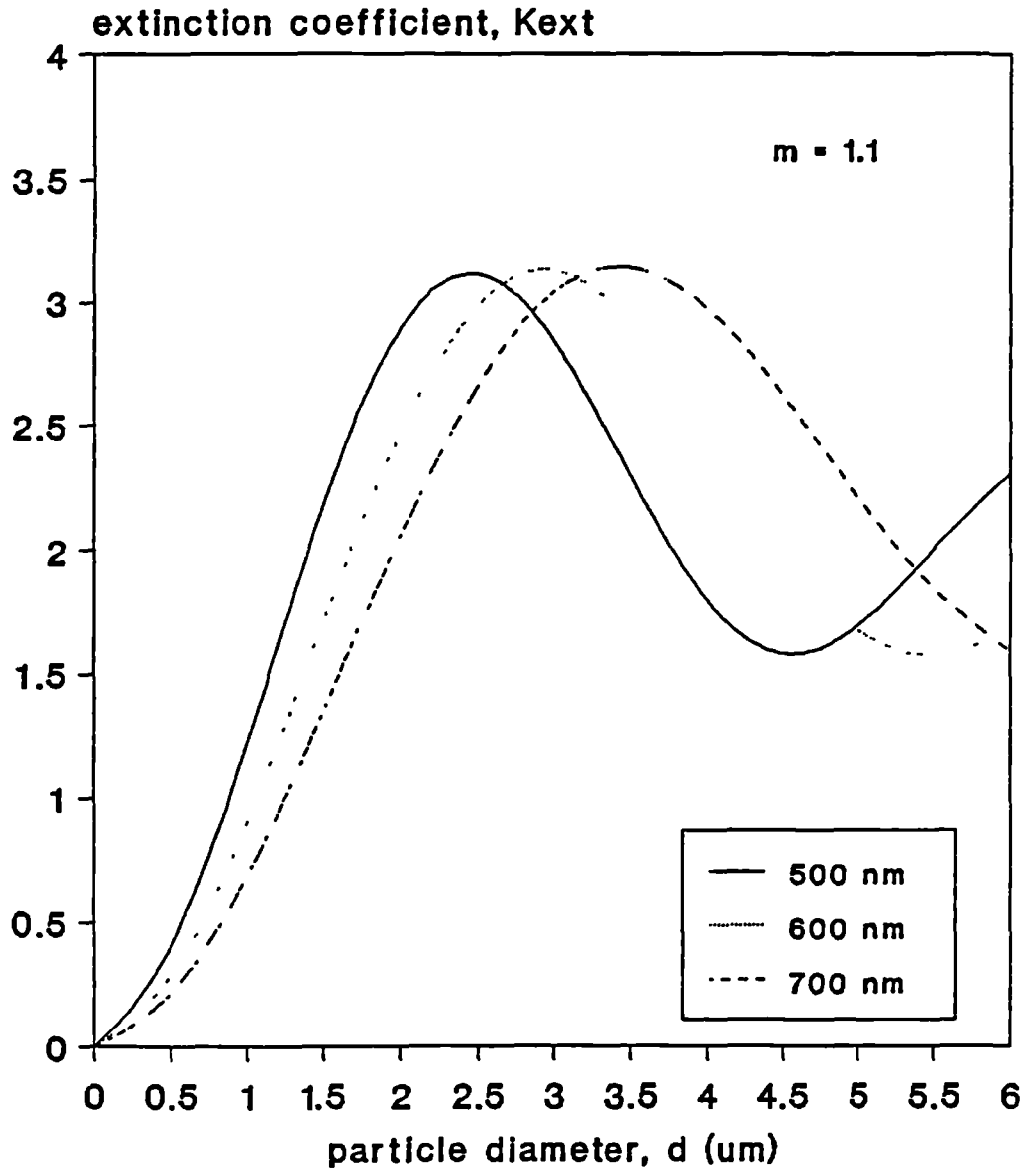

Figure 2.6: Change of extinction coefficient with particle diameter and wavelength at constant refractive index.

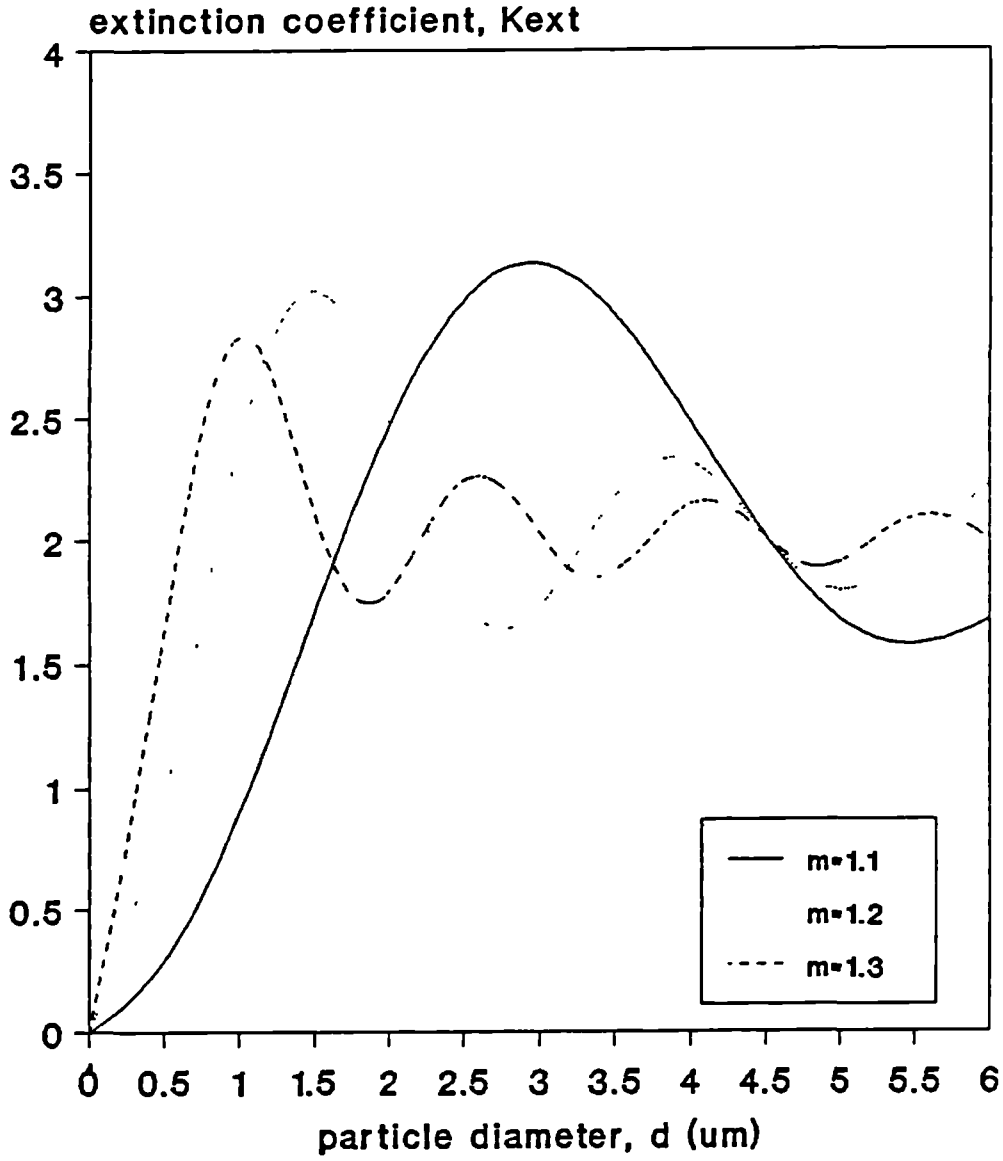

Figure 2.7: Change of extinction coefficient with particle diameter and relative refractive index at constant wavelength (λ=600 nm).

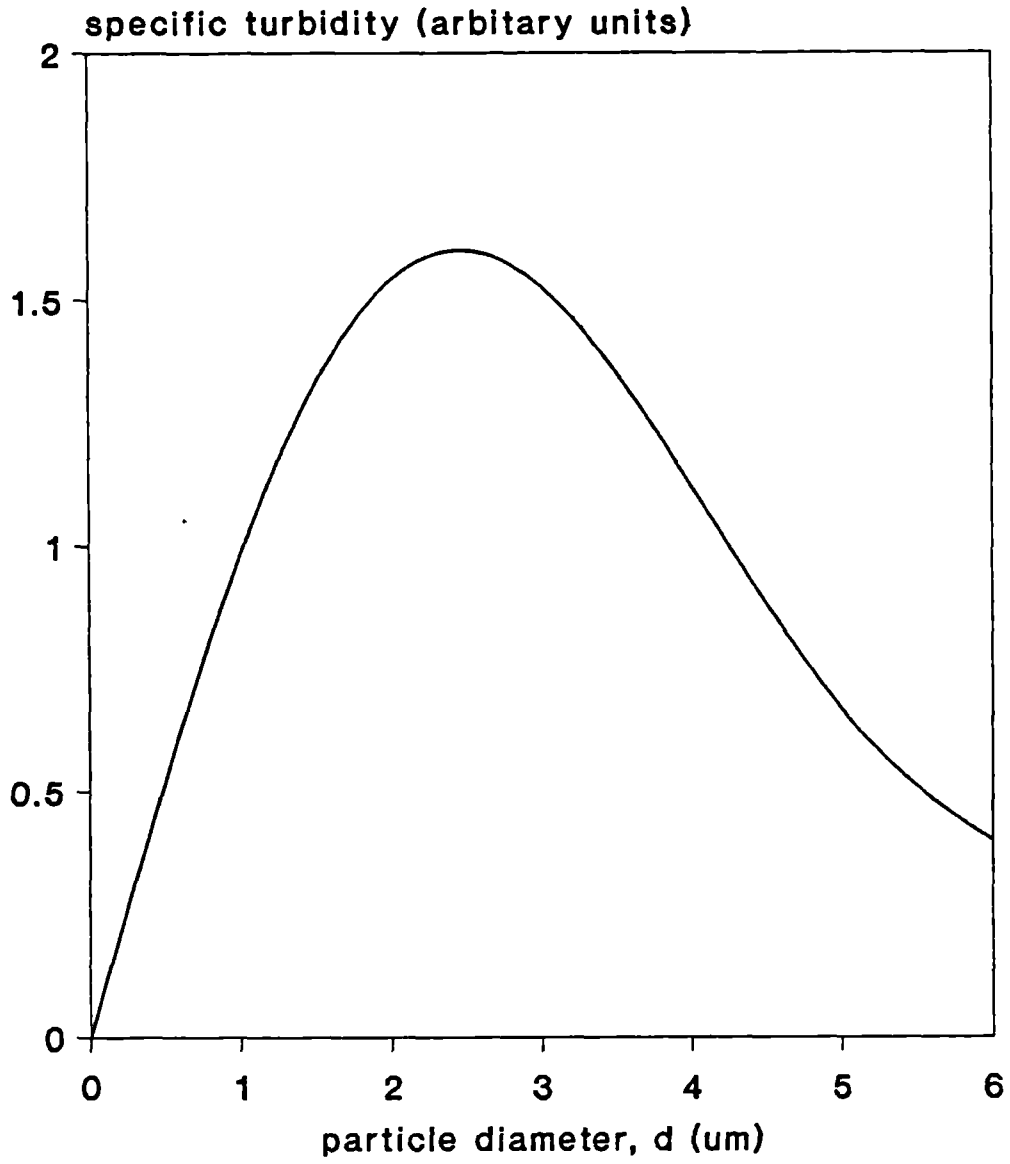

Figure 2.8: Change of the specific turbidity of a polyvinylacetate suspension with particle diameter.
Wavelength λ=690 nm, relative refractive index m=1.1

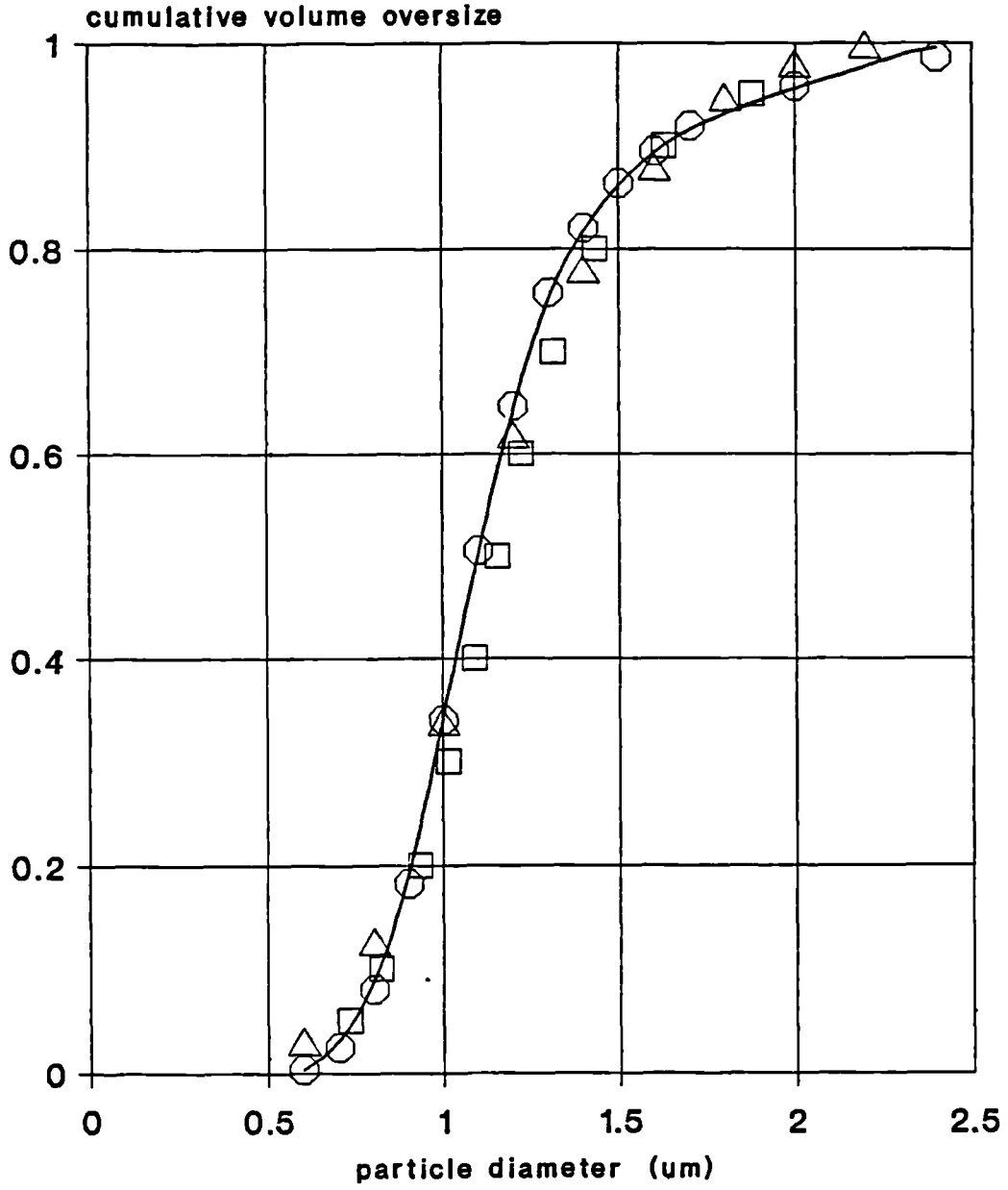

Figure 2.9: Cumulative volume oversize distribution of a polyvinylacetate suspension determined using different particle size analysing techniques.
(□) Electric zone sensing method (Elzone)
(○) Photo sedimentometer (Joyce Loebl)
(△) Calculated using Equation 2.12.

2.3.2 Tracer studies

Before examining the effects of settling area reduction on the separation performance of the centrifuge it was necessary to obtain information on the fluid flow pattern in the machine. Of particular interest was the tracer hold-up inside the separator and the time required for all the tracer to pass through the machine. The main results of these studies are summarized in Table 2.2. The effects of bowl rotation and active disc location on the hold-up volume and mean residence time is shown for a representative flowrate of 8.33 L min^{-1}. For other flowrates (300 and 400 L h^{-1}) the trends observed are very similar. Firstly, concentrating on the top and bottom arrangement (see Figure 2.5 A and B respectively) of the active discs two main trends may be detected. For a rotating bowl, a lower mean residence time with decreased dispersion is observed when the active discs are located at the bottom. When the bowl is not rotating larger mean residence times are noticed independent of active disc location, and equivalent to the longest residence time for a rotating bowl. These trends are attributed to the dispersion of fluid into the sediment holding space when the active discs are located at the top or when the bowl is not rotating.

The fluid volume required for nearly all the tracer material to be removed from the separator, V_{99}, is approximately 8.2 L independent of the active disc position. Hence steady state conditions may be assumed when more than 8 L of liquid have passed through the centrifuge which is equivalent to more than five volume changes. For particulate suspensions approximately 15 L flow is allowed before steady state is assumed.

From this observation, the conclusion is that if the bowl rotates at full speed and the discs are located at the bottom of the dummy disc stack then the fluid does not enter the solid holding space, whilst it is not prevented from doing so if the bowl is not rotating. The fluid in the sediment holding space is basically stagnant relative to the spinning bowl and the fluid exchange between liquid leaving the distributor and liquid occupying the sediment holding space is very poor. Removing the pressure from the sediment holding space by removing the centrifugal force field apparently opens the sediment holding space for the incoming liquid. Now the sediment holding space acts like a region of very stagnant fluid, or 'dead space'. Although most of the fluid passes through the centrifuge with

no delay, part of the fluid enters the deadwater region and is delayed causing an increase in the mean residence time.

Table 2.2: Summary of tracer study results

		Bottom		Top	
n	(rpm)	0	9200	0	9200
Q	(L/min)	8.33	8.33	8.33	8.33
t_m	(s)	21.0	16.8	22.2	22.8
V_h	(L)	2.92	2.33	3.08	3.17
V_{99}	(L)	8.2	8.2	6.8	8.2

t_m = mean residence time

V_h = holdup volume

V_{99}= throughput volume at which 99% of tracer material is removed from the centrifuge

top and bottom refers to position of active discs (see Figure 2.5 A, B)

2.3.3 Separation performance

2.3.3.1 General remarks on the preparation of the feed suspension

Before it is possible to use the polyvinylacetate suspension to measure the separation performance of the disc stack centrifuge (see section 2.1) it is necessary to destroy any agglomerates that may be present. This task was performed by ultrasonicating the diluted polyvinylacetate suspension for approximately 60 minutes. The application of ultrasonics in a liquid creates the phenomenon known as cavitation. Areas of compression and rarefaction occur and cavities, which form in the areas of rarefaction, rapidly collapse as the area changes to one of compression. The vapour bubbles produced in the cavities are thus compressed to several thousands of bars and on their collapse shock waves are generated which are thought to be responsible for the breakup of potential polyvinylacetate agglomerates (Scawen et al., 1986). Monitoring the dynamics of deagglomeration during the ultrasonication process showed a steady

reduction of the median particle size of the suspension from 3.5 μm to roughly 1.3 to 1.7 μm after 40 minutes. The final particle size was found to be dependent on the age of the polyvinylacetate concentrate. Freshly delivered polyvinylacetate concentrate gave smaller particle sizes after ultrasonic conditioning than somewhat older concentrate after it has been stored in the fridge at 4 °C for three months. Although the final particle size achievable by ultrasonic conditioning was already reached after about 40 minutes, it was considered good practice to leave the suspension for a further 20 minutes before using it.

The other question to be considered is whether the particle size of the polyvinylacetate suspension changes while it is being stirred in the feed vessel. Measuring various samples over a time period of 4 hours showed no indication of this happening. Generally, it appeared that the distribution was stable in respect to its size distribution provided it was constantly stirred. However, leaving the suspension over a long period, say more than 24 hours, resulted in a significant increase of the median particle size. Hence, it was essential to prepare a fresh batch of polyvinylacetate suspension prior to every experiment.

The particle sizes obtained by ultrasonic conditioning are by no means the final particle sizes. In order to reach the stage of only primary particles being left in the suspension, more drastic methods such as high pressure homogenisation are required. Nevertheless, a range of high shear experiments (such as capillary shear devices, centrifugal and gear pumps operated at high backpressure) using ultrasonically conditioned polyvinylacetate particles showed no significant change of the particle size distribution.

2.3.3.2 Effects of scale-down on the separation performance

The separation performance of a disc centrifuge has been examined for three operating parameters:

(i) fractional reduced settling area
(ii) active disc location
(iii) throughput capacity

In order to compare the results obtained at various operating conditions it is convenient to plot the grade efficiency curve as a function of the dimensionless diameter d/d_c. The value of the critical particle size d_c is determined using Equation 1.17. Any changes in the grade efficiency profile may be attributed directly to a change in the hydrodynamic behaviour of the fluid passing through the separator. Theoretically, if there are no effects of throughput capacity, separation area reduction or disc location on the separation performance then no change in the profile of the efficiency curve should occur.

The effects of a 75% reduction in the available separation area on the grade efficiency curve is illustrated in Figure 2.10. The number of discs in the stack were reduced from 72 to 17 discs and the discs were located on top of the blank inserts (Figure 2.5 A). The change in the profile of the grade efficiency curve due to changing the disc position is plotted using data for three flowrates in the range of 300 to 700 L h^{-1}.

The diagram shows the expected deviation from the theoretical grade efficiency curve calculated on the basis of Stokes Law (Equation 1.19). The observed grade efficiency curve reaches a value of 0.74 at the separation limit (d/d_c = 1), and approaches unity at approximately twice the separation limit. There is no observed trend of change in separation efficiency with change in flow rate. It was not possible to obtain grade efficiency values below a dimensionless particle size of approximately 0.6. However, it appears that there is an approach to the theoretical grade efficiency curve for lower dimensionless particle diameters.

For the same number of active discs placed at the bottom of the disc stack (Figure 2.5 B) the grade efficiency is clearly shifted to larger dimensionless particles diameters (Figure 2.11) indicating a reduction in the separation performance although again the separation curve is apparently independent of flow rate. The grade efficiency curve does not approach the theoretical curve.

The effect of a 90% reduction of separation area on the grade efficiency curve is shown in Figure 2.12. The overall trend of the grade efficiency curve is similar to the trend observed for a 75 % reduction of separation area. For active discs located at the top of the disc stack (Figure 2.5 A) the curve follows closely the theoretical grade efficiency curve for small dimensionless particle diameters and deviates from the theoretical curve

for larger particle sizes. Also a slight effect of flow rate on the grade efficiency is observed. At the separation limit the grade efficiency has a value of 0.70 which is a little below the value of 0.74 observed for 17 discs.

Figure 2.13 shows the grade efficiency curve of 7 discs located at the bottom of the disc stack. The trends already observed are amplified and show an increased reduction of efficiency if the disc location is switched from the top to the bottom position. At the separation limit the grade efficiency decreases with increasing flow rate from an average of 0.70 to a value as low as 0.4.

Since the aim was to avoid separation of solids in the sediment holding space but at the same time to ensure $T(d) \neq f(Q)$ the active discs were placed on top of the small blank insert (I1) located at the bottom of the disc stack (Figure 2.5 C). The effect of this measure on the grade efficiency is illustrated in Figure 2.14. As expected the grade efficiency was better than for disc position B (bottom arrangement) but worse than for position A (top arrangement) due to the decreased separation area available. At the separation limit a value of 0.6 is obtained which is lower than for the top position (0.74) but much higher than for the bottom position (0.40). The effect of flow rate may still be observed although the variation is considerably reduced when compared with the bottom disc arrangement. Scattering of the data points is less pronounced.

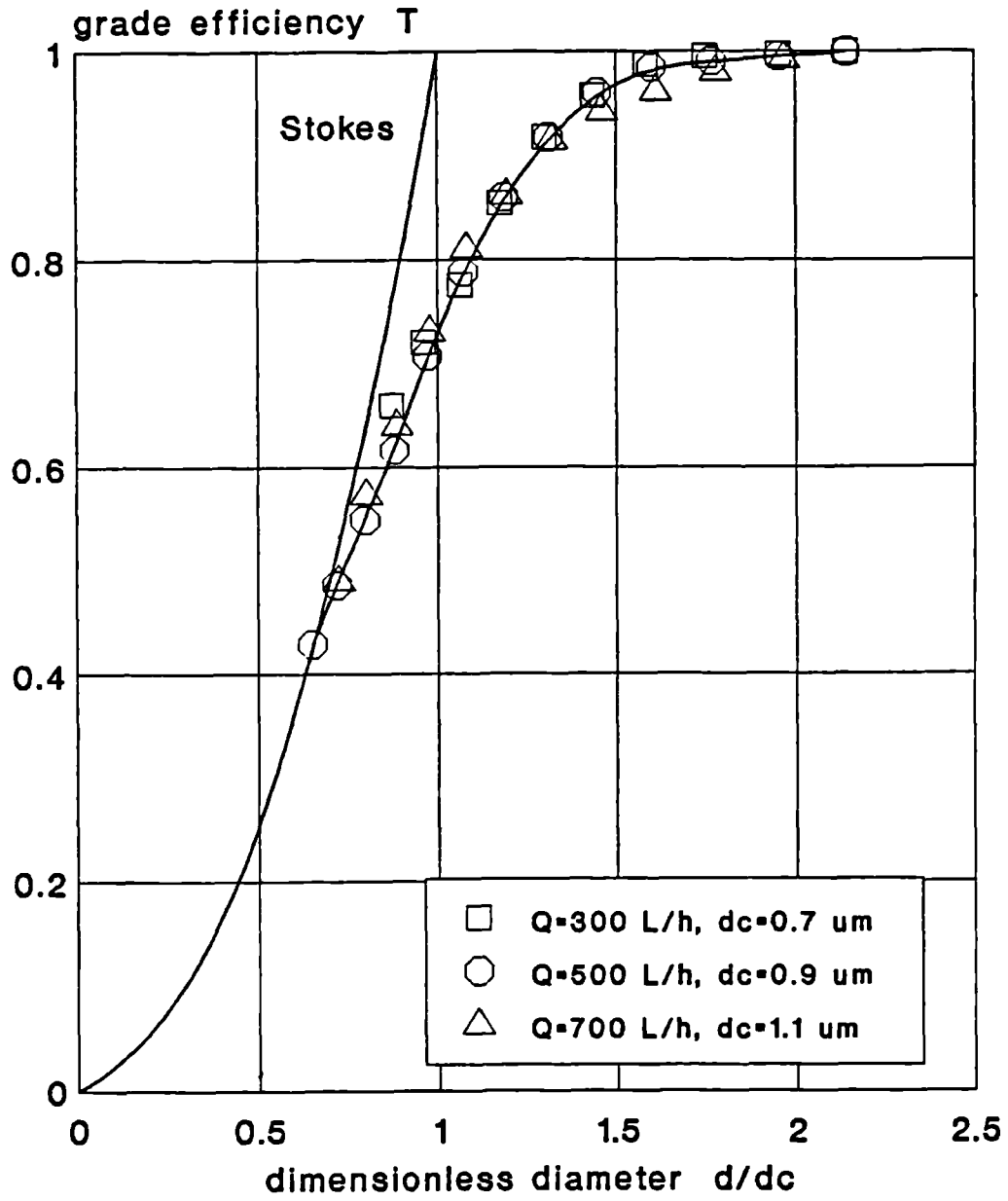

Figure 2.10: Grade efficiency curve of disc stack separator - the effect of disc location on separation performance. The number of discs is 17; top position (A) of discs (see Figure 2.5).

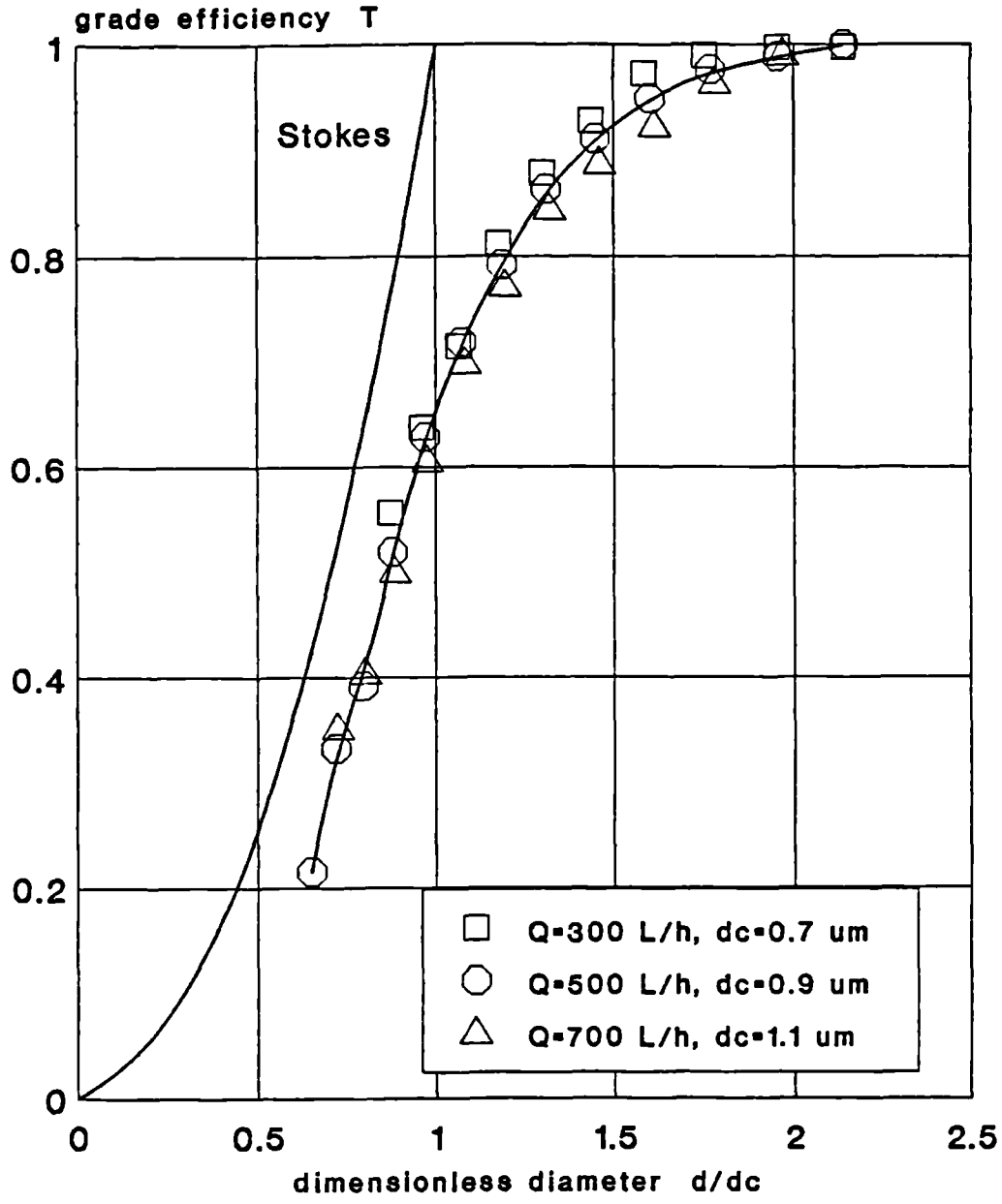

Figure 2.11: Grade efficiency curve of disc stack separator - the effect of disc location on separation performance. The number of discs is 17; bottom position (B) of discs (see Figure 2.5).

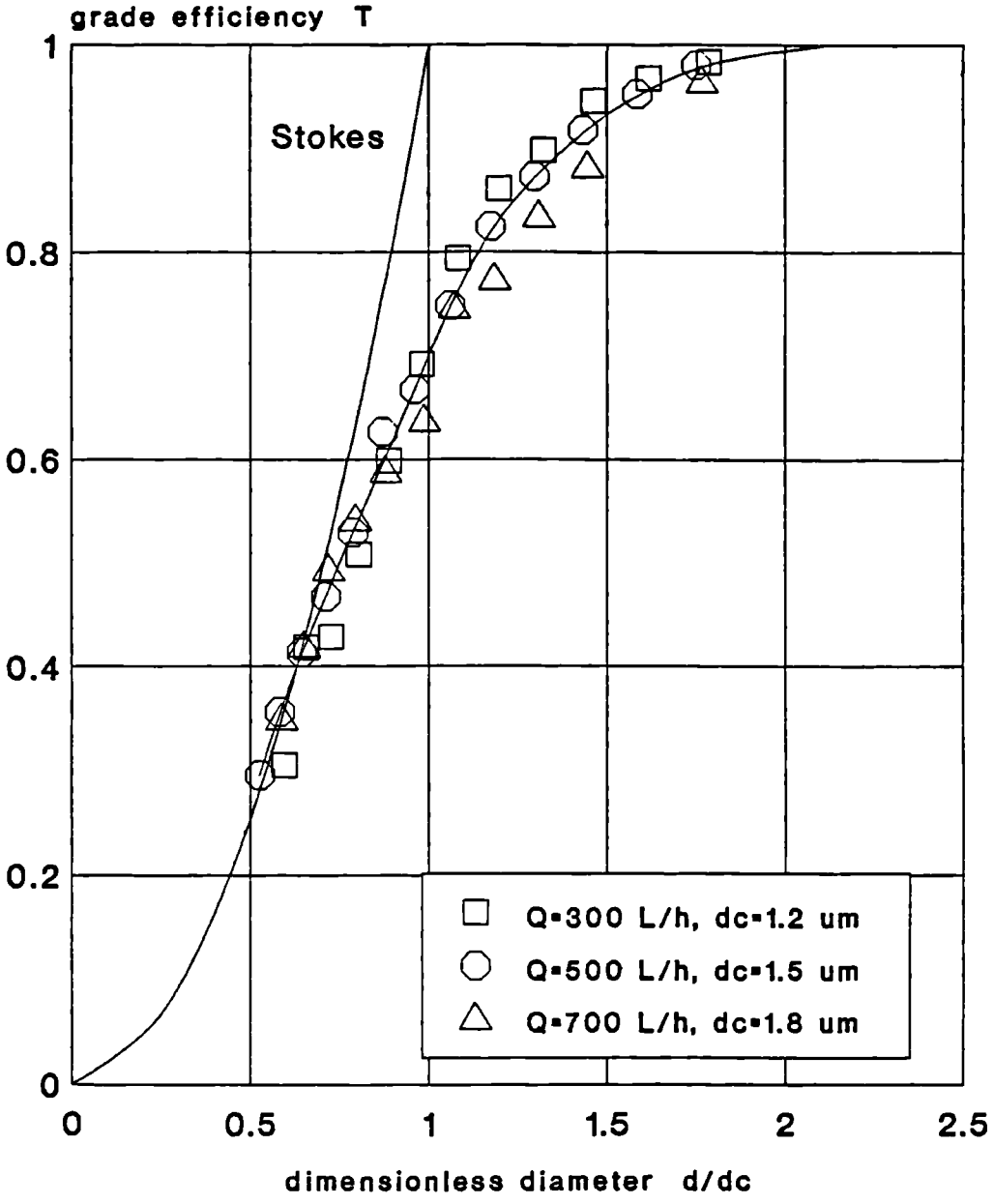

Figure 2.12: Grade efficiency curve of disc stack separator - the effect of disc location on separation performance. The number of discs is 7; top position (A) of discs (Figure 2.5).

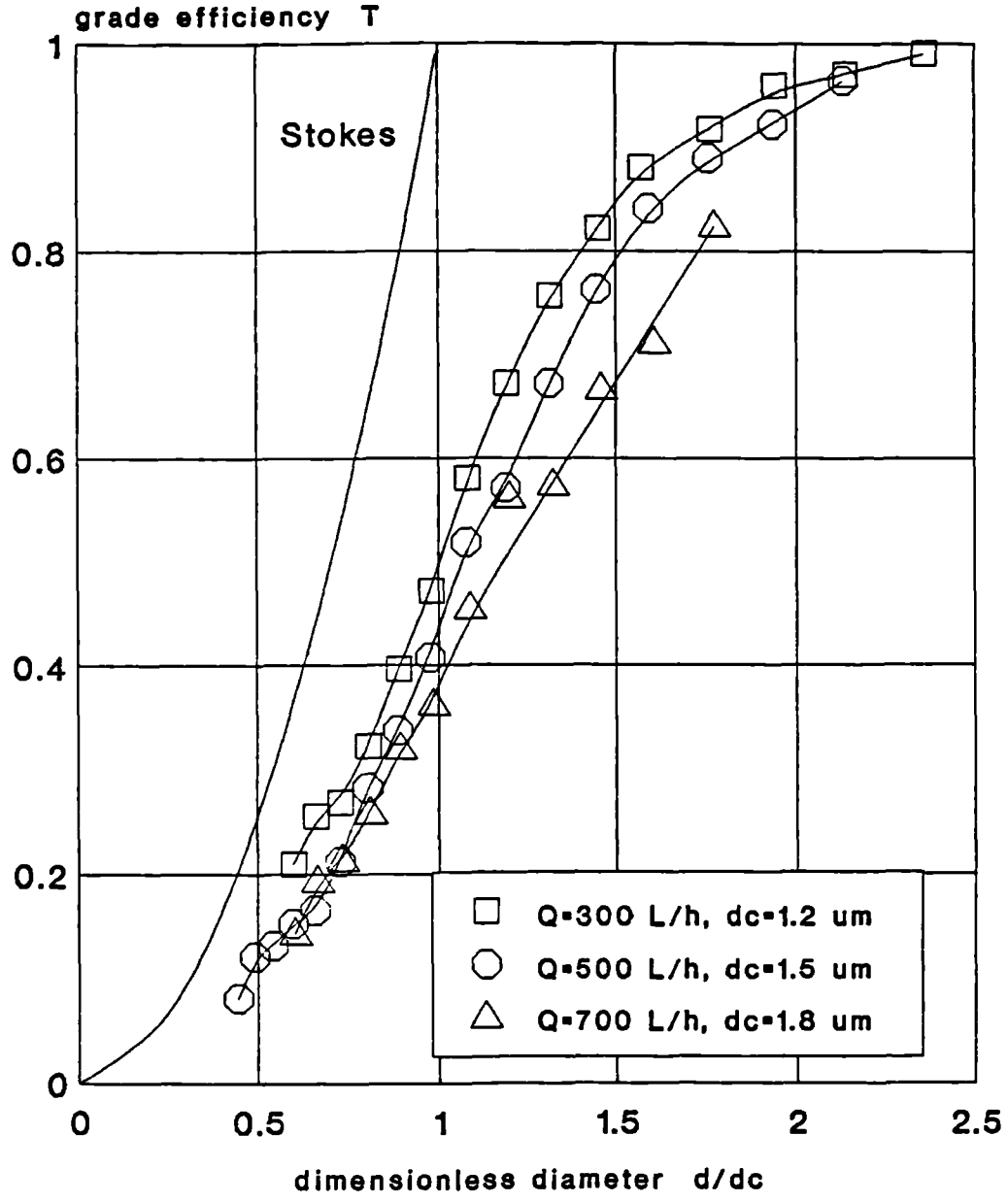

Figure 2.13: Grade efficiency curve of disc stack separator - the effect of disc location on separation performance. The number of discs is 7; bottom position (B) of discs (see Figure 2.5).

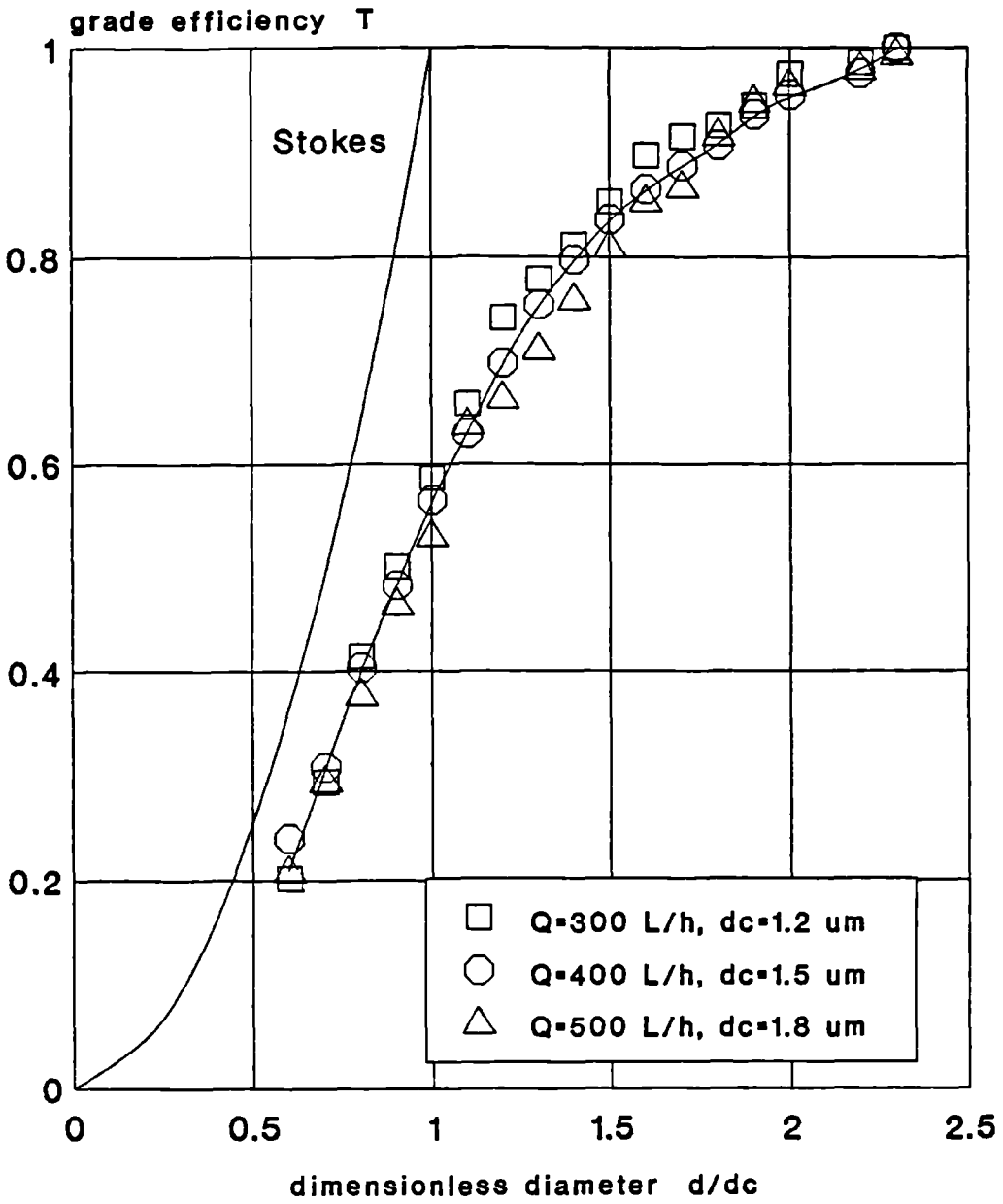

Figure 2.14: Grade efficiency curve of disc stack separator - the effect of disc location on separation performance. The number of discs is 7; top of insert I1 (see Figure 2.5 C).

2.3.4 Mathematical formulation of the grade efficiency curve

The separation performance of a centrifugal separator depends on the combination of three product parameter such as particle size, particle density and particle shape. Since the mass yield E_T, defined in Equation 2.13, depends very much on the settling characteristics of the feed solids, it is unsuitable as a general criterion for the efficiency of a separator. A single value of the mass yield cannot be used to describe the separation capability of the separation equipment for any materials other than the actual test material. The mass yield of a centrifuge is given by:

$$E_T = 1 - \frac{\dot{m}_1}{\dot{m}_o} \qquad 2.13$$

where $\dot{m}_1$ is the mass flow rate of solids in the clarified liquid discharge and $\dot{m}_o$ is the mass of solids in the feed suspension.

For a self-cleaning disc stack centrifuge the relationship between the mass flow rate, $\dot{m}$, and the solids concentration in the feed phase, $c_{m,o}$, and in the clarified liquid phase, $c_{m,1}$, is given by:

$$\dot{m}_o = \dot{m}\, c_{m,o}$$

and

$$\dot{m}_1 = \dot{m}\, c_{m,1}$$

The above relationship assumes that the mass flow rate of the fluid leaving the separator is approximately equal to the mass flow rate entering the machine. The amount of fluid lost through the solids discharge is considered to be negligible. Therefore, Equation 2.13 may be simplified to:

$$E_T = 1 - \frac{c_{m,1}}{c_{m,o}} \qquad 2.14$$

However, this simplification can not be applied for nozzle type disc stack separators because the flow of the sedimented solids through the discharge takes place continuously and is not negligible.

In order to describe the separation performance quantitatively and independently of the solids properties, the grade efficiency, T(x), is

introduced:

$$T(x) = \frac{\dot{m}_2(x)}{\dot{m}_o(x)} \qquad 2.15$$

where $\dot{m}_2(x)$ is the mass flow rate of solids of separation property x in the solids discharge (coarse fraction), $\dot{m}_o(x)$ is the mass flow rate of solids of separation property x in the feed (feed fraction). The variable x describes the separation property according to which separation takes place. In a centrifugal separator x is represented by the settling velocity of the particles. Since the particle density and the fluid viscosity are usually assumed constant for a given separation process the grade efficiency may be rewritten using:

$$T(d) = \frac{\dot{m}_2(d)}{\dot{m}_o(d)} \qquad 2.16$$

Since $\dot{m}_o(d) = \dot{m}_2(d) + \dot{m}_1(d)$, where $\dot{m}_1(d)$ is the mass flow rate of solids of size d in the supernatant fraction, Equation 2.16 may be expressed in terms of the size distribution in the clarified liquid phase:

$$T(d) = 1 - (1 - E_T)\frac{\Delta F_1(d)}{\Delta F_o(d)} \qquad 2.17$$

where $\Delta F_1(d)$ is the particle size distribution in the clarified liquid discharge and $\Delta F_o(d)$ is the particle size distribution in the feed to the centrifuge expressed in terms of the percent-in-range distribution respectively which means that the sum over all size fractions making up the particle size distribution is 100%.

At this point a few remarks on the representation of particle size distributions need to be made. Particles size distributions can be represented as number distributions if the type of quantity used is a number, as weight distributions if the type of quantity is a mass, or as area distributions if the type of quantity is a surface area. For a constant particle density, weight distributions and volume distributions are equal. Since number and volume distributions of the same particle suspension may differ considerably, the type of quantity measured or chosen when representing particle size distribution data has to be stated. Throughout this thesis the type of quantity measured or chosen for

representing particle size data is the particle volume if not stated otherwise.

Particle size distributions may be expressed as the so-called density distribution f(d), which represents the first derivative of the cumulative distribution, F(d), given by:

$$f(d) = \frac{dF(d)}{dd} \qquad 2.18$$

During particle size analysis the volume of particles within a finite size range is usually measured and plotted in form of a distribution histogram. The difference of two values of the cumulative distribution F(d) between two particle diameters d_1 and $d_2=d_1+\Delta d$ is given by:

$$dF(d_1,d_2) \approx \Delta F(d_1,d_2) = F(d_1) - F(d_2) \qquad 2.19$$

representing the so-called 'percent-in-range' distribution. Since $\Delta F(d)$ is obtained directly from particle size analysis it may be used in combination with Equation 2.17 to give the grade efficiency curve. The grade efficiency is obtained in the form of discrete grade efficiency values based on the arithmetic mean particle size $((d_1+d_2)/2)$ of the chosen size interval. Plotting the grade efficiency as a function of particle size and joining of the data points gives the grade efficiency curve.

The value of the grade efficiency is a probability rather than a certainty because different particles of similar size are subjected to different conditions when passing through the separator. A single particle of size d passing through the separator will either be separated or it will pass through with the fluid. The grade efficiency will, therefore, be either 0% or 100%. If two particles of the same size enter the separator, the grade efficiency may either be 0%, 50% or 100% depending upon whether the separator will separate neither, one or both particles. If a large amount of similar particles enter the separator then a certain probable amount of particles will be separated. The reasons for the probability character of the grade efficiency are:

(i) The finite dimensions of the input and output of the separator
(ii) The uneven conditions of separation at different points
(iii) The different surface properties of particles of the same size.

At this point the question arises about how the width of the size interval is to be selected. Theoretically, the smaller the chosen size intervals the more exact the grade efficiency curve. However, in practice the amount of scattering of the measured quantity within a given size interval Δd needs to be considered. These fluctuations depend on the total mass of solids analysed and the smaller the number of particles the larger the size range to be selected, hence the lower the resolution. The relative error increases with decreasing quantity of measured material in a given size range. In practice it is often necessary to combine several adjacent, narrow size bands into larger size intervals in order to obtain meaningful grade efficiency curves.

The Elzone particle sizer gives both the density volume (or number) and the cumulative volume (or number) distribution as a function of particle size logarithmically divided into 128 size channels. Owing to the reasons described earlier, these 128 size channels were subsequently reduced to 26 larger size intervals before the grade efficiency of each size interval was evaluated. Not only does this procedure reduce the relative error within small size intervals but also results in a certain degree of smoothing of the data points. Furthermore and without any loss of accuracy, 26 larger size intervals can be handled and be visualized more easily than 128 size channels.

The evaluation of the grade efficiency curve may be carried out graphically, in a table or by using a computer. Tabular and graphical procedures are cumbersome and time consuming and therefore a computer has been used to perform this task instead.

One exception to the rule of representing grade efficiency curves has to be stressed. Usually the independent variable is plotted on the abscissa describing the physical property chosen to characterise the size of the particles. The dependent variable, which describes the grade efficiency, is plotted on the ordinate. This would mean that for every separation process, using the same type of equipment, a new grade efficiency curve needs to be plotted if the settling velocity of the particles or if the operating conditions of the separator changes. Therefore, in order to make the grade efficiency curve invariant to solids properties, operating conditions and separator specifications the grade efficiency is plotted as a function of a dimensionless particle size (d/d_c), where d_c represents the critical particle size or the theoretical separation limit. The significance and

derivation of the theoretical separation limit for disc stack separators has been described in detail in chapter 1.3 of this thesis. Changes in the trend of this so-called dimensionless grade efficiency curve occur only if the flow pattern in the separator changes.

Once the grade efficiency curve has been determined in its graphical or tabular form it is often necessary for its further application that the grade efficiency curve is expressed in the form of a mathematical equation. Since the grade efficiency curve can be regarded as a key parameter of a separator, the curve in its mathematical form can be used as an essential part of an algorithm allowing computer simulated studies of the solids recovery process in a centrifuge for a wide range of operating conditions and solids properties.

As far as mathematical modelling of centrifugal separation is concerned, this is comparatively simple. The two main objectives are the evaluation of the separation efficiency of the separator and the associated particle size distribution of the particle suspension leaving the machine after separation. Knowing the particle size distribution and the quantity of material in the clarified liquid discharge is important for the design and operation of subsequent downstream processing stages. Some numerical examples on the mathematical modelling of centrifugal separation will be given in chapter 2.3.5 after the mathematical routines of grade efficiency curve fitting have been introduced.

The mass yield, which may be calculated from the grade efficiency curve, $T(d)$, and the size distribution in the feed, $\Delta F_o(d)$, is given by:

$$E_T = 1 - \sum_{d_{min}}^{d_{max}} [1-T(d)]\ \Delta F_o(d) \qquad 2.20$$

where d_{min} and d_{max} are the minimum and maximum particle size present in the feed suspension. The particle size distribution in the clarified liquid discharge is given by:

$$\Delta F_1(d) = \frac{1 - T(d)}{1 - E_T}\ \Delta F_o(d) \qquad 2.21$$

while the particle size distribution in the solids discharge phase, $\Delta F_2(d)$, is given by:

$$\Delta F_2(d) = \frac{T(d)}{E_T} \Delta F_o(d) \qquad 2.22$$

Since the mass yield is required for both the prediction of the particle size distribution in the clarified liquid overflow and the particle size distribution in the solids discharge phase, it always needs to be evaluated first using Equation 2.20.

For reasons described previously the grade efficiency curves need to be transformed into a mathematical expression describing the curve accurately with only few parameters. It is known that particle size distributions can be conveniently approximated by empirically determined distribution functions. Special graph paper has been developed where cumulative distributions following these functions follow straight lines. Owing to the similarity of form and shape of a cumulative distribution and the grade efficiency curve it is probable that the same curve fitting routines for particle size distributions should also apply to grade efficiency curves. For completeness three of the best known analytical distribution function shall be summarized briefly (see also Leschonski, 1984).

a) The power function

The power function, also known as the Gaudin-Schumann distribution:

$$F(d) = (d/d')^n \qquad 2.23$$

The spread parameter, n, is the slope of the straight line obtained by plotting the above function on a log F(d) - log d paper. The position parameter, d, is determined from the intercept of the straight line with the ordinate log F(d).

b) RRSB function

The Rosin-Rammler-Sperling-Bennet (RRSB) function is given by:

$$1 - F(d) = \exp(-(d/d')^n) \qquad 2.24$$

where d' represents the position parameter and n represents the slope of the straight line obtained when plotting lnln(1/R), where R = 1-F(d), on the ordinate and ln d on the abscissa.

c) Normal distribution

The third analytical function is the normal distribution given here in its general form:

$$f(z) = \frac{1}{\sqrt{\pi}} \exp(-z^2) \qquad 2.25$$

with z being a dimensionless variable describing the particle size. The standard deviation σ will be defined later in this section.

The cumulative distribution is obtained from:

$$F(z) = \int_{-\infty}^{z} f(z)\, dz \qquad 2.26$$

Normal distributions differ according to the definition of the variable z. The **Gaussian normal distribution** with linear abscissa:

$$z = (d - d_m)/(\sqrt{2}\ \sigma)$$

where d_m represents the median of the cumulative size distribution F(d) and σ represents the standard deviation or the spread of the distribution. For narrow distributions σ is small and for wide distributions σ is large and is obtained on probability graph paper when plotting F(d) on the ordinate and d on the abscissa. For Gaussian normal distributions with linear abscissa σ is given by:

$$\sigma = 0.5\ (d_{84} - d_{16}) = d_m - d_{16}$$

The **log-normal distribution:**

$$z = \ln(d/d_m)/(\sqrt{2}\ \sigma)$$

The standard deviation σ can be obtained when plotting the cumulative distribution data on log-probability paper. For log-normal distributions, σ can be calculated using:

$$\sigma = 0.5\ \ln(d_{84}/d_{16}) = \ln(d_m/d_{16})$$

The corresponding particle sizes can be acquired from a log-probability plot as described previously.

A slightly different form of the log-normal distribution is given by Herdan (1960) where the standard deviation σ is replaced by the geometric standard deviation σ_g given by:

$$\sigma = \ln\sigma_g$$

and therefore,

$$z = \ln(d/d_m)/(\sqrt{2}\ \ln\sigma_g)$$

By substituting the particle diameter d by the dimensionless diameter (d/d_c) the same curve fitting procedures applied for particle size distributions may be used for fitting an analytical function to grade efficiency curves. In the remainder of this chapter, results will be presented obtained by using a two-parameter model based on the RRSB-function and a Three-parameter model based on a modified log-normal distribution function.

2.3.4.1 Two-parameter model of grade efficiency curve

In order to approximate the grade efficiency curve by an expression defined only by two independent parameters the RRSB-distribution function is rewritten in a slightly modified form:

$$T(d) = 1 - \exp[-(k\ d/d_c)^n] \qquad 2.27$$

where k and n are the parameters describing the grade efficiency curve, d is the particle size and d_c is the critical particle size. Using Equation 2.27 and taking the logarithm twice an expression describing a straight line can be obtained.

$$\ln[-\ln(1-T(d))] = n\ \ln(k) + n\ \ln(d/d_c)$$

The first parameter n is obtained from the slope of the straight line, while the second parameter k is calculated using the intercept of the line with the ordinate:

$$k = \exp(\text{intercept}/n)$$

Figure 2.15 shows the change of grade efficiency, plotted as a function of dimensionless particle size, for four values of n. The value of k remained constant (k = 0.8) for this calculation. The values chosen for n ranged from 1.5 to 3.0. The curve describes a so-called sigmoidal course, starting

off at zero and converging to unity for large particle diameters which agrees with practical experiences. The smaller the particles the lower the grade efficiency while the larger the particles the higher the achievable recovery of the latter. With increasing values of n the curve becomes steeper and the convergence improves. As it is common for exponential functions all curves have a common point of intersection. Since this condition is only fulfilled if $(k \cdot d/d_c) = 1$ the coordinates of the point of intersection are a function of k. The corresponding value on the abscissa is given by k^{-1}. The corresponding ordinate value is independent of the coefficients k and n and may be calculated using Equation 2.27. In conclusion, a band of curves based upon the exponential equation (Equation 2.27) will have a common point of intersection given by the coordinates:

$$(d/d_c \; ; \; T)_s = (k^{-1} \; ; \; 0.632)$$

where $(d/d_c \; ; \; T)_s$ describes the coordinate of the common point of intersection. Owing to its good convergence to unity the practical error involved using the introduced two-parameter approximation of the grade efficiency curve is negligible.

Figure 2.16 shows the predicted course of a correlated grade efficiency curve for different values of k. The value of n remained constant (n = 2.0) during calculation. For small particles the curve increases rapidly with increasing particle size and approaches unity more rapidly for larger values of k. The graph shows a strong dependence of the grade efficiency approximation on k enhancing the requirement for special care and high accuracy during its evaluation.

The evaluation of the coefficients k and n from experimental data was performed by linear regression on a standard personal computer. In order to reduce the risk of error grade efficiencies $T(d/d_c) \geq 0.98$ were not included in the regression process. The reason for doing so becomes clear by looking at the axis division on RRSB graph paper. The effect of change of d/d_c on the grade efficiency is most effective between $0.05 < T > 0.98$. In this range a small change of d/dc results in a considerable change of the grade efficiency. However, at $T(d/d_c) \geq 0.98$ a considerable increase of the abscissa value gives only a small rise of the grade efficiency and consequently does not contribute a great deal to the overall error of the curve approximation. Therefore, the linear regression procedure should

concentrate on those data points contributing mostly to the overall error of the curve fitting process. For $T(d/d_c) \leq 0.05$ the same rules as above apply. However, such low grade efficiencies are rarely measured in practice.

For evaluation of experimental data linear regression is followed by a non-linear regression step in order to optimise the correlation coefficients. This procedure uses the experimental data and varies the coefficients k and n of Equation 2.27 until the deviation between measured grade efficiency and correlated grade efficiency is minimal. That means that the sum of errors squared in the following equation must be a minimum:

$$S = \sum_{i=1}^{m} (T_{i,theor} - T_{i,meas})^2$$

$$S = \sum_{i=1}^{m} [g(x_i,k,n) - T_{i,meas}]^2 \qquad \text{where } x_i = (d_i/d_c)$$

The minimum condition is fulfilled if the partial derivatives of the above equations become zero:

$$\frac{\partial S}{\partial k} = \frac{\partial S}{\partial n} = 0$$

Although defining the conditions to be met is simple, the actual solution of the problem is complicated and involves complex programming techniques. A numerical solution of non-linear regression analysis has been presented by Ebert (1983). The algorithm has been modified in order to correlate the coefficient k and n of Equation 2.27. The program requires initial guesses before it starts the calculation. For good convergence of the algorithm those initial guesses need to be fairly close (± 20%) to the final values of the correlated parameters. For this reason, non-linear regression is preceded by a linear regression procedure in order to provide good initial starting values of k and n. Furthermore, for non-linear regression all experimental data, including grade efficiency values of $T(d/d_c) \geq 0.98$, are included in the correlation procedure.

A typical example of a computer print out following such a correlation process in presented in Figure 2.17 with information of experimental conditions on top, followed by the results of the regression analysis and a table comparing experimental values ($T(d)_{obs}$) with correlated grade

efficiency values ($T(d)_{cal}$). Values of particle diameter, corresponding grade efficiency and separation limit are fed into the computer and the values of the coefficients k and n are determined by linear regression and are optimised by a non-linear regression algorithm. The experiment chosen as a typical representative for all other experimental trial is Run-No. V31, in which 7 discs were placed on top of insert I1 (small insert) followed by blank inserts I2 and I3. The flow rate was 400 L h^{-1} and the separation limit was 1.32 μm. The mean error of the fitted line provides an indication of how well the model equation is able to approximate the experimental data. This mean error includes all experimentally obtained grade efficiency values and is given by:

$$\varepsilon_c = \sqrt{\frac{1}{n-2} \sum_{i=1}^{m} (T(d)_{i,obs} - T(d)_{i,cal})^2} \qquad 2.28$$

where m is the number of size classes on which the calculation of the grade efficiency $T(d)_{obs}$ is based.

Figure 2.18 presents the correlated grade efficiency curve together with the measured grade efficiency values demonstrating visually the overall goodness of the curve fitting procedure. A summary of the results obtained during the curve fitting procedures applied on the grade efficiency data of various experiments are presented in Table 2.3.

Table 2.3: Summary of results obtained during grade efficiency approximation using Equation 2.27 and experimental data.

Run-No.	z	Q	Pos.	k	n	r_c	ε_c
V18	17	---	A	1.174	2.037	0.991	0.026
V19	7	---	A	1.115	1.883	0.990	0.028
V20a	7	300	B	0.859	2.332	0.998	0.012
	7	500	B	0.830	1.893	0.998	0.014
	7	700	B	0.745	1.717	0.990	0.029
V20b	17	---	B	0.976	2.679	0.987	0.034
V21	7	300	B	0.853	2.435	0.998	0.018
	7	500	B	0.787	2.435	0.999	0.015
	7	700	B	0.716	2.177	0.989	0.014
V28	7	---	C	0.846	2.054	0.989	0.020
V29	7	---	C	0.906	1.934	0.995	0.013
V30	7	---	C	0.869	2.127	0.999	0.012
V31	7	---	C	0.839	2.205	0.997	0.016
average V28...V31			C	0.865 (± 0.03)	2.080 (± 0.11)		

z: number of separation discs

Q: throughput capacity (L h^{-1}); if no item is given then data represent averages over a range of flow rates.

Pos: position of separating discs (see Figure 2.5).

k,n: coefficients obtained by regression analysis.

r_c: Pearson correlation coefficient

ε_c: mean error of estimate given by Equation 2.28.

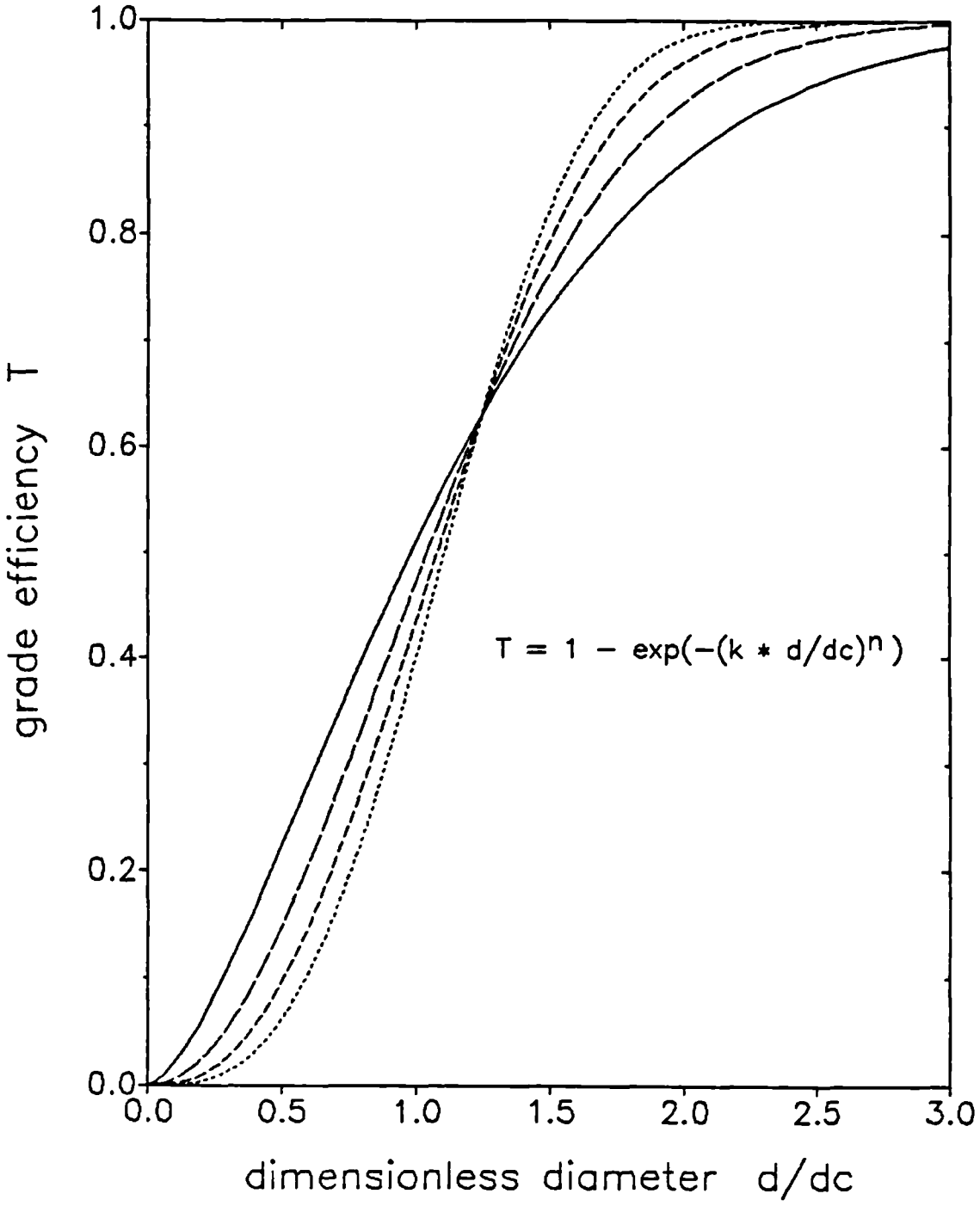

Figure 2.15: The change of grade efficiency T with increasing values of d/d_c. Calculation based on $T(d) = 1-\exp[-(k\ d/d_c)^n]$, k = 0.8 (constant).

(————), n = 1.5; (—— ——), n = 2.0;

(— — — —), n = 2.5; (--------), n = 3.0

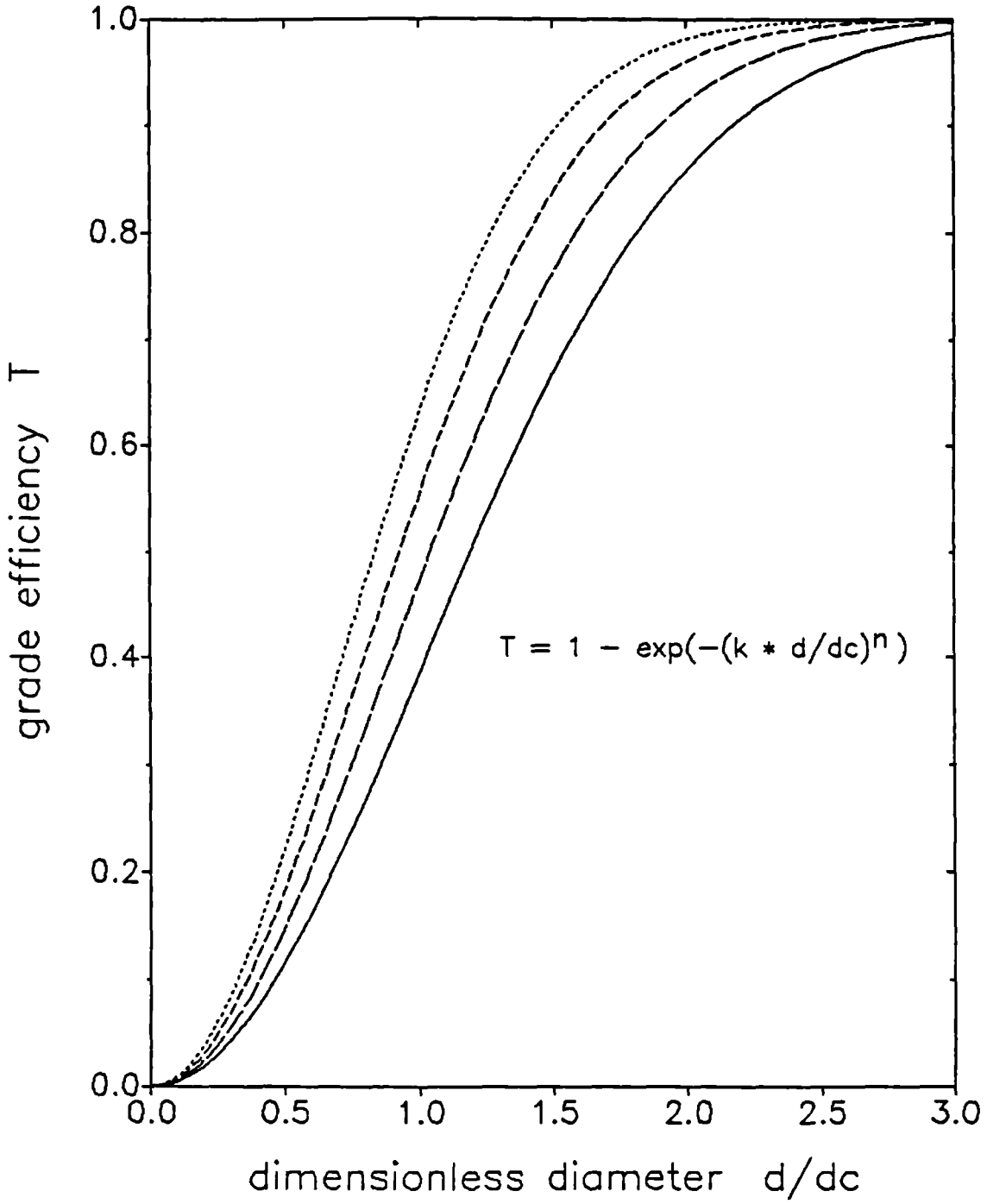

Figure 2.16: The change of grade efficiency T with increasing values of d/d_c. Calculation based on $T(d) = 1-\exp[-(k \cdot d/d_c)^n]$, n = 2.0 (constant).

(—————), k = 0.7; (—— ——), k = 0.8;

(— — — —), k = 0.9; (- - - - - - - - →), k = 1.0.

Run-No.:	V31	Datum:	18.12.1986
Product:	PVAc	Separator type:	BSB 7-47-476
Number of discs:	7	Position of discs:	C

Flow rate:	400 L/h
Separation area:	600 m^2
Specific throughput:	0.67 L/(h m^2)
Separation limit:	1.32 um

Regression line: $T(d) = 1 - \exp[-1*(k*d/dc)^n]$

Coefficients : k = 0.869
n = 2.194

d	d/dc	T(d) obs	T(d) cal	Error
um	/	/	/	abs.
0.792	0.600	0.192	0.213	-0.021
0.924	0.700	0.245	0.285	-0.040
1.056	0.800	0.352	0.363	-0.011
1.188	0.900	0.464	0.442	0.022
1.320	1.000	0.539	0.520	0.019
1.452	1.100	0.606	0.596	0.010
1.584	1.200	0.697	0.666	0.031
1.716	1.300	0.746	0.729	0.017
1.848	1.400	0.779	0.785	-0.006
1.980	1.500	0.816	0.833	-0.017
2.112	1.600	0.869	0.873	-0.004
2.244	1.700	0.887	0.905	-0.018
2.376	1.800	0.913	0.931	-0.018
2.508	1.900	0.939	0.950	-0.011
2.640	2.000	0.958	0.965	-0.007

mean error of fitted line: 2.061708E-02

Figure 2.17: Typical results sheet obtained after regression procedure.

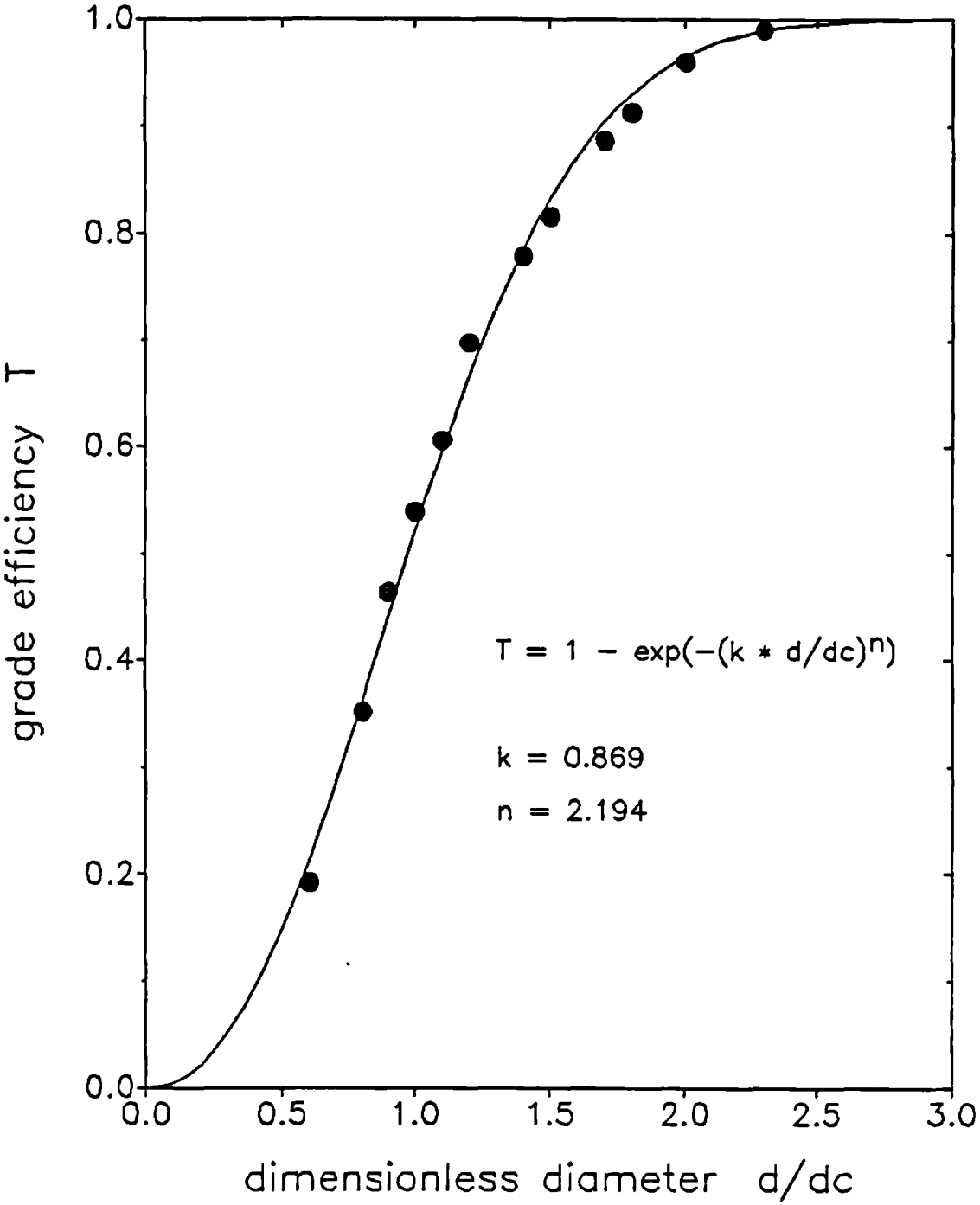

Figure 2.18: Plot of grade efficiency against dimensionless particle size. Solid circles represent experimental data points while the solid curve represents the best-fit line obtained after non-linear regression using Equation 2.27.

2.3.5 Application of the grade efficiency correlation function

In the following section the two-parameter approximation of the grade efficiency will be applied in order to estimate its capability of predicting the mass yield and the particle size distribution in the clarified liquid phase at given operating conditions of the centrifuge and particle size distributions in the feed phase. To predict the possible mass yield of the disc stack centrifuge, Equation 2.20 in conjunction with the mathematical form of the grade efficiency curve T(d) (Equation 2.27) was applied. In order to estimate the predictive power of the experimentally determined grade efficiency curve, data of the experimental trials V28 to V31 (Table 2.3) have been used to calculate the mass yield. A comparison between the theoretical and experimental mass yield values are presented in Figure 2.19 in which the ratio of experimentally determined mass yield and calculated mass yield are plotted against the volumetric single passage throughputs q (= Q/z). The calculation of the theoretical mass yield was based on the grade efficiency approximation given by Equation 2.27 with k=0.865 and n=2.08.

Figure 2.19 shows the general tendency of the grade efficiency function to underestimate the mass yield at low volumetric throughputs (R_c ($=E_{T,mass}/E_{T,pred}$) > 1), while at high throughputs the predicted values of the mass yield are larger than the actual measured values (R_c ($=E_{T,mass}/E_{T,pred}$) < 1). It appears that the dimensionless grade efficiency curve is to a certain degree influenced by the single passage throughput, q. This effect will be examined in more detail in section 3 of this thesis.

The capability of the two-parameter function to predict the recovery of bakers yeast cells was examined in a different type of experiment. The recovery of yeast cells was carried out in order to study an alternative shear-insensitive particle system and to demonstrate the validity of the polyvinylacetate-based model grade efficiency equation. The physico-chemical properties of bakers yeast has been studied in detail by Ward (1989). Owing to its high resistance to shear forces and its ease of handling, it is a biological particle system widely used for separation trials by centrifuge manufacturers.

The volumetric median particle size of bakers yeast cells is of the order of 4.5 to 5.5 µm and is considerably larger than the corresponding polyvinylacetate particle size. Measurement of the particle size

distribution using the electric sensing method gives varying particle sizes depending on the ionic strength of the electrolyte (Ward, 1989). At a high ionic strength of the electrolyte (> 1% (w/w) aqueous saline solution) the cell shrinks as a result of cell water diffusing out of the cell and into the surrounding fluid. At a low ionic strength (< 1% (w/w) aqueous saline solution) causes water to diffuse into the cell thereby increasing the volume of the cell. For this reason it is recommended to disperse the yeast cells in a buffer of the same ionic strength as the electrolyte used for particle size analysis. Therefore the described experiment was performed in a buffer made of 0.15 M sodium chloride (NaCl) and 0.10 M potassiumdihydrogen-phosphate (KH_2PO_4) adjusted to pH 6.5 using 2.5 M aqueous sodium hydroxide solution (NaOH). For the trials 0.35 kg bakers yeast were suspended into 350 L of buffer giving a final yeast concentration in the feed suspension of 0.1 % (w/w). According to Ward (1989) the density of the yeast cells suspended in a phosphate buffer is 1120 kg m^{-3} and the density of the buffer being 1015 kg m^{-3}. The viscosity of the buffer was assumed similar to the viscosity of water at 20 °C. The experiments were performed according to the same procedure applied for polyvinylacetate described in section 2.1 of this thesis. The separation area was reduced to 10 % of its original value by replacing most of the discs with blank inserts, leaving 7 separating discs located on top of insert I1 (see also arrangement C in Figure 2.5)

Table 2.4 shows the main results obtained in those experiments and compares the measured separator performance expressed as mass yield with the theoretically predicted performance. The theoretical mass yield was calculated using Equation 2.20. The grade efficiency curve was approximated using a two-parameter model equation (Equation 2.27) with the parameters n (= 2.08) and k (= 0.865). The particle size distribution of the unrecovered particles in the centrifuge $\Delta F_1(d)$ was determined by using the mass yield calculated with Equation 2.20 and inserting the particle size distribution in the feed phase $\Delta F_o(d)$ into Equation 2.21. From the limited data, it seems there is no significant difference between the measured and the predicted median particle diameter for various throughputs.

Table 2.4: Separation of bakers yeast cells in a scaled-down disc stack separator. Comparison of experimental and theoretically predicted separation performance.

			experimental		theoretical	
Q	q	d_c	E_T	d_m (2)	E_T (1)	d_m (2)
$L \cdot h^{-1}$	$L \cdot h^{-1}$	µm	/	µm	/	µm
500	71.4	1.97	0.995	3.76	0.987	3.93
600	85.7	2.15	0.983	4.10	0.977	4.01
700	100.0	2.33	0.975	4.20	0.963	4.18

(1) calculated using Equation 2.21 in conjunction with Equation 2.27.

(2) d_m represents the median particle size of the particles remaining in the clarified liquid discharge phase.

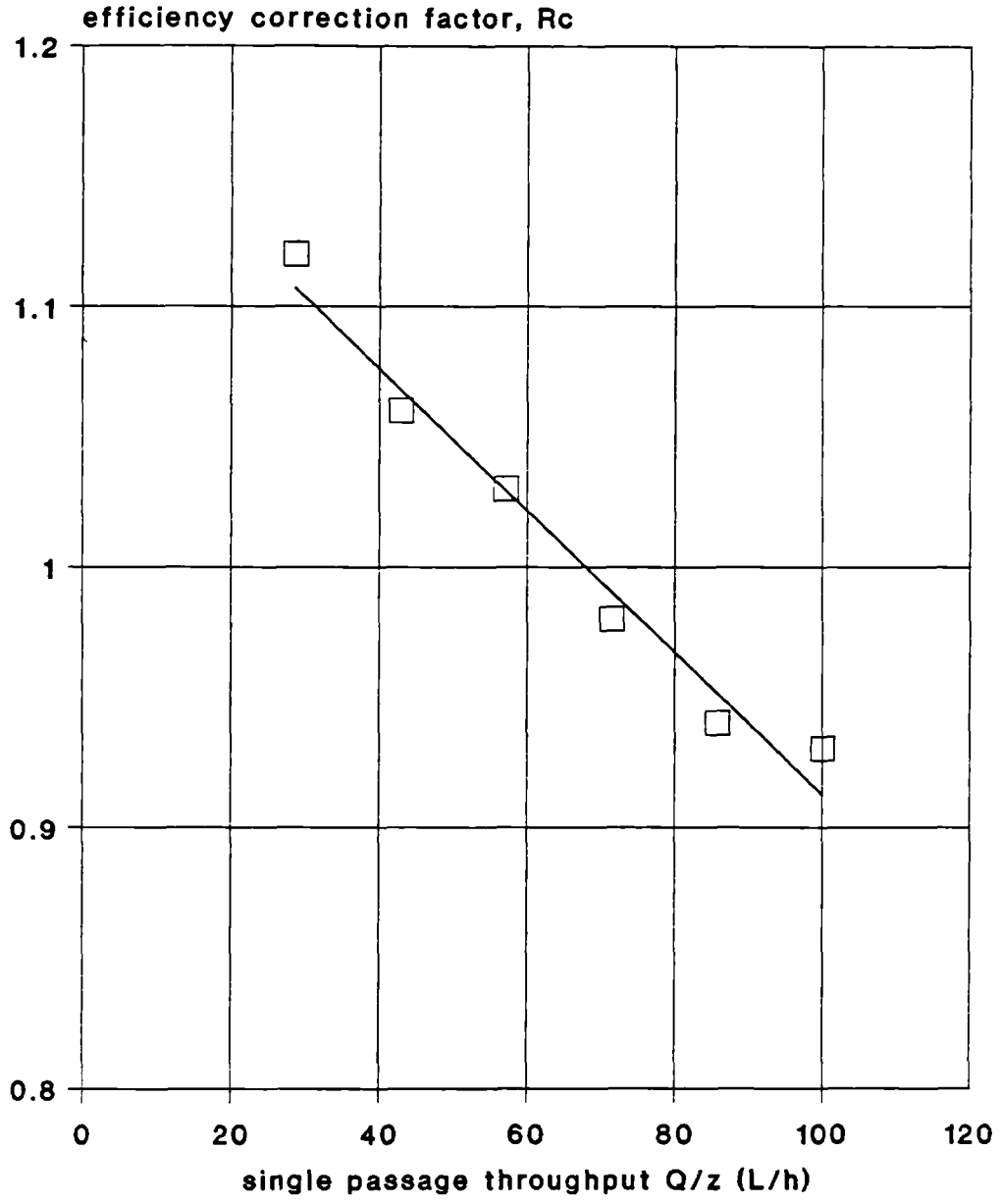

Figure 2.19: The effect of single passage throughput on the ratio of measured and calculated mass yield (R_c). The theoretical mass yield was calculated using Equations 2.20 and 2.27 with k = 0.865 and n = 2.08. Each point represents the mean of four measurements (SD = ± 0.03).

2.3.6 Rapid procedure of mass yield determination

The mass yield E_T is of primary importance when describing the separation performance of a centrifuge because it is one of the parameters which decides whether a particular machine is suitable for a given separation problem. Any deviations from normality during a separation procedure will be reflected in a change of the mass yield, usually giving a lower value. It is the first sign during a separation process which will tell the operator if something is not going according to plan. Therefore it may serve as a valuable tool in studies on separation performance. Changes of the mass yield are sensitive to changes in the operating conditions, hydrodynamics and product quality. For example during the studies on the scale down of a disc stack separator it was often necessary to get a quick overview on how certain changes in machine operation affect the solids recovery or the mass yield.

The mass yield of an intermittent disc stack separator may be determined by measuring the mass of solids in the clarified liquid phase and the mass of solids in the feed phase. At low concentrations this task was usually performed by measuring the particle concentration of a known sample volume using the electric zone sensing method. However, determination of the mass yield by using this method is complicated and slow. Therefore, a fast and reliable method of mass yield determination was required.

The turbidity of a sample is, by first approximation, proportional to the particle concentration. Unfortunately, other factors such as particle size, wavelength and detector geometry also affect the turbidity reading. However, based on the experience gained during the photosedimentometer studies of polyvinylacetate particles (chapter 2.3.1), there was reasonable ground for the application of turbidity measurements for mass yield determination. In order to evaluate the possibility of using turbidity measurements to estimate the mass yield of a centrifugation process, feed and supernatant samples were collected for each experimental trial performed with polyvinylacetate. Turbidity measurement was carried out by measuring the reduction of the intensity of a light beam passing through the sample.

The ratio of the intensity of the light beam after passing through the suspension and the incident light intensity was used as a measure for the turbidity (Lambert Beer's Law). In order to calculate the mass yield it was

assumed that the turbidity is directly related to the volume (= mass if particle density is constant) of suspended particles. Hence, the mass yield was calculated by inserting the corresponding turbidity readings into Equation 2.15. Rectangular plastic cuvettes (10 mm) were used for the measurement of the optical density. The wavelength of the incident light beam was 695 nm.

The result of this investigation is presented as a plot of the mass yield determined by using turbidity measurements (or optical density) versus the mass yield based on measurements using the electric zone sensing principle (Elzone) in Figure 2.20. It can be seen that the mass yield readings follow closely a 45°-line confirming the possibility of using turbidity readings at 695 nm to estimate the mass yield of a separation process. The mean error of the optically determined mass yield in respect to the mass yield determined by the electric zone sensing method was ± 3% absolute.

Practical experience has shown that in order to get good agreement between mass yields determined by the two described techniques it is essential to avoid settling of the particles in the sample flasks and to measure the turbidity as soon as possible. Tiny air bubbles interfere with turbidity readings and should be avoided.

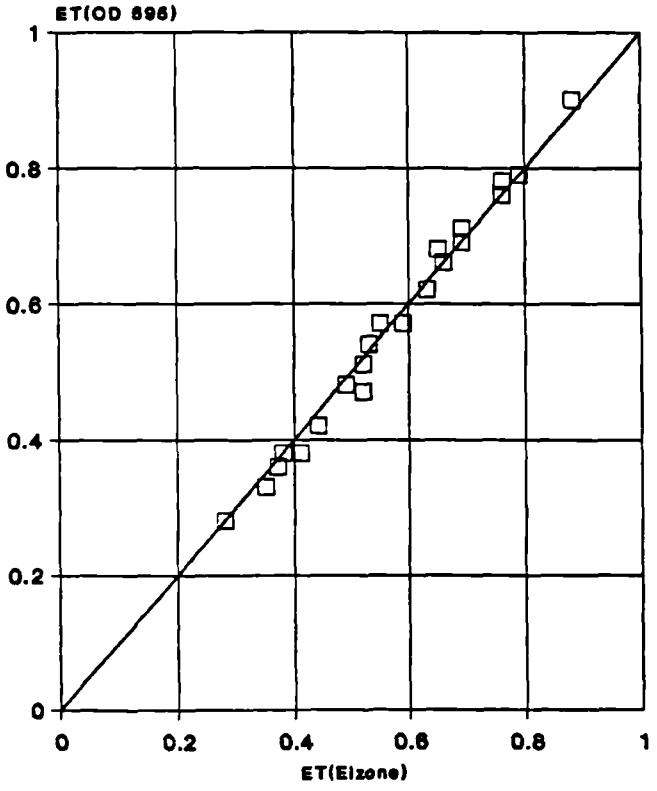

Figure 2.20: Plot of the mass yield determined by electric zone sensing technique and optical density measurement.

3. Preliminary studies of aggregate breakup in feed zones to disc stack centrifuges

In the following paragraphs the experimental procedure of examining the level of aggregate breakup in a disc centrifuge will be presented. The model system used for the studies is introduced and the associated problems are discussed. The objective is to use the experience gained during centrifuge scale-down and to test the particle system described in section 1.6.2 in respect to breakup when subjected to hydrodynamic shear forces inside a disc stack centrifuge.

3.1 Preparation of the protein precipitate suspension

The overall experimental set-up is illustrated in Figure 3.1 which shows the various experimental stages such as total water extract preparation, protein precipitation and centrifuge operation in the form of a process flow sheet.

Defatted soya flour was suspended in an extraction vessel (A1) and the protein dissolved by adjusting the suspension to pH 9.2 using an aqueous sodium hydroxide solution from reservoir (B1). Insoluble proteins and carbohydrates were removed using batch centrifuge (S1) and the supernatant containing the soluble proteins and carbohydrates was diluted into the precipitator (A2). Precipitation was performed by pumping sulphuric acid (P1) from the reservoir (B2) into the precipitator until pH 4.8 was reached. On completion of the precipitation the precipitate suspension was aged and then diluted into 0.07 M sodium acetate buffer (pressure vessel A3). By means of air pressure inside the feed vessel the precipitate suspension was pushed through the disc stack centrifuge (S2). Samples of the precipitate suspension were collected from the feed and supernatant stream, analysed and examined for possible particle breakup. Protein concentrations were determined using the Biuret technique with bovine serum albumin as calibration standard (BSA: Fraction V, 96-99% Albumin). This method of protein measurement is based on the reaction of peptide bonds with copper ions in alkali leading to the formation of a violet-coloured complex which can be quantified photometrically (Kresze, 1980).

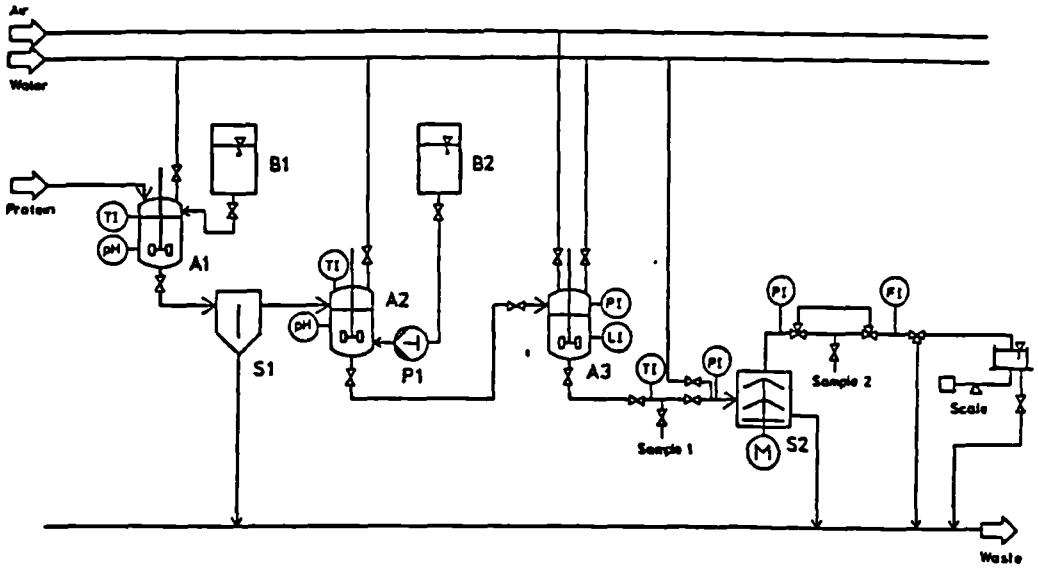

Figure 3.1: Process flow sheet of experimental setup.
A1: protein extraction vessel (V=2 L); A2: precipitation vessel (V=40 L); A3: feed vessel (V=1500 L); B1, B2: alkali and acid containers, respectively; S1: bench top centrifuge; S2: disc stack centrifuge (z=variable, R_i=0.036 m, R_a=0.076 m, h=0.5 mm, n=9300 min^{-1}, φ=38°); P1: positive displacement pump (Q=9 mL min^{-1}); PI: pressure gauges; FI: magnetic-inductive flow meter; pH: pH-meters; TI: theromcouples, LI: liquid level indicators.

3.1.1 Total water extract

The total water extract (TWE) was prepared in a 2.7 L baffled vessel (I.D. 125 mm, height 220 mm, four baffles; width 5mm) equipped with a 6-blade Rushton turbine impeller (I.D. 50 mm), temperature sensor, pH-probe and impeller speed control. 0.25 kg of defatted soya flour (Soya fluff 200W, Interfood Ltd., England) was dispersed in 2 L of distilled water at maximum impeller speed (1500 rpm). In order to extract the soluble protein approximately 20 mL of 10 % (w/w) sodium hydroxide solution (NaOH) were added until pH 9.2 was reached. The suspension was aged for 0.5 hours prior to removal of the insoluble carbohydrates (raffinose, stachyose, etc. - Salt, 1980) in a refrigerated centrifuge (Mistral 4L, MSE Ltd., London) operated at 2200 rpm and 15 °C for two hours. After centrifugation the solids fraction containing the insoluble carbohydrates and proteins was discarded. The supernatant containing the soluble proteins and carbohydrates, also known as 'total water extract', was stored for about 12 hours in a fridge at a temperature of 4 °C. In order to restrict bacterial growth, approximately 1 mg of sodium azide (NaN_3) was added to the total water extract. The overall yield of extract was about 1.5 L per batch with an average protein content of 60-65 kg m^{-3}.

3.1.2 Isoelectric protein precipitation

Protein precipitation was performed in a purpose-build precipitation vessel (Figure 3.2), equipped with a temperature sensor, pH-probe and impeller speed control. The design specifications of the precipitation vessel are listed in Table 3.1. The total water extract was diluted into an appropriate volume of soft water adjusted to pH 9.2 (10% (w/w) sodium hydroxide solution) to give a protein concentration of 3-3.5 kg m^{-3}. Protein precipitation was initiated by adding sulphuric acid (30% v/v) at a constant rate using a small piston pump (Micro Pump Series II, Head Size 3, F.A. Hughes & Co. Ltd., Surrey, U.K.; flow rate 9 mL min^{-1}) at an impeller speed of 250 rpm. To ensure rapid dispersion in the vessel, the acid was added via a capillary syringe just below the rotating impeller. When the pH of the suspension reached pH 4.8, acid addition was stopped and the suspension was aged for 0.5 hours at a reduced impeller speed of 200 rpm. The suspension temperature was approximately 20 °C throughout protein precipitation. Typically 75-83% of the soluble protein in the total water extract were precipitated.

Table 3.1: Precipitation reactor dimensions

Diameter T (= Depth H)	0.37 m
Volume	0.035 m^3
Impeller clearance ratio, h/H	0.33
Impeller/Tank ratio, D/T	0.33
Baffles (4 off)	0.1 T
Base	Flat
Material	Perspex[1]

[1] Poly (methyl meth-acrylat) (PMMA)

Bell and Dunnill (1981) have shown that the maximum strength of protein precipitate prepared in a batch precipitator is obtained at an aging parameter, $G \cdot t$, greater than $1 \cdot 10^5$ where G is the root-mean-square velocity gradient (see section 1.4):

$$G = \sqrt{\frac{P}{V \cdot \mu}} \qquad 3.1$$

where P is the power dissipated in the liquid by a rotating agitator, V is the volume of the liquid in which the agitation power is dissipated and μ is the dynamic viscosity of the liquid. For low viscosity fluids, this power is closely related to the agitator diameter Di and speed n by the relationship

$$P = Po\ \rho\ n^3\ D_i^5 \qquad 3.2$$

where n is the impeller rotational speed in revs s^{-1}, D_i is the impeller diameter in m. The power number Po is a function of mixing Reynolds number ($= \rho n Di^2/\mu$), the Froud number ($= n^2 Di/g$) and other geometrical data. For geometrically similar, fully baffled vessels without a centrifugal vortex and turbulent conditions ($Re > 2 \cdot 10^4$) the power number is a constant independent of the Reynolds number but dependent on the agitator type. A collection of power numbers for Rushton disc turbines (6 blades) obtained by Bujalski (1987) shows a vast variation of the Po values obtained by different workers, ranging from values as low as 2.74 to values as high as 6.3. In order to be consistent with work already performed by Bell and Dunnill (1982) on the isoelectric precipitation of soya proteins, Po = 4.5 was used for the calculation of the rms velocity

gradient. Under the experimental conditions, the ageing parameter G·t was about $6 \cdot 10^5$ and the root-mean-square velocity gradient G was in the order of 345 s^{-1}.

After completion of the precipitation and ageing stage the protein precipitate suspension was then withdrawn from an 8 mm port at the vessel base and immediately diluted into 400 L of sodium acetate buffer (ionic strength 0.07 M, pH 4.8). The final particle concentration was approximately 10^9 particles/L with a median particle diameter of 5.3 ± 0.4 µm (by volume).

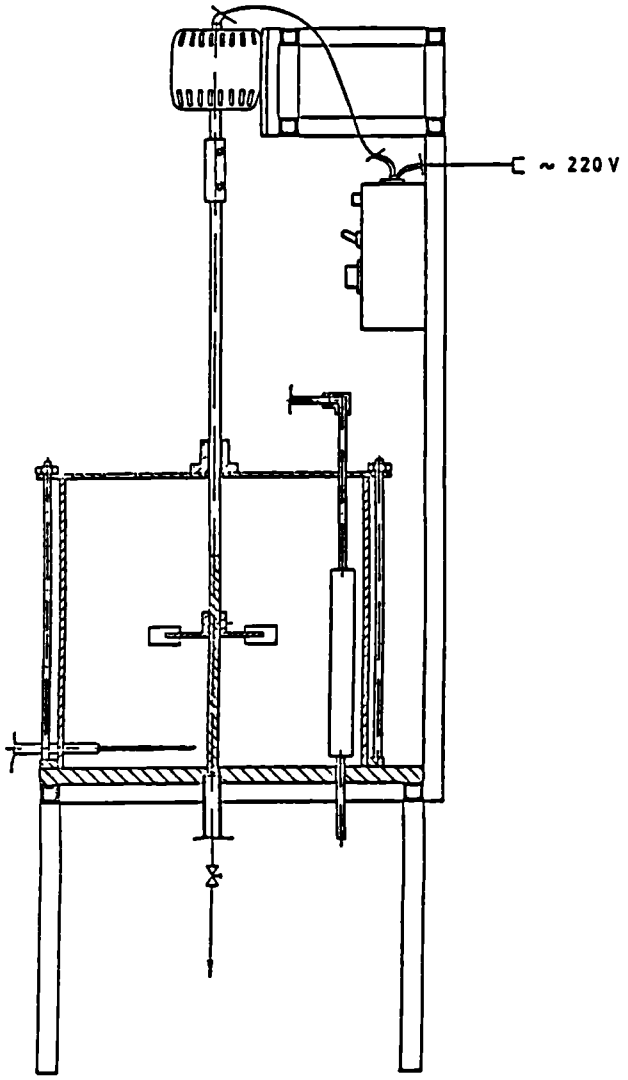

Figure 3.2: Schematic diagram of the pilot scale vessel used for the isoelectric precipitation of soluble soya protein.

3.2 Centrifuge operation

The separator was started up with mains water flowing through the machine as described in the operation manual. The suspension storage tank was pressurised and the suspension gently stirred and fed to the centrifuge using air pressure (maximum pressure 1.5 bar gauge). An average bowl speed of 9150 rpm was used for all experiments. Samples were collected at the feed inlet and directly from the clarified liquid discharge. A by-pass system was used to avoid potential particle breakup during the sampling process. For each trial four throughput capacities in the range between 300 and 600 L h^{-1} were evaluated. For each flow setting 15 kg of suspension were carried through the centrifuge before a supernatant sample was collected (steady state condition). Feed samples were collected after the feed was switched back to mains water. Prior to each new flow setting the collected solids were discharged and the machine was rinsed three times with water. A magnetic-inductive flow meter was used for the monitoring of the throughput capacities. The average temperature of the feed suspension was 20 °C.

3.3 Particle size analysis

All size distributions were measured on an Elzone particle sizing instrument by means of the electric zone sensing principle. A 30 µm orifice tube was used for measuring the particle size distribution. Samples were accurately diluted to an appropriate concentration in sodium acetate buffer (0.07 M, pH 4.8) which was filtered using 0.2 µm Sartobran Filter Capsules (Sartorius AG, West Germany). Otherwise particle size analysis was performed as described for polyvinylacetate (section 2.2.1).

Mass balance studies of particle size distributions (Virkar et al, 1982) measured after varying times of precipitate dilution showed that the precipitate particles did not redissolve in the electrolyte solution to a measurable extent. Preliminary studies on samples recycled after a particle size measurement showed that no significant breakup of aggregates occurred during the passage of the electrolyte through the orifice. Treweek (1977) has demonstrated that owing to the effect of aggregate porosity on the particle conductivity the electronic counter measures only the particulate matter within a aggregate which is smaller than justified by the actual particulate content. However, Bell and co-workers (1982)

showed that on the basis of particle size analysis using different techniques the electric zone sensing method accounts for at least 93% of the diameter of 6 μm precipitate particles. The small effect of conductivity on the size measurement of precipitate particles is explained by the theory that free electrolyte in a pore closed at one or both ends will be non-conductive.

3.4 Physico-chemical properties of protein precipitate

The main physico-chemical properties of the soya protein precipitate are listed in Table 3.2. The protein density was determined by measuring the settling velocity of the precipitate particles using the Joyce Loebl disc photosedimentometer and fitting the obtained settling velocity distribution data to the particle size distribution (volume basis) determined using the electric zone sensing principle. The viscosity of the carrier liquid was determined using an Ostwald capillary viscosity meter calibrated with distilled water at 20 °C.

Table 3.2: Some important physico-chemical properties of a soya protein precipitate suspension (20 °C). Values given represent the mean of three measurements.

Precipitate density[1]	1092	kg m^{-3}	±10
Density of carrier liquid	1002	kg m^{-3}	±1
Viscosity of carrier liquid	0.001	Pa·s	$\pm 5 \cdot 10^{-5}$

[1] assumes that particles are spherical.

3.5 Results

3.5.1 Preliminary experiments and results

a) Effect of laminar shear on large scale processed soya precipitate

The field of aggregate breakup in laminar shear fields has been extensively studied and presented in the thesis by Bell (1982). However, in order to characterize the shear associated properties of the precipitate prepared on a larger scale than the precipitate used by Bell some preliminary shear experiments were performed. To examine the resistance to shear disruption, the precipitate was subjected to capillary shear in an Instron 1141 Food Tester (Instron LTd., High Wycombe, Bucks., England) modified to house a range of capillary tubes of different length and bore width. To test the protein aggregate an average shear rate of $9 \cdot 10^4$ s^{-1} at exposure times between 0.004 and 0.022 s were chosen. The tube bore diameter was 330 µm. To examine the shear damage at lower shear rates one single trial was performed at an average shear rate of $1.7 \cdot 10^4$ s^{-1} and an exposure time of 0.044 s. In this case a 575 µm tube bore diameter was used. The precipitate was prepared as described in section 3.1.

As already demonstrated by Bell (1982), at high shear rates ($9 \cdot 10^4$ s^{-1}), the ratio d_m/d_m^o (where d_m^o represents the median particle size before shear breakup and d_m represents the median particle size after shear exposure) decreases proportionally with increasing exposure times. However, in contrast to Bell a significantly stronger dependence of d_m/d_m^o on the exposure time was observed (Figure 3.3). The reason for this deviation is explicable by different precipitate preparation conditions. Bell used a smaller precipitation vessel (0.69 L) and much higher protein concentrations (30 kg m^{-3}). Using the highest exposure time of 0.022 s the final volume median diameter was reduced to 3.5 µm. At the lowest shear rate of $1.7 \cdot 10^4$ s^{-1} (575 µm tube bore) little aggregate breakup was observed even for long exposure times. The initial volume median diameter changed only slightly from 6.204 µm to 6.101 µm.

b) Effect of diaphragm valve on shear disruption in feed to centrifuge

In order to control the flow rate to the centrifuge it was necessary to establish whether a valve in the feed line to the disc centrifuge causes any shear associated damage to the protein aggregates. The precipitate was

prepared as described in section 3.1. The centrifuge was passed by using a short cut between feed pipe and the bypass assembly. The feed vessel was pressurised to 0.5 bar (gauge) and the flow rate was adjusted to four values between 300 and 600 L h^{-1} using a diaphragm valve. Special care was taken to avoid any particle disruption during the sampling process.

The result of this experiment is illustrated in Figure 3.4, which shows the cumulative volume oversize distribution at various flow rates plotted against the particle diameter. The initial particle size was 4.9 µm and the protein concentration prior to precipitation was 3 kg m^{-3}. The non-shear flow condition (i.e. valve completely open) is represented by the solid squares. A considerable reduction of the volume median size is observed at flowrates of Q = 300 L h^{-1} and Q = 600 L h^{-1} in which the size of the precipitate particles are reduced to 2.7 and 3.4 µm respectively.

From these results it becomes evident that valves in the feed line to the disc centrifuge must strictly be avoided if particle breakup shall only be restricted to the centrifuge feed zone. Therefore it was necessary to control the feed rate entirely by the pressure level inside the pressure vessel and a needle valve which is located after the by-pass assembly.

c) Optical density of soya precipitate suspensions

In section 2.3.6 the optical density (or turbidity) was used to obtain the overall mass yield E_T. The optical density of a dilute polyvinylacetate suspension was linearly proportional to the solids concentration of the examined suspension and the mass yield E_T was obtained by:

$$E_T = 1 - OD(supern)/OD(feed) \quad \text{at} \quad \lambda = 695 \text{ nm}$$

Applying the same principle for protein precipitate showed that the mass yield based on optical density measurement deviates considerably from the mass yield derived using the Elzone particle size analyser. The potential source of this behaviour is demonstrated in Figure 3.5 and 3.6.

In Figure 3.5 the total protein concentration is plotted against the optical density at a wavelength of the incident beam of λ = 695 nm for a series of samples obtained from the centrifugation trials involving soya precipitate. Up to an optical density of approximately 0.25 the particle volume increases linearly proportional to the optical density. However, at

higher optical densities the total particle volume is no longer proportional to the optical density but rises exponentially.

Optical densities below readings of 0.25 arise from supernatant samples exhibiting particle size distributions similar to each other. In the feed samples, however, corresponding particle concentrations give quite different optical density values depending on the volume based median particle diameter. This behaviour indicates that the turbidity of a soya aggregate suspension of constant concentration changes significantly with particle size and is particularly influenced by large aggregates.

This trend is further supported by a plot shown in Figure 3.6 where the optical density is plotted against the volume based median particle diameter at a constant precipitate concentration. It can be seen that the optical density falls with increasing particle diameter. The reason for this relationship between optical density and particle size may be explained with a denser, more homogeneous structure of smaller aggregates leading to higher turbidity values.

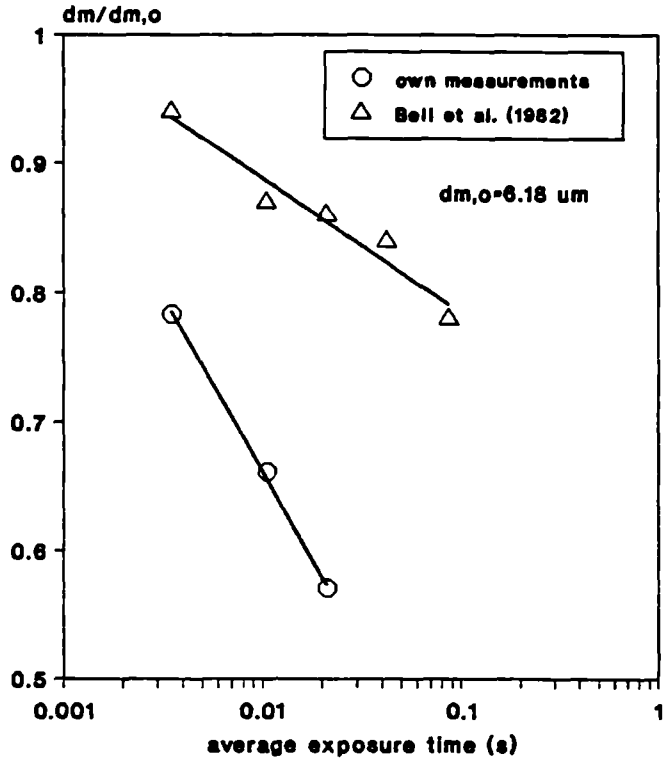

Figure 3.3: Effect of shear rate and exposure time on particle breakup in a laminar shear device - $d_{m,o}$ and d_m are the median particle diameters before and after shear, respectively. Total protein concentration prior to protein precipitation was 3 kg m^{-3}.

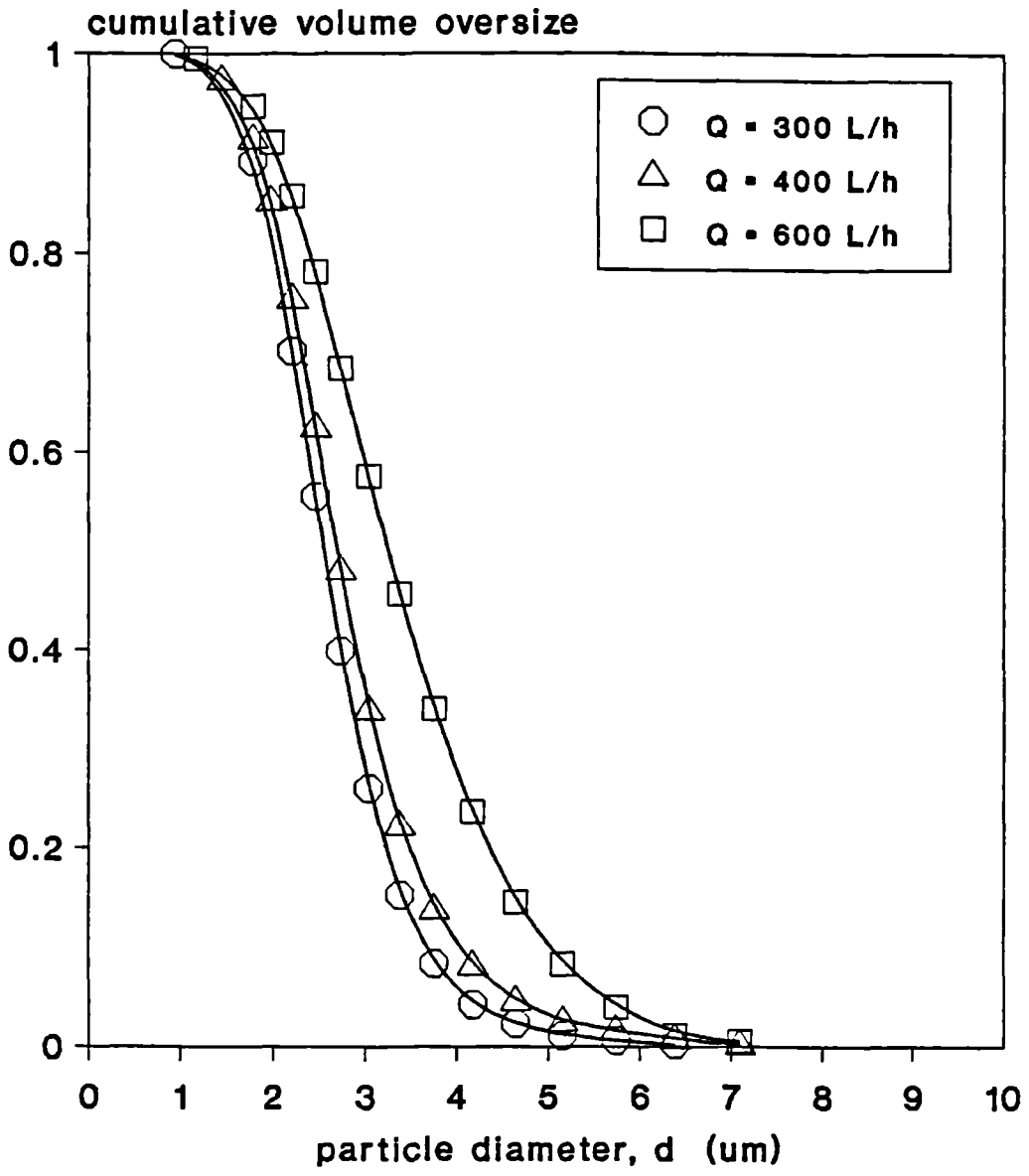

Figure 3.4: The change in cumulative volume oversize from exposure to shear in a diaphragm valve. d_m^o = 4.9 μm. Total protein concentration prior to protein precipitation was 3 kg m^{-3}.

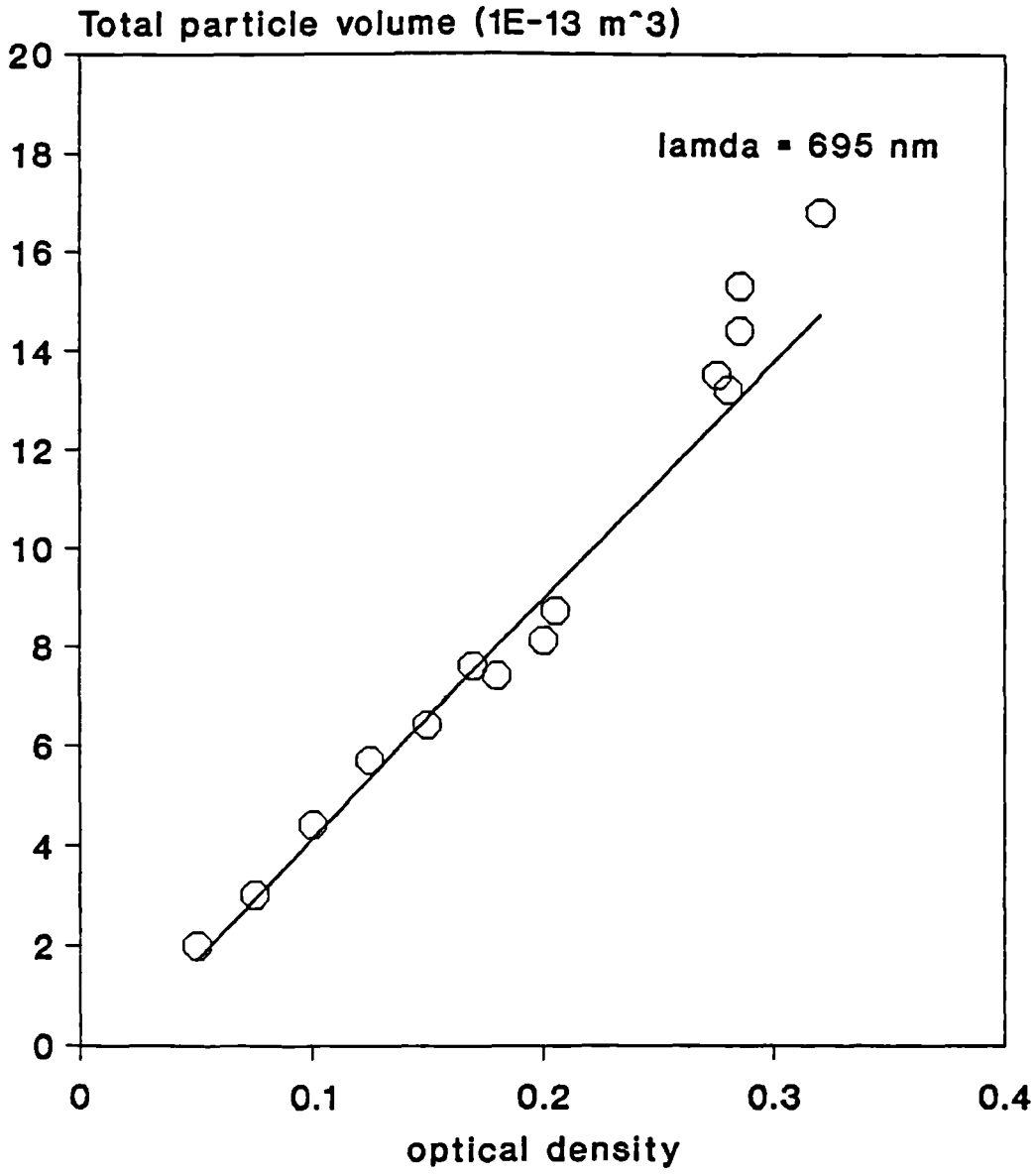

Figure 3.5: The effect of total protein concentration on the optical density of precipitate samples. λ = 695 nm.

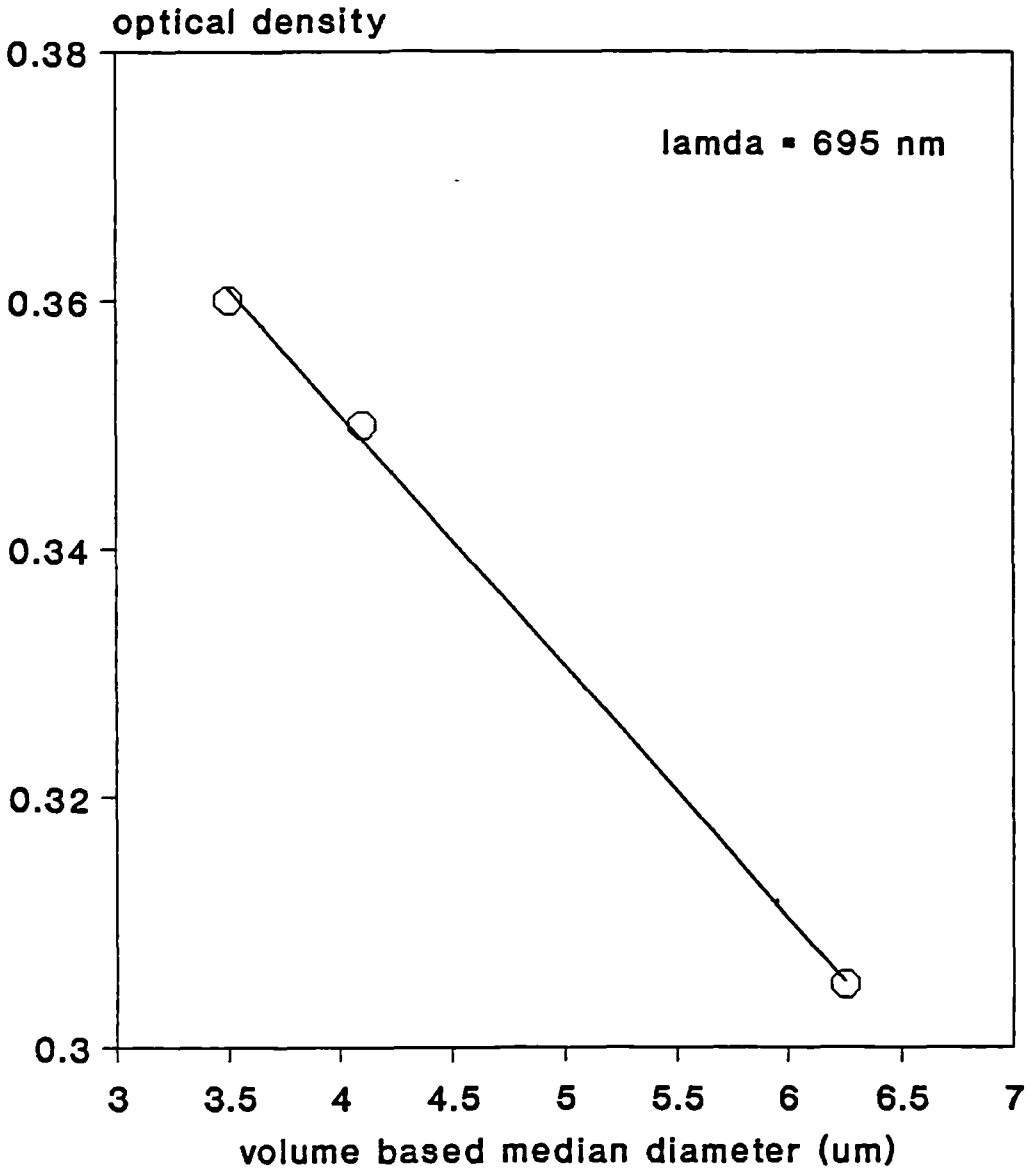

Figure 3.6: The effect of median particle size on the optical density of a protein precipitate of constant concentration.

3.5.2 Aggregate breakup in feed zone to disc centrifuge

3.5.2.1 Effect of particle breakup on mass yield

Figure 3.7 shows a typical percent-in-range particle size distribution (volume) of soya precipitate measured in the feed phase entering the disc centrifuge. Included in Figure 3.7 is the corresponding grade efficiency curve as a function of particle size for throughput capacities of 300, 400 and 500 L h^{-1}. The grade efficiency curve was calculated on the basis of the two-parameter function given in section 2.3.4.1 with the coefficients k = 0.865 and n = 2.08. The graph indicates that most of the precipitate particles should be recovered in the disc centrifuge under the given operating conditions. However, computing the mass yield on the basis of the particle size distribution in the feed to the centrifuge and the mathematised form of the grade efficiency curve (Equation 2.20) shows a significant deviation between theoretical to experimental values of the mass yield. Table 3.3 lists the mass yields obtained from such a calculation and compares the results with experimental data.

Table 3.3: Predicted and measured mass yields for precipitate particles separated in a full-hermetic disc centrifuge.

Q	$E_{T,pred}$	$E_{T,meas}$
L h^{-1}	/	/
300	0.985	0.795
400	0.973	0.680
500	0.957	0.531
600	0.938	0.466

Figure 3.8 shows the result of calculating the dimensionless grade efficiency curve using the precipitate distribution in the feed to the centrifuge and in the supernatant leaving the centrifuge. Included in Figure 3.8 is the dimensionless grade efficiency curve obtained using shear-insensitive polyvinylacetate particles.

The grade efficiency for precipitate particles is better than the polyvinylacetate curve for large values of d/d_c followed by a sharp decline for smaller values of d/d_c. The precipitate curve actually extends further down into the negative region indicating the formation of smaller fragments which were not present in the feed suspension. Breakup of larger aggregates leads to apparently better grade efficiencies at the top end of the grade efficiency curve while the fragments which are more difficult to recover cause the loss of recovery efficiency at smaller particle sizes.

At this point it needs to be recalled that in reality the dimensionless grade efficiency curve of the disc centrifuge has not changed at all. As a matter of fact the grade efficiency curve based on precipitate particles uses only the wrong basis of calculation. Owing to particle breakup the particle size distribution in the feed is different from the particle size distribution entering the disc stack. Since particles are subjected to breakup forces while travelling through the feed zone, larger aggregates will break into smaller fragments which are more difficult to recover. If this size distribution entering the disc stack was known then the grade efficiency curve would essentially be the same as for polyvinylacetate particles.

In the full-hermetic disc stack centrifuge the clarified liquid is discharged by means of an in-built centrifugal pump with an impeller diameter of 50 mm. This discharge pump is necessary to provide enough backpressure to enable the lip seals, separating the supernatant side from the feed side, to function properly. In addition, the pump transforms the rotational energy of the fluid into kinetic and pressure energy used to transport the fluid away from the centrifuge. The effect of pumps and in particular of centrifugal pumps to particle breakup has been examined in detail by Narendranathan (1981) who demonstrated that particles are broken almost immediately in centrifugal pumps to give uniform particle size distributions. If aggregates are not broken in the feed zone but in the clarified liquid discharge a grade efficiency curve similar to the one shown in Figure 3.8 would be obtained. However since the overall particle volume is conserved during breakup, breakup of particles due to shear action of the discharge pump cannot explain the observed loss of mass yield. This reduction is only possible if the size of the particles in the feed suspension has been altered in the feed zone prior to particle separation. Any further particle breakup (e.g. discharge pump) has no effect on the overall mass yield of the separator.

Therefore, the particle size distribution of the precipitate after the feed zone affects the separation efficiency or the overall mass yield of the disc centrifuge. If it was possible to determine this distribution then it could be used as a measure of particle breakup. Furthermore, from the particle size distribution conclusions could be drawn on the mechanisms responsible for particle breakup. The remainder of this section will be devoted to this problem.

The two processes of particle breakup and particle recovery may be divided into two distinct processes as shown in the diagram below:

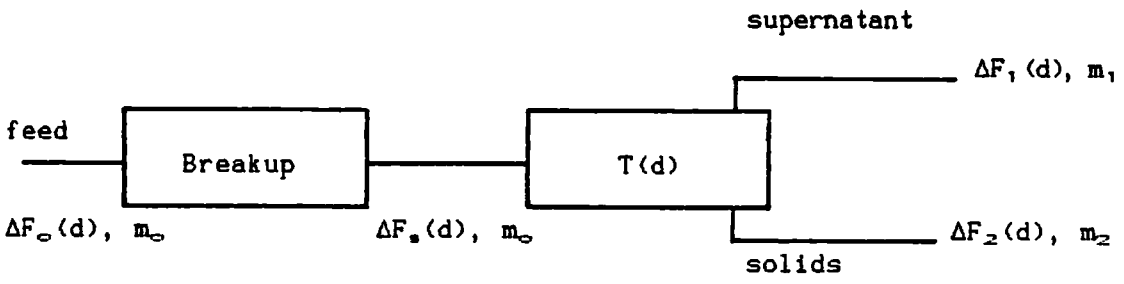

Provided that the overall particle volume before and after particle breakup is preserved and the grade efficiency curve of the centrifuge under examination is known then Equation 2.21 of section 2.3.4, allowing the calculation of the supernatant particle size distribution, may be rearranged to give the sheared feed size distribution $\Delta F_s(d)$:

$$\Delta F_s(d) = \frac{1 - E_T}{1 - T(d)} \Delta F_1(d) \qquad 3.3$$

which represents the particle size distribution of the feed suspension after the feed zone but before the suspension is entering the disc stack for phase separation. Of course, since the breakup term in the above diagram disappears for shear insensitive particles, Equation 3.3 may also be used to determine the feed size distribution $\Delta F_0(d)$ from the particle size distribution in the clarified liquid discharge $\Delta F_1(d)$ and the mass yield, E_T, of the disc centrifuge.

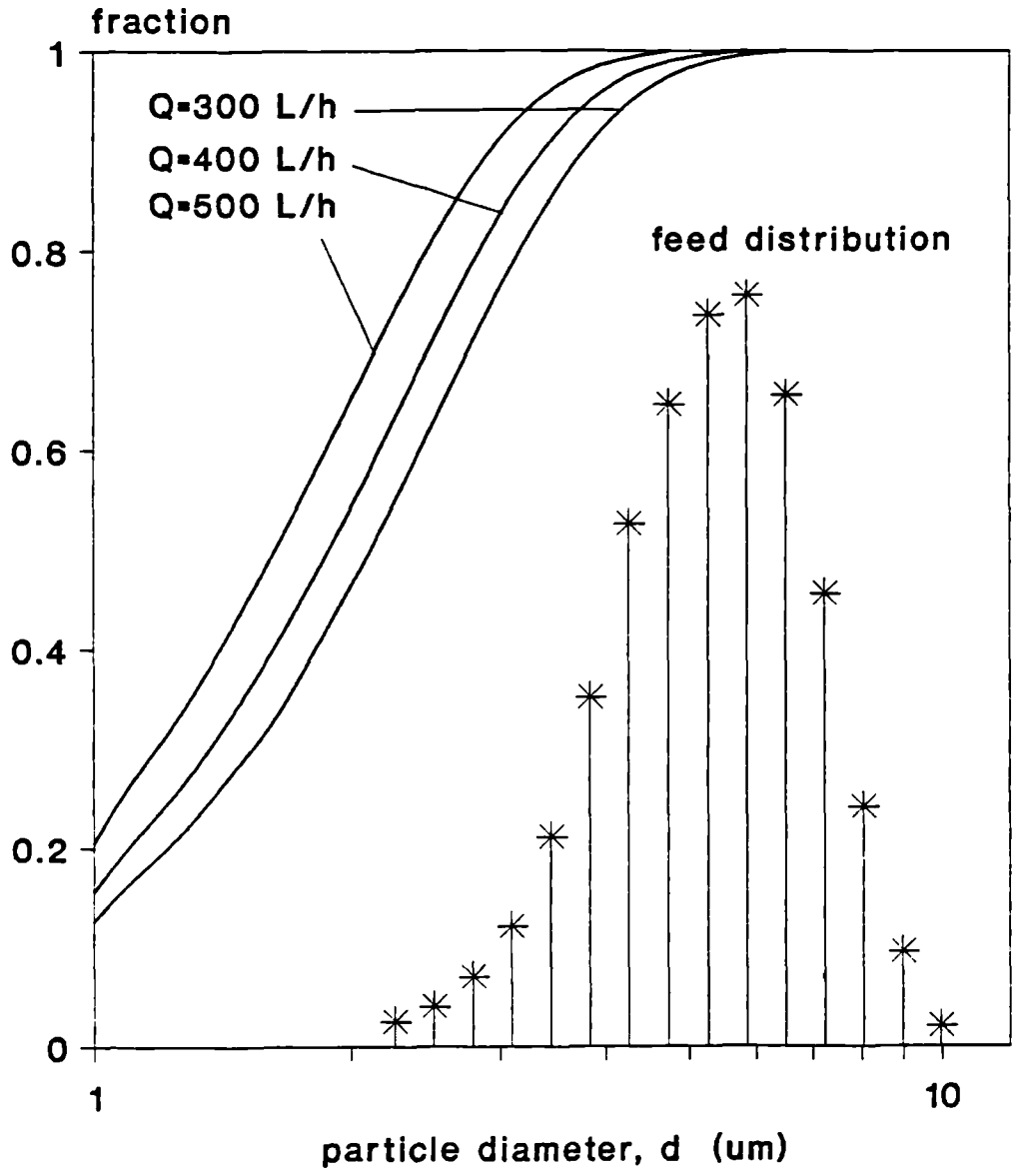

Figure 3.7: Particle size distribution of protein precipitate entering the disc centrifuge and grade efficiency curves for precipitate particles at different flow rates calculated on the basis of Equation 2.25 with the coefficients k = 0.865 and n = 2.08.

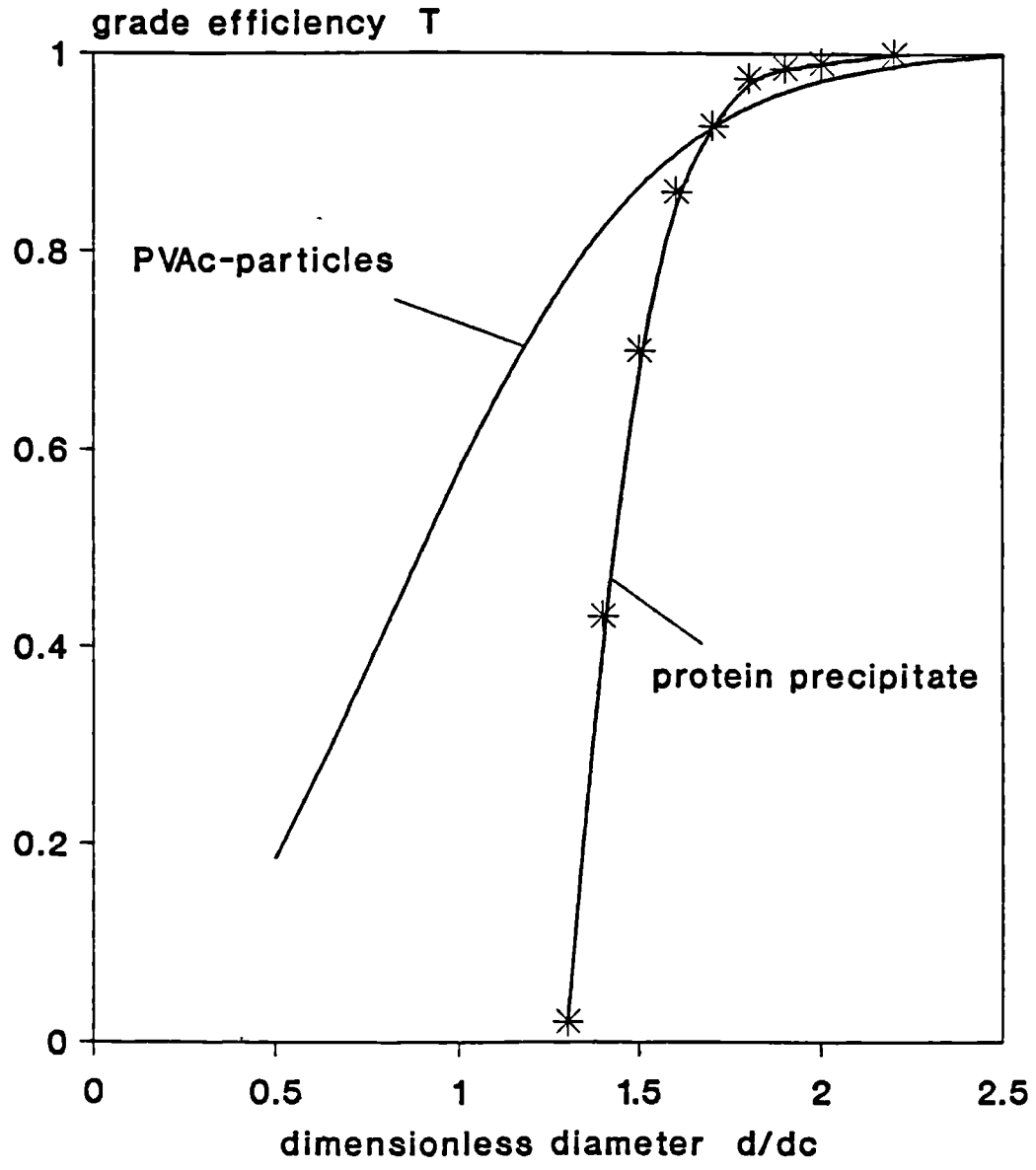

Figure 3.8: Shear breakup in centrifuge feed zone demonstrated in form of dimensionless grade efficiency curves of polyvinylacetate and precipitate particles.

Unfortunately, Equation 3.3 does not hold what it promises. In practice it is very difficult to obtain a meaningful form of the sheared feed size distribution using the derived equation. As a matter of fact, even using particle size distributions $\Delta F_1(d)$ of shear insensitive particles such as polyvinylacetate it is not possible to obtain the corresponding, measured feed size distribution. For instance although it was possible to predict the mass yield and the supernatant particle size of baker's yeast particles after separation in a disc centrifuge (see section 2.3.5) which agreed well with the measured data, it was not possible to use the actual measured cell distribution of the supernatant and to calculate the corresponding feed size distribution via Equation 3.3. The calculated feed distribution showed no resemblance to the actual measured yeast cell distribution.

The reasons for this disagreement between the measured and calculated distributions lie in the high sensitivity of Equation 3.3 to small errors in the supernatant particle size distribution $\Delta F_1(d)$ which are unavoidable in practice. As the grade efficiency curve approaches unity the value of $\Delta F_s(d)$ becomes very large when the supernatant contains only a few particles more than should be present theoretically. Integration of the sheared feed size distribution, $dF_s(d)$, over all particle sizes gives:

$$\int_{d_{min}}^{d_{max}} dF_s(d) > 1$$

An additional problem is that Equation 3.3 is also sensitive to particle breakup in the clarified liquid discharge. If breakup of aggregates occurs during supernatant discharge then smaller particles than should be present are measured in the supernatant and backcalculation of the sheared feed size distribution results in:

$$\int_{d_{min}}^{d_{max}} dF_s(d) < 1$$

These problems highlight the need for a new approach to estimate the sheared feed size distribution which is insensitive to variation of the particle size distribution in the clarified liquid discharge. A possible solution is provided by the mass yield, since particle breakup in the feed zone will always be accompanied by a significant reduction of the mass yield which will be the lower the higher the degree of breakup. Nevertheless some caution is necessary when interpreting the mass yield results. For instance Table 3.3 shows an increase between the estimated

and measured mass yield with flow rate. However, this increase does not necessarily mean that particle breakup is a function of flow rate, rising with increasing throughput capacities. In practise the relative difference between estimated and measured mass yield values will increase even if particle breakup is invariant to flow rate, because the sheared feed size distribution, containing a larger fraction of small particles is affected differently by the grade efficiency curve, compared to the original feed size distribution upon which calculation of the estimated mass yield is based. In the first case (sheared feed size distribution) a small change of flow rate results in a significant change of the mass yield while in the second case (unsheared feed size distribution) a similar change in the throughput hardly reflects in the mass yield because the particle sizes of the original feed distribution are on average significantly larger than the critical particle size d_c (i.e. sizes above the separation limit) while the particle size distribution after shear breakup is on average close or smaller than the separation limit.

3.5.2.2 Estimation of sheared size distribution using an inversion algorithm

The use of an inversion algorithm as an indirect means to obtain a particle size distribution originates from examinations of the size distributions of natural aerosols in the submicron size range. The common problem is the determination of size distributions from a limited number of experimental observations represented by the weighted integrals of the distribution over all particle sizes. In general the problem can be characterised by the equation:

$$G(y_i) = \int_0^\infty \Phi(x, y_i)\ f(x)\ dx \qquad 3.4$$

where $\Phi(x,y_i)$ is designated as the kernel, $f(x)$ the size distribution function and $G(y_i)$ the value of the integral.

Replacing $G(y_i)$ by the mass yield $E_T(d_c)$, $\Phi(x,y_i)$ by the grade efficiency function $T(d,d_c)$ and $f(x)\,dx$ by the feed size distribution $dE_0(d)$ illustrates that the problem of solving Equation 3.4 is similar to the problem of solving Equation 2.20 which expresses the mass yield as a function of feed size distribution and grade efficiency. In respect to centrifugal separation the basic idea is to measure the emerging mass yield $E_T(d_c)_1$, $E_T(d_c)_2$... for

different grade efficiency functions $T(d,d_c)_1$, $T(d,d_c)_2$... and therefrom, by suitable mathematical manipulation, the particle size distribution $dF(d)$.

The problem lies in finding a suitable mathematical manipulation which allows inversion of the data set $E_T(d_c)_1$, $E_T(d_c)_2$... $E_T(d_c)_n$ to obtain $dF(d)$. In fact one cannot obtain a unique particle size distribution $dF(d)$ and in some way a most acceptable solution from many possibilities needs to be selected. Nevertheless, by means of suitable constraints, solutions can be obtained which give tolerable results if substituted back into the integral on the right-hand-side of Equation 3.4 to give values of $E_T(d_c)_i$ very close to the real values.

A comparison of generic inversion algorithms for characterising particle size distribution has been introduced by Yu and co-workers (1987). Examples of other algorithms and their application are given by Twomey (1975 and 1981) and Gras (1983).

The 'apparent size' method is the algorithm used here in order to obtain the sheared feed size distribution. The chosen algorithm is the simplest to apply but, in some respect, is the most restricted, for in its most widely used form it assumes that the particle size distribution fits to an analytical distribution function such as a normal- or log-normal (see also section 2.3.4). It relies on mean or average values to characterise the particle size distribution and is therefore unsuitable for the detection of bi- or polymodal size distributions.

The solution of Equation 3.4 is given by the roots of the expression:

$$G(y_i)_{meas} - \int_a^b \Phi(x,y_i)\ f(x_g,\sigma_g)\ dx = 0 \qquad 3.5$$

or as far as centrifugal separation is concerned, by:

$$E_T(d_c)_{meas} - E_T(d_g,\sigma_g) = 0 \qquad 3.6$$

where $E_T(d_g)$ represents the estimated mass yield of a feed size distribution (Equation 2.20) characterised by the geometric mean size d_g and the standard deviation σ_g. For a log-normal particle size distribution the geometric mean size d_g and the median size d_m are identical.

If the conditions,

(i) $dF_s(d)$ is log-normal

(ii) σ_g of the unknown distribution is available or instead, if the particle size distribution in the clarified liquid discharge can be obtained

(iii) $T(d)$ is a stable and steady function of particle size

(iv) E_T can be obtained accurately

are met, then the sheared feed size distribution may be determined numerically by obtaining the roots of Equation 3.6. In order to perform this task a computer program was written for an microcomputer using Microsoft Basic as a programming language. The block diagram of the program is given in Figure 3.9. The median particle diameter of the sheared feed size distribution is determined by varying d_g, using the Regula Falsi Algorithm (Bartsch, 1977), until the condition of Equation 3.6 is fulfilled. The results are presented in form of the parameters which characterise the feed size distribution such as median particle size and geometric standard deviation.

In order to verify the possible use of such an inversion algorithm to obtain an estimate of the particle size after feed zone breakup the algorithm was first tested using the data obtained for the separation of polyvinylacetate. Since in this case no breakup of particles occurs the retrieved median particle size should ideally correspond to the one obtained from the measured feed size distribution. The results of this calculation are presented in Table 3.4 which illustrates the good agreement between the median particle sizes of the measured and predicted feed size distribution.

Table 3.5 lists the results obtained for isoelectric protein precipitate and compares the predicted sheared feed size distribution which represents the state of the particle size distribution before entering the disc stack. The results presented show a considerable reduction of the particle size due to particle breakup in the feed zone to the centrifuge. The median particle diameter of the protein precipitate in the feed distribution is reduced by about 44% from 5.3 μm to 2.3 μm while passing through the feed zone.

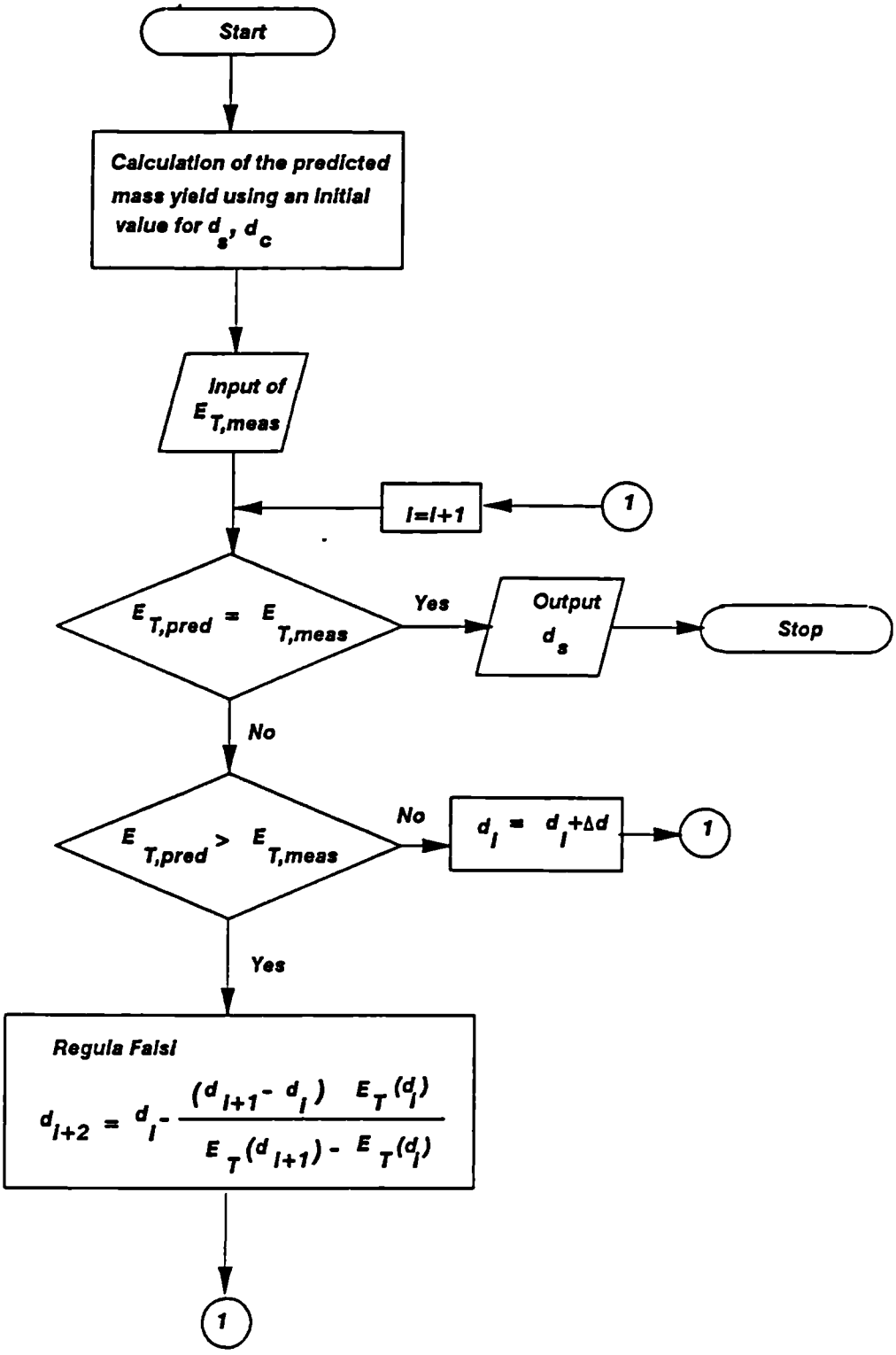

Figure 3.9: Block diagram of the computer program used to solve Equation 3.6 in order to calculate the sheared feed size distribution.

Table 3.4: Predicted and measured median particle diameters of polyvinylacetate particles in feed to disc centrifuge.

Run	Q	$d_{o,pred}$	$d_{o,ave}$	$d_{o,meas}$
/	L/h	µm	µm	µm
V28	300	1.33		
	400	1.31	1.31	1.33
	500	1.29		
	600	1.37		
V29	300	1.25		
	400	1.22	1.21	1.21
	500	1.22		
	600	1.21		
V30	300	1.57		
	400	1.70	1.65	1.63
	500	1.65		
V31	300	1.56		
	400	1.61	1.61	1.62
	500	1.60		
	600	1.64		

$d_{o,pred}$ = predicted median particle size of PVAc in feed

$d_{o,ave}$ = arithm. average of $d_{o,pred}$

$d_{o,meas}$ = measured median particle size of PVAc in feed

inversion was based on: A_e = 598 m²

$\Delta\rho$ = 190 kg m^{-3}

μ = 1.0 cP

Table 3.5: Predicted median particle diameters of isoelectric protein precipitate before and after shear breakup in full-hermetic feed zone to disc centrifuge.

Run	Q	d_s	$d_{s,ave}$	$d_{o,meas}$
/	L/h	µm	µm	µm
V36	300	2.59		
	400	2.24	2.35	5.26
	500	2.32		
	600	2.23		
V38	300	2.42		
	400	2.42	2.31	5.38
	500	2.20		
	600	2.20		

d_s = sheared median particle size

$d_{s,ave}$ = arithm. average of sheared median size, d_s

$d_{o,meas}$ = median size of protein precipitate in feed

inversion was based on: A_s = 598 m^2

$\Delta\rho$ = 90 kg m^{-3}

μ = 1.0 cP

4. The examination of different feed zone designs in respect to shear associated particle breakup

4.1 Objective

The objective of this section is to apply the two model particle systems to compare the full-hermetic with the semi-hermetic and a newly developed hydro-hermetic feed zone design. The aim is to quantify the separation performance of disc centrifuges equipped with various feed zone designs using shear sensitive particles and in particular to examine the separation performance of the newly designed hydro-hermetic feed zone in respect to particle breakup.

4.2 Description of the various feed zone designs

The feed zone to a centrifuge is composed of mainly two parts, the cylindrical feed pipe and the distributor. The feed suspension is fed into the rotating bowl via a cylindrical feed pipe, is then tangentially accelerated in the cylindrical part of the distributor (distributor neck) and by radial ribs located in the conical part of the distributor (distributor foot) and finally, the feed suspension is distributed evenly across the disc stack. According to the design of the feed and clarified liquid discharge zone three types of intermittent discharge disc stack centrifuges may be distinguished.

4.2.1 The semi-hermetic disc centrifuge

This type of centrifuge is called semi-hermetic because it is only hermetic in respect to the clarified liquid discharge. The ingoing suspension is fed into the rotating bowl via a stationary feed pipe (Figure 4.1). Discharge of the clarified liquid is aided by means of a stationary centripetal pump which is immersed into the rotating supernatant. The fluid flows through channels from the outside to the inside of the disc and the rotational energy of the fluid is transformed into pressure energy. The pressure produced is a function of rotational speed of the bowl, the external diameter of the centripetal pump and the depth of immersion of the stationary centripetal pump into the rotating

liquid circle. An increase of the hydraulic throughput capacity will also increase the depth of immersion which in turn results in an increased pumping rate of the centripetal pump, i.e. within certain limits the centripetal pump adjusts itself automatically to changes of the hydraulic throughput capacity. Figure 4.2 shows a schematic diagram of a semi-hermetic disc centrifuge. By means of a throttle valve in the discharge line a back-pressure is created which suppresses foam formation and avoids the release of aerosols into the environment. The distributor itself is not completely filled with suspension but only to a radius which depends on the depth of immersion of the centripetal pump and the hydraulic resistance of bowl and disc stack to fluid flow. The higher the back-pressure the deeper the immersion of the centripetal pump. However, the level of back-pressure is limited by overflow of the discharge liquid into the space surrounding the bowl (centripetal pump overflow).

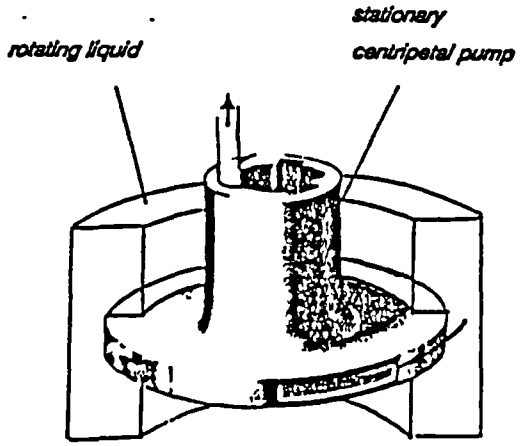

Figure 4.1: Operating principle of centripetal pump.

Attention needs also be paid to the hydraulic capacity of the centrifuge which determines the flow that can be handled just before the distributor starts overflowing (distributor overflow). The physical meaning of this is that as the hydraulic throughput capacity is increased the radius of the air/liquid interface in the open distributor will move towards the axis of rotation until it becomes smaller than the inner radius of the distributor. The results is overflow of the distributor and, as described before, liquid discharge into the space surrounding the bowl.

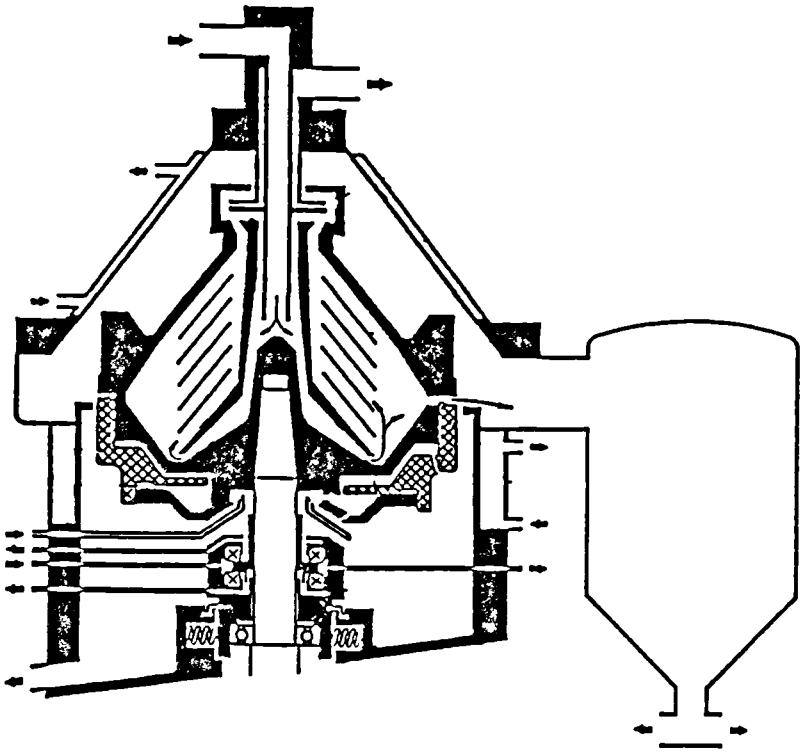

Figure 4.2: Semi-hermetic version of intermittent disc-stack centrifuge (Type BSB 7, Westfalia Separator, Germany).

The merits of the semi-hermetic feed zone design is the absence of seals allowing the machine to run dry, i.e. without feed suspension flowing through it, and the ease of operation. Air-liquid interfaces in the outlet line are reduced to a very small area represented by the cylindrical surface of the rotating liquid ring. Its major disadvantage is the fact that the feed suspension is subjected to very harsh conditions inside the distributor which includes air-liquid interfaces, impingement of the feed suspension on the rotating stainless steel walls and sudden acceleration at and along the ribs of the distributor which are thought to inflict significant damage and breakup of shear sensitive material entering the centrifuge.

4.2.2 The full-hermetic disc centrifuge

The main characteristic of the full-hermetic disc centrifuge is the mechanical seals used to separate the feed and outlet lines from each other and from the space surrounding the bowl (Figure 4.3). Contact between the two liquid streams is avoided by the use of three rubber seals. A further characteristic of the full-hermetic design is the rotating, cylindrical feed pipe which together with the mechanical seals enables the

centrifuge to be completely filled with liquid to the centre of the bowl at all times (except during solids discharge) thereby avoiding air-liquid interfaces. Other advantages of the full-hermetic feed zone design may be summarised as follows:

1. it may be used in pressurized process lines

2. it is better for use where the suspension is: (i) susceptible to oxidation, (ii) of low volatility, or (iii) contains dissolved gases.

3. it offers a gentler feed system for shear sensitive solids because the initial impact upon the particles entering the rotating bowl is avoided.

4. the potential foaming of fluid systems containing soluble proteins is completely suppressed. Foaming is caused by protein-oxygen-compounds which arise from the destruction of natural protein-OH-compounds in the presence of air-liquid interfaces (Hemfort, 1987).

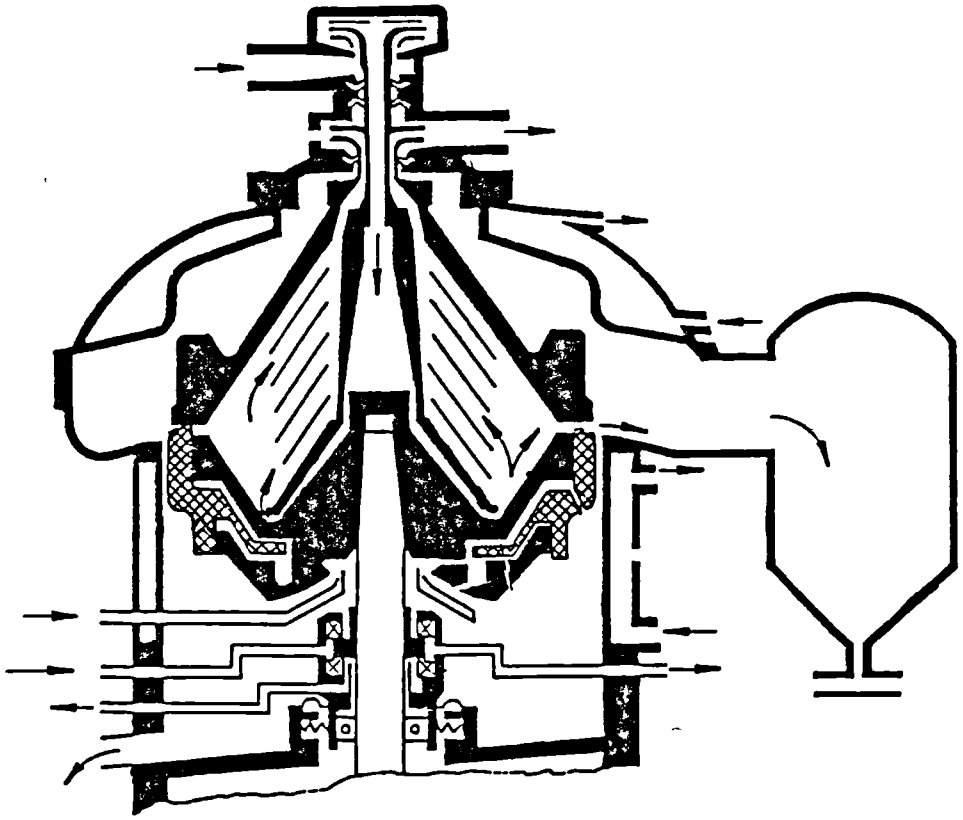

Figure 4.3: Full-hermetic version of intermittent disc-stack centrifuge (Type BSB 7, Westfalia Separator, Germany).

Discharge of the clarified liquid is performed at the top of the bowl near the centre line via a rotating discharge pump. The action of the discharge pump is similar to that of a centrifugal pump. The fluid flows through the vanes of a rotating impeller from a small diameter to a larger diameter increasing the kinetic energy of the discharge liquid. Using a throttle valve located in the discharge line the kinetic energy is transformed into pressure energy which causes the lip seals located in the outlet line to be pressed against the rotating feed pipe thereby facilitating sealing of the feed and outlet lines from each other. Furthermore, the discharge pump also enables the transport of the fluid away from the centrifuge. Reducing the pressure in the outlet line below a certain minimum value (approximately 1 bar gauge) causes penetration of air into the discharge liquid from the space surrounding the bowl. The entry of air into the system can easily be detected by the presence of air bubbles in the outlet line.

The major disadvantage of this type of centrifuge is that it relies on the sealing power of the mechanical seals. In practice the rubber lip seals need to be cooled at all times by the feed suspension and are susceptible to wear and tear and require regular attention. Damaged seals cause liquid to flow from the region of high pressure (usually the discharge line) to the region of low pressure (the feed line) causing internal liquid circulation and as a result loss of separation performance. Under no circumstances should the centrifuge be allowed to operate dry i.e. in a state without feed or water running through it, because this causes considerable damage to the lip seals and necessitates their immediate replacement. In practice a minimum flow rate of 50 L h^{-1} is required to provide sufficient cooling of the lip seals.

4.2.3 The hydro-hermetic disc centrifuge

The hydro-hermetic version combines both the advantages of the full-hermetic and of the semi-hermetic disc centrifuge. As for the semi-hermetic feed zone design the feed suspension is fed into the rotating bowl via a stationary feed pipe. Discharge of the clarified liquid is performed by means of a centripetal pump. However, in contrast to the semi-hermetic feed version the bowl is filled to the centre with feed suspension, just like the full-hermetic centrifuge, but with the advantage of no mechanical seals being present which are used to separate the feed

and outlet streams. Since the feed suspension is injected into a liquid filled distributor the conditions experienced by the entering suspension are thought to be far less violent compared with the semi-hermetic feed zone design. The formation of air-liquid interfaces is also reduced to a small area created by the free surface of the liquid circle around the rip-body in the upper neck section of the distributor.

The basic design of hydro-hermetic disc centrifuge type is very similar to the semi-hermetic centrifuge. The only significant difference lies in the so-called rib-body and the hydro-hermetic disc which are located in the neck-section of the distributor (Figure 4.4). This rip-body enables the feed suspension to fill the space underneath the hydro-hermetic disc to the centre and to immerse the stationary feed pipe into the feed suspension. Diagrams showing different rib-body designs are given in the experimental section of this chapter. Furthermore and in contrast to the full- and semi-hermetic feed types, the walls in the neck-section of the distributor are not equipped with axial ribs and are very smooth.

The function of the rib-body is to compensate the pressure generated by the radial ribs located in the conical foot-section of the distributor. Otherwise this pressure would cause overflow of the feed suspension out of the distributor. Due to the ribs of the rib-body the fluid rotates with the same angular velocity as the bowl generating a sealing liquid circle above the hydro-hermetic disc between the wall of the distributor and the stationary feed pipe.

In order to ensure proper functioning of the hydro-hermetic feed zone the centrifuge has to be operated within distinct boundaries which are determined by the pressure in the feed and discharge line and the hydraulic throughput capacity at which the machine is operated. Operation is limited by the following events:

(i) the feed pipe is not immersed in the feed suspension because the feed pressure is too low.

(ii) distributor overflow occurs because the feed pressure is too high.

(iii) centripetal pump overflow occurs because the clarified liquid discharge pressure is too high.

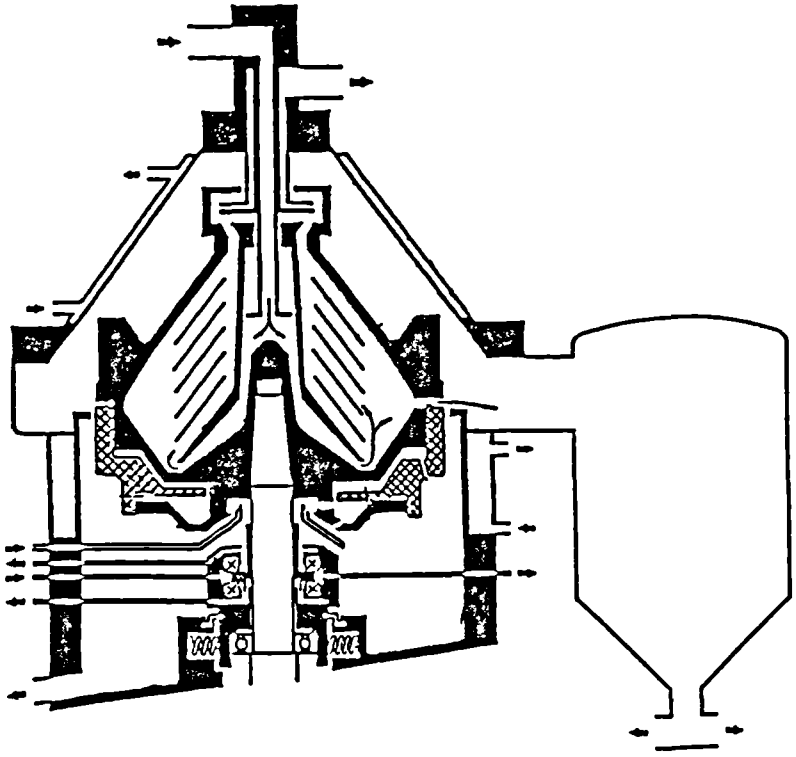

Figure 4.4: Hydro-hermetic version of intermittent disc-stack centrifuge (Type BSB 7, Westfalia Separator, Germany).

The typical range of operation of a BSB 7 type centrifuge equipped with a hydro-hermetic feed zone is illustrated in Figure 4.5. The disc centrifuge can be operated safely in respect to separation performance within the hatched area of the two diagrams. As the diagram indicates overflow of the discharge pump is more likely at low hydraulic capacities while distributor overflow occurs mainly for high throughput capacities. In practice the machine should be operated between the two boundary conditions given by the immersion of the hydro-hermetic disc and overflow of the feed or discharge liquid. For example at a hydraulic throughput capacity of 750 L h^{-1} the minimum feed pressure at which the centrifuge can be operated is approximately 0.5 bar (gauge), whereas the maximum feed pressure is approximately 1.7 bar (gauge). For the same conditions the discharge pressure may vary between the boundaries given by 0.7 bar and 2.5 bar (gauge) respectively. If the machine is operated in the middle of these boundary conditions then small changes in the pressure conditions have no effect on the operation of the centrifuge. During the examination of the hydro-hermetic feed disc stack centrifuge in respect to shear-associated particle breakup three design models of the rib-body were investigated. Considering the flow of the feed suspension in, out and around the vicinity of the rip-body it is thought that the it may act like an impeller which is rotating at a very high velocity (more than 9000 rpm) causing even more

damage to shear-sensitive particles than the distributor without the hydro-hermetic assembly. Therefore three different types of rib-body designs, of which one is shown in Figure 4.6, were manufactured and tested using shear-sensitive protein precipitate particles. The different rib-body design are conveniently defined as follows:

1) Rib-body design A which has the same dimensions as the design illustrated in Figure 4.6 but consists of 6 long ribs with sharp edges.

2) Rib-body design B which is the one actually illustrated in Figure 4.6 and in contrast to design A consists of four long ribs with rounded edges.

3) Rib-body design C which again is similar to the one shown but this time the rib-body consists of four short ribs (Length: 25 mm) with rounded edges.

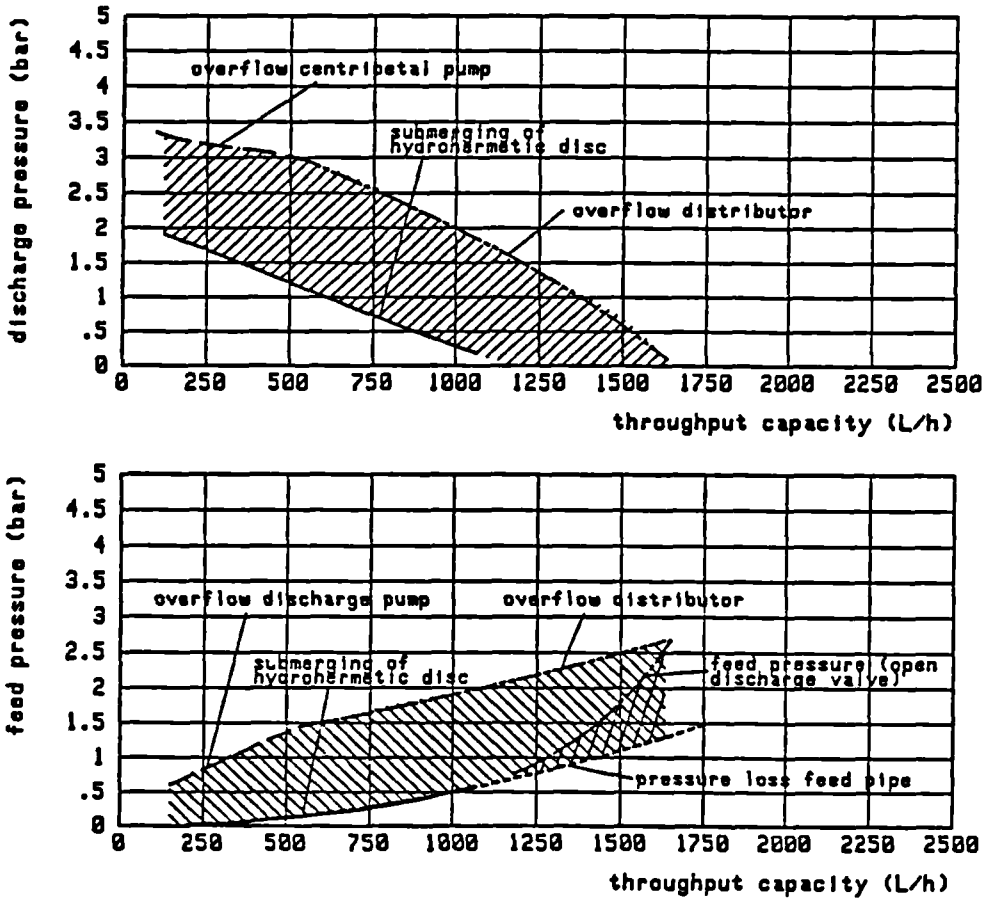

Figure 4.5: Practical operating area of hydro-hermetic disc stack centrifuge (Type BSB 7, Westfalia Separator, Germany).

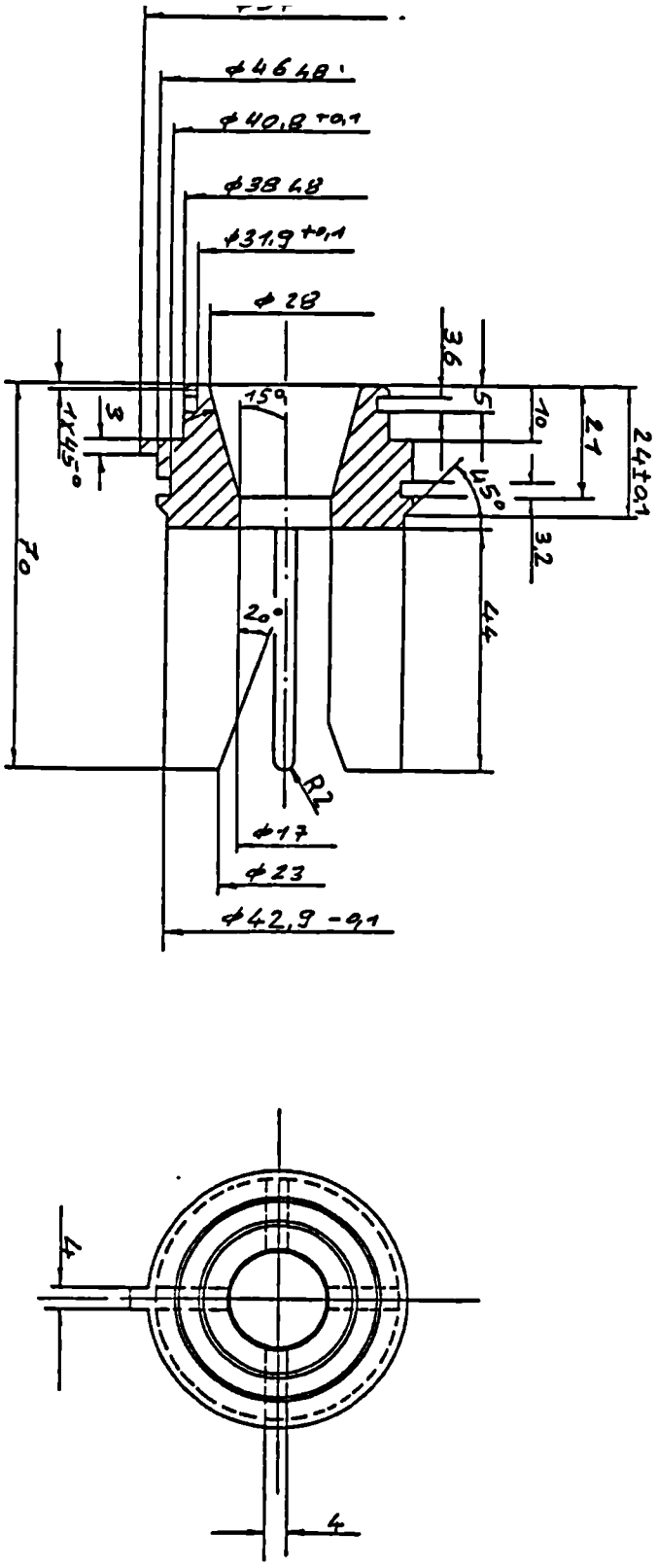

Figure 4.6: Sectional view of rib-body used in hydro-hermetic disc centrifuge (Design version B).

4.3 Experimental

4.3.1 Preparation of feed suspension

4.3.1.1 Polyvinylacetate suspension

The feed suspension containing approximately 0.5 g L^{-1} polyvinylacetate was prepared as follows.

0.125 kg of polyvinylacetate (Mowilith D 50, Hoechst AG, Frankfurt, W.-Germany) were dispersed in 0.8 L of water (purified by reverse osmosis) and then diluted in an ultrasonic bath to give a final liquid volume of 8 L. Potential agglomerates of polyvinylacetate particles were disrupted by ultrasonic conditioning of the suspension for approximately one hour. In order to reduce heating of the suspension during the conditioning process the suspension was cooled by means of a cooling device circulating coolant through a heat exchanger placed in the suspension (coolant temperature: 0°C). Prior to experimentation the suspension was diluted further in a pressure vessel (working volume: 400 L) containing 250 L of tap water. A slowly rotating paddle impeller (90 rpm) was used to ensure adequate dispersion of polyvinylacetate particles in the suspension.

4.3.1.2 Isoelectric soya protein precipitate suspension

Total water extract

Preparation of the water extract containing approximately 3 kg m^{-3} soluble protein was performed as follows: 0.25 kg of soya flour (Soya Fluff Basic, Interfood Ltd., Hemel Hempstead, U.K.) was dispersed in 5 L of water (from reverse osmosis) by means of a 6-blade Rushton turbine impeller (i.d. 50 mm) rotating at an impeller speed of 1000 rpm. To extract the soluble protein approximately 20 mL of 10% (w/w) sodium hydroxide solution (Merck Chemicals, Darmstadt, W.-Germany) was added until pH 9.2 was reached (Knick pH-meter, Model PORTACON 652-1X, Berlin, W.-Germany). Then the impeller speed was reduced to 800 rpm and the suspension was aged for further 0.5 hours.

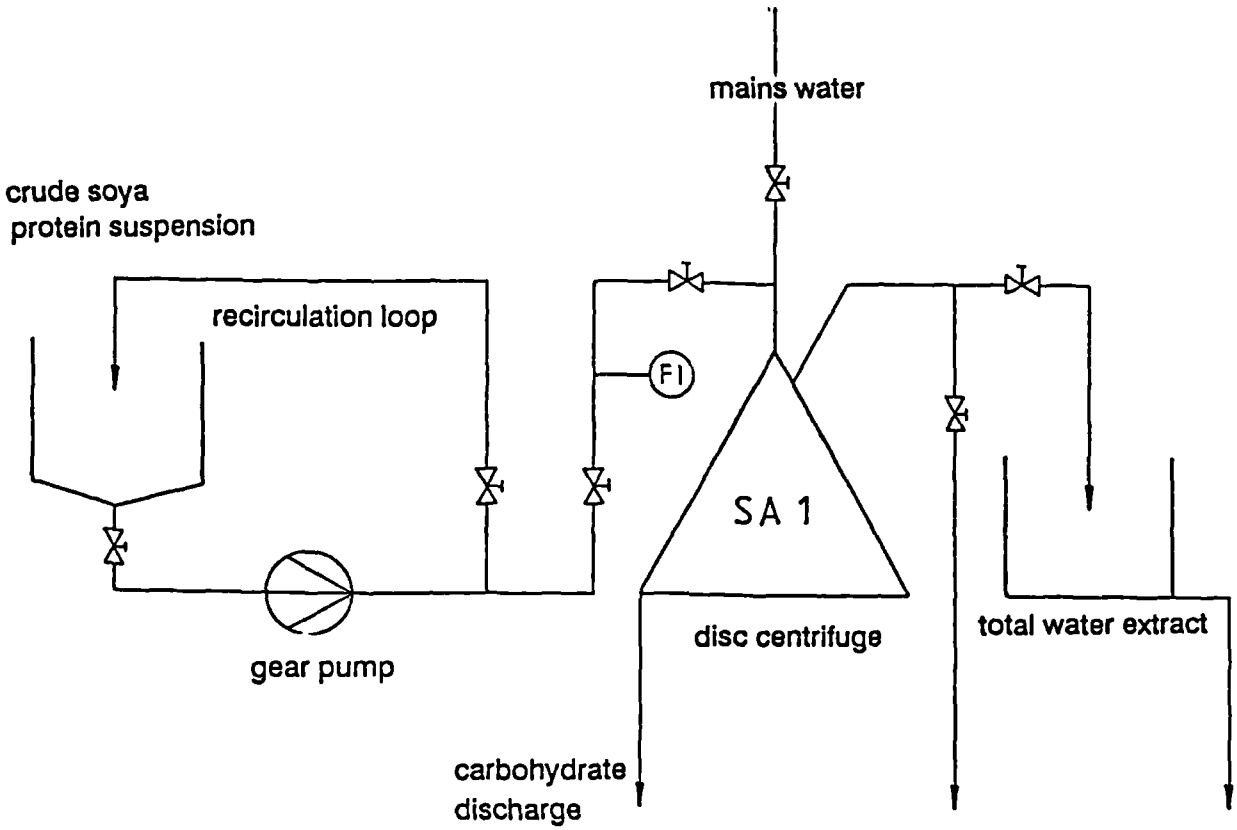

Figure 4.7: Experimental setup of total water extract preparation.

The experimental setup used to separate the insoluble carbohydrates and proteins from the soluble protein fraction is shown in Figure 4.7 which consists of a small intermittent disc centrifuge (Model SA 1, Westfalia Separator, Oelde, W.-Germany), a gear pump, a feed and discharge collecting vessel and a rotameter to monitor the hydraulic throughput through the separator. At first the whole system was cleaned with water circulating through the centrifuge and the connecting pipe work. After cleaning of the centrifuge the water was removed by discharging the machine several times. Then the feed tank was filled with 5 L of clean tap water and the pH of the water adjusted to 9.2 using a few drops of concentrated sodium hydroxide solution while it was circulating through the centrifuge. During water circulation the clarified liquid discharge was fed back into the feed vessel. The flow rate of 40 L h^{-1} was maintained using a by-pass control loop with one branch leading back to the feed vessel and the other branch leading to the disc centrifuge (Figure 4.7). The discharge pressure was adjusted and kept constant at a value of 1 bar.

Once water circulation was stable, 5 L of the prepared protein extract were diluted into the feed vessel. Mixing of the feed vessel was maintained by the circulating feed suspension. After 5 L of suspension had passed through the centrifuge, samples of the feed and the clarified liquid discharge were collected and analysed for their solids content. Then the flow of suspension was switched to tap water and the solids were removed from the sediment holding space using the intermittent discharge mechanism of the centrifuge.

After displacing the water from the sediment holding space, separation of the insoluble solids fraction continued until all the suspension was used up. The protein content of the clarified liquid discharge was determined using the Biuret technique. On average the feed to the disc stack centrifuge contained approximately 5 to 6 vol% solids (wet weight) while the solids content in the clarified liquid discharge was < 0.03 vol%. The protein content of the prepared total water extract was approximately 9 to 11 kg m^{-3}. The water extract was diluted further to the required protein concentration using tap water (pH=9.2). The amount of water required was determined by:

$$V_w^* = \frac{V_{tw} \cdot C_{tw}}{C_x} - V_{tw}$$

where V_w is the required water volume (L), V_{tw} is the volume of the

protein extract (L), C_{tw} is the protein concentration of the prepared water extract (mg/ml) and C_x is the required protein concentration after dilution (mg/ml).

Isoelectric precipitation of soya protein

Isoelectric precipitation of the soluble soya protein was performed according to the same technique which has already been described in section 3.3.2.2 of this thesis. The efficiency of precipitation which is defined as the ratio of the soluble protein concentration after acid addition to the concentration of soluble protein before precipitation was in the order of 75 to 80%.

After precipitation and ageing for 0.5 hours, the precipitate suspension was diluted in 250 L of 0.07 M sodium acetate buffer (pH 4.8) which was prepared by dissolving 400 g of sodium hydroxide pellets in 250 L of tap water and the addition of approximately 1.8 - 2.0 L of glacial acetic acid (Merck Chemicals, Darmstadt, W.-Germany) until pH 4.8 was reached. In order to minimize particle breakup transfer of the precipitate suspension from the precipitator (see Figure 3.2) into the feed vessel was carried out via a wide diameter pipe (i.d. 50 mm) which was immersed into the buffer solution.

4.3.2 Experimental setup

In order to examine different feed zone designs independent of the exact physico-chemical nature of the testing material two separators of exactly the same specifications were setup in such a way that they could be supplied with the suspension from the same feed vessel (Figure 4.8). Since it was not possible to feed the same suspension to two different feed zone designs at the same time the machines were operated in sequence. For this reason it was necessary to ensure a very rapid switch-over from one machine to the other. In view of the use of shear sensitive particles transport of the feed suspension to the centrifuge was designed as soft as possible. Pumps and valves were avoided in the feed line and the feed suspension was pushed through the centrifuges by using air to pressurise the feed vessel. The hydraulic throughput capacity was

controlled by means of increasing or reducing the feed pressure and a valve situated in the clarified liquid discharge line.

In order to limit the time necessary to obtain stable operation of the machines basic pressure and throughput adjustment were performed while water (from tap) was flowing through the centrifuges. Afterwards, by operating a ball valve, feed was switched rapidly from water to product flow. In order to avoid product damage during the sampling process it was necessary to collect feed and discharge samples by means of a by-pass assembly.

4.3.3 Experimental procedure

In the following section the experimental procedure, which is invariant of the feed suspension, will be explained in detail using a specific example. In order to ensure consistent feed product specifications only one hydraulic throughput capacity was examined for both machines at a time. In other words for a given flow rate samples were collected for both machines and analysed before a new flow rate was adjusted. Since the operating and product conditions are exactly the same for both centrifuge versions, potential difference of separation performance when using shear sensitive particles may then solely be attributed to the varying level of shear of the different feed zone designs.

For convenience the disc centrifuge equipped with the full-hermetic feed version shall simply be termed SEP1 in the subsequent text while the disc centrifuge with either the hydro-hermetic or with the semi-hermetic feed version shall simply be called SEP2. As mentioned earlier in order to avoid damage the lip seals (used to separate the feed from the outlet line from each other and from the space surrounding the bowl in the full-hermetic disc centrifuge) need to be constantly cooled with liquid and the pressure in the clarified liquid discharge line should not exceed 8 bar (gauge). The hydraulic throughput capacity through the centrifuges was measured using magnetic-inductive flow meters (Fischer & Porter, Göttingen, W.-Germany). The corresponding pressure in the feed and outlet lines were measured using electric pressure transducers. The valve position belonging to the various centrifuge operating stages given by (i) start-up of disc centrifuges with fresh water, (ii) feed zone examination using SEP2, (iii) feed zone examination using SEP1 are best summarised in tabular form.

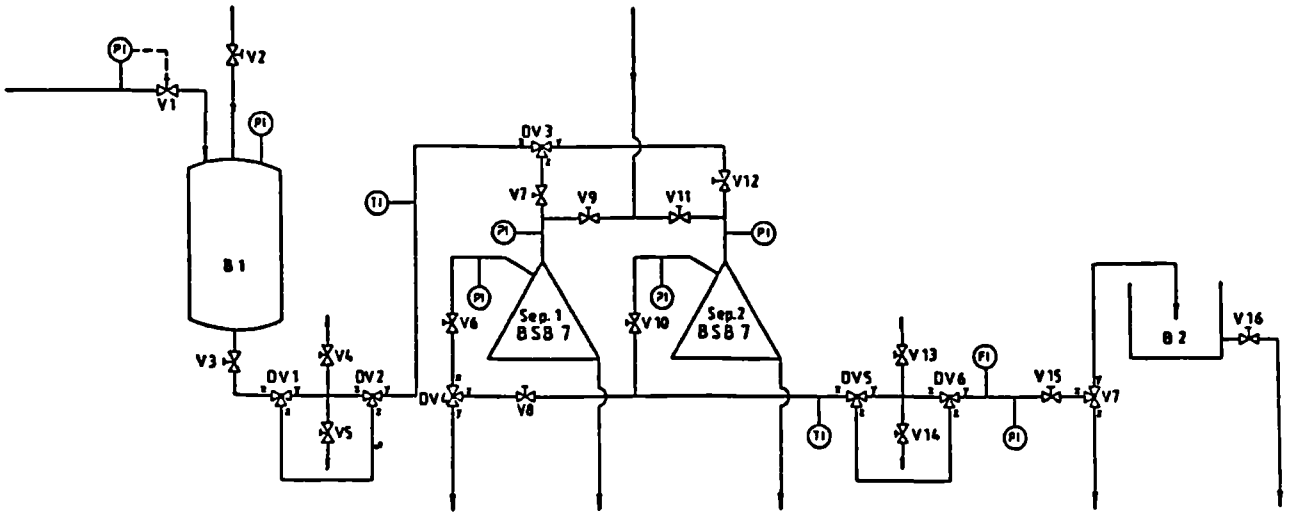

Figure 4.8: Experimental setup for the study of the shear associated particle breakup in different feed zone designs.

(i) Start-up of disc centrifuges using fresh water

Valve No	closed	open
V 1	*	
V 2	*	
V 3	*	
V 4	*	
V 5	*	
V 6		*
V 7	*	
V 8	*	

Valve No	closed	open
V 9		*
V 10		*
V 11		*
V 12	*	
V 13	*	
V 14	*	
V 15		*
V 16	*	

Three way valve No	direction x	direction y	direction z
DV 1	*	*	
DV 2	*	*	
DV 3	*	*	
DV 4	*	*	
DV 5	*	*	
DV 6	*	*	
DV 7	*		*

The hydraulic throughput capacity of fresh water flowing through both centrifuges was approximately 400 L h^{-1}. The clarified liquid discharge pressure of SEP1 was adjusted to approximately 4 bar (gauge) using valve V 6 which is located in the discharge line.

(ii) Feed zone examination of SEP2

Valve No	closed	open	Valve No	closed	open
V 1		*	V 9		*
V 2	*		V 10		*
V 3		*	V 11	*	
V 4	*		V 12		*
V 5	*		V 13	*	
V 6		*	V 14	*	
V 7	*		V 15		*
V 8	*		V 16	*	

3-way valve No	direction x	direction y	direction z
DV 1	*	*	
DV 2	*	*	
DV 3	*	*	
DV 4	*	*	
DV 5	*	*	
DV 6	*	*	
DV 7	*		*

In order to examine the effect on particle breakup of the hydro-hermetic feed zone, pressure inside the feed vessel was increased to 0.6 bar (gauge). The permissible pressure range depends on the working area of the hydro-hermetic disc centrifuge (Figure 4.5). After switching valve V 7 from water to product flow valve V15 is used to adjust and regulate the hydraulic product flow rate through the centrifuge. Then the 3-way valve DV 7 is switched from direction x - z to x - y. Once approximately 20 L of liquid has passed through the centrifuge feed, discharge samples are collected. For this purpose the two 3-way valves DV 5 and DV 6 are switched in direction x - z and z - y. The discharge sample is collected

first by opening valve V 13 (vent) and then by opening valve V 14. The feed sample is collected accordingly by switching the 3-way valves DV 1 and DV 2 in direction x - z and z - y and opening of valves V 4 (vent) and V 5. This procedure ensures that potential particle breakup during the sampling process is reduced to a minimum.

After the samples are collected the valves are switched back to fresh water operation and the separator is rinsed and completely discharged (solids discharge line) for at least three times. Vessel B 2 which is used to collect and measure the volume of the clarified liquid discharge is emptied by opening valve V16.

Examination of the semi-hermetic feed zone version is performed according to exactly the same procedure. However, the pressure in the feed vessel is only increased to approximately 0.2 bar (gauge) since otherwise overflow of the clarified liquid discharge occurs.

(iii) Feed zone examination of SEP1

In order to examine the full-hermetic feed zone version the pressure inside the feed vessel is increased to approximately 2.4 bar (gauge). Before feed is switched from fresh water to product valve V 6 is opened completely and the required hydraulic throughput capacity is adjusted using valve V 15. After switching to product flow the centrifuge is vented and the hydraulic throughput capacity is re-adjusted to its desired value.

The 3-way valve DV 7 is switched from direction x - z to x - y. Once approximately 20 L of liquid have passed through the centrifuge feed and discharge samples are collected. For this purpose the 3-way valves DV 5 and DV 6 are switched in direction x - z and z - y. The discharge sample is collected first by opening valve V 13 (vent) and then by opening valve V 14. The feed sample is collected by switching the 3-way valves DV 1 and DV 2 in direction x - z and z - y and opening of valve V 4 (vent) and V 5.

After the samples are collected the valves are switched back to fresh water operation and the separator is rinsed and completely discharged (solids discharge line) for at least three times. Vessel B 2 which is used to collect and measure the volume of the clarified liquid discharge is emptied again by opening valve V 16.

Valve No	closed	open	Valve No	closed	open
V 1		*	V 9	*	
V 2	*		V 10	*	
V 3		*	V 11	*	
V 4	*		V 12	*	
V 5	*		V 13	*	
V 6		*	V 14	*	
V 7		*	V 15		*
V 8		*	V 16	*	

3-way valve No	direction x	direction y	direction z
DV 1	*	*	
DV 2	*	*	
DV 3	*		*
DV 4	*		*
DV 5	*	*	
DV 6	*	*	
DV 7	*		*

4.3.4 Scale-down of disc centrifuge

Scale-down of the disc centrifuge was accomplished by using the same method and materials already described in section 2 of this thesis. In order to use small quantities of testing material the equivalent separation area was reduced from originally 6400 m^2 to 625 m^2, 1250 m^2 and 1875 m^2 respectively by replacing parts of the separating discs with blank aluminium inserts (see Figure 2.1.). In order to maintain a constant specific throughput capacity in the range of 0.3 L/(h m^2) to 0.8 L/(h m^2), the throughput capacity was also raised with increasing separation area.

Based on the experience gained on the previously described scale-down trials, the position of the separating discs was kept constant on top of the small blank insert (Figure 2.5 C) for all experiment.

4.3.5 Particle size analysis

Particle size analysis was performed using an Elzone 180 XY particle sizing instrument (Particle Data Europe, A.A.R.L., Luxemburg) applying the electric zone sensing technique (see section 2.2.1.1).

Particle size analysis of the polyvinylacetate suspension was accomplished by dispersing 1 mL of the particle sample in 50 mL of 10% (w/w) sodium chloride electrolyte (0.02 µm filtered) and by using a 12 µm orifice capillary. Measurement was performed at a vacuum pressure of 160 mbar and a automatic stop time was 20 s giving a measurable particle size range in the order of 0.5 to 5 µm.

Particle size analysis of the protein precipitate particles was performed by dispersing 1 mL of the particle sample in 50 mL of 0.07 M sodium acetate buffer (pH 4.8, 0.02 µm filtered) and by using a 24 µm orifice capillary. As previously, the vacuum pressure was adjusted to 160 mbar and the automatic stop time was 20 s giving a measurable particle size range in the order of 0.8 to 12 µm.

Evaluation of the particles size analysis data, including calculation of the mass yield and the grade efficiency curve, was performed automatically using a Hewlett-Packard workstation (HP 9000 series).

4.4 Results

As mentioned earlier the primary objective of this investigation was to examine the contribution of the feed zone design to particle breakup. In section 3.5.2.1 it has been shown that the degree of particle breakup is directly reflected in a comparable loss of mass yield. Therefore if two separators of exactly the same specification are operated using identical operating conditions, the same feed product, but equipped with different feed zones then the difference in the mass yield could then be used as a measure for the level of particle breakup in the respective feed system.

It is obviously not possible to apply this approach if the feed zone changes the grade efficiency curve measured using shear-insensitive polyvinylacetate particles. From theoretical considerations the feed zone should have no influence on the performance of the disc stack centrifuge. In practice, however, different designs may alter the conditions of the feed suspension on entry to the disc stack. For these reasons extensive examination of the effect of feed zone design and centrifuge operation on the grade efficiency curve were necessary prior to the studies using protein precipitate.

Among the parameters examined were different levels of equivalent separation area ranging from 625 m^2 to 1875 m^2, different hydraulic throughput capacities (200 L h^{-1} to 1200 L h^{-1}), and for the hydro-hermetic feed zone different rib-body designs and two bowl speed settings of 7800 rpm and 9350 rpm. Another important feature was to examine the reproducibility of the grade efficiency curve trials. Obviously there was little point in applying this method of mass yield comparison if reproducibility i.e. similar grade efficiency curves for the same experimental conditions, could not be guaranteed.

Owing to the way the experiments were performed and the use of the relative mass yield (full-hermetic feed zone = 1) to describe the level of particle breakup, the exact physical nature of the protein precipitate was irrelevant to evaluation and interpretation of the results.

4.4.1. Results obtained using polyvinylacetate particles

Table A1 given in the Appendix lists the various operating conditions applied during the separation of a polyvinylacetate suspension using BSB 7 type disc centrifuges equipped with different feed zone types. Included in the table are all important results related to the separation performance of the centrifuge.

Figure 4.9 shows the grade efficiency curves obtained for the full-hermetic, hydro-hermetic and semi-hermetic disc centrifuge operated at various specific throughput capacities ranging from 0.32 L/(h m²) to 0.64 L/(h m²). Included in the graph is the theoretical grade efficiency curve determined according to Equation 1.19 (Stokes Law). The symbols represent the arithmetic mean value of at least three grade efficiency values for a given feed zone design and specific throughput capacity. The regression curve drawn through the data points was obtained by taking the arithmetic average of the corresponding values of the correlation model parameters k and n which were calculated utilising the two-parameter fitting routine described in section 2.3. The curves indicate that for a given specific throughput capacity, the grade efficiency curve is invariant to the design of the feed zone, as there is very little noticeable deviation of the data points from a single line. Comparing the curves obtained for different specific throughput capacities shows that the grade efficiency decreases slowly with increasing values of q_m. This observation is supported by a corresponding drop of the correlation parameter k and n. The deviation of the grade efficiency curve from the Stokes curve is typical for the used position (position C; Figure 2.5) of the blank inserts and compares well with earlier results described in section 2.3.3.

Plotting the two model parameters k and n of all experiments against the specific throughput capacity on semi-logarithmic paper then the following relationship can be obtained:

$$k = -0.116 \ln(q_m) + 0.718$$
$$n = -0.863 \ln(q_m) + 1.687 \qquad 4.1$$
$$\text{for } 20 \text{ L/(h m}^2) < q_m < 100 \text{ L/(h m}^2)$$

In order to calculate the mass yield based on separator specifications, operating conditions and the physical properties of feed product (polyvinylacetate suspension) Equation 4.1 was used in conjunction with

Equation 2.22. The results of this calculation is compared with the measured mass yield obtained in all trials and is given in Table A1 (Appendix).

Figure 4.10 shows the grade efficiency curves obtained for three equivalent clarification area sizes increasing from 625 m^2 to 1875 m^2. The change of the separation area was brought about by varying the number of separating discs in the disc stack. The Figures are similar to the one shown previously since Figures 4.10 implicitly contains changes of the equivalent clarification area dimension.

The disc centrifuges were operated at various specific throughput capacities ranging from 0.32 L/(h m^2) to 0.64 L/(h m^2). Included in the graph is the theoretical grade efficiency curve determined according to Equation 1.2.19 (Stokes Law). The symbols represent the grade efficiency values of a chosen feed zone design determined for this particular specific throughput capacity and equivalent separation area. The regression curve drawn through the data points was obtained using the corresponding values of the correlation parameters k and n.

The curves indicate that in accordance with theory, for a given specific throughput capacity, the grade efficiency curve is invariant to the number of separating discs in the disc stack i.e. the separation area. As before, comparing the curves obtained for different specific throughput capacities reveals that the grade efficiency decreases slowly with increasing values of q_m.

The experimental reproducibility is illustrated in Figure 4.11 which shows the grade efficiency curves obtained at different days of experimentation but applying the same experimental conditions. The figures show some representative examples of different feed zone designs, equivalent separation area dimension and specific throughput capacities. The regression line was calculated using the arithmetic average of the corresponding model parameters k and n.

It appears that the reproducibility of the performed grade efficiency determination experiments is sufficiently good in order to ensure the correct application of the dimensionless grade efficiency function. It is observed that the scatter of the grade efficiency values increases with increasing specific throughput capacities. However, calculations have shown

that the effect of data scattering on the calculation of the overall mass yield is negligible.

Another approach to reduce the equivalent separation area is to decrease the centrifugal force acting upon the settling particle by operating the centrifuge at a lower angular bowl velocity. The corresponding dimensionless grade efficiency curve obtained in such an experiment is illustrated in Figure 4.12 which shows the grade efficiency as a function of the dimensionless particle diameter and angular bowl velocity. In the described experiments the bowl speed was decreased from 9350 rpm (A_Σ = 625 m^2) to 7800 rpm (A_Σ = 435 m^2) using a frequency-controlled variable speed drive.

The results shown in Figure 4.12 indicate that for both the full-hermetic as well as for the hydro-hermetic disc centrifuge a reduction of the angular bowl velocity has no consequences on the course of the dimensionless grade efficiency curve. In terms of the relative mass yield, $E_{T,rel}$, the results obtained so far mean, that for a given shear insensitive particle suspension, separated in disc centrifuges of exactly the same specification, but fitted with different feed zone designs, operated at comparable operating conditions, the relative mass yield should be close to unity. This conclusion is illustrated in Figure 4.13, where the relative mass yield obtained using the semi-hermetic and hydrohermetic disc centrifuge is plotted for different specific throughput capacities.

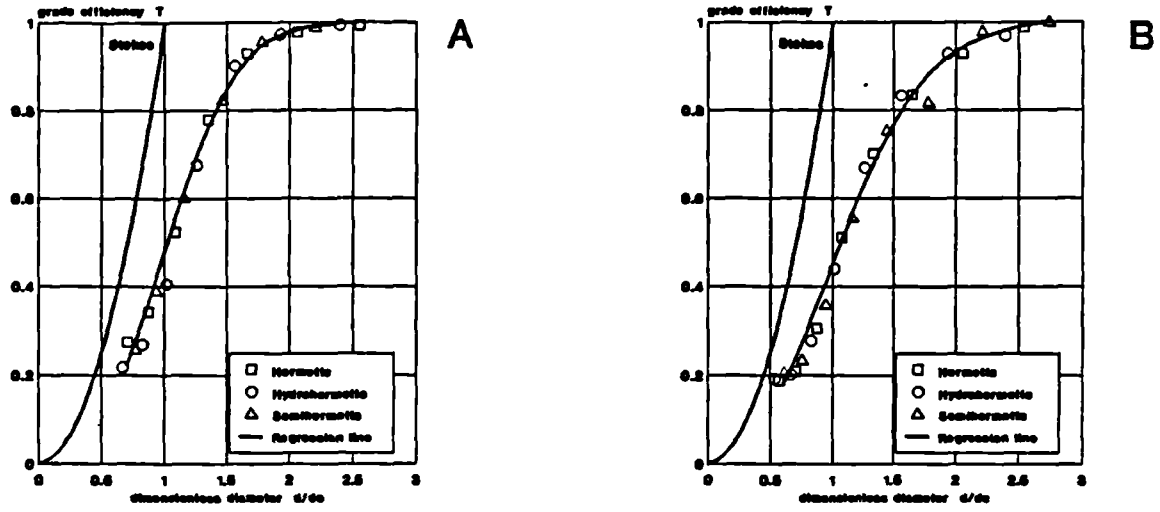

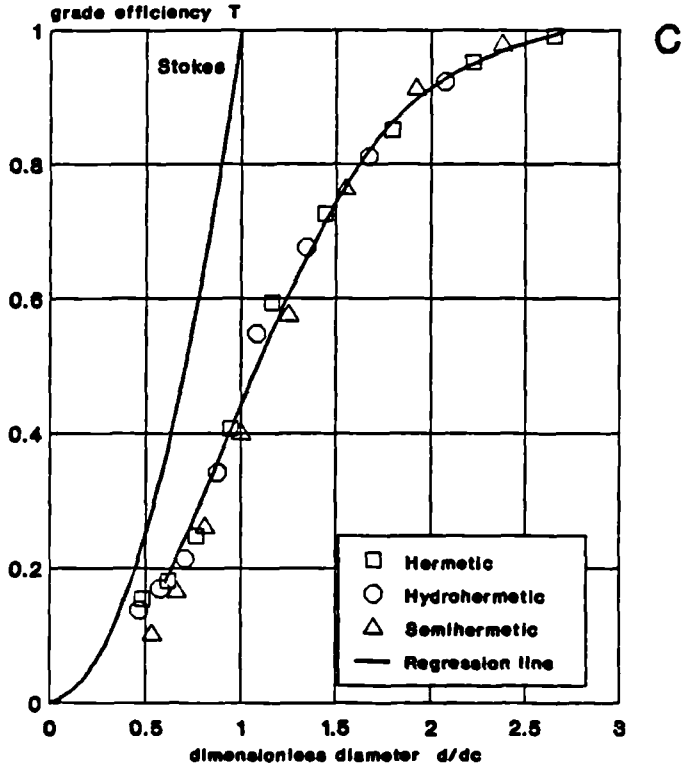

Figure 4.9: Effect of feed zone design on separation performance. Plot of grade efficiency against the dimensionless particle diameter for three different feed zone designs using a polyvinylacetate/water suspension as model product.

(A): specific throughput capacity, q_s=0.32 L/(h m²).

(B): specific throughput capacity, q_s=0.48 L/(h m²).

(C): specific throughput capacity, q_s=0.64 L/(h m²).

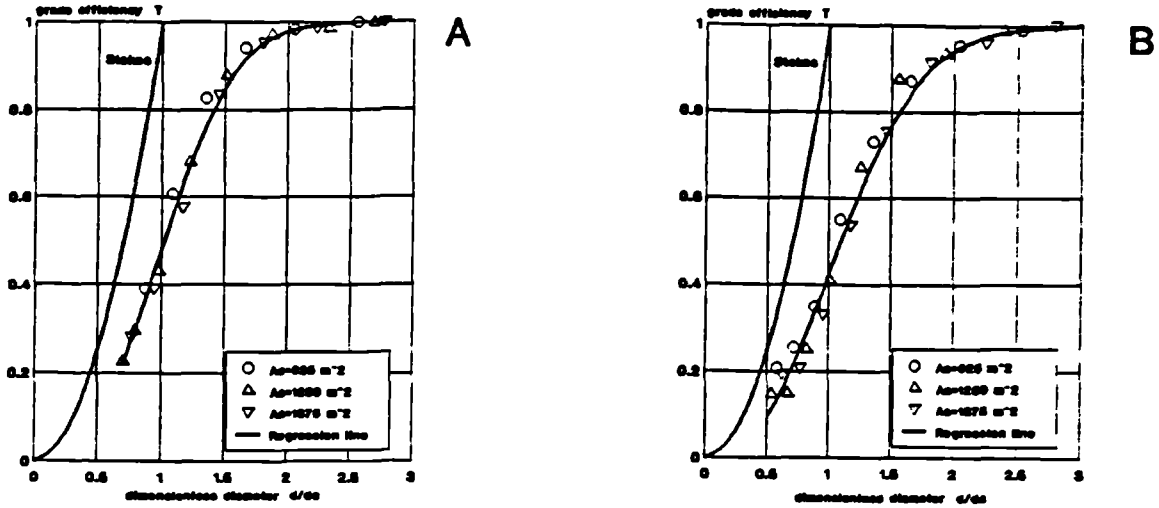

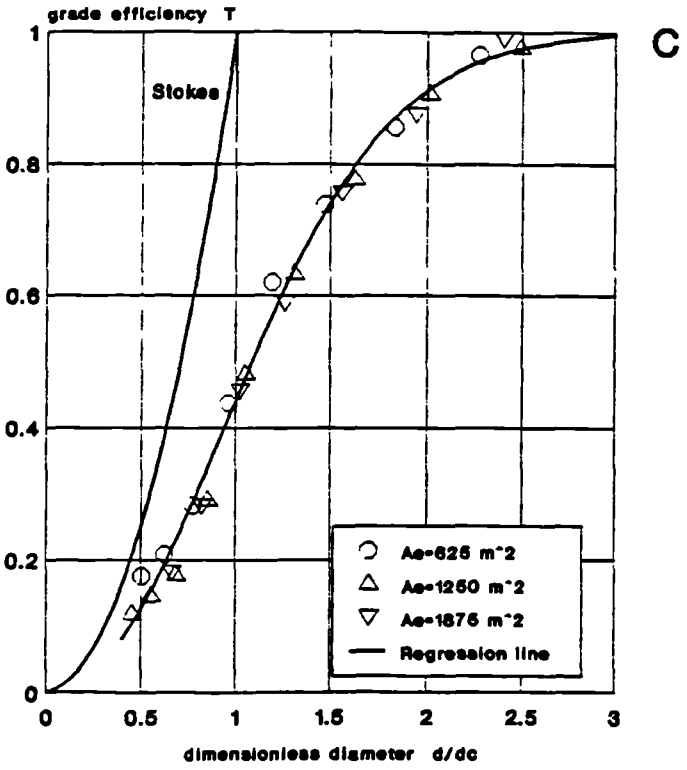

Figure 4.10: Effect of separation area scale on separation performance. Plot of grade efficiency against the dimensionless particle diameter for three separation area sizes using a polyvinyl-acetate/water suspension as model product.
(A): q_a=0.32 L/(h m²), full-hermetic feed zone.
(B): q_a=0.48 L/(h m²), hydro-hermetic feed zone.
(C): q_a=0.64 L/(h m²), full-hermetic feed zone.

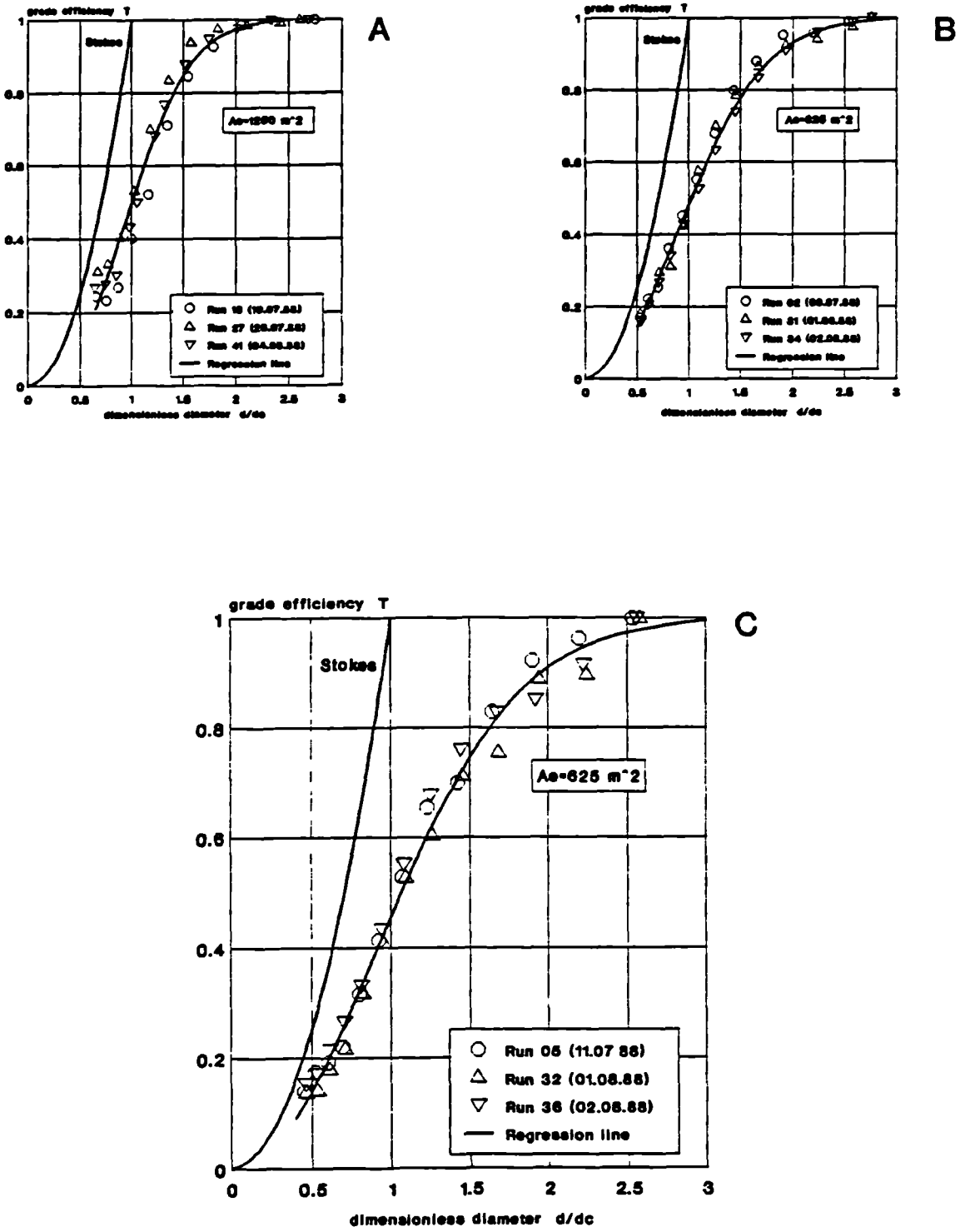

Figure 4.11: Reproducibility of separation performance results.
Plot of grade efficiency against the dimensionless particle diameter for three independent experimental trials using a polyvinylacetate/water suspension as model product.
(A): q_s=0.32 L/(h m²), full-hermetic feed zone.
(B): q_s=0.48 L/(h m²), hydro-hermetic feed zone.
(C): q_s=0.64 L/(h m²), hydro-hermetic feed zone.

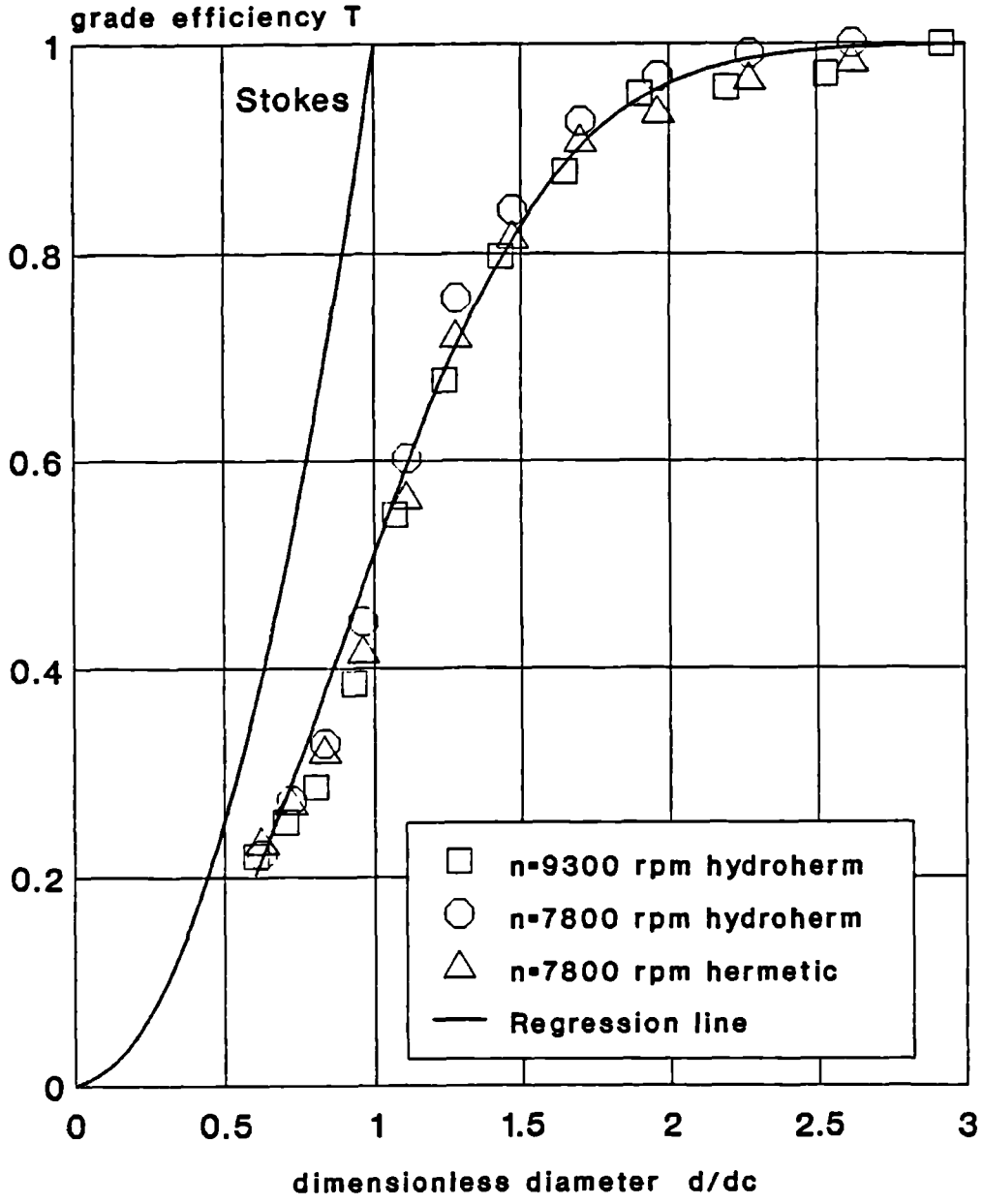

Figure 4.12: Comparison of the dimensionless grade efficiency curve of a disk stack centrifuge operated at different bowl speeds using a polyvinylacetate/water model suspension.

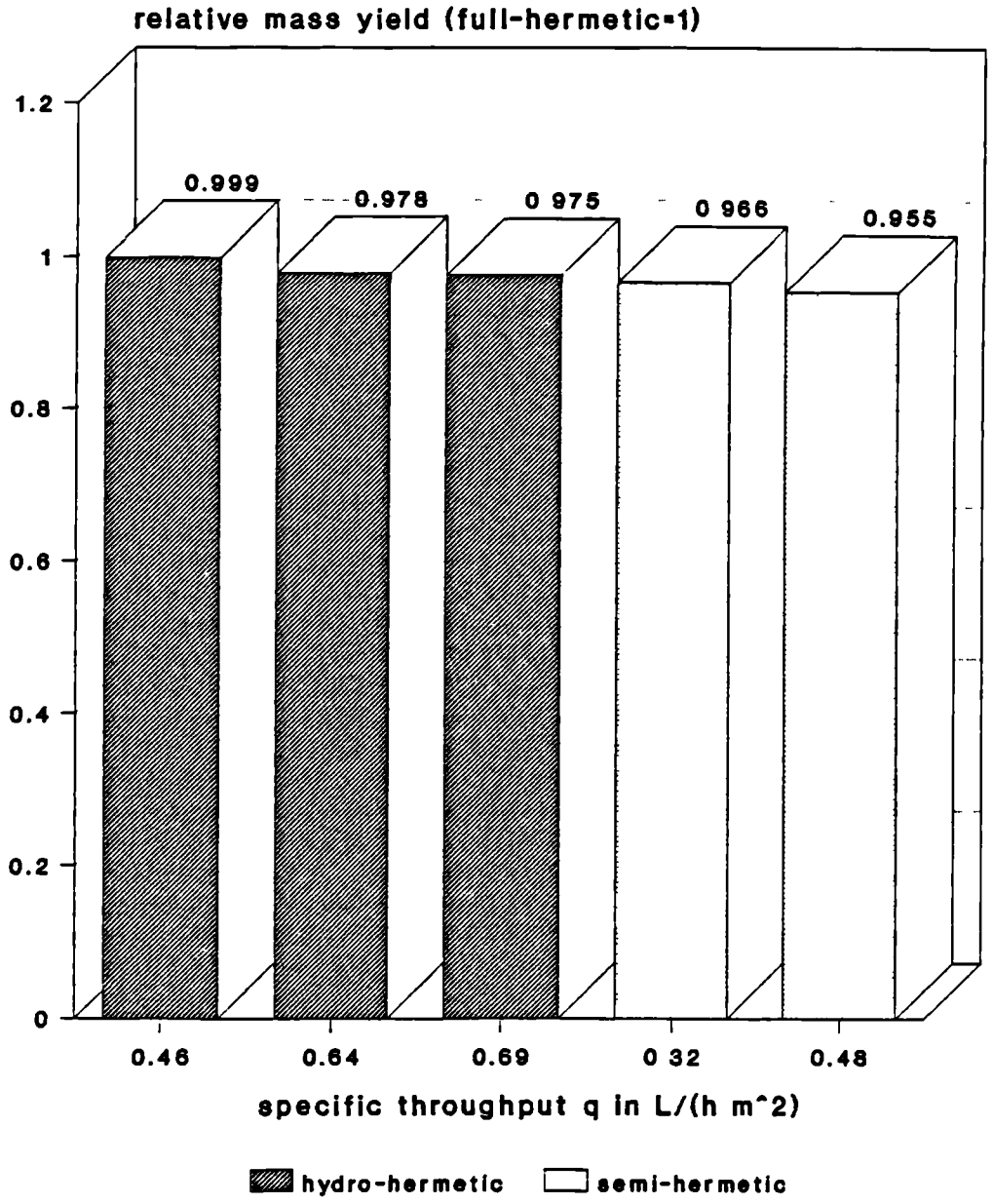

Figure 4.13: Relative mass yield obtained for a polyvinylacetate/water model suspension at different specific throughput capacities (full-hermetic feed zone = 1).

4.4.2 Results obtained using protein precipitate particles

In the previous section it has been shown that the design of the feed zone has no or only a minor effect on the separation performance. In order to examine the effects of feed zone design on particle breakup a protein precipitate suspension was separated in a disc centrifuge applying exactly the same procedure which has already been used for the separation of polyvinylacetate particles. From previous studies (see section 3.5) it was known that protein precipitate particles are readily disrupted in the strong shear fields generated in feed zones to centrifuges. It was also known that the degree of particle breakup is related to the rate of shear experienced by the particle (Bell, 1982). Consequently, if different feed zone designs exert different levels of shear then this difference should be reflected in the relative recovery performance of the centrifuges. The higher the shear rate the smaller the resulting particles and therefore, since particle recovery is proportional to the square of the particle diameter, the poorer the mass yield.

In section 3.5.2.2 it is demonstrated how the sheared particle size distribution (i.e. the particle size distribution of the feed suspension leaving the feed zone before entering the disc gap) can be calculated indirectly using the mass yield and a mathematical inversion algorithm. However in order to apply this algorithm correctly the exact physico-chemical properties of the suspension has to be available which is not always the case in practice. For example, it is very likely that the particle density and the particle strength varies from batch to batch of prepared precipitate. Although there are means to determine these fluctuations, they are far too laborious and too time consuming to be performed for each batch of protein precipitate. Additionally the experiments were far too important to rely solely on the reproducibility of the protein precipitate preparation technique assuming that the product is of constant specification and then argue that differences in the separation performance are only due to feed zone effects rather than altered precipitate properties.

Therefore, for reasons of importance and reliability of the performed experiments, queries relating to the physico-chemical nature of the product were eliminated by using two disc centrifuges equipped with different feed zones and operated almost simultaneously (see section 4.3). Additionally using the relative mass yield where the mass yield of the full-hermetic

disc centrifuge serves as a standard, it was possible to compare results of experiments performed on different days using freshly prepared batches of protein precipitate.

Figure 4.14 gives examples of the variability of the prepared precipitate particles. The figure illustrates variations of the precipitate size distribution in the feed suspension to the disc centrifuge. The changes are expressed in terms of the median and mode particle size (volume basis) which are defined as the diameter at which 50% of the particles have a smaller volume, and 50% have a larger volume, and the diameter of those particles which contribute most to the total particle volume, respectively. With the exception of the first experiment (WS14) the median particle sizes of the prepared precipitate suspension fluctuated around a mean value of 5.6 ± 0.3 µm with the mode diameter following closely. The small difference between median and mode particle diameter indicates a fairly symmetrical particle size distribution (Figure 4.14).

The results of the particle size analysis are documented in the form of a table in which both the relative number and volume particle concentrations measured in a given size range are listed. The program was written by the author in corporation with Mr. E. Wenzel of Westfalia Separator, Oelde, West Germany using HP-BASIC as programming language. The program itself is too long to be included in this thesis but a copy can be obtained on request from the author. In order to increase the resolution at the fine end of the size distribution the size ranges increase logarithmically from small to large particles. A statistics routine gives the total number of measured particles and calculates the corresponding total particle volume. In addition the three characteristic particle diameter represented by the median, mode, and mean particle size for both the number and volume distributions are also listed.

Calculation of the mass yield was based on the respective volume distribution of the precipitate size distribution in the feed to the centrifuge and in the clarified liquid outlet of the disc centrifuge. The results obtained from this examination are summarised in Table 4.1. In order to interpret this table correctly only experiments using the same specific throughput capacity may be compared with each other. While for example the relative mass yield obtained in experiment WS14 and WS15 for a specific throughput capacity of 0.64 L/(h m^2) may be set against each other, the decrease of the relative mass yield from a value of 0.821 to

0.701 if the specific throughput capacity is increased from a value of 0.64 L/(h m^2) to 0.96 L/(h m^2) does not necessarily mean that the particles are subjected to greater shear forces at higher flow rates. The reason for this becomes clear if the sheared particle size distribution of the full-hermetic and the hydro-hermetic feed zone is computed using the inversion algorithm introduced in section 3.3.2.2. The inversion technique can safely be applied here since only the relative change within a single experiment is of interest.

Experiment WS17 examines the effect of flow rate on particle breakup in such a way that the flow rate was doubled while the specific throughput remained constant at a value of 0.64 L/(h m^2). If the relative mass yields obtained for the hydro-hermetic feed zone operated at a flow rate of 400 and 800 L h^{-1} are averaged then a small drop from a value of 0.802 to 0.759 can be noted. The loss of mass yield for the full-hermetic feed zone in absolute terms is illustrated in Figure 4.15. The figure compares the mass yield obtained in various experiments operated at different flow rates using the same specific throughput capacity.

The effect of feed pressure has been examined in experiment WS20. Since the radius of the liquid circle inside the rib-body above the hydro-hermetic disc is a function of the feed pressure it was interesting to find out whether this pressure had a significant effect on particle breakup. The hydro-hermetic disc centrifuge was operated at a feed pressure of 1.15 and 0.75 bar. The mass yields indicate no significant loss of separation performance with feed pressure variation. The mass yields were in of order of 0.555 and 0.556 respectively.

For reasons described in section 4.2.3 experiments WS18, WS20 and WS21 analyse the possible effect of rib-body design on particle breakup using rib-body design A, B, and C respectively (see Figure 4.6). The results are shown in Figure 4.16 and no influence of the rib-body design on particle breakup emerges from the diagram. The relative mass yield is plotted for three different rib-body designs. the centrifuges were operated at a specific throughput capacity of 0.64 L/(h m^2).

Experiment WS20 included examination of possible effects of bowl speed on particle breakup. Therefore both the full-hermetic and hydro-hermetic disc centrifuges were operated at 7800 rpm. The specific throughput capacity of 0.64 L/(h m^2) was maintained by an appropriate reduction in flow rate. The

change from 9350 rpm to 7800 rpm resulted in a significant rise of the relative mass yield hence decreasing levels of shear breakup in the hydro-hermetic feed zone. The relative mass yield increased from a value of 0.752 at 9350 rpm to a value of 0.937 at 7800 rpm. In absolute terms, the mass yield obtained in the hydro-hermetic centrifuge increased from a value of 0.555 to 0.743 at 9350 rpm and 7800 rpm respectively while, although to a smaller extent, the mass yield increased from a value of 0.738 to 0.793 in the full-hermetic centrifuge. A similar trend was noted in experiment WS18 where similar trials were performed but in contrast to WS20 different specific throughput capacities were used.

The effect of the semi-hermetic feed zone design on particle breakup was examined in experiment WS22 and WS23. The relative mass yields observed for the semi-hermetic feed zone were reduced even further compared to those values obtained for the hydro-hermetic centrifuge. In both experiments the operating conditions of the centrifuges were exactly the same and, not surprisingly, the relative mass yields were 0.654 and 0.660 respectively. Compared to the hydro-hermetic feed zone this result indicates an even higher level of shear in this type of feed zone.

In Figure 4.17 the effect of feed zone design, flow rate and bowl speed on the extent of particle breakup is expressed in terms of relative mass yield. Since it has been shown earlier that for shear-insensitive particles the relative mass yields obtained using the hydro-hermetic and semi-hermetic centrifuge are close to unity (Figure 4.13) the figure quantifies correctly the levels of shear as a function of operating condition and feed zone design.

Table 4.1: Examination of separation performance of disc centrifuge equipped with different feed zone designs using protein precipitate particles.

No	Type	p_{in}	p_{out}	Q	ϑ	z	n_{bowl}	A_e	q_s	$d_{m,o}$	E_T	$E_{T,rel}$
	/	bar	bar	L h^{-1}	°C	/	rpm	m^2	L/h m^2	µm	/	/
WS14	HH	0,70	2,34	400	17,2	7	9350	625	0,64	6,35	0,620	
	H	2,32	5,49	400	17,1	7	9350	625	0,64	6,45	0,791	0,784
WS15	HH	0,82	2,57	400	17,3	7	9350	625	0,64	5,61	0,652	
	H	1,97	5,07	400	17,4	7	9350	625	0,64	5,62	0,794	0,821
	H	2,07	5,03	600	17,3	7	9350	625	0,96	5,64	0,739	0,701
	HH	0,71	1,87	600	17,5	7	9350	625	0,96	5,64	0,518	
WS17	HH	0,97	1,59	800	16,6	14	9350	1250	0,64	5,76	0,571	
	H	2,30	5,00	800	16,7	14	9350	1250	0,64	5,76	0,740	0,772
WS18	H	3,40	5,10	800	16,1	14	9350	1250	0,64	5,38	0,757	0,754
	HH	1,20	1,70	800	16,2	14	9350	1250	0,64	5,45	0,571	
	HH	1,05	1,47	670	16,2	14	7800	870	0,77	5,45	0,685	
	H	2,20	4,80	670	16,3	14	7800	870	0,77	5,45	0,771	0,888
WS20	HH	1,15	1,64	800	15,9	14	9350	1250	0,64	5,76	0,555	
	H	2,43	5,12	800	15,9	14	9350	1250	0,64	5,81	0,738	0,752
	HH	0,75	1,33	800	16,1	14	9350	1250	0,64	5,84	0,556	
	HH	0,80	1,46	560	16,4	14	7800	870	0,64	5,84	0,743	
	H	2,35	5,15	560	16,4	14	7800	870	0,64	5,81	0,793	0,937
WS21	HH	0,97	1,51	800	16,4	14	9350	1250	0,64	5,10	0,515	
	H	2,17	5,08	800	16,4	14	9350	1250	0,64	5,16	0,681	0,756
WS22	S	0,20	1,60	400	16,1	7	9350	625	0,64	5,68	0,538	
	H	2,20	5,40	400	16,2	7	9350	625	0,64	5,68	0,823	0,654
WS23	S	0,15	1,90	400	15,6	7	9350	625	0,64	5,96	0,543	
	H	2,40	5,40	400	15,9	7	9350	625	0,64	6,10	0,823	0,660

No: Number of experiment
Type: feed zone (distributor) type (i) H = full-hermetic; (ii) HH = hydro-hermetic; (iii) S = semi-hermetic
p_{in}: feed pressure
pout: discharge pressure
Q: throughput capacity or feed flow rate
ϑ: temperature of feed suspension
z: number of separating discs
n_{bowl}: rotational velocity of bowl
A_e: equivalent separation or clarification area (Equation 1.14), relevant centrifuge specifications are listed in Table 2.1.
q_s: specific throughput capacity (= Q/A_e)
$d_{m,o}$: median size of particle size distribution in feed to centrifuge
E_T: mass yield
$E_{T,rel}$ relative mass yield (full-hermetic feed zone = 1)

Remarks: WS18: rib-body design A; WS20: rib-body design B; WS21: rib body design C.

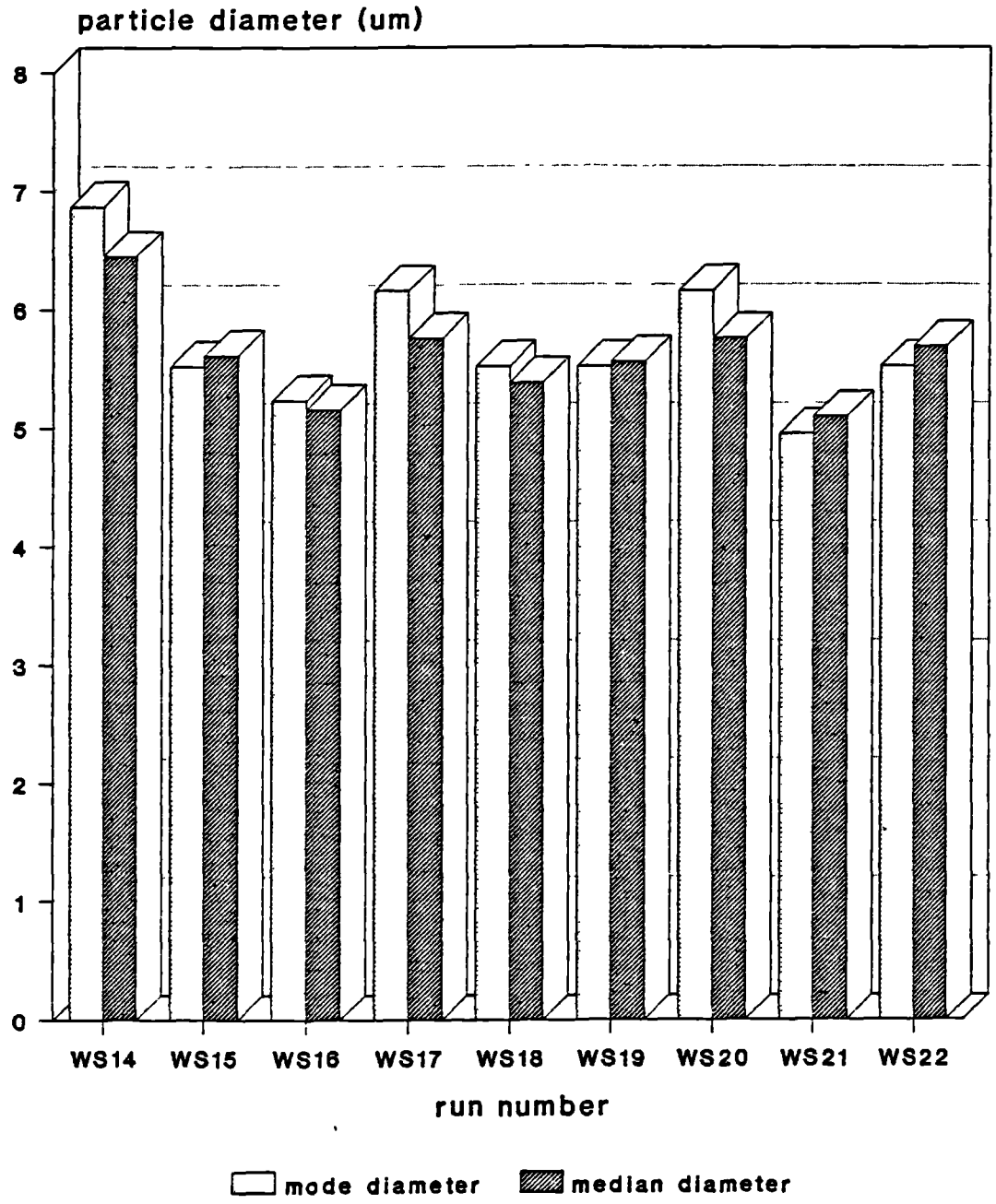

Figure 4.14: Reproducibility of a batch-prepared soya protein precipitate applying constant preparation and precipitation conditions as described in section 4.3.1.2.

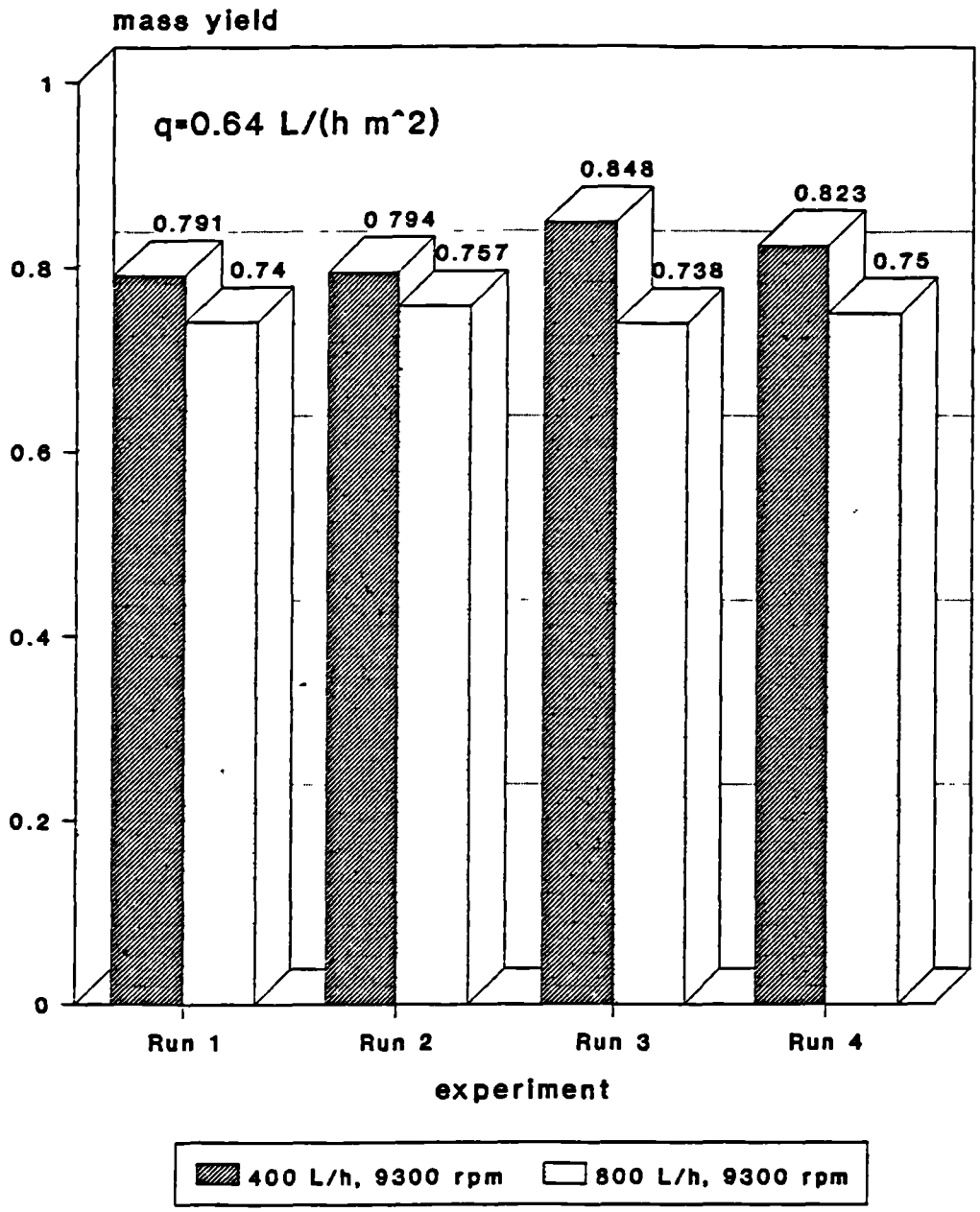

Figure 4.15: Mass yield obtained for the separation of soya protein precipitate separated in a full-hermetic disc stack centrifuge operated at two different throughput capacities (q_s = 0,64 L/(h m²)).

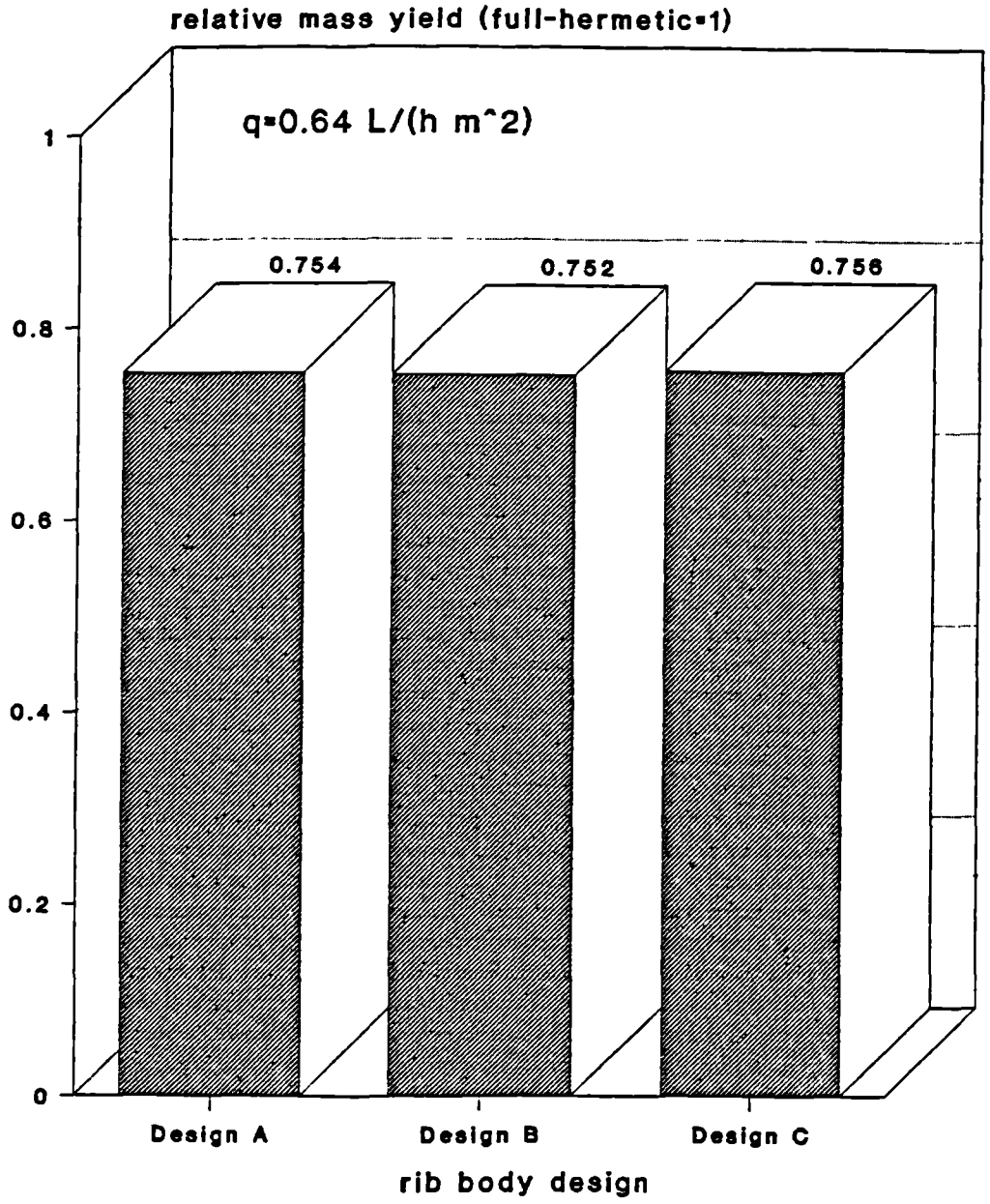

Figure 4.16: Effect of rib-body design (Figure 4.6) on the relative mass yield obtained for the separation of a protein precipitate suspension (Full-hermetic = 1).
Design A: 6 ribs, long, sharp edges
Design B: 4 ribs, long, rounded edges
Design C: 4 ribs, short, rounded edges

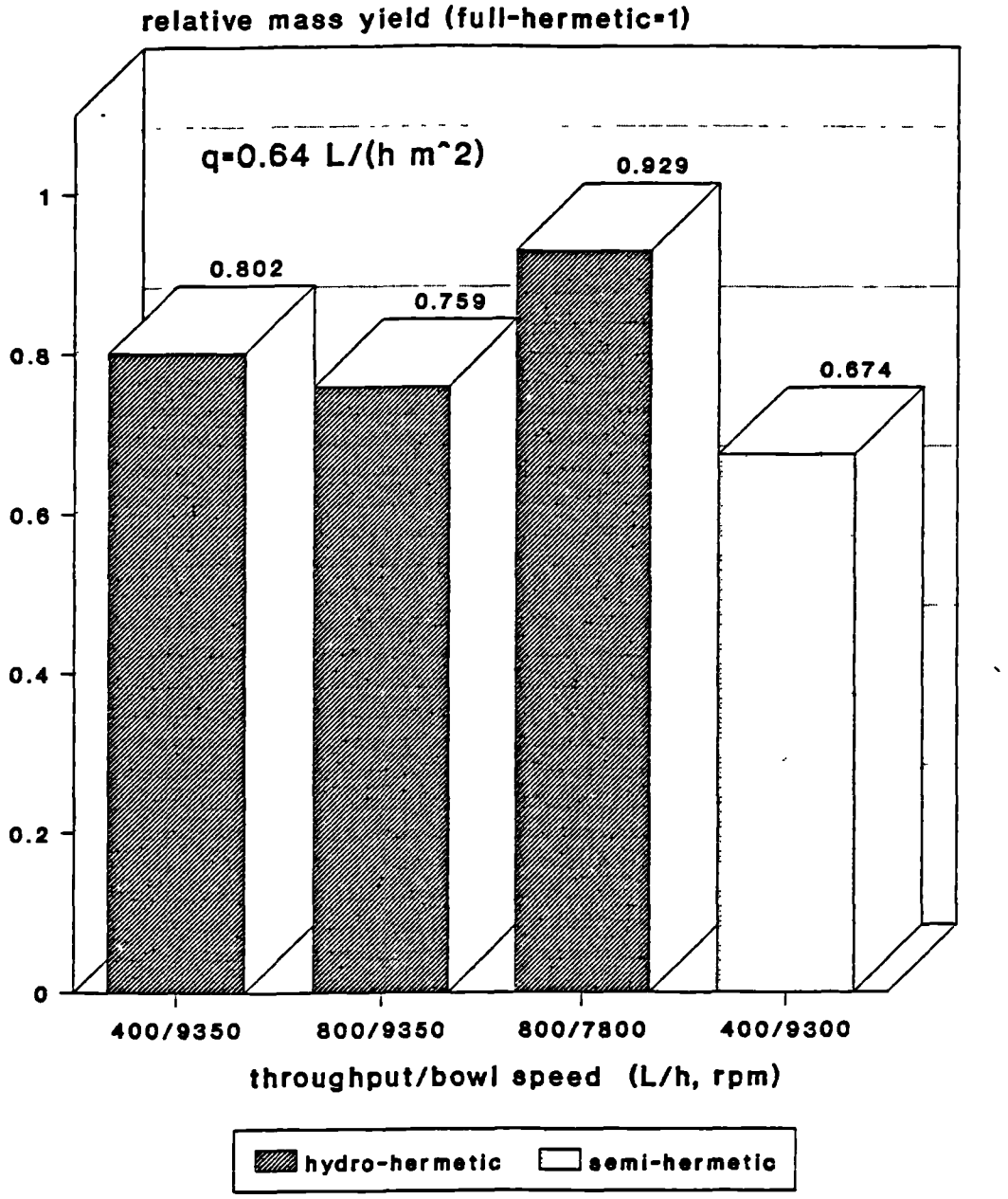

Figure 4.17: Relative mass yield obtained for a protein precipitate suspension separated in disc stack centrifuges of different feed zone designs, throughput capacity and bowl speed (Full-hermetic feed zone = 1).

5. Discussion

5.1 Evaluation of the separation characteristics of a scaled-down industrial disc centrifuge

In downstream processing it is often necessary to develop scale-down techniques to model or simulate the operation of larger, pilot or production scale, equipment. If reliable simulation techniques are available, the biochemical engineer could then more quickly and less expensively screen both product preparation conditions and operating conditions that affect capital and operating cost and to a certain degree optimise the clarification process.

In order to evaluate the use of disc centrifuges for a particular process duty it is necessary to use a centrifuge of such size that scale-up to industrial machines is possible. One main limitation is the ability to control solids discharge and such a restriction leads to the use of a centrifuge capable of operating at high hydraulic throughput capacities of > 1000 L h^{-1}. Such a throughput is considerably larger than that available in many development facilities.

The aim of the first part of this thesis was to examine how the separation performance of an industrial centrifuge may be assessed using relatively small amounts of process fluid. This necessitated scale-down of the centrifuge and for this purpose the reduction in the active proportion of disc stacks available for separation was examined.

The study has shown that in scale-down the degree of scale-down and the location of the active discs (discs with spaces between) have a marked effect on the profile of the dimensionless grade efficiency curve. Firstly, the effect of altering the disc location on the residence time of a dye tracer can be appreciated from the data given in Table 2.2. The change of the discs from position B (bottom) to position A (top) involves an increase in the mean residence time of almost 36%. At a flow rate of 500 L h^{-1}, this corresponds to an increase of the hold-up volume of approximately 0.85 L. In order to confirm this observation a series of trials were performed at different volumetric flow rates. The hold-up volumes obtained were 3.35 L (±0.15 L) and 2.43 L (± 0.06 L) for disc position A (Figure 2.5) and for disc position B respectively again a difference of approximately 0.9 L. This increased hold-up volume is assumed to be

provided by the sediment holding space the volume of which totals about 1.5 L. The data presented are limited to the mean residence time and hold-up volume. The dispersion number (Levenspiel, 1972), a measure of the degree of dispersion of the flow within the centrifuge indicated a considerable extent of fluid mixing; within the feed zone, the sediment holding space, the disc gap and the exit zone all giving rise to partially mixed regions. The relative error of the dispersion numbers was too high to allow more meaningful interpretation of the data.

The results show that the incoming fluid is dispersed to a certain degree at the foot of the distributor. Upward flow towards the top discs is not limited to the peripheral distribution channels but involves parts of the sediment holding space. Thus, because the grade efficiency curve plotted as a function of the dimensionless diameter d/d_c is only dependent on the flow pattern inside the disc centrifuge it should show a distinct difference depending on the position of the active discs in the stack. The results obtained using a polyvinylacetate/water suspension were as predicted from the dye tracer studies studies. In general, the grade efficiency curve based on the top position of the active discs is considerably better than the bottom based curve. The dimensionless median cut size, corresponding to the dimensionless particle size at 50% separation, increases by about 60% in relative terms from $(d/d_c)_{50} = 0.8$ to $(d/d_c)_{50} = 1.25$ if the discs are transfered from the top (position A) to the bottom position B. This is not to say that the discs in the top position are more effective as separators but rather that the theory should take into account the settling that occurs in the sediment holding space. Since this will become negligible for a completely active disc stack it is preferred not to modify the theory but rather to choose the arrangement where such settling is minimized. In practice it must always be better to slightly underestimate the separation performance during process development and to be on the safe side during scale-up.

Placing the discs in position C (Figure 2.5) is a compromise between the two other possibilities. For scale-down purposes this location is favoured, since it does not exhibit the significant effect of flow rate experienced by a settling particle at the bottom position (B) and settling of large particles in the sediment holding space is avoided.

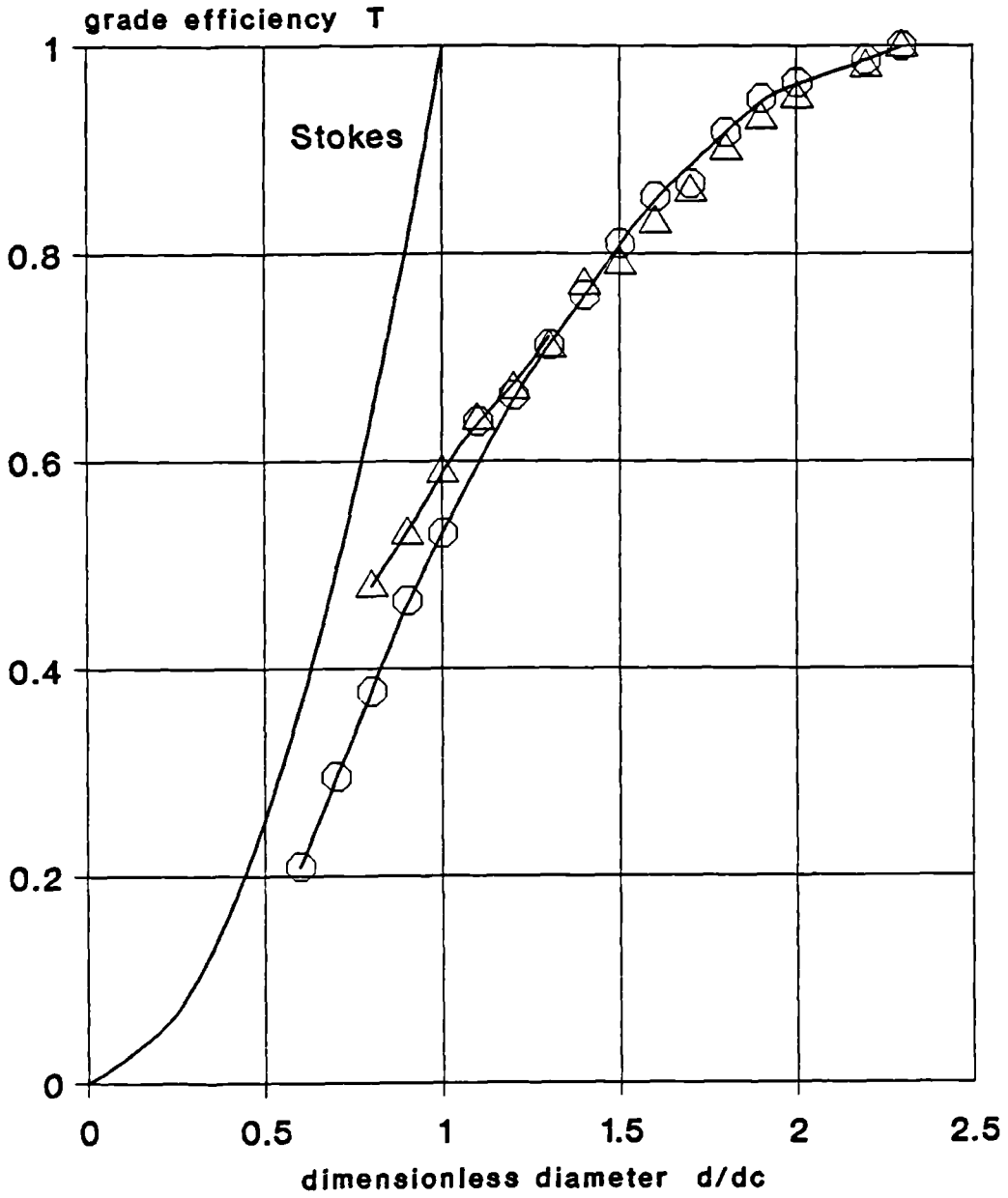

Figure 5.1: Comparison of grade efficiency curves of a disc stack with reduced sedimentation area and a full set of discs of an industrial disc stack centrifuge. (O) reduced disc stack; 7 discs; position C (see Figure 2.5), (Δ) Data obtained by Brunner (1979) using an industrial disc centrifuge (z=57, R_i=0.045 m, R_a=0.1 m, h=0.8 mm, n=6300 min^{-1}).

How those data compare with a full disc stack is illustrated in Figure 5.1. The data for the full stack were obtained by Brunner (1979) who used an industrial disc centrifuge containing a set of 57 discs.

The graph indicates that the grade efficiency curves obtained using a reduced disc stack (90% reduction of separation area, position C) compares reasonably well with the curve of a full stack. For the scaled-down version of an industrial disc centrifuge the loss of efficiency near the separation limit is not of concern when examining the operation of the centrifuge for full particle recovery ($d/d_c > 2$).

The figure shows that a disc centrifuge may be scaled down to 10% of its total available separation area in order to examine particle recovery. If the centrifuge is to be used such that a high proportion of a particle species are to appear in the overflow than subsequent scale-up will lead to an underestimation of performance (e.g. approximately 20% underestimation of flow rate for 40% recovery of particles in the overflow). If the centrifuge is to be used for almost complete (> 95%) particle recovery, as is normally the case, then the prediction of the required throughput will be only slightly (< 1%) underestimated. On this basis large scale operation may be simulated on a much smaller and less expensive scale by reducing the equivalent separation area, batch size and flow rates etc. by the same factor. Once fully optimized on a smaller scale, the extrapolation to a larger scale for particle recovery should be predictable and reliable. The other main function of a centrifuge such as dewatering and solids discharge were not a feature of this study.

The grade efficiency profiles presented are not atypical for disc stack separators with peripheral flow distribution channels (Brüning, 1987). Earlier in the paper it was mentioned that the limiting particle diameter of a well designed separator, d_{100}, is given by:

$$d_{100} = \sqrt{2}\, d_c$$

Figure 2.11 which shows the dimensionless grade efficiency curve for the top arrangement (position A) reveals that the limiting particle diameter of discs with peripheral distribution channels is rather given by:

$$d_{100} = \sqrt{3}\, d_c$$

In contrast, due to the dependency of the grade efficiency profile on the

throughput capacity for the bottom arrangement (position B) no clear statement on the separation limit can be made.

In subsequent experiments (see section 4.3) the effect of feed zone design on separation performance was examined in more detail. Based on the experiences gained during method development (section 2.3) the active discs were placed on top of the small blank insert (position C; Figure 2.5). The data obtained reveal no significant differences between type of feed zone and different scales expressed in terms of equivalent separation area available for particle separation. However, in contrast to the previous data (see Figure 2.16) the results showed a distinctive trend of the dimensionless grade efficiency curve towards a reduced separation performance of the centrifuge at increased specific throughput capacities. Generally it was observed that lower specific throughput capacities increased the steepness of the grade efficiency curve. For example the $(d/d_c)_{50}$, at which 90% of particles of the given dimensionless size are separated, increased from 1.60 at q_w = 0.32 L/(h m²) to a value of 2.20 at the higher specific throughput capacity of q_w = 0.64 L/(h m²). Since no differences in the separation performance were observed for the different feed zone designs this result may be regarded as typical for all separation experiments performed using a polyvinylacetate suspension. This trend is also reflected in the value of the correlation parameters which were used to express in a functional form the relationship between the grade efficiency, the particle diameter, centrifuge specifications and operating conditions. It is this dimensionless grade efficiency function which will be discussed further.

5.2 Modelling of grade efficiency curve

The merits of using the grade efficiency curve in the form of a mathematical expression have been discussed in section 2.3.4. Various possible approaches to model the grade efficiency curve were introduced such as the simple two-parameter model which expresses the grade efficiency by means of an exponential function involving two-parameters and the more complex three-parameter model which assumes a log-probability relationship between the dimensionless particle diameter and the grade efficiency.

Subsequent application of the two grade efficiency models revealed that the two-parameter model was sufficiently accurate to predict the separation performance of the machine. The absolute errors made by predicting the mass yield from the physico-chemical properties of the solids suspension, the feed particle size distribution, the centrifuge specifications and the throughput capacity was in the order of ± 0.03. No additional accuracy was gained using the three-parameter model. Apart from its simplicity the parameters k and n of the two-parameter model were very sensitive to changes of the separation performance caused by secondary effects such as disc stack configuration (Table 2.3) and throughput capacity (Table A1 and Equation 4.1).

Analysis of Table 2.3 indicates that the correlation-parameter k approaches values in the range of 0.9 to 1.2 for a good grade efficiency curve obtained for the experiments V18 and V20b where 17 active discs were placed on top of the disc stack (position A; Figure 2.5). A good grade efficiency curve may be defined as the grade efficiency curve which follows the Stokes' separation curve over a wide range of dimensionless particle diameters. A bad grade efficiency curve (Figure 2.15) shows smaller values of k which are typically of the order of 0.70 to 0.75.

In a diagram plotting the grade efficiency against the dimensionless particle diameter a shift of the grade efficiency curve towards the left-hand-side indicates an improvement of the separation performance of the centrifuge and is accompanied by an increase of the correlation parameter k. A shift towards the right-hand-side indicates a drop in the separation performance and is accompanied by a decrease of k.

The corresponding effects on the correlation parameters n are less obvious mainly because changes of n have a much smaller effect on the grade efficiency curve than variations of k (Figure 2.17 and 2.18). Basically n may be regarded as a measure of the steepness of the grade efficiency curve. A large value of n is a sign for a steep grade efficiency curve while a small value indicates a flat curve extending over a wide range of particle sizes.

The Stokes' separation curve may to a certain extent also be approximated by the two-parameter correlation. The parameters, and in particular the value of k, may be regarded as a measure for the deviation from the experimentally determined separation performance from Stokes' separation.

Since Stokes separation is regarded as the maximum achievable separation performance of the centrifuge a value of k_{max} = 1.3 may be used to define the upper limit of the parameter k, i.e. if the dimensionless grade efficiency curve follows close to the Stokes' curve the parameter k of the two-parameter correlation equation (Equation 2.27) will be close to a value of 1.3 while it decreases with reduced separation performance.

For a value of n ≈ 2.5 the relationship between k and the dimensionless grade efficiency curve may be summarised as follows:

(1) $1.2 < k < 1.3$: Grade efficiency curve follows Stokes' Law over a wide range of particle diameters. Minor deviations between Stokes separation curve and grade efficiency curve occur for particles for which $(d/d_c) > 0.9$.

(2) $1.0 < k < 1.2$: Grade efficiency curve follows Stokes' Law over a small range of particle diameters. Deviations between Stokes separation curve and grade efficiency curve occur for particles for which $(d/d_c) > 0.7$.

(3) $0.6 < k < 1.0$: Grade efficiency curve does not follow Stokes' Law. Considerable deviation between Stokes separation curve and grade efficiency curve in such that grade efficiency curve is always worse.

It needs to be stressed that the boundaries of k given in the above summary represent approximate values. The lower limit of k (= k_{min}) is of the order of 0.6 which is imposed by experimental restrictions. In practice such small values of k have never been observed during experimentation (see Table A1 in the appendix).

The significance of n, which may be regarded as a measure of the slope of the grade efficiency curve, is less obvious and for the approximation of the Stokes separation curve a value of n = 3.0 may be used. However, since changes in n do not effect the course of the grade efficiency curve as much as changes in k the parameter n may, in some instances, approach values larger than this. A large value of n does not necessarily imply that the centrifuge exhibits a good separation performance since it only refers to the slope and not to the position of the grade efficiency curve in respect to the Stokes separation curve. In practice values of n ranging

from 2.0 to 3.0 are most common (Table A1). Smaller values of n indicate inadequacy of the centrifuge to separate large particles with dimensionless particles sizes of $(d/d_c) > 2.5$; this is undesirable.

In the early stage of method development a correction factor R_c was introduced in order to account for the deviations between measured and theoretically determined mass yield (section 2.3.5). Calculation of the correction factors of the experiments V28 to V31 using the correlation parameters k = 0.865 and n = 2.08 showed a steady decline of R_c with increasing flow per active disc gap, q. The linear relationship between the correction factor R_c and q is also illustrated in Figure 2.19 in which R_c, expressed as the arithmetic mean of all R_c-values calculated for each single passage throughput, is plotted as a function of q on semi-logarithmic paper.

Figure 5.2 expresses the data obtained for the correction factor R_c as a function of the single passage throughput capacity, q, in which the theoretical mass yield ($E_{T,pred}$) was calculated using 4.1 in conjunction with Equation 2.20 and the given separator specifications, operating conditions and physico-chemical properties of the feed suspension. As can be seen the relationship between R_c, expressed as the arithmetic mean of all R_c-values and q is described by a horizontal line with a mean value of R_c close to unity. These results confirm that the determined correlation between the parameters k and n (Equation 4.1) and the single passage throughput is sufficient to correct theoretical mass yield calculations for secondary flow effects.

The grade efficiency diagram may be used to examine the effect of altering the operating conditions required in the recovery of so-called protein inclusion bodies, insoluble particles of partially folded foreign protein which often occur when rDNA techniques are employed. They appear in cross sections of microorganisms viewed by electron microscopy as dark masses. When the cell has been disrupted the inclusion bodies must be separated from the resulting cell debris but inclusion bodies are very small. The size distribution of γ-interferon and calf prochymosin inclusion bodies were examined by (Taylor et al, 1986) and the median diameters were of the order of 0.8 μm and 1.3 μm respectively.

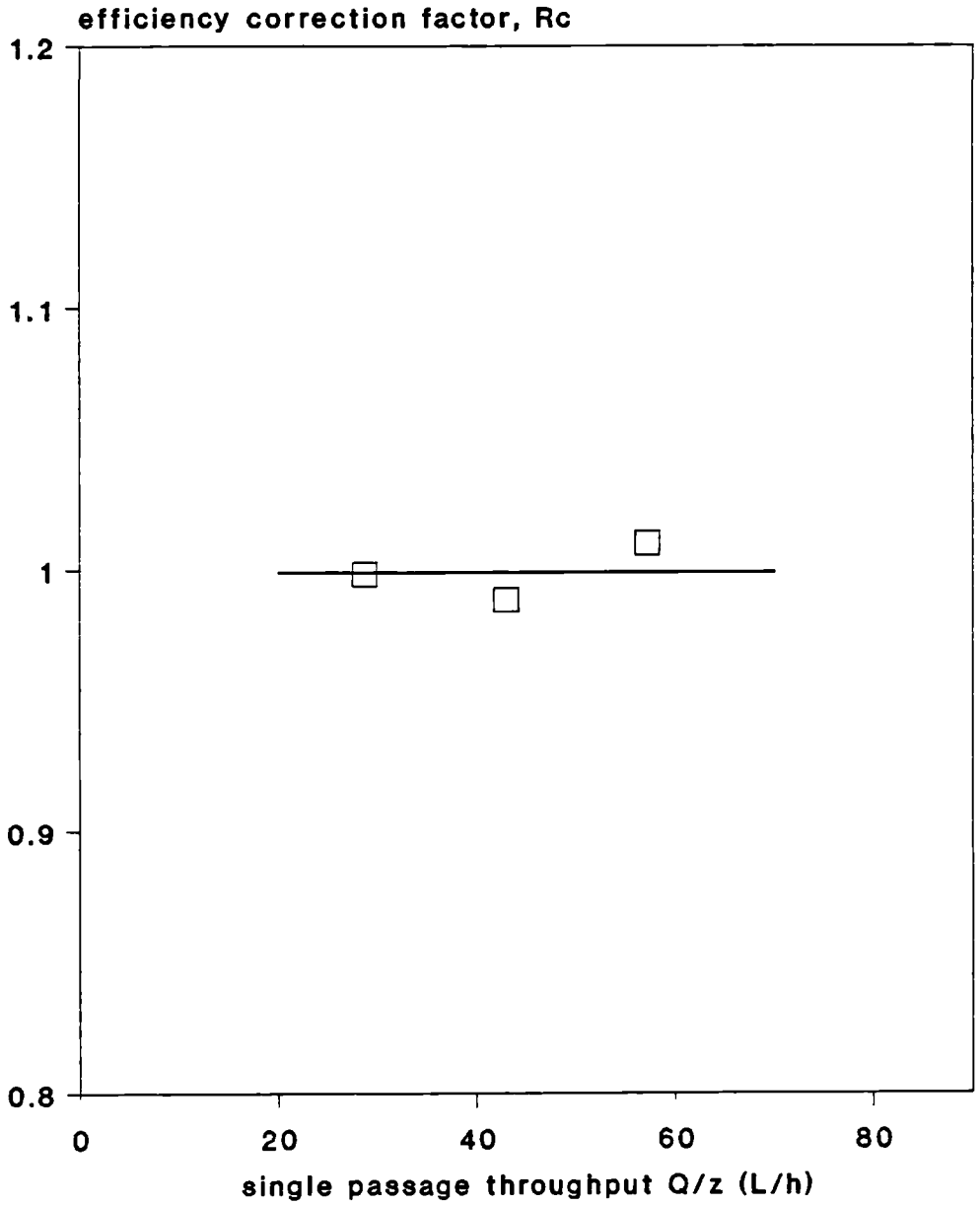

Figure 5.2: The effect of single passage throughput on the ratio of measured and predicted mass yield (R_z). The predicted mass yield was calculated using Equation 2.20 in conjunction with Equation 4.1. Each point represents the mean of three measurements (SD = 0.03).

Separate experiments showed voidages accessible to suspending fluid of 70% for γ-interferon and 85% for prochymosin. To recover the inclusion bodies free from the debris on a large-scale requires operation of industrial disc centrifuges based on this analytical work. Based on simulating the separation process by using the grade efficiency curve the performance of such a centrifuge has been examined (Figure 5.3). At low flow rate through the rotor there is a good recovery of the inclusion bodies but poor removal of cell debris which is also sedimented under these conditions. At high throughput the inclusion bodies are only partially recovered, but separation from debris is good because it is too small to sediment. The optimum lies at a flow rate of 200 L h^{-1} for this machine. Subsequent experimental studies confirmed the simulated results (Olbrich et al, 1988).

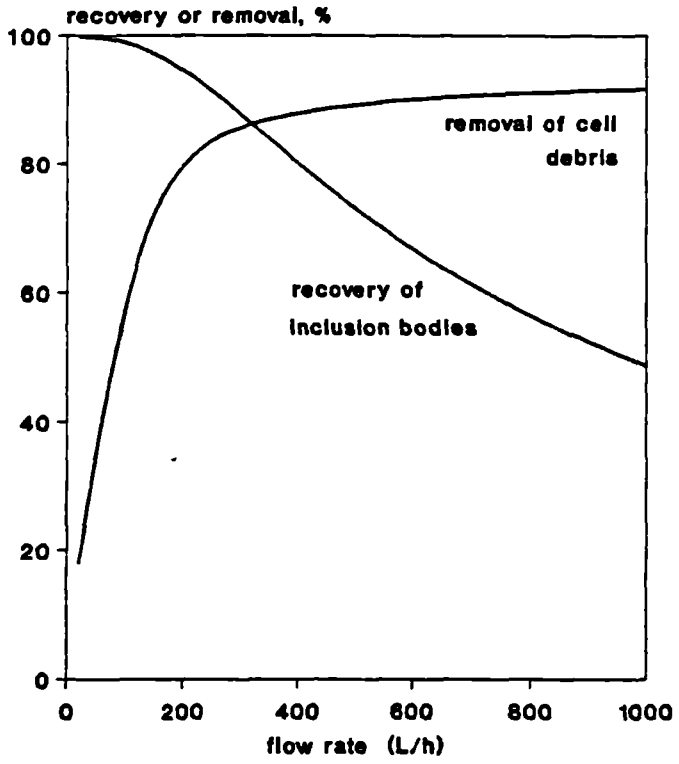

Figure 5.3: Simulated recovery of prochymosin inclusion bodies in an industrial disc centrifuge and extent of removal of cell debris from the inclusion bodies.

So far it has been shown that an industrial disc centrifuge can successfully be scaled-down to approximately 10% of its original separation area without affecting the hydrodynamics and settling characteristics inside the machine. In order to characterize and pre-

calculate the separation performance a two-parameter correlation equation was formulated and applied successfully. However, despite these apparent successes the question as to what causes the effect of single passage throughput on the course of the dimensionless grade efficiency curve remains to be answered.

One possibility to explain these single passage throughput effects would be to argue that it may be caused as a result of inadequate particle size analysis. However the trends observed have been confirmed by good agreement between the mass yield values based on particle size analysis and the mass yield values based on optical density measurement (section 2.3.6).

During his studies on the separation performance of a disc centrifuge operated under a variety of conditions, Brunner (1979) has also shown that a polyvinylacetate/water suspension is highly sensitive to changes of the hydrodynamic conditions experienced by the particle suspension. With increasing throughput capacity a significant reduction of separation performance was observed. The reason for this reduction lies to a great extent in the level of cross-flow at the disc periphery. Partially confirmed by dye tracer studies, not all of the suspension is fed into the disc gaps via the peripheral flow distribution channels but some is fed via the periphery of the disc. This causes separated solids to be partially remixed into the freshly supplied feed suspension flowing into the next disc gap on top. As a consequence the solids are only partly separated (Figure 1.6). This hypothesis explains the flow rate dependency of the separation results since the level of cross-flow increases with increasing single passage throughput.

In this respect the findings presented so far are in line with observations made by other research workers. However in order to confirm this hypothesis more detailed experiments regarding the effects of peripheral suspension loading on separation efficiency are needed. In particular it is recommended to avoid entry of the feed suspension into the solids holding space and by the use of internal feed distribution channels.

5.3 Evaluation of shear breakup in feed zones to disc centrifuges

The effect of shear on suspensions of protein precipitates and its influence on particle recovery was studied in three different types of centrifugal feed zones. As described in section 1.5 a precipitate particle will be disrupted if placed in a shear field exceeding a critical stress value. The rate and mechanism of breakup is a complex function of particle strength and size and the hydrodynamic properties of the shear field. Since particle strength is related to particle size, the larger the aggregate the lower the yield strength and consequently larger aggregates are more susceptible to shear associated breakup than smaller ones which have higher critical strengths. Hence, the rate of particle breakup is faster at higher rates of shear and larger aggregates breakup faster than smaller ones.

Therefore, if different feed zones exert different levels of shear then as observed in section 4.4.2 the separation performance of the centrifuge will be the lower the higher the shear rate in the feed zone. The results showed that most shear breakup occurred in the semi-hermetic, followed by the hydro-hermetic feed zone design. The least amount of particle breakup was observed for the full-hermetic feed zone. In contrast to the hydro- and full-hermetic feed zone versions the semi-hermetic feed zone comprises a variety of locations which may contribute more or less to the breakup effects (Van der Linden, 1987).

(1) The primary contact between the centrifuge and the feed suspension takes place at the lock-nut, which, because of its conical shape, deflects the liquid flow, which is ejected from the stationary feed pipe with high velocity. Owing to the short contact time little momentum is expected to be transfered in angular direction.

(2) The second location comprises the acceleration ribs in the distributor where intensive contact between the distributor and the feed suspension takes place.

(3) The third location is thought to be the trajectory in between the distributor rib and the liquid surface situated at the pressure side of the guiding rib.

(4) Fourth location is the inner wall of the distributor where axial shear becomes predominant when the feed liquid surface radius is positioned outwards resulting in low liquid depths.

(5) Finaly the fifth location for particle breakup is the conical shaped lower end of the distributor where high shear rates may occur.

In practice breakup is probably the result of the combined action of all the locations just described each contributing more or less to the level of breakup.

From the point of view of the equipment manufacturer evaluation of the location which brings about most of the particle disruption seems to be the most formidable task whereas the mechanisms of breakup are of less importance.

Examining the disruption data of the full-hermetic feed zone shows a considerable reduction in the possible solids recovery efficiency caused by a substantial drop in the feed particle size distribution as a result of aggregate disruption in the centrifugal feed zone. The initial volume median size falls from 5.1 μm in the original feed size distribution to approximately 2.3 μm after the feed zone which represents a size reduction of almost 55%. This is surprising because this type of feed zone is classified as 'soft feed' designed to be especially gentle on aggregates. The questions are what level of shear is experienced by the solids aggregate inside the full-feed zone and which factors contribute to this high level of particle size reduction.

In order to obtain some impressions on the level of shear inside the centrifuge feed zone the first step is to calculate the root-mean-square velocity gradient, G. As mentioned in section 1.3.5 the breakup of aggregates in a fluid suspension generally is directly associated with the hydrodynamic state of the fluid as for example: laminar or turbulent flow, scale of turbulence and the size of the energy transferring eddies. However in order to calculate the root-mean-square velocity gradient, G, it is first necessary to determine the dissipated power per unit volume of liquid which is used to approximate the intensity of turbulence in an agitated liquid. This principle has proved useful in the scale-up of agitator vessels, where geometrically similar vessels and agitator

arrangements of differently sized equipment require constant power per unit volume in order to produce the same homogenisation of suspension.

In a full-hermetic disc centrifuge the power dissipated inside the feed zone is related to the pressure drop across the distributor. Applying the power - pressure drop relationship given by:

$$P_s = Q\ \Delta p_s \qquad 5.1$$

then the the power dissipated in the centrifuge can be calculated. In respect to particle breakup, only the power dissipated in the feed zone is of interest. The pressure drop across the disc centrifuge is the sum of the pressure drop across the disc stack, the distributor and the liquid discharge line. If the latter is neglected then the pressure drop across the distributor Δp_{dist} may be estimated by:

$$\Delta p_{dist} = \Delta p_s - \Delta p_{disc} \qquad 5.2$$

The disc pressure drop can be estimated using an expression derived by Brunner (1956) during his studies on the centrifugal separation of oil/water emulsions. For disc stacks equipped with long caulks Carlsson (1986) suggests:

$$\frac{\Delta p_{disc}}{\Delta p_{sym}} = \frac{N^{o}(\lambda)^2}{N^{o}(\lambda)^2 - M^{o}(\lambda)^2} + \frac{4\ \sin\varphi\ \ln(\sqrt{2}+1)}{z_L\ \ln(Ra/Ri)}\ \frac{M^{o}(\lambda)^2}{N^{o}(\lambda)^2 + M^{o}(\lambda)^2} \qquad 5.3$$

$$\Delta p_{sym} = \frac{\rho_f\ \omega\ Q\ \ln(R_a/R_i)}{\pi\ h\ z\ N^{o}(\lambda)} \qquad 5.4$$

where ρ is the density of the precipitate suspension, ω is the angular bowl velocity, Q is the throughput capacity, h is the gap width, z is the number of discs and $N^{o}(\lambda)$ is the tangential fluid velocity profile.

The meridian and tangential velocity profiles $M^{o}(\lambda)$ and $N^{o}(\lambda)$ can be obtained using:

$$N^{o}(\lambda) = \frac{1}{\lambda}\ \frac{\sinh(\lambda) - \sin(\lambda)}{\cosh(\lambda) + \cos(\lambda)} \qquad 5.5$$

and

$$M^{\circ}(\lambda) = 1 - \frac{1}{\lambda} \frac{\sinh(\lambda) + \sin(\lambda)}{\cosh(\lambda) + \cos(\lambda)} \qquad 5.6$$

where

$$\lambda = h\sqrt{\frac{\omega \sin\theta}{\nu}} \qquad 5.7$$

For values of $\lambda > 10$ the above equations can be simplified to

$$N^{\circ}(\lambda) = 1/\lambda \qquad \text{and} \qquad M^{\circ}(\lambda) = 1 - 1/\lambda \qquad 5.8$$

Subsequent calculation using the specifications listed in Table 2.1 showed that the pressure drop, Δp_{disc}, across a full disc stack ($z = 72$) is very small and therefore the pressure drop across the disc centrifuge may directly be used to express the pressure drop across the distributor which finally can be applied to determine the power dissipation:

$$P_{dist} = \Delta p_{s} \, Q \qquad 5.9$$

The root-mean-square velocity gradient G is then given by:

$$G_{dist} = (P_{v,dist}/\mu)^{1/2} \qquad 5.10$$

where $P_{v,dist}$ represents the power dissipated per unit volume of liquid ($= P_{dist}/V_{dist}$). Numerical evaluation of the above equations ($Q = 300$ L h^{-1}, $\Delta p_{dist} \approx 0.5$ bar, $V_{dist} \approx 0.3$ L) shows that the mean power dissipated per unit volume in the distributor of a disc stack centrifuge equipped with a full-hermetic feed zone is of the order of 15 kW/m^3, which corresponds to a high degree of turbulence. For similar scales of power dissipation considerable breakup of protein precipitates has been found in centrifugal pumps by Narendranathan (1981).

Alternatively the specific power dissipated in the entry zone may be estimated from the momentum balance and the law of conservation of energy applied to the liquid entering and leaving the centrifuge. The liquid mass m enters the centrifuge with no kinetic energy or momentum and leaves the centrifuge at the discharge radius r_d, with the rotational speed equal to that of the bowl, i.e. a velocity u in the tangential direction. The angular momentum is then:

$$L = m \, r_d \, u \qquad 5.11$$

According to the laws of momentum conservation this increase in angular

momentum is equal to a driving torque given by:

$$T = \dot{m}\, r_d\, u \qquad 5.12$$

which corresponds to a driving power:

$$P_o = T\omega = \dot{m}\, u^2 \qquad 5.13$$

or, written in a more convenient form given by:

$$P_o = Q\rho\omega^2 r_d^2 \qquad 5.14$$

where Q is the flow rate of the discharge stream and ρ is the fluid density.

Equation 5.14 shows that a bowl discharging the fluid at a radius $r_d = 0$ requires ideally no power. Actually, viscous drag of the fluid in the passage of the bowl is present and has to be overcome by an external source since no energy is available from the centrifuge. In practice the stream is discharged at a radius other than zero and a small part of the power computed by Equation 5.14 is consumed to overcome the viscous drag resulting from the flow of that stream through the centrifuge. A second part appears as kinetic energy in the discharge fluid and the rest of this power is dissipated in heat and turbulence. Gössele (1980) suggests that approximately half the driving power is transformed into kinetic energy of the fluid discharge while the other half is dissipated within the feed zone of the centrifuge.

$$P_{dist} = 1/2\ P_o = 1/2\ Q\rho\omega^2 r_d^2 \qquad 5.15$$

Using the experimentally determined, effective fluid discharge radius (r_d = 0.0109 m) of the full-hermetic feed zone, a flow rate of 300 L h^{-1} and a angular bowl velocity of 965 s^{-1} a power value P_{dist} of roughly 4.6 W can be calculated. On the basis of a distributor volume of 0.3 L it is possible to calculate the specific power dissipated in the full-hermetic feed zone. The value of $P_{v,dist}$ = 15.4 kW/m^3 is of the same order of magnitude as the value calculated before using the pressure-drop approach.

The major disadvantage in applying the power dissipation per unit volume approach in order to explain the various levels of particle breakup lies in the difficulties to measure the dissipated power in feed zones other than the full-hermetic and in the problem to define the liquid into which volume the power is actually dissipated. However, comparing the hydro-

hermetic and the semi-hermetic feed zone versions, it would appear that a similar amount of power is dissipated in a smaller volume of liquid. As a consequence the levels of particle breakup increase. Calculating the root-mean-square velocity gradient according to Equation 1.43, shear levels of the order of $G_{dist} \approx 3700\ s^{-1}$ are obtained. These levels of shear are approximately four times greater than those of a precipitation reactor where considerable particle breakup was observed (Glatz et al, 1986). Particle breakup as a result of particle collision with the distributor ribs seems to be the most likely cause for particle breakup. This would also explain, apart from the different levels of power dispersion, the considerable differences in terms of particle breakup between the hydro-hermetic and full-hermetic feed zone versions. The rotational velocity of the distributor rib is given by:

$$v_{rib} = \omega \cdot r_{rib} \qquad 5.16$$

where r_{rib} is the inner rib radius. Since the frequency and the impact of collision with the rib will be proportional to the circumferential velocity of the rib, particle breakup should be a function of the bowl speed and the rib radius, i.e. particle breakup should be reduced if v_{rib} is decreased. On the other hand similar levels of particle breakup should be observed if v_{rib} remains constant.

Examining the hermetic and hydro-hermetic feed zone versions shows that the effective rib-radius of the full-hermetic feed zone is roughly 0.021 m, while the effective rib-radius for the hydro-hermetic feed zone is of the order of 0.0275 m. Hence, provided the assumptions made earlier are correct, then it is not surprising that for the same angular bowl velocity, considerably more particle breakup is observed for the hydro-hermetic feed zone compared with the full-hermetic feed zone.

As a matter of fact, reducing the rib-velocity of the hydro-hermetic distributor to a value close to the rib-velocity of the full-hermetic distributor, increases the relative mass yield to values close to unity provided the specific throughput capacity is kept constant (see mass yield data of WS20, Table 4.1).

Since the observed level of particle breakup was even higher for the semi-hermetic feed zone, these additional levels of breakup are attributed to impingement of the feed suspension onto the rotating distributor walls after deflection from the lock nut and in particular the impact with the

rotating tips of the distributor ribs which, according to Van der Linden (1987) contribute considerably towards higher levels of shear-associated particle damage.

One aspect which so far has not yet been considered is the effect of flow rate on the level of particle breakup. Although Figure 4.15 indicates a trend to more particle breakup at higher flow rates the data have to be treated carefully since the experiments were not performed using the same batch of precipitate particles. The results shown would only be in correspondence with Equation 5.15 which, if correct, implies that the higher the flow rate the greater the power dissipated and hence the higher the levels of particle breakup. On the other hand, however, it is important to remember that particle breakup is also a function of the time a particle is exposed to shear (Bell, 1982) which in itself is inversely proportional to the flow rate, Q. Therefore, it may well be that the increase of shear is partly offset by a reduction of the corresponding shear exposure time.

In conclusion the study of the behaviour of suspensions of protein precipitate in feed zones to disc centrifuges has provided valuable information which are useful for quantifying the levels of particle disruption and for the design of new, low shear feed zone versions.

In order to confirm the above findings a detailed examination of the effect of the distributor-rib diameter on the level of particle breakup is currently under way. Based on the results presented in this thesis new distributor types allowing acceleration of the feed suspension close to the centre axis of rotation are being build and tested by centrifuge manufacturers.

6. Conclusions

The separation performance has been studied for a scaled-down version of an industrial disc centrifuge. It has been shown that a disc centrifuge may be scaled down to 10% of its total available separation area in order to examine particle recovery. It has also been shown that the separation performance of the scaled-down disc centrifuge is influenced by the location of the active discs within the partially blanked disc stack.

The most unfavourable location of the active discs in respect to separation performance was found to be near the distributor foot where the feed suspension leaves the distributor and enters the spacing in between the discs. Secondary effects of the flow rate on the separation performance are observed showing a decrease in the performance of the disc centrifuge with increasing single passage throughputs.

Effects of scale on the separation performance due to variation of the number of active discs were not observed. It has been shown that a two-parameter equation can be used successfully in order to express the grade efficiency curve in a mathematical form which is very useful for computer simulation purposes.

When placed in a shear field protein precipitates are readily fragmented into smaller particles of which the fragment size is related to the size of the particle, the particle strength and the strength of the shear field. Using these properties it has been show that in the high shear fields of feed zones to centrifuges precipitate particles are easily disrupted into smaller particles resulting in a considerable loss of separation performance.

It has also been shown that the level of particle breakup is related to the design of the feed zone. A high level of particle breakup has been observed for the semi-hermetic feed zone while far less shear damage was observed for the full-hermetic feed zone.

In respect to particle breakup the hydro-hermetic feed zone design showed less particle breakup than the semi-hermetic but more breakup than the full-hermetic feed zone versions. When the bowl speed is reduced the level of particle disruption is also decreased resulting in an improved performance of the disc centrifuges. The exact mechanism of aggregate rupture in feed zones has not been solved yet but collision forces between particles and the rotating distributor ribs together with turbulence seem to be the most likely cause for particle breakup.

List of symbols

		dimension
A_e	equivalent separation area	m^2
$A_{e,\perp}$	effective equivalent separation area	m^2
A_n	net sectional area	m^2
b_L	caulk width	m
C	floc strength constant	-
C_1	floc strength constant (inertial convective subrange)	-
C_2	floc strength constant (viscous dissipation subrange)	-
$c_{m,0}$	solids concentration in feed	$kg\ m^{-3}$
$c_{m,1}$	solids concentration in supernatant	$kg\ m^{-3}$
$c_{m,2}$	solids concentration in solids discharge	$kg\ m^{-3}$
c_s	soluble protein concentration	$kg\ m^{-3}$
c_v	volumetric solids concentration	$kg\ m^{-3}$
D	diffusivity	$cm^2\ s^{-1}$
D_i	impeller diameter	m
D_s	dielectric constant	-
d	particle diameter	m
d_c	critical particle diameter	m
d_{100}	particle diameter of 100% recovery	m
d_m	median particle diameter	m
d_{max}	maximum particle diameter	m
d_s	sheared particle diameter	m
$d_{s,ave}$	arithmetic average of sheared particle diameters	m
$d_{0,meas}$	median particle diameter in feed to centrifuge	m
E	electric field strength	$V\ m^{-1}$
E(k,t)	energy spectrum	W
E_T	mass yield	-
$E_{T,pred}$	predicted mass yield	-
$E_{T,meas}$	measured mass yield	-

		dimension
F_b	floc binding force	N
f	shape factor	-
f_o	number frequency distribution	-
f_3	volume frequency distribution	-
F_o	cumulative number distribution	-
F_3	cumulative volume distribution	-
$\Delta F_o(d)$	normalised volume frequency distribution in feed	-
$\Delta F_1(d)$	normalised volume frequency distribution in supernatant	-
$\Delta F_2(d)$	normalised volume frequency distribution in solids discharge	-
f_L	correction factor	-
g	gravity constant (= 9.81 ms^{-2})	
G	root-mean-square velocity gradient	s^{-1}
G_{dist}	root-mean-square velocity gradient in distributor	s^{-1}
h	height	m
I	current	A
k	wavenumber (= λ^{-1})	m
K	constant	-
K_1	constant	-
K_2	constant	-
K_3	constant	-
K_A	rate constant	-
K_{eff}	collision efficiency factor	-
K_{ext}	extinction coefficient	-
K_O	constant	-
K_B	Boltzman constant (= $1.381 \cdot 10^{-23}$ J K^{-1})	
L	length scale of energy dissipating eddies	m
l_m	central distance between particles	m
m	mass	kg
m	number of size classes	-
m	relative refractive index	-
$\dot{m}$	mass flow rate	kg s^{-1}
$\dot{m}_o$	mass flow rate of feed	kg s^{-1}

		dimension
$\dot{m}_1$	mass flow rate of supernatant	kg s^{-1}
$\dot{m}_2$	mass flow rate of solids discharge	kg s^{-1}
$M^o(\lambda)$	meridian fluid flow profile	m s^{-1}
n	impeller rotational speed	rev s^{-1}
N	number of particles	-
N_o	initial number of particles	-
N_{max}	maximum possible number of primary particles in an aggregate	-
$N^o(\lambda)$	tangential fluid velocity profile	m s^{-1}
P	dissipated power	W
Po	power number	-
P_f	dissipated power in feed zone	W
$P_{v,dist}$	dissipated power per distributor unit volume	W m^{-3}
Δp_s	pressure drop across separator	bar
Δp_{dist}	pressure drop across distributor	bar
Δp_{disc}	pressure drop across disc stack	bar
Q	hydraulic throughput capacity	m^3 s^{-1}
q	single passage throughput	m^3 s^{-1}
q_s	specific throughput capacity	L $m^{-2}h^{-1}$
r	radius	m
r_c	Pearson correlation coefficient	-
r_d	liquid discharge radius	m
r_{rib}	inner rib radius	m
R	particle radius	m
R_a	outer disc radius	m
Re	Reynold number	-
R_i	inner disc radius	m
Ro	Rosby number	-
S	protein solubility	kg m^{-3}
S_o	extrapolated protein solubility	kg m^{-3}
t	time	s
t	shear exposure time	s
t_m	mean residence time	s

		dimension
T	grade efficiency	-
T_{abs}	absolute temperature	K
$T_{i,theor}$	calculated grade efficiency value	-
$T_{i,meas}$	measured grade efficiency value	-
u	circumferential bowl velocity	$m\ s^{-1}$
u_a	fluid velocity at outside radius of disc	$m\ s^{-1}$
u_λ	mean eddy velocity	$m\ s^{-1}$
ΔU	voltage pulse	V
V	volume	m^3
V	potential energy of interaction	$J\ m^{-1}$
V_{dist}	volume of distributor	m^3
v_g	gravitational settling velocity	$m\ s^{-1}$
v_g^*	hindered settling velocity	$m\ s^{-1}$
$v_{g,c}$	critical settling velocity	$m\ s^{-1}$
V_h	holdup volume	m^3
v_p	meridian particle velocity	$m\ s^{-1}$
$v(h)$	fluid velocity profile across width of disc	$m\ s^{-1}$
v_{rib}	circumferential velocity of distributor rib at r_{rib}	$m\ s^{-1}$
v_z	centrifugal settling velocity	$m\ s^{-1}$
V_{cube}	volume of a cube	m^3
V_{sphere}	volume of a sphere	m^3
z	number of discs	-
z	dimensionless variable	-
z_L	number of caulks	-

Greek Symbols

		dimension
β	constant	-
Δ	difference	-
ε	energy dissipated per unit mass	$W\ kg^{-1}$
ε_c	mean error	-
η	microscale	-
λ	stream parameter	-
λ	wave length	m
λ_o	wavelength of light in vacuum	m
ν	kinematic viscosity	Pa·s
π	3.14159	-
ρ	density	$kg\ m^{-3}$
ρ_m	density of aggregates	$kg\ m^{-3}$
ρ_l	density of liquid phase	$kg\ m^{-3}$
ρ_s	density of solids	$kg\ m^{-3}$
ρ_R	electric resistivity	Ω
$\Delta\rho$	density difference	$kg\ m^{-3}$
σ	yield strength constant	$N\ m^{-2}$
σ	arithmetic standard deviation	m
σ_g	geometric standard deviation	m
τ	turbidity	-
φ	half disc opening angle	°
ω	angular velocity	$rad\ s^{-1}$

References

Alex W., Koglin B. and Leschonski K., Teilchengrößenanalyse, Chemie-Ingenieur-Technik, 46 (1974) pp 729-732.

Ambler C.M., The evaluation of Centrifuge performance, Chemical Engineering Progress, 3 (1952) pp 150-158.

Argaman Y. and Kaufman W.J., Turbulence and Flocculation, Journal of the Sanit. Eng. Div., ASCE, Vol. 96, No SA2, Proc. Paper 7201, (April 1970) pp 223-241.

Aronson A. and Quilter J., Design and Installation of Disc Stack Separators for Biotechnology, priv. com. 1986

Barnea E. and Mizrahi J., A Generalized Approach to the Fluid Dynamics of Particulate Systems - Part 1: General Correlation for Fluidization and Sedimentation in Solid Multiparticle Systems, The Chemical Engineering Journal, 5 (1973) pp 171-189.

Bartsch H.J.: Mathematische Formeln. VEB Fachbuchverlag Leipzig, 1977.

Batchelor G.K.: The Theory of Homogeneous Turbulence, Cambridge Univ. Press, Cambridge, England, 1958.

Bell D.J., Ph.D. Thesis, University of London, 1982

Bell D.J. and Dunnill P., Shear Disruption of Soya Protein Precipitate Particles and the Effect of Aging in a Stirred Tank, Biotechnology and Bioengineering, 24 (1982) pp 1271-1285.

Bell D.J., Hoare M. and Dunnill P., The Formation of Protein Precipitates and their Centrifugal Recovery, Advances in Biochemical Engineering /Biotechnology, 26 (1983) pp 1-72.

Bell D.J., Heywood-Waddington D. and Hoare M., The Density of Protein Precipitates and its Effect on Centrifugal Sedimentation, Biotechnology and Bioengineering, 24 (1982) pp 127-141.

Bender W. and Koglin B., Mechanische Trennung von Bioprodukten, Chemie-Ingenieur-Technik, 58 (1986) pp 565-577.

Bott E.W., Clarification as an Alternative to Filtration in the Wine Industry, Filtration & Separation, Sept./Oct. 1980, pp 426-451.

Bohman H., Hydrodynamics of the Liquid in the Disc Stack of a Centrifugal Separator, First European Conference on Mixing and Centrifugal Separation, 9th-11th September 1974, Paper F3.

Brown L.D. and Glatz E.C., Aggregate Breakage in Protein Precipitation, Paper prepared for presentation at the Annual Meeting of the AIChE, Chicago, Illinois, November, 1985.

Brugger K., The Particle Size Determination of Pigments with the Disc Centrifuge, Powder Technology, 13 (1976) pp 215-221.

Brunner A., Ph.D. Thesis, University of Zürich, Switzerland, 1956.

Brunner K.H., Ph.D. Thesis, University of Erlangen, W.-Germany, 1979.

Brunner K.H., Separators in Biotechnology, Westfalia Separator AG, Germany.

Brunner K.H. and Molerus O., Partikelbewegung im Tellerseparator, vt Verfahrenstechnik, 11 (1977) pp 538-541.

Brunner K.H. and Molerus O., Theoretical and Experimental Investigation of Separation Efficiency of Disc Centrifuges, German Chemical Engineering 2 (1979) 228-233.

Bujalski W., Nienow A.W., Chatwin S. and Cooke M., The Dependency on Scale of Power Numbers of Rushton Disc Turbines, Chemical Engineering Science, Vol. 42, " (1987) pp 317-326.

Burt M.W.G., The Accuracy and Precision of the Centrifugal-Disc Photosedimentometer Method of Particle Size Analysis, Powder Technology, 1 (1967) pp 103-115.

Camp T.R. and Stein P.C., Journal of the Boston Society of Civil Engineers, 30 (1943) p 219.

Carlsson C.G., Ph.D. Thesis, University of Göteborg, Sweden, 1979.

Coll H. and Searles C.G., Use of Density Gradients in a Disk Centrifuge, J. of Colloid and Interface Science, 110 (1986) pp 67-72.

Coll H. and Searls C.G., Particle Size Analysis with the Joyce-Loebl Disk Centrifuge: A Comparison of the Line-Start with the Homogeneous-Start Method, J. of Colloid and Interface Science, 115 (1987) pp 121-129.

Coulter W.H., Means for Counting Particles suspended in a fluid, U.S. Patent 2 656 508 (1953).

Daniels W., Polyvinylacetate, Kirk-Othmer Encyclopedia of Chemical Technology, 3rd Edition, 23 (1983) pp 817-847.

Datar R., Centrifugal and Membrane Filtration Methods in Biochemical Separation, Filtration & Separation, Nov./Dec. 1984, pp 402-404.

Devereux N., Hoare M. and Dunnill P., Membrane Separation of Protein Precipitates: Unstirred Batch Studies, Biotechnology and Bioengineering, 28 (1986) pp 88-96.

Dixon M. and Webb E.C.: Enzymes. Longmans, London (1979).

Ebert K. and Ederer H.: Computeranwendungen in der Chemie. Verlag Chemie, Weinheim (1983).

Erikson R.A., Disc Stack Centrifuges in Biotechnology, Chemical Engineering Progress, December 1984 pp 51-54.

Foster P. and Watt J.G.: The CSUM fractionation process. In "Methods of Plasma Fractionation" (Ed. J. Curling), Academic Press London and New York (1980) pp 17-31.

Fisher R.R., Glatz, C.E. and Murphy P.A., Effects of Mixing During Acid Addition on Fractionally Precipitated Protein, Biotechnology and Bioengineering 28 (1986) pp 1056-1063.

Frampton G.A., Evaluating the Performance of Industrial Centrifuges, Chemical Process Engineering, August 1983, pp 401-412.

Francis A.W., Physics, 4 (1933) p 403.

Fuchs N.A.: The Mechanics of Aerosols, Pergamon Press, Oxford, 1964, p 334.

Glasgow L.A. and Barkley A.W., Particle Size Reduction by Breakage in Biological Waste Water Treatment, Biotechnology and Bioengineering, 25 (1983) pp 901-918.

Glasgow L.A. and Hsu P.J., An Experimental Study of Floc Strength, AIChE Journal, 28 (1982) 5 pp 779-785.

Glasgow L.A. and Luecke H.R., Mechanisms of Deaggregation for Clay-Polymer Flocs in Turbulent Systems, Industrial Engineering Chemical Fundamentals, 19 (1980) pp 143-156.

Glatz C.E., Hoare M. and Landa-Vertiz J., The Formation and Growth of Protein Precipitates in a Continuous Stirred-Tank Reactor, AIChE Journal 32 (1986) pp 1196-1204.

Gras J.L., An Investigation of a Non-Linear Iteration Procedure for Inversion of Particle Size Distributions, Atmospheric Environment 17 (1983) 4 pp 883-894.

Greenspan H.P.: The theory of rotating fluids, Cambridge University Press, England, 1968.

Gregory J., Turbidity Fluctuations in Flowing Suspensions, Journal of Colloid & Interface Science, 105 (1985) 2 pp 357-371.

Gupta S.K., Scale-up Procedures for Disc Stack Centrifuges, Chemical Engineering Journal, 22 (1981) pp 43-49.

Gösele W., Scale-up of Helical Conveyor Type Decanter Centrifuges, German Chemical Engineering, 3 (1983) pp 353-359.

Hao Y.L., Ingham K.C. and Wickerhauser M.: Fractional precipitation of proteins with polyethylene glycol. In "Methods of Plasma Protein Fractionation" (Ed. J. Curling), Academic Press, London and New York (1980) pp 57-74.

Hemfort H. and Kohlstette W., Chemical Industry, (Düsseldorf) 37 (Juni 1985) pp 3-7.

Hemfort H. and Kohlstette W., Entwicklungstendenzen im Separatoren- und Dekanterbau, Vorträge des VLT Seminars zum Thema: Trenntechniken, 19/20 Februar 1987 in Flein, pp 121-147.

Herdan, G.: Small Particle Statistics. Butterworth, London (1960)

Hinze J.O.: Turbulence, 2nd ed., McGraw Hill, New York, 1975, pp 222, 305-310.

Hoare M. and Dunnill P., Biochemical Engineering Process Design for the Recovery and Fractionation of Proteins by Precipitation, Paper presented at the Third European Congress on Biotechnology, Munich, 10th-14th Sept. 1984.

Hoare M. and Dunnill P., Precipitation of Food Proteins and their Recovery by Centrifugation and Ultrafiltration, Journal of Chemical Technology Biotechnology 34B (1984) pp 199-205.

Horak D., Peska J. Svek T. and Stamberg J., Powder Technology, 31 (1982) p 263

Huck P.M. and Keith L.M., Kinetic Model for Flocculation with Polymers, Journal of the Environmental Engineering Division, EE4, Paper 13950 (August 1978) pp 767-784.

Hsu H.W.: Separations by centrifugal phenomena. Techniques of Chemistry, Vol. XVI (1983), John Wiley & Sons.

Kachel V., Investigation into Coulter Sizing of Biological Particles; Theoretical Background and Instrumental Improvements, Particle Characterisation 3 (1986) pp 45-55.

Kerker M.: The Scattering of Light and Other Electromagnetic Radiation. Academic Press New York, 1969.

Koglin B., Experimentelle Untersuchungen zur Sedimentation von Teilchenkomplexen in Suspensionen, Chemie-Ingenieur-Technik 44 (1972) pp 515-521.

Kresze G.B.: Methods for Protein Determination; in Bergmeyer: Methods of Enzymatic Analysis. Vol. II, 3rd. Edition (1980) pp 84-98.

Kruyt, H.R., Colloid Science, 1 (1952) Elsevier Amsterdam

Kula M.R., Honig W. and Foellmer, H.: Polyethylene glycol precipitation. In "Proceedings of International Workshop on Technology for Protein Separation and Improvement of Blood Plasma Fractionation" (Ed. H.E. Sandberg), National Institute of Health Puplication No 78-1422, Washington DC USA (1977) pp 361-371.

Ladenburg R., Analen der Physik, 20 (1903) p 287.

Langer G., Zur Sedimentationsanalyse wäßriger Kunststoffdispersionen mit der Scheibenzentrifuge, Colloid & Polymer Science, 257 (1979) pp 522-532.

Levenspiel O.: Chemical Reaction Engineering 2 (1972).

Leschonski K., Representation and Evaluation of Particle Size Analysis Data, Particle Characterisation, 1 (1984) pp 89-95.

Levich V.G.: Physico-Chemical Hydrodynamics, Prentice Hall Inc., Englewood Cliffs, N.J., 1962.

Luther H., Claus A., Büttner W. and Schuster E., Untersuchungen zur Separation aufgeschlossener Hefesuspensionen, Acta Biotechnologica 3 (1983) 2 pp 133-142.

Matsuo T. and Unno H., Forces Acting on Floc and Strength of Floc, Journal of the Sanitary Engineering Division, ASCE, Vol. 107, No EE3, Proc. Paper 16300 (June 1981) pp 527-545.

Murkes J. and Carlsson C.G., Mathematical Modelling and Optimisation of Centrifugal Separation, Filtration & Separation, Jan./Feb. 1978 pp 18-22

Murray K.R., The Effect of Flow Reversal through the Disc Stack of a High Speed Disc Centrifuge, First European Conference on Mixing and Centrifugal Separation, 9th-11th September, 1974, Paper F4.

Muschelknautz E., Laufende Grundlagenuntersuchungen im Bereich der Hochschulen, in GVC - Preprints: Mechanische Flüssigkeitsabtrennung (1987) pp 223-243.

Narendranathan T.J., Ph.D. Thesis, University of London, 1981.

Nash A.M., Kwolek W.F. and Wolf W.J., Denaturation of Soybean Proteins by Isoelectric Precipitation, Cereal Chemistry 48 (1971) pp 360-368.

Nelson C.D. and Glatz C.E., Primary Particle Formation in Protein Precipitation, Biotechnology and Bioengineering, 27 (1985) pp 1434-1444.

Obukhoff A.M. and Yaglom A.M., Prikladnaya Matematica i Mekhanika, 15 (1951) 3.

Olbrich R., Mannweiler K., Fish N.M. and Hoare M., The Separation and Reduction of E.coli Cell Debris from Protein Inclusion Bodies, to be puplished.

Pandya J.D. and Spielman L.A., Floc Breakage in Agitated Suspensions: Effect of Agitation Rate, Chemical Engineering Science, 38 (1983) 12 pp 1983-1992.

Parker D.S., Kaufman W.J. and Jenkins D.J., Floc Breakup in Turbulent Flocculation Processes,Journal of the Sanitary Engineering Division, ASCE, Vol. 98, No SA1, Proc. Paper 8702 (Febr. 1972) pp 79-99.

Patterson I. and Kamal R.M., Shear Deagglomeration of Solid Aggregates Suspended in Viscous Liquids, The Canadian Journal of Chemical Engineering, 52 (1974) pp 306-315.

Pearse M.J. and Barnett J., Chemical Treatments for Thickening and Filtration, The Second World Filtration Congress, 1979.

Petenate A.M. and Glatz C.E., Isoelectric Precipitation of Soy Protein: I. Factors Affecting Particle Size Distribution, Biotechnology and Bioengineering, 25 (1983) pp 3049-3058.

Petenate A.M. and Glatz C.E., Isoelectric Precipitation of Soy Protein: II. Kinetics of Protein Aggregate Growth and Breakage, Biotechnology and Bioengineering 25, (1983) pp 3059-3078.

Richardson J.F. and Zaki W.N., Transaction of the Institution of Chemical Engineers. 32 (1954) pp 35-53.

Salt D.J., Leslie R.B., Lillford P.J. and Dunnill P., Factors Influencing Protein Structure During Acid Precipitation: A Study of Soya Protein, Europ. Journal of Applied Microbial Biotechnology 14 (1982) pp 144-148.

Scawen M.D. and Hammond P.M.: Protein Recovery. In "Bioactive Microbial Products 3 - Downstream Processing" (Ed. J.D. Stowell et al.), Academic Press, London and New York (1986) pp 77-101.

Skvortsov L.S., A Study of Separation in the Settling Space of a Centrifugal Cleaner-Separator, Theoretical Foundations of Chemical Engineering, 18 (1984) 3, pp 226-233.

Skvortsov L.S. and Rachitskii V.A., Estimating the Flow Rate of Solids Particles in the Rotor of a Centrifugal Separator, Theoretical Foundations of Chemical Engineering, 12 (1978) pp 526-529.

Smith D.K.W. and Kitchner J.A., The Strength of Aggregates Formed in Flocculation, Chemical Engineering Science, 33 (1978) pp 1631-1639.

Smith T.N., Recovery Fractions in Centrifuges, Chemical Engineering Journal, 13 (1977) pp 21-26.

Sokolov V.I. and Dolzhanova G.A., Influence of the angular velocity of Centrifuge and Separator Rotors on Separation Efficiency, Theoretical Foundations of Chemical Engineering, 45 (1972) pp 1063-1066.

Sokolov V.I., Rusakova A.A. and Gorbunova V.V., Influence of Solids-Phase Concentration in Suspension on Process of Thin-Layer Centrifugal Separation, Theoretical Foundations of Chemical Engineering 9, (1975) 4, pp 537-543.

Sokolov V.I., Semenov E.V. and Gorbunova V.V., Calculating the Throughput Capacity of a Centrifuge Separator, Theoretical Foundations of Chemical Engineering, 11 (1977) pp 220-224.

Sokolow W.J.: Moderne Industriezentrifugen, VEB Technik Verlag, Berlin 1971.

Stanley J.H. and Locke W.L., Continuous Centrifugation in a Disc Centrifuge, AIChE Journal, 3 (1957) pp 480-483.

Tambo N. and Watanabe Y., Physical Characteristics of Flocs: I. The Floc Density Function and Aluminium Floc, Water Research, 13 (1979) pp 409-419.

Tambo N. and Watanabe Y., Physical Aspects of Flocculation Process -I. Fundamental Treatise, Water Research, 13 (1979) pp 429-439.

Tambo N. and Hozumi H., Physical Characteristics of Flocs: II. Strength of Floc, Water Research, 13 (1979) pp 421-427.

Thomas D.G., Turbulent Disruption of Flocs in Small Particle Size Suspensions, AIChE Journal, 10 (July 1964) pp 517-523.

Tomi D.T. and Bagster D.F., A Model of Floc Strength under Hydrodynamic Forces, Chemical Engineering Science, 30 (1975) pp 269-278.

Tomi D.T. and Bagster D.F., The Behaviour of Aggregates in Stirred Vessels: Part II- An Experimental Study of the Flocculation of Gelena in a Stirred Tank, Transactions of the Institution of Chemical Engineers, 56 (1978) pp 9-19.

Treasure C.R.G., in T. Allen: Particle Size Measurement, Chapman and Hall London, 3rd Edition, 1981.

Treweek, G.P. and Morgan J.J., Size Distributions of Flocculated Particles: Application of Electronic Particle Counters, Environmental Science & Technology, 11 (1977) 7 pp 707-714.

Twineham M., Hoare M. and Bell, D.J., The Effects of Protein Concentration on the Breakup of Protein Precipitate by Exposure to Shear, Chemical Engineering Science, 39 (1984) pp 509-513.

Twomey S.A., Comparison of Constrained Linear Inversion and an Iterative Nonlinear Algorithm Applied to the Indirect Estimation of Particle Size Distributions, Journal of Computational Physics, 18 (1975) pp 188-200.

Twomey S.A. and Zalabsky R.A., Multifilter Technique for Examination of the Size Distribution of the Natural Aerosol in the Submicrometer Size Range, Environmental Science & Technology, 15 (1981) 2 pp 177-184.

Ullrich W.J., Modern Developments in Powder Metall., Vol. 1, Fundamentals and Methods, Rhenum (1966) p 125.

Van der Linden J.P., Ph.D. Thesis, University of Delft, Netherlands, 1987.

Virkar, P.D., Hoare M., Chan M.Y.Y. and Dunnill P., Kinetics of the Acid Precipitation of Soya Protein in a Continuous-Flow Tubular Reactor, Biotechnology and Bioengineering, 24 (1982) pp 871-887.

Ward P., Ph.D. Thesis, University of London 1989

Willus C.A. and Fitch, B., Flow Patterns in a Disc Centrifuge, Chemical Engineering Progress, 69 (1973) 9, pp 73-74.

Wolf W.J., Dayle A.S. and Babcock G.E., Denaturation of Soybean Globulins by Aqueous Isopropanol, Cereal Chemistry, 41 (1961) pp 328-339.

Yu P.Y. and Gentry J., Comparison of Generic Inversion Algorithms for Characterising Particle Size Distributions, Powder Technology, 50 (1987) pp 79-89.

Zastrow J., Theoretical Calculation of the Performance of Disc Centrifuges, International Chemical Engineering, 16 (1976) 3, pp 515-518.

Zimmels J., Hindered Motion of Particulate System in Newtonian Fluids - Acceleration and Steady Regime, Powder Technology, 34 (1983) pp 191-202.

Appendix

Table A1: Examination of separation performance of disc centrifuge equipped with different feed zone designs using polyvinylacetate particles.

No	Type	p_{in}	p_{out}	Q	θ	ρ_s	ρ_l
	/	bar	bar	L h^{-1}	°C	kg m^{-3}	kg m^{-3}
1	H	2.31	5.23	300	20	1190	998.2
2	HH	0.50	2.45	300	16	1190	998.9
3	H	2.40	5.20	300	16	1190	998.9
4	HH	0.58	2.56	300	15	1190	999.1
5	HH	0.55	2.23	400	15	1190	999.1
6	HH	0.53	1.90	500	15	1190	999.1
7	H	1.80	3.40	400	18	1190	998.6
8	S	0.10	1.50	200	17	1190	998.8
9	S	0.10	1.40	300	16	1190	998.9
10	S	0.20	1.50	400	16	1190	998.9
11	H	2.25	4.95	800	14	1190	999.2
12	H	2.30	5.15	600	14	1190	999.2
13	H	2.15	4.80	600	14	1190	999.2
14	HH	0.61	2.44	400	17	1190	998.8
15	HH	0.54	2.00	400	17	1190	998.8
16	HH	0.60	1.90	600	17	1190	998.8
17	HH	0.65	1.40	800	17	1190	998.8
18	H	2.48	5.34	400	17	1190	998.8
19	HH	0.58	1.94	600	17	1190	998.8
20	HH	1.00	1.36	600	18	1190	998.6
21	HH	0.69	1.03	900	17	1190	998.8
22	H	2.40	5.25	600	18	1190	998.6
23	H	2.40	5.22	900	18	1190	998.6
24	H	2.40	5.10	1200	18	1190	998.6
25	HH	0.90	2.15	900	18	1190	998.6
26	H	2.20	4.40	300	18	1190	998.6
27	H	2.20	5.22	400	18	1190	998.6
28	H	1.82	4.73	200	16	1190	998.9
29	H	2.09	5.45	300	16	1190	998.9
30	HH	0.59	2.52	200	16	1190	998.9
31	HH	0.58	2.43	300	16	1190	998.9
32	HH	0.65	2.20	400	16	1190	998.9
33	H	2.11	5.16	300	16	1190	998 9
34	HH	0.65	2.52	300	16	1190	998.9
35	H	2.03	5.10	400	16	1190	998.9
36	HH	0.65	2.19	400	16	1190	998.9
37	H	1.80	3.87	200	16	1190	998.9
38	HH	0.50	1.87	200	16	1190	998.9
39	H	2.27	3.65	300	17	1190	998.8
40	HH	0.51	1.53	300	17	1190	998.8
41	H	1.90	4.80	400	15	1190	999.1
42	S	0.10	1.50	400	15	1190	999.1
43	S	0.30	1.35	600	15	1190	999.1
44	H	2.14	4.90	600	15	1190	999.1

The density data of the carrier liquid (water) were obtained from the Chemiker Kalender, 2nd Edition, Springer-Verlag, Heidelberg (1974)

Table continued...

No	Type	Q	$\Delta\rho$	μ_f	z	n_{bowl}	$A_{e,L}$
	/	L h^{-1}	kg m^{-3}	mPa s	/	rpm	m^2
1	H	300	191.8	1.002	7	9350	625
2	HH	300	191.1	1.109	7	9350	625
3	H	300	191.1	1.109	7	9350	625
4	HH	300	190.9	1.139	7	9350	625
5	HH	400	190.9	1.139	7	9350	625
6	HH	500	190.9	1.139	7	9350	625
7	H	400	191.4	1.053	7	9350	625
8	S	200	191.2	1.081	7	9350	625
9	S	300	191.1	1.109	7	9350	625
10	S	400	191.1	1.109	7	9350	625
11	H	800	190.8	1.169	14	9350	1250
12	H	600	190.8	1.169	14	9350	1250
13	H	600	190.8	1.169	14	9350	1250
14	HH	400	191.2	1.081	14	9350	1250
15	HH	400	191.2	1.081	14	9350	1250
16	HH	600	191.2	1.081	14	9350	1250
17	HH	800	191.2	1.081	14	9350	1250
18	H	400	191.2	1.081	14	9350	1250
19	HH	600	191.2	1.081	21	9350	1875
20	HH	600	191.4	1.053	21	9350	1875
21	HH	900	191.2	1.081	21	9350	1875
22	H	600	191.4	1.053	21	9350	1875
23	H	900	191.4	1.053	21	9350	1875
24	H	1200	191.4	1.053	21	9350	1875
25	HH	900	191.4	1.053	21	9350	1875
26	H	300	191.4	1.053	14	7800	870
27	H	400	191.4	1.053	14	7800	870
28	H	200	191.1	1.109	7	9350	625
29	H	300	191.1	1.109	7	9350	625
30	HH	200	191.1	1.109	7	9350	625
31	HH	300	191.1	1.109	7	9350	625
32	HH	400	191.1	1.109	7	9350	625
33	H	300	191.1	1.109	7	9350	625
34	HH	300	191.1	1.109	7	9350	625
35	H	400	191.1	1.109	7	9350	625
36	HH	400	191.1	1.109	7	9350	625
37	H	200	191.1	1.109	7	7800	435
38	HH	200	191.1	1.109	7	7800	435
39	H	300	191.2	1.081	7	7800	435
40	HH	300	191.2	1.081	7	7800	435
41	H	400	190.9	1.139	14	9350	1250
42	S	400	190.9	1.139	14	9350	1250
43	S	600	190.9	1.139	14	9350	1250
44	H	600	190.9	1.139	14	9350	1250

The viscosity data of the carrier liquid (water) were obtained from the CRC-Handbook of Chemistry and Physics, 55th Edition, CRC Press, (1974/1975).

Table continued...

No	Type	Q	q_m	d_c	E_{in}	E_{out}	$E_{T,E}$
	/	L h^{-1}	L/(h m^2)	µm	/	/	/
1	H	300	0.48	1.21	0.602	0.248	0.588
2	HH	300	0.48	1.21	0.630	0.223	0.645
3	H	300	0.48	1.21	0.639	0.228	0.638
4	HH	300	0.48	1.21	0.626	0.222	0.645
5	HH	400	0.64	1.40	0.603	0.313	0.481
6	HH	500	0.80	1.57	0.608	0.359	0.410
7	H	400	0.64	1.35	0.624	0.302	0.516
8	S	200	0.32	0.95	0.652	0.226	0.653
9	S	300	0.48	1.20	0.652	0.372	0.429
10	S	400	0.64	1.38	0.656	0.470	0.284
11	H	800	0.64	1.42	0.602	0.377	0.374
12	H	600	0.48	1.23	0.598	0.324	0.458
13	H	600	0.48	1.23	0.598	0.323	0.460
14	HH	400	0.32	0.97	0.588	0.159	0.730
15	HH	400	0.32	0.97	0.588	0.159	0.730
16	HH	600	0.48	1.19	0.586	0.278	0.526
17	HH	800	0.64	1.37	0.586	0.350	0.403
18	H	400	0.32	0.97	0.587	0.159	0.729
19	HH	600	0.32	0.97	0.575	0.137	0.762
20	HH	600	0.32	0.95	0.556	0.120	0.784
21	HH	900	0.48	1.19	0.572	0.226	0.605
22	H	600	0.32	0.96	0.574	0.103	0.821
23	H	900	0.48	1.19	0.574	0.189	0.671
24	H	1200	0.64	1.37	0.574	0.253	0.558
25	HH	900	0.48	1.18	0.576	0.227	0.601
26	H	300	0.34	0.99	0.596	0.165	0.723
27	H	400	0.32	0.95	0.605	0.155	0.744
28	H	200	0.32	0.97	0.603	0.143	0.763
29	H	300	0.48	1.19	0.603	0.252	0.582
30	HH	200	0.32	0.97	0.607	0.151	0.751
31	HH	300	0.48	1.19	0.608	0.271	0.554
32	HH	400	0.64	1.37	0.602	0.348	0.422
33	H	300	0.48	1.19	0.521	0.208	0.601
34	HH	300	0.48	1.19	0.521	0.205	0.607
35	H	400	0.64	1.38	0.518	0.262	0.494
36	HH	400	0.64	1.38	0.520	0.271	0.479
37	H	200	0.46	1.17	0.514	0.195	0.621
38	HH	200	0.46	1.17	0.513	0.196	0.618
39	H	300	0.69	1.42	0.518	0.277	0.465
40	HH	300	0.69	1.42	0.515	0.282	0.452
41	H	400	0.32	0.99	0.602	0.208	0.654
42	S	400	0.32	0.99	0.601	0.222	0.631
43	S	600	0.48	1.21	0.600	0.355	0.408
44	H	600	0.48	1.21	0.597	0.327	0.452

Table continued...

No	Type	Q	$d_{m,o}$	k	n	$E_{T,exp}$	$E_{T,pred}$
	/	L h^{-1}	µm	/	/	/	/
1	H	300	1.53	0.771	2.017	0.610	0.641
2	HH	300	1.59	0.841	2.046	0.672	0.657
3	H	300	1.59	0.853	2.119	0.683	0.656
4	HH	300	1.48	0.837	2.340	0.656	0.624
5	HH	400	1.44	0.799	2.064	0.519	0.499
6	HH	500	1.44	0.790	1.952	0.460	0.429
7	H	400	1.45	0.769	1.867	0.539	0.506
8	S	200	1.14	0.844	2.705	0.643	0.635
9	S	300	1.15	0.799	2.132	0.448	0.445
10	S	400	1.15	0.751	2.412	0.302	0.352
11	H	800	1.25	0.750	2.120	0.390	0.408
12	H	600	1.28	0.752	2.377	0.477	0.522
13	H	600	1.25	0.793	2.435	0.496	0.505
14	HH	400	1.32	0.851	2.896	0.721	0.723
15	HH	400	1.42	0.808	2.894	0.732	0.769
16	HH	600	1.31	0.794	2.815	0.543	0.561
17	HH	800	1.31	0.745	2.535	0.410	0.455
18	H	400	1.44	0.794	2.537	0.727	0.773
19	HH	600	1.45	0.851	2.649	0.764	0.773
20	HH	600	1.57	0.773	2.938	0.781	0.822
21	HH	900	1.59	0.738	2.340	0.623	0.676
22	H	600	1.61	0.845	2.417	0.813	0.829
23	H	900	1.60	0.790	2.200	0.674	0.680
24	H	1200	1.63	0.751	2.274	0.569	0.579
25	HH	900	1.52	0.762	2.454	0.619	0.656
26	H	300	1.27	0.901	2.407	0.713	0.682
27	H	400	1.23	0.921	2.392	0.739	0.693
28	H	200	1.29	0.909	2.500	0.757	0.711
29	H	300	1.28	0.861	1.980	0.592	0.541
30	HH	200	1.29	0.889	2.662	0.741	0.713
31	HH	300	1.29	0.820	2.098	0.562	0.543
32	HH	400	1.27	0.752	1.998	0.423	0.431
33	H	300	1.36	0.843	1.965	0.617	0.582
34	HH	300	1.36	0.795	2.041	0.580	0.581
35	H	400	1.37	0.799	1.874	0.512	0.480
36	HH	400	1.36	0.797	1.971	0.500	0.472
37	H	200	1.36	0.849	2.175	0.623	0.599
38	HH	200	1.36	0.875	2.336	0.632	0.595
39	H	300	1.36	0.796	1.715	0.495	0.455
40	HH	300	1.36	0.785	1.821	0.482	0.452
41	H	400	1.27	0.866	2.563	0.689	0.685
42	S	400	1.26	0.847	2.617	0.666	0.683
43	S	600	1.27	0.740	2.290	0.458	0.516
44	H	600	1.25	0.760	2.249	0.479	0.512

Key to Table A1:

No:	Number of experiment
Type:	feed zone (distributor) type (i) H = full-hermetic (ii) HH = hydro-hermetic (iii) S = semi-hermetic
p_{in}:	feed pressure
pout:	discharge pressure
Q:	throughput capacity or feed flow rate
θ:	temperature of feed suspension
ρ_s:	density of solids phase
ρ_l:	density of liquid phase
$\Delta\rho$:	density difference between solids and liquid phase (= $\rho_s-\rho_l$)
μ_f:	dynamic viscosity of liquid phase
z:	number of separating discs
n_{bowl}:	rotational velocity of bowl
$A_{e,L}$:	equivalent separation or clarification area (Equation 1.20), relevant centrifuge specifications are listed in Table 2.1.
q_m:	specific throughput capacity (= Q/A_e)
d_c:	critical particle diameter (Equation 1.17)
E_{in}:	extinction reading of feed suspension at λ=695 nm
E_{out}:	extinction reading of clarified liquid discharge at λ=695 nm
$E_{T,E}$:	extinction based mass yield of separation process (= $1-(E_{out}/E_{in})$)
$d_{m,e}$:	median particle size of the solids size distribution in the feed to centrifuge
k:	parameter of grade efficiency curve correlation function
n:	parameter of grade efficiency curve correlation function
$E_{T,Siz}$:	size distribution based mass yield of separation process
$E_{T,pred}$:	predicted mass yield based on the corresponding feed size distribution and grade efficiency function expressed by the expression $T = 1 - \exp[-(k\cdot d/d_c)^n]$, where k, n = $f(q_m)$ (Eqn. 4.1).